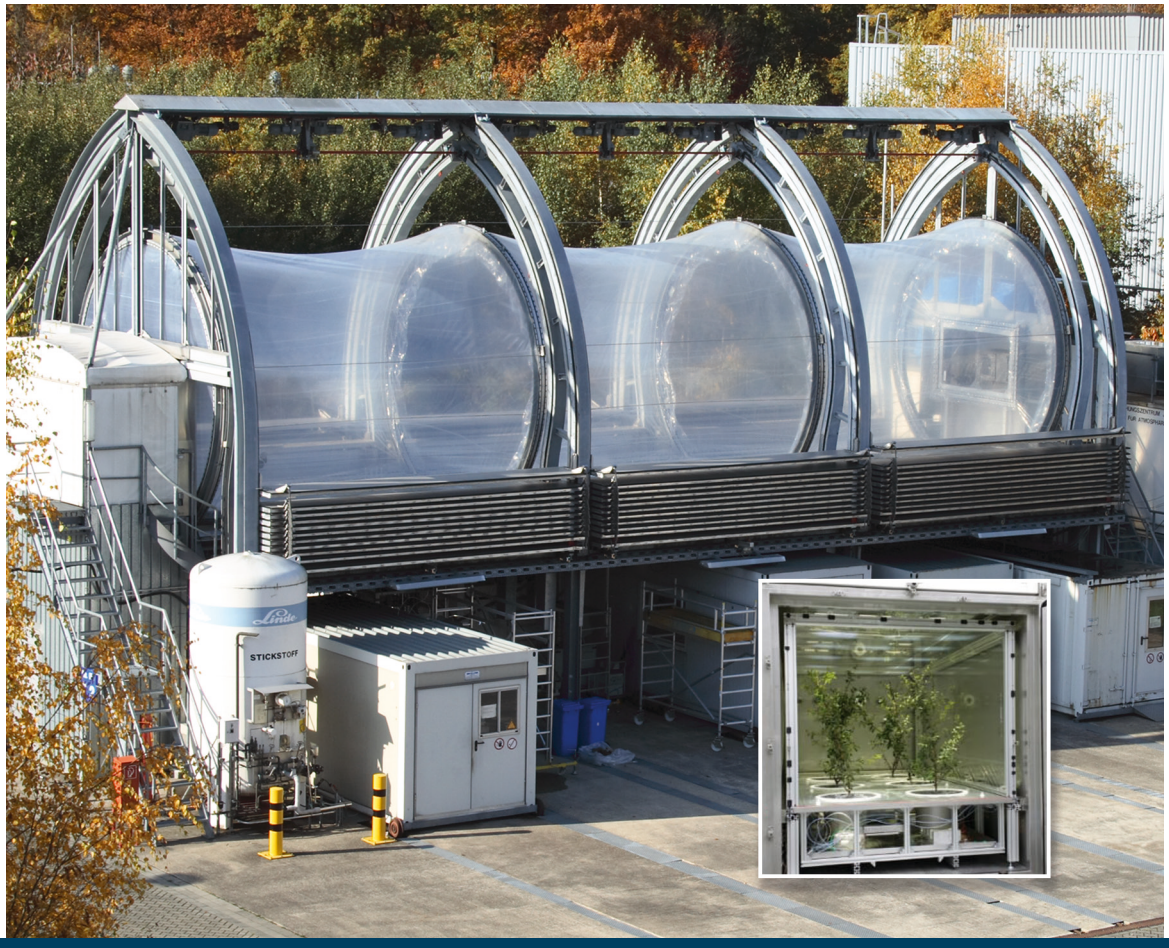

Chamber study of biogenic volatile organic compounds: plant emission, oxidation products and their OH reactivity

Zhujun Yu

Energie & Umwelt / Energy & Environment
Band / Volume 436
ISBN 978-3-95806-356-3

Mitglied der Helmholtz-Gemeinschaft

JÜLICH
Forschungszentrum

Schriften des Forschungszentrums Jülich
Reihe Energie & Umwelt / Energy & Environment Band / Volume 436

Forschungszentrum Jülich GmbH
Institut für Energie- und Klimaforschung
Troposphäre (IEK-8)

Chamber study of biogenic volatile organic compounds: plant emission, oxidation products and their OH reactivity

Zhujun Yu

Schriften des Forschungszentrums Jülich
Reihe Energie & Umwelt / Energy & Environment Band / Volume 436

ISSN 1866-1793 ISBN 978-3-95806-356-3

Bibliografische Information der Deutschen Nationalbibliothek.
Die Deutsche Nationalbibliothek verzeichnet diese Publikation in der
Deutschen Nationalbibliografie; detaillierte Bibliografische Daten
sind im Internet über http://dnb.d-nb.de abrufbar.

Herausgeber und Vertrieb:	Forschungszentrum Jülich GmbH Zentralbibliothek, Verlag 52425 Jülich Tel.: +49 2461 61-5368 Fax: +49 2461 61-6103 zb-publikation@fz-juelich.de www.fz-juelich.de/zb
Umschlaggestaltung:	Grafische Medien, Forschungszentrum Jülich GmbH
Druck:	Grafische Medien, Forschungszentrum Jülich GmbH
Copyright:	Forschungszentrum Jülich 2018

Schriften des Forschungszentrums Jülich
Reihe Energie & Umwelt / Energy & Environment, Band / Volume 436

D 468 (Diss., Wuppertal, Univ., 2018)

ISSN 1866-1793
ISBN 978-3-95806-356-3

Vollständig frei verfügbar über das Publikationsportal des Forschungszentrums Jülich (JuSER)
unter www.fz-juelich.de/zb/openaccess.

Abstract

Volatile organic compounds (VOC)(Fuchs et al., 2017) are ubiquitous in the atmosphere with an estimated atmospheric VOC species of 10^4-10^5. Natural and anthropogenic activities emit VOCs into the atmosphere, with about 90% of the global VOC emissions originating from land vegetation. VOCs play a vital role in the global carbon budget and in the regional formation of ozone in the troposphere. They can also serve as a source of secondary organic aerosol (SOA). Atmospheric lifetime of VOCs varies from minutes to years and is predominantly determined by the reactions with hydroxyl radical (OH), nitrate radical (NO_3), or ozone (O_3). By atmospheric VOCs oxidation intermediate products are formed. The detailed chemical mechanisms involved are insufficiently known to date and need to be understood for air quality management and climate change predictions.

OH radical as the primary oxidant in the troposphere, initiates the degradation of nearly all types of VOCs. The total OH reactivity is the first-order loss rate of OH in reaction with compounds present in ambient air, which provides an insight of the total loading of reactive compounds in the atmosphere. Previous studies comparing directly measured OH reactivity with that calculated from VOC measurements often reported a "missing OH reactivity" in the calculated one, suggesting the existence of unquantified OH sink terms.

This work presents the emission of Biogenic VOCs (BVOCs) from 7 sets of trees and the oxidation of VOCs in a chamber system. The focus of this work is to investigate the atmospheric degradation of VOCs and to improve the knowledge of the sum of reactive trace gases involved in atmospheric processes by using the OH reactivity parameter.

A Proton-Transfer-Reaction Time-of-Flight Mass Spectrometer (PTR-TOF-MS) was used for real-time measurements of VOCs. Monoterpene and sesquiterpene speciations from an offline gas-chromatograph (GC) measurements were adopted for OH reactivity calculation due to the reaction rate coefficient difference among different monoterpenes and sesquiterpenes. The intercomparison between PTR and online GC during the selected campaigns exhibited that the measured concentrations of the main reactants used in this study (isoprene, monoterpenes and benzene-D_6) were linearly correlated and differed within 15%.

The newly built plant chamber SAPHIR-PLUS was characterized with the average BVOCs transfer efficiency of 0.85 from inlet to outlet, and 0.8 from PLUS to the atmosphere simulation chamber SAPHIR.

The BVOCs emission pattern from *Quercus ilex* trees has been determined by the use of SAPHIR-PLUS. The detected BVOCs emissions were dominated by monoterpenes, with minor emissions of isoprene and methanol, consistent with the overall emission pattern typical for *Quercus ilex* trees in the growing season. Monoterpenes and isoprene emissions showed to be triggered by light rather than temperature, because these two compounds have no storage pools in *Quercus ilex*, their release are thus directly connected with the photosynthesis processes in the plant. Additionally, their emissions showed clear exponential temperature dependence under constant light condition, with a slope of 0.11 ± 0.02 $^{\circ}C^{-1}$ for monoterpenes emission. As a tracer for leaf growth, methanol emission exhibited an abrupt increase at the beginning of illumination. This was explained as instantaneous release from stomata of leaves, that stored produced methanol during the night and opened upon light exposure. Emission of methanol increased linearly with temperature.

The ozonolysis of β-pinene, limonene, two monoterpenes mixtures, and four plant-emitted BVOCs were conducted individually in the atmosphere simulation chamber SAPHIR, as well as photo-oxidations of injected and tree-emitted isoprene, to examine the gas-phase oxidation product yields from these reactions. Oxidation products such as formic and acetic acids and acetone were detected, with particular products for different oxidations. The nopinone molar yield was determined to be 0.41 ± 0.04 from the reaction of β-pinene with O_3. No significant oxidation products from the reaction of limonene with O_3 were observed. In the presence of nitric oxide (NO), isoprene in reaction with OH lead to the formation of methyl vinyl ketone (MVK) and methacrolein (MACR). In this study, the MVK + MACR yields under high- and mid- NO conditions were 0.79 ± 0.15 and 0.83 ± 0.16, respectively. When NO is low, isoprene photooxidation is expected to yield the hydroxy hydroperoxides (ISOPOOHs). ISOPOOHs identified as the major products from low-NO isoprene photo-oxidation, had a yield of 0.8 ± 0.15. MVK + MACR yield from photo-oxidation of tree-emitted isoprene was 0.57 ± 0.11 and was in agreement with the literature.

The total OH reactivity was determined with VOCs measurements from the PTR, and directly measured by laser flash photolysis-laser induced fluorescence (LP-LIF) at the same time. Comparison of these two OH reactivity measurements showed an increase of missing OH reactivity in the presence of oxidation products of VOCs, indicating a strong contribution to missing OH reactivity from uncharacterized oxidation products. The biggest missing OH reactivity was observed during the limonene ozonolysis, presumably due to undetected oxidation products by using the PTR technique. The oxidation of plant emissions containing sesquiterpenes showed higher missing OH reactivity than emissions containing monoterpenes, indicating the existence of highly reactive sesquiterpenes oxidation products, that were generated rapidly and were not measured by the PTR. Overall the missing OH reactivities were smaller in photochemical degradation of air masses containing AVOCs, in accordance with previous studies, where less missing OH reactivity was observed in urban areas.

For all selected 36 experiments, the missing OH reactivity emerged a upward tendency with the atomic oxygen-to-carbon (O/C) ratio of the VOC mixture, suggesting again that the more oxidized the system, the more unknown OH sinks. Furthermore, the sum of unidentified compounds measured by the PTR was tentatively used to explain the observed missing OH reactivity. An averaged reaction rate constant k^*, of about 1×10^{-11} cm^3 molecule^{-1} s^{-1} was obtained, and therefore is recommended for VOCs without reported rate constants in further OH reactivity studies.

Contents

Abstract **iii**

1 Introduction **1**
1.1 Volatile Organic Compounds (VOCs) . . . 1
1.1.1 Sources of atmospheric VOCs . . . 1
1.1.2 Sinks of atmospheric VOCs . . . 4
1.2 Atmospheric oxidants . . . 8
1.2.1 Tropospheric OH radicals formation . . . 8
1.2.2 Tropospheric O_3 formation . . . 8
1.2.3 Tropospheric NO_3 radicals formation . . . 9
1.3 Total OH reactivity . . . 10
1.3.1 Introduction to total OH reactivity . . . 10
1.3.2 Missing k_{OH} in the world . . . 11
1.4 Focus of this thesis . . . 13

2 Methods and Instruments **15**
2.1 Proton Transfer Reaction-Time Of Flight-Mass Spectrometry (PTR-TOF-MS) . 15
2.1.1 Ion-molecule reactions . . . 16
2.1.2 Mass separation and ion detection . . . 18
2.1.3 Mass spectra analysis . . . 19
2.1.4 Quantification of VOCs concentrations . . . 20
2.2 Gas-Chromatograph (GC) . . . 22
2.3 Laser Flash Photolysis-Laser Induced Fluorescence (LP-LIF) . . . 24

3 Experimental section **27**
3.1 Chamber svaporystem . . . 27
3.2 Experiments characterizing plant emission intensity and patterns . . . 31
3.3 VOCs oxidation experiments . . . 32
3.3.1 BVOCs Oxidation . . . 32
3.3.2 AVOCs Oxidation . . . 34

4 Data evaluation **37**
4.1 Product yields determination . . . 37
4.2 Missing OH reactivity investigation . . . 39
4.3 O/C ratio calculation . . . 42

5 Plant emitted BVOC measurements **45**
5.1 Overall plant emissions . . . 45
5.2 Light- and temperature-dependent plant emissions . . . 47

6 Product yields from BVOCs oxidations **51**
6.1 Single BVOCs . . . 51
6.2 BVOC mixture . . . 60
6.3 BVOCs from plant emission . . . 61

7 Results and discussion of the OH reactivity **65**
7.1 Missing OH reactivity for BVOCs oxidations 65
7.2 Missing OH reactivity for AVOCs oxidations 69
7.3 Discussion of missing OH reactivity 72

8 Summary and conclusion **81**

A Sensitivity table **85**

B kOH comparison time series **89**

C Yield plot **111**

Bibliography **129**

Acknowledgements **139**

List of Figures

1.1 Structure of some terpenoids . . . 2
1.2 Structure of some AVOCs . . . 4
1.3 Atmospheric fate of VOCs . . . 5
1.4 Atmospheric fate of VOCs . . . 7
1.5 Isoprene degradation . . . 7
1.6 kOH world map . . . 12

2.1 Schema of the PTR-TOF-MS . . . 15
2.2 Separation of isobaric molecules . . . 19
2.3 Calibration of α-pinene . . . 21
2.4 Comparison between PTR and GC measurements . . . 23
2.5 OH decay curve in synthetic air . . . 24

3.1 SAPHIR chamber . . . 27
3.2 Chamber schema . . . 28
3.3 Transfer efficiency of the chamber system . . . 29

4.1 Nopinone yield from β-pinene ozonolysis . . . 38
4.2 Calculation of OH reactivity from PTR-TOF-MS measurements. . . . 39
4.3 Unidentified compounds from PTR-TOF-MS measurements . . . 40

5.1 *Quercus ilex* emission example . . . 47
5.2 Light dependent emissions . . . 48
5.3 Temperature dependent emissions . . . 49

6.1 β-pinene ozonolysis . . . 51
6.2 β-pinene oxidation product structure . . . 52
6.3 acetone yield from β-pinene ozonolysis . . . 54
6.4 Limonene ozonolysis product structure . . . 56
6.5 Isoprene photo-oxidation product structure . . . 57
6.6 Products yields from isoprene photo-oxidations. . . . 60

7.1 k_{OH} of experiment BS2 . . . 66
7.2 k_{OH} of experiment BM3 . . . 67
7.3 k_{OH} of experiment BP1 . . . 68
7.4 k_{OH} of experiment BP6 . . . 69
7.5 k_{OH} of experiment AS1 . . . 70
7.6 k_{OH} of experiment AM2 . . . 71
7.7 k_{OH} of experiment AB3 . . . 72
7.8 kOH comparison overview . . . 73
7.9 kOH comparison overview1 . . . 74
7.10 kOH comparison overview2 . . . 75
7.11 kOH comparison overview3 . . . 76
7.12 kOH comparison overview4 . . . 77
7.13 $k_{OH}^{cal}/k_{OH}^{meas}$ vs O/C . . . 78

7.14 k^* for measured unidentified compounds 79
7.15 reported k for VOC species 80

A.1 Sensitivity comparison 88
A.2 GC vs PTR 88

B.1 Single VOC k_{OH} 93
B.2 BVOC mixture k_{OH} 95
B.3 Plant emitted BVOC k_{OH} 101
B.4 Single AVOC k_{OH} 102
B.5 Urban mixture k_{OH} 103
B.6 AVOC + BVOC (*Fagus sylvatica*) k_{OH} 107

C.1 Product yield from β-pinene ozonolysis 113
C.2 Product yield from limonene ozonolysis 115
C.3 Product yield from isoprene photo-oxidation (high NO) 116
C.4 Product yield from isoprene photo-oxidation (middle NO) 117
C.5 Product yield from isoprene photo-oxidation (low NO) 117
C.6 Product yield from ozonolysis of BM1 120
C.7 Product yield from ozonolysis of BM2 122
C.8 Product yield from ozonolysis of *Quercus ilex* tree emission 123
C.9 Product yield from ozonolysis of *Pinus sylvestris* tree emission 125
C.10 Product yield from ozonolysis of *Fagus sylvatica* tree emission 125
C.11 Product yield from ozonolysis of mix tree emission 126
C.12 Product yield from photo-oxidation of *Quercus robur* emission 127

List of Tables

1.1 Global BVOCs emission 3
1.2 Lifetime of BVOCs 6

2.1 Proton affinity table 17

3.1 List of instruments in SAPHIR 30
3.2 Summary of BVOCs oxidation experiments 33
3.3 Summary of AVOCs oxidation experiments 35

4.1 Rate constant table 41
4.2 Rate constant error 42

5.1 Monoterpene and sesquiterpene speciation from different tree species 46

6.1 Product yields from β-pinene ozonolysis 53
6.2 Product yields from limonene ozonolysis 56
6.3 Product yields from isoprene photo-oxidation 58
6.4 Product yields from ozonolysis of BVOC mixture 61
6.5 Product yields from oxidation of plant emissions 62

A.1 Sensitivity table for the diffusion source calibrations 85
A.2 Sensitivity table for gas standard calibrations 87

B.1 A summary of experiments of BVOCs oxidation. 108
B.2 A summary of experiments of AVOCs oxidation. 109

Chapter 1

Introduction

1.1 Volatile Organic Compounds (VOCs)

Tens of thousands of organic compounds have been detected in the air we breath, lots of them have been found to be relevant to atmospheric chemistry. The concentrations of Volatile organic compound (VOCs) detected in the atmosphere are very low and in the range of parts per trillion by volume (pptv) to parts per million by volume (ppmv). Despite the insignificant fraction of VOCs in the atmosphere (< 1%), they are numerous and ubiquitous in the global atmosphere, most scents or odors are of VOCs. Goldstein et al., 2007 have conjectured that 10^4-10^5 different atmospheric VOCs have been measured, and it might be much smaller than the number of compounds which is actually present. VOCs play a vital role in the global carbon budget and in the regional formation of ozone in the troposphere; they can also serve as a source of secondary organic aerosol (SOA). There is no general quantitative definition of what VOCs are. Often VOCs are also named NMVOCs (non-methane volatile organic compounds). This notation excludes methane because it differs from the other VOCs by its high abundance and slow reaction with OH. CO and CO_2 are not regarded as VOC for the same reason. The term "VOC" was defined by the Environment Protection Agency (EPA) in the United States as any compound that participate in atmospheric photochemical reaction (Koppmann, 2008). More quantified definitions have been made, the term "VOCs" being referred later is regarded as organic compounds having 15 or less carbon atoms, a vapor pressure higher than 10 Pa at 25°C, and a boiling point of up to 260°C at atmospheric pressure. This definition excluded the semi-volatile organic compounds (SVOCs) which undergo different transport chemistry and partition to the aerosol phase. Recently, the research on oxygenated volatile organic compounds (OVOCs) has come into the focus of research, OVOCs are generally more reactive in the atmosphere than the alkanes from which they are derived (Mellouki et al., 2015). In this study, the term VOCs include all trace amount hydrocarbons (HCs) and OVOCs.

1.1.1 Sources of atmospheric VOCs

The sources of atmospheric VOCs are essentially associated with life and are found in remote oceans, tropical forests as well as urban environments. Biogenic VOCs (BVOCs) account for more than 90% of the global VOC emissions (Guenther et al., 1995; Koppmann, 2008). The BVOCs are emitted into the atmosphere mainly from oceans and land vegetation. The ocean (5 Tg yr^{-1}) is considered a source of VOC since it is supersaturated with VOC with respect to the atmosphere. Vegetation is found to be the dominant source of the atmospheric BVOCs. Total BVOC emissions have been estimated at 1007 Tg for the year 2000 (Guenther et al., 2012) (Table 1.1), although quantification and attribution of sources can vary considerably depending on the approach of estimation.
The terpenoids are the most important class of emitted BVOCs, whose carbon skeletons are composed of characteristic C_5 units including hemiterpenes (C_5, e.g., isoprene), monoterpenes (C_{10}, e.g., pinenes, myrcene, limonene), and sesquiterpenes (C_{15}, e.g., caryophyllene,

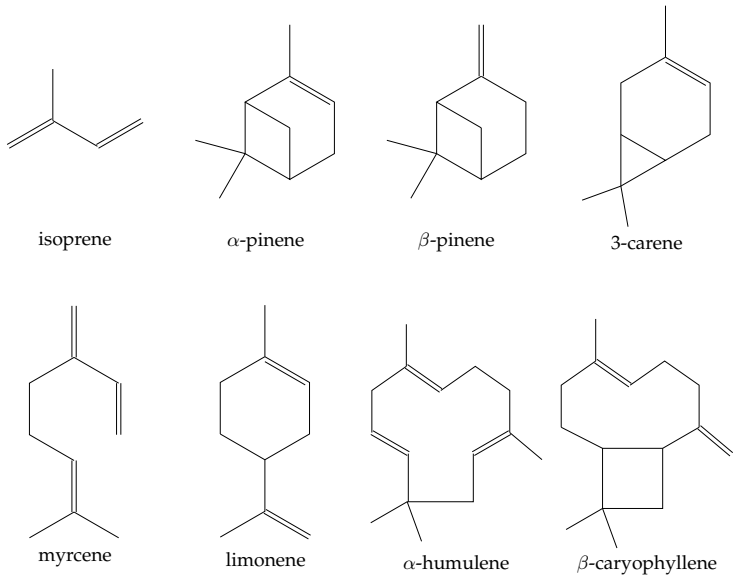

FIGURE 1.1: Structure of some terpenoids.

humulene), up to polyterpenes with more than C_{45} units. Figure 1.1 shows the chemical structure of a number of different terpenoids. Isoprene is the most emitted (∼53%, Table 1.1) in the global BVOC emissions. It is emitted from a large variety of plants when photosynthetic activity is present, isoprene is never stored in plants after its production, but is rapidly lost by volatilization, thus its emission ceases within minutes under dark conditions. Isoprene-emitting plants are more often found in woody plant species than in herbs and crops (Kesselmeier et al., 1999). Over 1000 monoterpenes found in various plants emissions account for ∼15% of the total BVOC emission (Guenther, 2002). Global monoterpene emissions are dominated by α-pinene, β-pinene, Δ^3-carene, limonene, camphene, myrcene, sabinene, and β-phellandrene, yet others can be regionally important (Geron et al., 2000). Biogenic emissions of isoprene and monoterpenes are essentially influenced by temperature and light, on the other hand, relative air humidity is not an important factor for their emissions. Although BVOC emissions are influenced by many factors, different plant species are found to emit their characteristics BVOCs. Two oak species *Quercus robur* and *Quercus ilex* are respectively characterized as an isoprene and a monoterpenes emitter (Rapparini et al., 2004; Sabillón et al., 2001; Schnitzler et al., 2015). The species-dependent emission adds additional challenge for understanding the interaction between plants and the atmosphere. Sesquiterpenes appear to be of minor importance in the global BVOC budget, and are emitted in higher rates by stressed trees. About 3% of the global BVOC emission is contributed by sesquiterpenes, and only a few (e.g., β-caryophyllene, farnescenes) out of roughly 3000 sesquiterpenes are responsible for almost all sesquiterpene emissions (Geron et al., 2000; Nölscher et al., 2012). None of the approximately 2000 diterpenes is found to have a significant emission.

In addition to terpenoids, there are many other oxygenated VOCs that are emitted by plants into the atmosphere, including alcohols, aldehydes, ketones, organic acids, etc. Methanol, the simplest alcohol, is the largest oxygenated VOC emission, which contributes about 10% of the total global BVOC emission (Table 1.1). Contrary to highly volatile compounds such as isoprene and monoterpenes, which cannot be controlled by stomata, the more soluble

TABLE 1.1: Global annual total BVOCs emissions for the year 2000 (adapted from Guenther et al., 2012.

Class	**Compounds**	**Emission (Tg yr^{-1})**
isoprene	isoprene	535
monoterpene	α-pinene	66.1
	$trans$-β-ocimene	19.4
	β-pinene	18.9
	limonene	11.4
	sabinene	9.0
	myrcene	8.7
	3-carene	7.1
	camphene	4.0
	β-phellandrene	1.5
	terpinolene	1.3
	additional 31 monoterpenes	14.9
sesquiterpene	β-caryophellene	7.4
	α-farnescene	7.1
	β-farnescene	4.0
	α-humulene	2.1
	additional 28 sesquiterpenes	8.4
alcohol	methanol	99.6
	ethanol	20.7
ketone	acetone	43.7
aldehyde	formaldehyde	5.0
	acetaldehyde	20.7
organic acid	formic acid	3.7
	acetic acid	3.7
other VOC	propene	15.8
	ethene	26.9
	butene	8.0
total	sum of 146 VOC	1007

compound methanol is controlled by stomatal conductance and is in particular highly emitted in young growing leaves (Niinemets et al., 2003). Methanol is also used as an additive to gasoline, emissions from anthropogenic sources are of minor importance for the global methanol budget (Mellouki et al., 2015). Acetone, the most abundant ketone and the ubiquitous component of the atmosphere, accounts for about 4% of the total global BVOC emission. Acetone is notably emitted from evergreen tree species, the diurnal pattern and the response to temperature of acetone emission is similar to that of monoterpenes. However, acetone released from anthropogenic activities, directly or indirectly, is seen to be the largest source on the global emission (Janson et al., 2001). Formaldehyde and acetaldehyde are the most abundant aldehydes, together comprise less than 3% of the total BVOC emission. The main contribution to the atmospheric aldehydes budget is the secondary production from oxidations of biogenic/anthropogenic VOCs such as isoprene, monoterpenes, and methanol. Even though higher concentrations are found in large cities, considerable direct emission of both

aldehydes from trees (e.g., *Quercus ilex* and *Pinus pinea*) has been reported (J. Kesselmeier et al., 1997). Acetaldehyde released from trees is also known as stress-induced emission. Formic and acetic acids from anthropogenic sources are not substantial for the global organic acids budget, the oxidation of ethene and propene, as well as automobile exhaust, industrial combustion, and biomass burning could lead to their production. However, the emission of formic and acetic acids from trees is prominent in the tropospheric organic acids budget (Keene et al., 1986). Both acids are significantly emitted from several plant species and are indirectly produced at a minute quantity from photo-oxidations of other VOCs. Despite the small amount of plant emitted formic and acetic acids in comparison to other BVOCs, they are the main influence of the acidification in boreal forests (Kesselmeier et al., 1999).
The importance of BVOCs in atmospheric chemistry is becoming more and more clear due to their predominance in the global VOCs emission and their high reactivity in reaction with atmospheric oxidants. BVOCs affect both gas-phase and heterogeneous chemistry in the atmosphere. Therefore, the sources, sinks and atmospheric residence time of BVOCs are the subject of many current researches.
The anthropogenic contribution to the atmospheric VOCs is dominated by solvent using, gasoline evaporation and biomass combustion. On a global scale, the emissions of AVOC including alkanes, alkenes, and aromatic compounds, are estimated to be approximately 100 Tg yr^{-1} (Kansal, 2009; Von Schneidemesser et al., 2015). However, on regional scales AVOC can exceed BVOC emission, especially in urban environment. 1-pentene, toluene, and o-xylene are widely used in petrol productions (direct emissions) and released from combustion processes as well. Certain AVOCs such as benzene, are potentially carcinogenic for human health. Benzene emitted mainly from cigarette smoke and exhaust from cars, is 10 times higher in smokers than in nonsmokers (Dales et al., 2008). Figure 1.2 shows the chemical structure of several AVOCs.

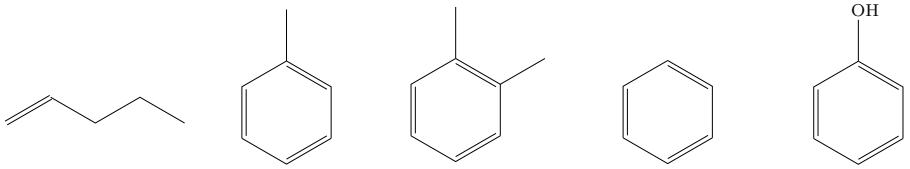

FIGURE 1.2: Structure of some AVOCs and oxygenated AVOCs.

1.1.2 Sinks of atmospheric VOCs

VOCs from both biogenic and anthropogenic sources undergo numerous physical and chemical processes leading to their transformation in the atmosphere or removal from the atmosphere. The possible atmospheric fates of the emitted VOC are chemical oxidation, photolysis, and deposition. A sketch of atmospheric VOC removal processes is shown in Figure 1.3. Overall, the predominant VOC removal process is the reaction with hydroxyl radical (OH), nitrate radical (NO_3), or ozone (O_3), VOC is then transformed into lower-vapor-pressure or more soluble OVOCs products that subsequently transform into SOA, or ultimately into CO_2. It is estimated that most (>75%) of the VOCs in the atmosphere are degraded into CO_2. About 80% of emitted isoprene, was found to be completely oxidized to CO_2 (Guenther, 2002). Some VOCs can absorb the sunlight at wavelengths > 290 nm and their photolysis is an important radical source, photolysis of VOC lead to smaller fragments and promote photochemical ozone formation (Chapter 1.2.2). For most VOCs, deposition is probably of minor importance, deposition can occur on surfaces such as vegetation or aerosols (dry deposition)

or in rain (wet deposition). The deposited amount of VOCs without any chemical reactions is more than 10% for methanol and about 5% for more reactive compounds such as isoprene (Cleveland et al., 1997).

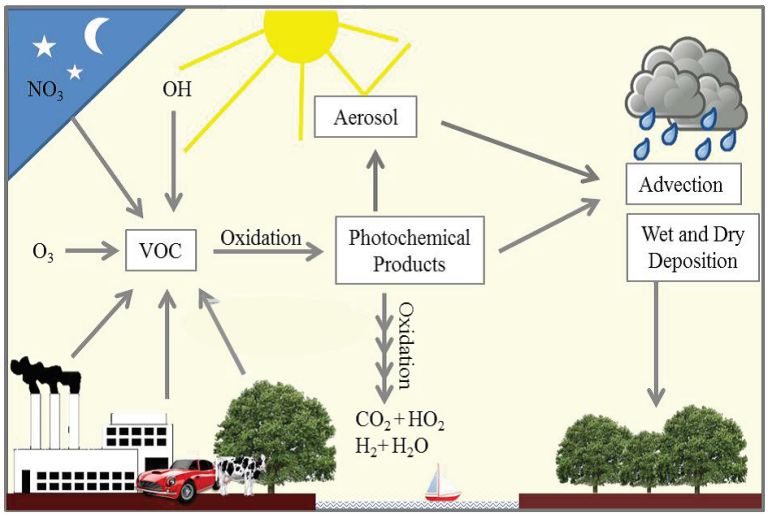

FIGURE 1.3: Sketch of various processes affecting the atmospheric fate of VOCs, ranging from oxidation, particle formation, advection and deposition. (Adapted from Jäger, 2014).

The atmospheric lifetime of VOCs varies from minutes to years and is determined by the respective rate coefficients of the reactions with OH, O_3, and NO_3 as well as the respective deposition velocities. The lifetimes listed in Table 1.2 are calculated by using the following: [OH] = 2.0 $\times$ 10^6 molecule cm^3, [O_3] = 7 $\times$ 10^{11} molecule cm^3 and [NO_3] = 2.5 $\times$ 10^8 molecule cm^3. The lifetimes listed here provide simply a perspective on the rank of reactivity of atmospheric VOCs. Bare in mind that many other factors can impact such reactions, for example, meteorological condition, season, latitude, even the chemical composition of the air mass containing other VOCs. Isoprene lifetime in reaction with OH is estimated to be only 1.4 hours, whereas for the more stable methanol the lifetime with OH is about 12 days. α-pinene has a longer lifetime with OH comparing to β-pinene, yet it is more reactive than β-pinene towards O_3 and NO_3. Some sesquiterpenes are very reactive in the atmosphere, both β-caryophyllene and α-humulene have only 2 mins lifetime with O_3, consequently sesquiterpene measurement in the atmosphere can be very difficult due to their low volatility and high reactivity. In contrast, because of the lower atmospheric reactivity of most AVOCs compared to many BVOCs, the atmospheric lifetime of AVOCs is more variable and usually longer than that of BVOCs. Calculated lifetimes of AVOCs are typically days or years compared to a few hours or less for most BVOCs (see Table 1.2). Therefore, BVOCs are reckoned to play a dominant role in the chemistry of the lower troposphere and atmospheric boundary layer.
In general, the chemical degradation/transformation of VOCs in the troposphere can be sketched by Figure 1.4 (Atkinson et al., 2003a). The OH, O_3 and NO_3 initiated reactions of a VOC (RH) in the presence of nitric oxide (NO) lead to the formation of intermediate radicals such as alkyl ($R^\bullet$), alkyl peroxy ($RO_2^\bullet$), and alkoxy ($RO^\bullet$) radicals. The reactions with OH radicals are the main sink for VOCs during the daytime, whereas the reactions with O_3 and NO_3 are important VOCs sink at nighttime.

TABLE 1.2: List of calculated atmospheric lifetimes of some atmospheric VOCs (adapted from Atkinson, 2000; Atkinson et al., 2003b)

VOCs	Lifetime for reaction with		
	OH[a]	**O_3**[b]	**NO_3**[c]
isoprene	1.4 h	1.3 day	1.6 h
α-pinene	2.6 h	4.6 h	11 min
β-pinene	1.8 h	1.1 day	27 min
3-carene	1.6 h	11 h	7 min
limonene	49 min	2.0 h	5 min
myrcene	39 min	50 min	6 min
β-caryophyllene	42 min	2 min	3 min
α-humulene	28 min	2 min	2 min
acetone[d]	61 day	> 4.5 year	> 8 year
methanol	12 day	> 4.5 year	2.0 year
formaldehyde[d]	1.2 day	> 4.5 year	166 day
acetaldehyde	8.8 h	> 4.5 year	34 day
toluene	2.1 day	> 4.5 year	3.6 year
benzene	9.5 day	> 4.5 year	> 8 year
phenol	5.3 h		18 min

[a] Assumed OH radical concentration: 2.0×10^6 molecule cm^3, 12-h daytime average.

[b] Assumed O_3 concentration: 7×10^{11} molecule cm^3, 24-h average

[c] Assumed NO_3 radical concentration: 2.5×10^8 molecule cm^3, 12-h nighttime average.

[d] Will also undergo photolysis. Calculated photolysis lifetime is ∼60 day for acetone and ∼4 h for formaldehyde.

The reaction starts by addition of the OH radicals, NO_3 radicals and O_3 to a C=C bond, or abstraction of a H-atom from a C−H bond by OH and NO_3 radicals. O_3 reacts only by addition to C=C bonds. VOCs having C=C double bonds usually react by addition of the oxidants to the double bonds, while the H-atom abstraction occurs from various C-H bonds in alkanes, ethers, alcohols, carbonyls and esters. The latter is also important for aldehydes containing C=C bonds (e.g., methacrolein), but is of minor importance for isoprene, monoterpenes and sesquiterpenes. Both pathways lead to the formation of alkyl radicals,

$$\mathrm{RH} + \mathrm{OH} \longrightarrow \mathrm{R}^\bullet + \mathrm{H_2O} \tag{1.1}$$

forming an $R^\bullet$ and water. The alkyl radical $R^\bullet$ will typically react rapidly with O_2,

$$\mathrm{R}^\bullet + \mathrm{O_2} \longrightarrow \mathrm{RO_2}^\bullet \tag{1.2}$$

leading to the formation of a peroxy radical $RO_2^\bullet$ which reacts with NO when present,

$$\mathrm{RO_2}^\bullet + \mathrm{NO} \longrightarrow \mathrm{RO}^\bullet + \mathrm{NO_2} \tag{1.3}$$

and is readily converted to a alkoxy radical $RO^\bullet$ via the oxidation of NO to NO_2, the $RO^\bullet$ reacts with O_2 and produces stable organic nitrates products and hydroperoxy radicals HO_2.

$$\mathrm{RO}^\bullet + \mathrm{O_2} \longrightarrow \mathrm{carbonyls} + \mathrm{HO_2} \tag{1.4}$$

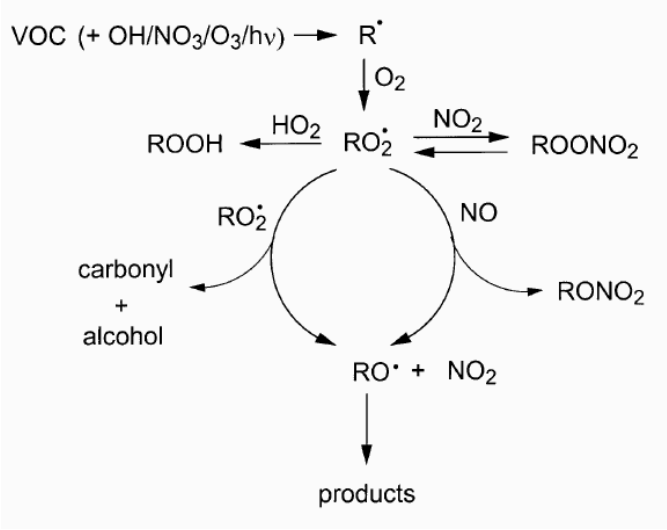

FIGURE 1.4: Schematic of the OH initiated degradation of VOCs in the presence of NO Adapted from (Atkinson et al., 2003a).

At low NO conditions, the $RO_2^\bullet$ reacts with HO_2 to form a peroxide (ROOH), or with another $RO_2^\bullet$ to form $RO^\bullet$, or products such as carbonyls and alcohol.

$$RO_2^\bullet + HO_2 \longrightarrow \text{peroxide} + O_2 \tag{1.5}$$

$$RO_2^\bullet + RO_2^\bullet \longrightarrow \text{carbonyls, alcohol} \tag{1.6}$$

Reactions with HO_2 dominate the fate of $RO_2^\bullet$ under pristine conditions. $RO_2^\bullet$ radicals formed from OH-initiated isoprene oxidation, generally undergo two distinct pathways (Figure 1.5): a) reaction with NO to form methyl vinyl ketone (MVK) / methacrolein (MACR), formaldehyde, and HO_2; or b) reaction with HO_2 to form hydroperoxides (ISOPOOHs). The low-NO products ISOPOOHs can subsequently transform to isoprene epoxides (IEPOXs) and regenerate OH radicals, IEPOXs are potentially important precursors for atmospheric aerosols.

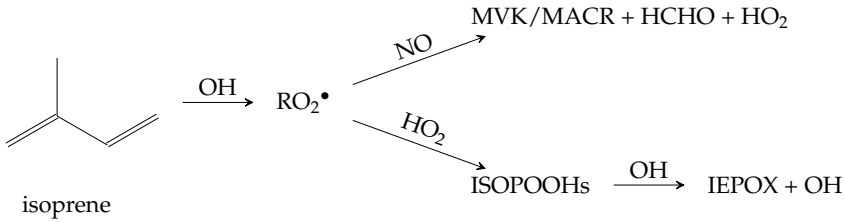

FIGURE 1.5: Schematic of the OH initiated degradation of isoprene under high- and low-NO level. (Adapted from Fuchs et al., 2013; Rivera-Rios et al., 2014; St. Clair et al., 2015).

1.2 Atmospheric oxidants

As outlined in the preceding sections, VOCs are removed from the atmosphere mainly by reactions with atmospheric oxidants such as OH, O_3 and NO_3. Reaction with chlorine (Cl) atoms may also be important in some regions. The processes leading to the formation of OH radicals, O_3, and NO_3 radicals in the troposphere are briefly discussed below.

1.2.1 Tropospheric OH radicals formation

The predominent source of tropospheric OH radicals is the photolysis of O_3 in the presence of water vapor (Atkinson et al., 2003b):

$$\mathrm{O_3} + h\nu \xrightarrow{\lambda \leq 350nm} \mathrm{O_2} + \mathrm{O}\,(^1\mathrm{D}) \tag{1.7}$$

$$\mathrm{O}\,(^1\mathrm{D}) + \mathrm{H_2O} \longrightarrow 2\,\mathrm{OH} \tag{1.8}$$

This requires sufficient sunlight irradiation and water, therefore higher OH concentrations are encountered in areas exposed to strong actinic fluxes and having higher humidity (i.e., the tropics).
Additionally, the intermediate HO_2 radicals formed during VOCs degradation reacts with NO, converting NO to NO_2 and recycling OH (Atkinson, 2000; Winiberg et al., 2016):

$$\mathrm{HO_2} + \mathrm{NO} \longrightarrow \mathrm{OH} + \mathrm{NO_2} \tag{1.9}$$

However, unexpectedly large OH concentrations were recently revealed from measurements in some low-NO forest regions, OH regeneration without the involvement of NO was proposed to explain the observed high levels of OH radicals in isoprene-rich environments (Fuchs et al., 2014, 2013).
There are some other sources of OH radicals in the troposphere, such as the photolysis of nitrous acid (Rohrer et al., 2005):

$$\mathrm{HONO} + h\nu \xrightarrow{\lambda < 400nm} \mathrm{OH} + \mathrm{NO} \tag{1.10}$$

and the photolysis of formaldehyde and other carbonyls in the presence of NO, and ozonolysis of alkenes.

1.2.2 Tropospheric O_3 formation

Stratospheric O_3 absorbs most of the ultraviolet (UV) radiation and protects life on Earth. To the contrary, O_3 in the troposphere is a secondary air pollutant acting as a greenhouse gas and a potent respiratory hazard to animals and plants. Because of the high O_3 mixing ratios of several ppm (parts-per-million) in the stratosphere, a net O_3 transport by eddy diffusion from the stratosphere into troposphere accounts for 10% of the annual tropospheric O_3 production (Mellouki et al., 2015). A large part of tropospheric O_3 is formed photochemically from the photolysis of NO_2 (Atkinson, 2000; Pitts et al., 2000):

$$\mathrm{NO_2} + h\nu \xrightarrow{\lambda < 430\ nm} \mathrm{NO} + \mathrm{O}\,(^3\mathrm{P}) \tag{1.11}$$

$$\mathrm{O}(^3\mathrm{P}) + \mathrm{O_2} + \mathrm{M} \longrightarrow \mathrm{O_3} + \mathrm{M} \quad (\mathrm{M} = \mathrm{N_2}, \mathrm{O_2}) \tag{1.12}$$

the O_3 quickly oxidizes NO back to NO_2,

$$O_3 + NO \longrightarrow NO_2 + O_2 \tag{1.13}$$

Reactions 1.11, 1.12 and 1.13 result in a balance among O_3, NO_2 and NO, hence a steady concentration of O_3 is obtained in the troposphere, 10-40 ppb (parts-per-billion) in remote areas but often exceeding 100 ppb in polluted urban regions.
However, in the presence of nitrogen oxides (NO, NO_2, collectively called NO_x), the degradation reactions of VOCs lead to the production of intermediate peroxy radicals, which replace O_3 in the reaction converting NO to NO_2 (Reaction 1.3). Besides that, photolysis of VOCs produce smaller fragments and HO_2, for example, the photolysis of formaldehyde (Von Schneidemesser et al., 2015):

$$HCHO + h\nu \xrightarrow{O_2} + HO_2 + CO \tag{1.14}$$

HO_2 also competes with O_3 in the oxidizing reaction of NO to NO_2 as demonstrated in Reaction 1.9. The produced NO_2 then photolyzes to form O_3 as shown in Reaction 1.11, 1.12. This results in a net production of tropospheric O_3, therefore VOCs play an important role in the tropospheric ozone formation. Under certain environmental conditions, reaction of peroxy radicals with NO (Reaction 1.3) produces organic nitrates, in particular peroxyacetyl nitrate (PAN). The formation of PAN involves consumption of $RO_2^{\bullet}$ and NO, thereby lowers the potential of O_3 formation in the source region (Chapleski et al., 2016). PAN represents a reservoir and a transportation for NO_x, because it is chemically more stable than NO_x and can be transported to clean, remote environments, in where PAN eventually decomposes into NO_x and promote the O_3 formation in the new region.

1.2.3 Tropospheric NO_3 radicals formation

Another important atmospheric oxidant is NO_3. In the troposphere, the main source of NO_3 is the chain reactions in the presence of NO:

$$NO + O_3 \longrightarrow NO_2 + O_2 \tag{1.15}$$

$$NO_2 + O_3 \longrightarrow NO_3 + O_2 \tag{1.16}$$

NO_3 reacts with certain VOCs through addition or hydrogen abstraction reactions, yielding the temporary NO_x reservoir PAN, hence alters the O_3 formation in such way (Chapleski et al., 2016).
NO_3-initiated oxidation can be important at night because the rapid photolysis of NO_3 radical under sunlight results in a NO_3 lifetime of $\sim$5 s and a negligible concentration at daytime (Atkinson, 2000).

$$NO_3 + h\nu \longrightarrow NO + O_2 \quad (\sim 10\%) \tag{1.17}$$

$$NO_3 + h\nu \longrightarrow NO_2 + O(^3P) \quad (\sim 90\%) \tag{1.18}$$

1.3 Total OH reactivity

1.3.1 Introduction to total OH reactivity

The hydroxyl radical OH is the primary oxidant in the troposphere, initiating the degradation of nearly all VOCs and thereby, controls the oxidizing efficiency of the global atmosphere. OH exhibits a high reactivity towards many VOCs, and some inorganic compounds like carbon monoxide (CO), NO_x. Atmospheric OH lifetime is very short (< 1 s), the OH concentration in the atmosphere is in a steady-state between production and destruction of OH radicals (Lou et al., 2010). A globally averaged OH concentration of 1.0×10^6 molecule cm^{-3} has been reported by Prinn et al., 2001. The production of OH is elaborated above (see Chapter 1.2.1). The destruction of OH is the first-order loss rate of reaction with compounds present in ambient air, also called as the total OH reactivity, k_{OH}, which represents the reciprocal atmospheric OH lifetime, τ_{OH}^{-1}. Thus the overall OH sink term is estimated by calculating OH loss frequencies (concentration and rate constant) for all individually measured species and summing them.

$$k_{OH} = \sum_i k_{OH+X_i} \times [X_i] = \tau_{OH}^{-1} \tag{1.19}$$

Here, $[X_i]$ represents the measured concentration of a reactive component (CO, NO_x, VOCs, etc.) in ambient air, k_{OH+X_i} denotes the corresponding bimolecular reaction rate constant, and $k_{OH+X_i} \times [X_i]$ is the OH reactivity of X_i.
The OH reactivity serves as an estimate of the total loading of reactive compounds in the troposphere, a high k_{OH} implies the high potential of ozone and SOA formation and therefore interesting. To date, the total OH reactivity can be measured directly by two main approaches. In the first method, artificially generated OH radicals are added into a flow tube with sampled ambient air, OH is added into the flow tube either by laser flash photolysis of ozone (Lou et al., 2010; Sadanaga et al., 2004) or by a moveable OH injector (Ingham et al., 2009; Kovacs et al., 2003), and the OH loss rate is monitored via a FAGE apparatus (Fluorescence Assay by Gas Expansion, Dusanter et al., 2009) or a LIF (Laser-Induced Fluorescence, Lou et al., 2010). Thus the OH reactivity is retrieved from the measured decay of OH radicals due to the reaction with trace gases in the sampling flow. A detailed description of the LIF method can be found in the Chapter 2.3. In the second method, the OH reactivity is measured directly with the Comparative Reactivity Method (CRM). The principle of this technique is the competitive reaction of a reactive molecule, which is not present in the atmosphere and competes for the artificially produced OH radicals when ambient air is sampled (Sinha et al., 2008). The selected reactive molecule, whose reactivity with OH is well known, so far always pyrrole, is passed through a glass reactor and its concentration is monitored with a detector such as Proton Transfer Reaction Mass Spectrometer (PTR-MS) or a Gas Chromatography Photo Ionization Detector (GC-PID).
In less than 20 years development since the first measurements of OH reactivity, numerous studies have reported OH reactivity in various environments: from branch enclosures/plant cuvettes (Kim et al., 2011; Nölscher et al., 2013) to flow tubes and environmental chambers (Nakashima et al., 2012; Nölscher et al., 2014); from ground-based ambient measurements at field sites (Edwards et al., 2013; Lee et al., 2009; Ren et al., 2003) to airborne measurements with airplanes or Zeppelins (Jäger, 2014; Mao et al., 2009). An accurate OH sink term can constrain models and thus interpret the potential reasons for discrepancies between models and measurements (Sinha et al., 2008). However, the total OH reactivity is not well comprehended currently, as the OH reaction involving a multitude of species, all of which compete for the available OH. The comprehension of the relatively few important inorganic compounds (NO_x, O_3, CO) has become better in the last years thanks to accessible instruments

and accurate rate coefficients. Nevertheless, measurements of VOCs are still challenging due to the large variety of VOCs (10^4-10^5 different species). In most field campaigns only a limited number of VOCs (< 100 species) are analyzed due to the knowledge of existing VOCs and the limit of instrument, this results in great uncertainties in the quantification (Goldstein et al., 2007).

1.3.2 Missing k_{OH} in the world

Previous studies have reported the measured OH reactivity ranging from 4 s^{-1} in an airplane measured above the Pacific Ocean (Mao et al., 2009) and 200 s^{-1} in Mexico City (Shirley et al., 2006). Figure 1.6 shows the different sites in the world where the OH reactivity was reported. Green, grey and dark blue frames indicate the type of environment where the measures were performed: forests, urban and coastal areas, respectively, light blue frames are airborne measurements. Red font highlights the site where a k_{OH} > 50 s^{-1} is reported, which is mostly found in megacities and tropical forests. Maximum OH reactivity observed in polluted megacities are remarkable: 200 s^{-1} in Mexico City (Shirley et al., 2006), 130 s^{-1} in Paris (Dolgorouky et al., 2012), 100 s^{-1} in Tokyo (Yoshino et al., 2006), New York City (Ren et al., 2006), and Beijing (Lu et al., 2013). k_{OH} of more than 70 s^{-1} were observed in the tropical rainforest of Suriname (Sinha et al., 2008) and Borneo (Edwards et al., 2013), where natural emissions of isoprene and other BVOCs dominated the OH reactivity. The coastal site El Arenosillo was found to have a k_{OH} < 3.5 s^{-1} in clean marine air masses but a k_{OH} up to 85 s^{-1} when the air masses were transported from polluted big cities as Madrid and Sevilla (Sinha et al., 2012). High k_{OH} of up to 120 s^{-1} was also observed in the subtropical rural site in Pearl River Delta with the highest k_{OH} correlated with anthropogenically emission (Lou et al., 2010). A measured maximum k_{OH} of 76 s^{-1} from heat-stressed tree emission was reported in a boreal forest in Hyytiälä (Nölscher et al., 2012).
Considerably lower calculated OH reactivity derived from equation 1.19 have been reported, the gap between measured and calculated OH reactivity is usually regarded as "missing OH reactivity". An unexplained fraction of up to 89% was reported in the Hyytiälä boreal forest, this missing OH reactivity was speculated to be from stressed tree emissions (e.g., sesquiterpenes, aldehydes) which were not successfully detected by their instruments (Nölscher et al., 2012). About 30% of missing OH reactivity was found in the rural site in Michigan, which is due to unmeasured temperature dependent monoterpenes emission (Di Carlo et al., 2004). At the Suriname tropical rainforest, more than 60% of measured k_{OH} could not be clarified by calculating the k_{OH} with all detected reactants, this was hypothesized to be from unmeasured biogenic compounds (Sinha et al., 2008). More than 30% missing OH reactivity was found in New York City in the winter of 2004, most likely from primary emitted OVOCs like aldehyde and ketone (Ren et al., 2006). Only 1.6 $^{-1}$ OH reactivity was calculated from all the OH reactants measurements during the airborne pacific ocean measurements, lead to 60% of missing OH reactivity, possibly related to some unmeasured highly reactive VOCs (Mao et al., 2009). Results from the campaign in Paris demonstrated a missing OH reactivity up to 75%, which was presumed to be caused by highly oxidized compounds from photochemically processed anthropogenic air masses (Dolgorouky et al., 2012). As for the other tropical rainforest in Borneo, approximately 40% of missing OH reactivity was observed, correspond to unmeasured photochemically produced isoprene oxidation products (Edwards et al., 2013). About 50% of missing OH reactivity was found in the rural site in Pearl River Delta, resulting from photochemically formed unmeasured OVOCs (Lou et al., 2010).
Less missing OH reactivities were found in urban sites. The Zeppelin flew over Netherlands and Italy in 2012 reported no significant missing OH reactivity (Jäger, 2014). Model calculated k_{OH} had a good agreement with the measured k_{OH} on most days during the campaign

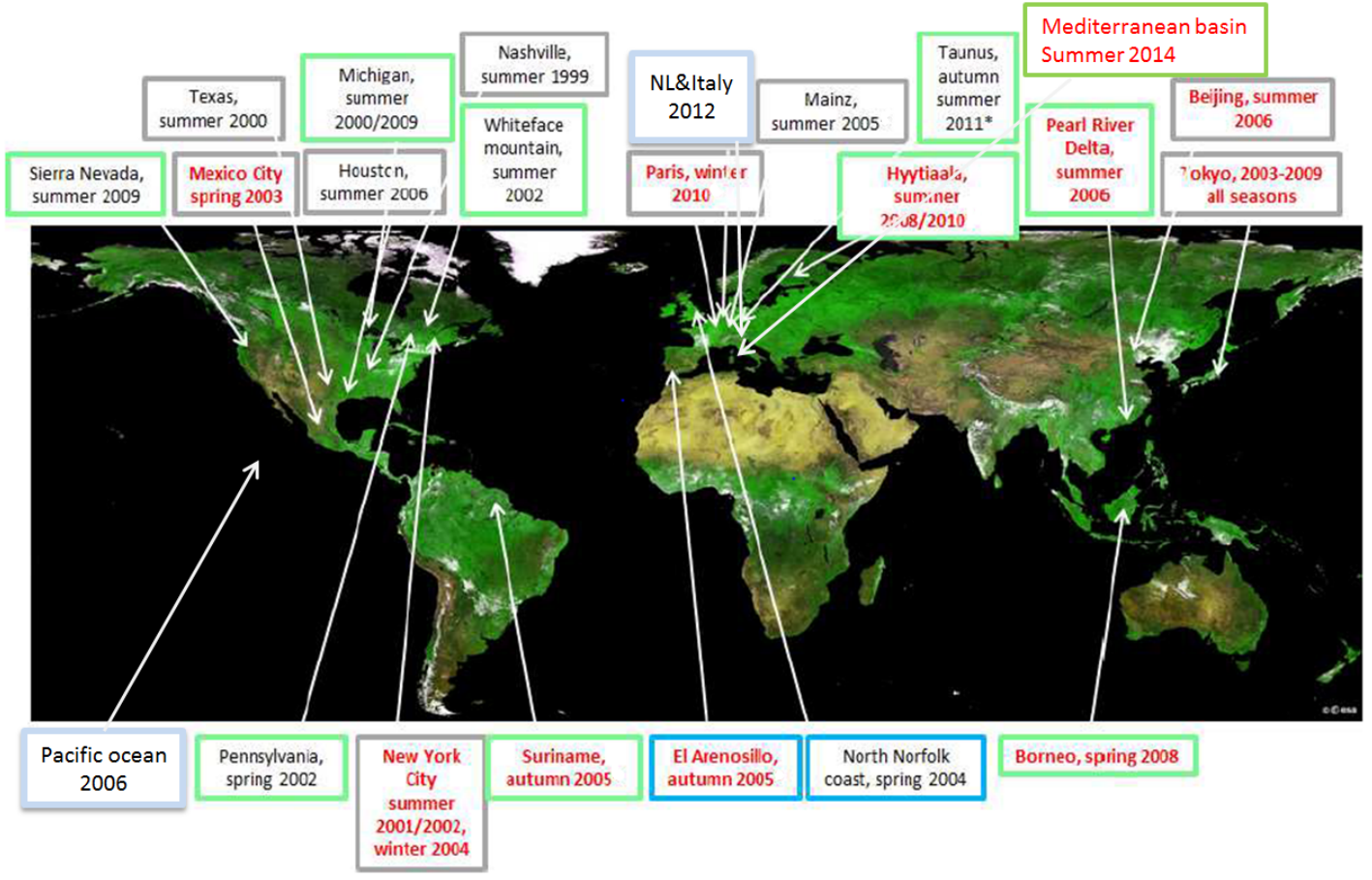

FIGURE 1.6: OH reactivity measurements world map adapted from Zannoni, 2015. Green frames refer to forest sites, grey frames are urban sites, dark blue are coastal sites and light blue are airborne measurements. Red font highlights the site where a OH reactivity > 50 s^{-1} is reported.

in Beijing (Lu et al., 2013). In Nashville, the calculated OH reactivity agreed to within a 10% of measured OH reactivity when including measured short-lived VOCs (Kovacs et al., 2003). No missing OH reactivity was found in New York City during another campaign in the summer of 2001, where the maximum k_{OH} was only 25 s^{-1} (Ren et al., 2003). Moreover, no remarkable missing OH reactivity was observed in Houston during the campaign in summer 2006 (Mao et al., 2010).
The introduced previous field studies of OH reactivity indicate that primary emitted anthropogenic species are better characterized than primary biogenic species. It also seems like that unknown species contributing to the missing OH reactivity, are from both primary and secondary origin. Furthermore, because of unknown existence of some secondary products and the lack of analytical means to measure them, the secondary products formed from oxidations of VOCs are more difficult to characterized. Finally, uncertainties in reaction rates of BVOCs with OH that propagate to calculated OH reactivity uncertainties, could also lead to the observed missing OH reactivity. In many studies, the rate coefficients are only estimated as there is no experimental data exists for many reactions between OH and VOC. Mogensen et al., 2011 have reported that the rate coefficient could differ by a factor of 2 or more for the same reaction evaluated by different groups. They multiplied the rate constants by a factor of 2 for several important compounds (e.g., isoprene, monoterpenes, acetone) observed in the Hyytiälä measurements, and achieved an increase of 40% of the calculated OH reactivity.

1.4 Focus of this thesis

This work analyzes experiments performed in a chamber system (SAPHIR and SAPHIR-PLUS, see Chapter 3.1) to explore the plant emission pattern, the VOC oxidation mechanism, and the OH reactivity under simulated atmospheric conditions.
A number of instruments measuring from VOCs to the total OH reactivity enable the cross validation of VOC data and also the comparison of the OH reactivity parameter. The instrumentation is described in details in Chapter 2. Experiment procedures of selected 36 experiments are displayed in Chapter 3, the benefits of using our chamber system in Forschungszentrum Jülich, Germany, is outlined as well.
Chapter 4 explains how the data from our chamber experiments is evaluated, illustrating the data analysis of VOC measurements and the calculation of k_{OH} with all trace gas measurements. Moreover, other parameters derived from VOC measurements are shown.
Chapter 5 presents the VOC emissions in the plant chamber SAPHIR-PLUS. Results of plant emission patterns under different light and temperature conditions is compared to the literature. To test if the product yields from complex VOC mixture are comprehensible based on known product yields from single compound, product yields of VOC oxidations are compared in the Chapter 6. An increased complexity of the simulated atmosphere system is explored: from single BVOC to BVOC mixtures and eventually to the real plant emissions.
Chapter 7 exhibits the total OH reactivity results, in order to i) test the ability of measuring k_{OH} in controlled experiments; and to ii) examine if the k_{OH} in compound specific single VOC oxidation is in accordance with k_{OH} in oxidation of a more complicated atmosphere system. This chapter discusses the total OH reactivity, and the comparison between the measured OH reactivity and that calculated from the trace gas measurements. The comparison enables the analysis of the integrity of the VOC measurements, with respect to the OH reactivity. Missing OH reactivity is investigated in biogenic and anthropogenic VOC oxidations, again, with increasing complexity of the atmosphere system. The measured OH reactivity and thus the major OH sinks can be determined for the different atmosphere systems. Throughout the selected 36 different oxidation scenarios, the results from this thesis can help to interpret OH reactivity measurements and to predict the potential missing OH

sink terms in field studies, therefore to better constrain the total atmospheric constituents and understand VOCs degradation processes.

Chapter 2

Methods and Instruments

2.1 Proton Transfer Reaction-Time Of Flight-Mass Spectrometry (PTR-TOF-MS)

vapor

The instrument used for measuring VOCs in this study is a commercially available high sensitivity PTR-TOF-MS built by Ionicon Analytik (Jordan et al., 2009; Lindinger et al., 1998). As shown in the schematic drawing of the PTR-TOF-MS instrument (Figure 2.1), the set-up consists of 1) a hollow cathode discharge ion source to produce the H_3O^+ reagent ions, 2) the drift tube reaction chamber, in which the proton-transfer reactions between H_3O^+ and VOCs take place, and 3) the transfer lens system together with the Tofwerk orthogonal acceleration reflectron time-of-flight mass spectrometer. Additionally the two modes of operation of the TOF are outlined, namely the V-and the W-mode.

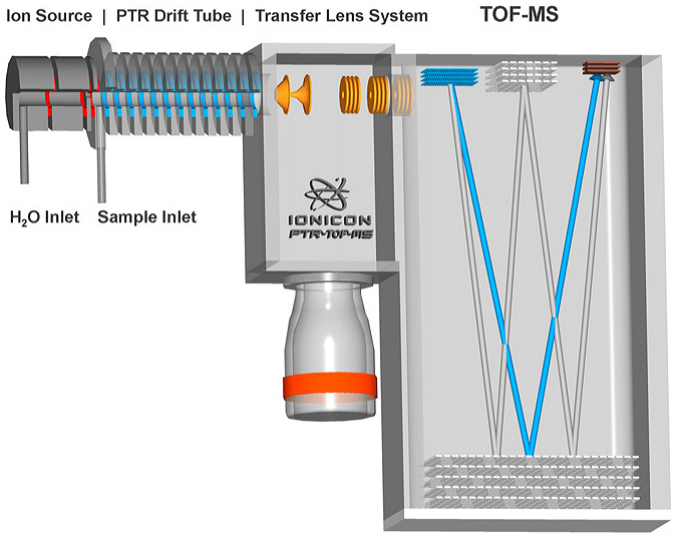

FIGURE 2.1: Schema of the PTR-TOF-MS instrument (Jordan et al., 2009).

The ion source is made up of a hollow cathode discharge which generates high energy (hundreds of electron-volts) electrons, the electrons generate ions in collision with water vapor introduced from a liquid water reservoir:

$$\begin{aligned} e^- + H_2O &\longrightarrow H_2O^+ + 2\,e^- \\ &\longrightarrow {H_2}^+ + \cdots \\ &\longrightarrow H^+ + \cdots \end{aligned}$$

$$\longrightarrow O^+ \quad + \cdots$$

In a small intermediate chamber, ions from the hollow-cathode are further converted into H_3O^+ ions while being continuously transported towards the drift tube. The most relevant reactions are listed below (Hansel et al., 1995).

$$\begin{aligned}
H_2{}^+ \quad &+ H_2O \longrightarrow H_2O^+ \quad + H_2 \\
H^+ \quad &+ H_2O \longrightarrow H_2O^+ \quad + H \\
O^+ \quad &+ H_2O \longrightarrow H_2O^+ \quad + O \\
H_2O^+ &+ H_2O \longrightarrow H_2O \cdot H^+ + OH
\end{aligned}$$

The ion source usually provides H_3O^+ ions with a purity of about 99% or higher, leading to high count rates of primary H_3O^+ ions typically at several 10^6 cps (counts per second). The most significant impurity observed is constituted by $O_2{}^+$ and NO^+ ions, which are introduced from the air streaming back from the drift tube into the ion source. The $O_2{}^+$ and NO^+ ions go through charge-transfer reactions with most VOCs including species like alkanes that are normally not detectable by using H_3O^+ as a chemical ionization agent (De Gouw et al., 2007). Higher impurity could cause false peak identification in mass spectra analysis.

2.1.1 Ion-molecule reactions

The drift tube consists of a number of stainless steel rings, separated by Teflon rings which seal the vacuum and isolate the drift rings electrically. Primary ions produced in the ion source are extracted by a voltage gradient into the drift tube, where the analyte gas sample is also injected via a gas inlet system. The proton transfer reactions take place as the mixture proceeds along the drift tube. Protons transfer from primary H_3O^+ ions to the trace gases R, that have higher proton affinity than water:

$$H_3O^+ + R \rightleftharpoons RH^+ + H_2O$$

For PTR-MS using H_3O^+ as reagent ions, molecules with a proton affinity smaller than water (165.2 kcal/mol) cannot be detected. This helps to exclude reactions with any of the major components present in air (i.e., O_2, N_2, CO_2, H_2O), and also allows the air sample to be analyzed and used directly as buffer gas to maintain the pressure conditions (typical pressures are between 2.2 and 2.4 mbar) in the drift tube. Most VOCs have proton affinities larger than water, Table 2.1 shows the proton affinities of some common components present in clean air and of various organic components. Atmospheric trace gases which undergo proton transfer reactions include unsaturated and aromatic hydrocarbons, and also most of the oxygenated VOCs (aldehydes, ketones, alcohols, acids, etc.) (De Gouw et al., 2007). However, although the proton transfer is favourable in reaction with formaldehyde (HCHO), the proton affinity of formaldehyde is not sufficiently larger than that of water. Therefore, the back reaction of protonated HCHO with water is substantial and reduces the sensitivity of detection:

$$H \cdot HCHO^+ + H_2O \longrightarrow HCHO + H_3O^+$$

Significant underestimations (a factor of 3 to 5) of HCHO concentrations measured by PTR-TOF-MS were reported (Vlasenko et al., 2010). In addition, low accuracy of HCHO measurement caused by the humidity dependence was observed. In this study formaldehyde data were preferably taken from the Hantzsch measurements if available (Kelly et al., 1994).
The collision energy in the drift tube is controlled by the parameter E/N used in ion mobility studies, where E denotes the applied electric field and N the number density of the gas in

TABLE 2.1: Proton Affinities of common components in clean air and of various organic components (adapted from Lindinger et al., 1998).

Substance	**Formula**	**Mass**	**Detected mass**	**Proton Affinity** $(kcal.mol^{-1})$
Hydrogen	H_2	2	-	100.9
Helium	He	4	-	42.5
Neon	Ne	20	-	48.6
Argon	Ar	40	-	88.2
Oxygen	O_2	32	-	100.6
Krypton	Kr	84	-	101.5
Nitrogen	N_2	28	-	118.0
Xenon	Xe	132	-	118.6
Carbon monoxide	CO	28	-	141.7
Carbon dioxide	CO_2	44	-	129.2
Water	**H_2O**	**18**	**-**	**165.2**
Hydrogen sulphide	H_2S	34	35	168.5
Formaldehyde	CH_2O	30	31	170.4
Methanol	CH_4O	32	33	180.3
Propene	C_3H_6	42	43	179.6
Acetaldehyde	C_2H_4O	44	45	183.8
Formic acid	CH_2O_2	46	47	177.3
Ethanol	C_2H_6O	46	47	185.6
Acetonitrile	C_2H_3N	41	42	186.2
Acetone	C_3H_6O	58	59	194.1
Acetic acid	CH_4O_2	60	61	190.2
Isoprene	C_5H_8	68	69	198.9
Butanal	C_4H_8O	72	73	189.5
Benzene	C_6H_6	78	79	179.3
Toluene	C_7H_8	92	93	187.4
Phenol	C_6H_6O	94	95	195.0
Xylene	C_8H_{10}	106	107	190.0

the drift tube. De Gouw et al., 2003 reported that the effect of humidity on the cluster ion distribution becomes very minor at an E/N of 120 Td (1 Td=10^{-17} V cm^2). Consequently, in this study the E/N parameter in the PTR-TOF-MS was kept at about 130 Td with a drift tube voltage of 560 V. The pressure in the drift tube was set at 2.3 mbar to obtain a good sensitivity, as the proton reaction frequency increases with drift tube pressure under constant E/N value (De Gouw et al., 2007). The average reaction time of the ions in the drift tube is usually $\sim 1.0 \times 10^{-4}$ s. Investigations show that exothermic proton transfer reactions are always proceeding at a reaction rate close to the collision rate. Reaction rate constants k_{PTR} for many proton transfer reactions are reported in the literature and are typically in the order of 10^{-9} cm^3 molecule^{-1}sec^{-1} (Hansel et al., 1995; Wisthaler et al., 2001). The energy transferred during a reaction, given as the difference of the proton affinities plus the collision energy, is usually lower than the bond energies of volatile organic molecules, leading to a low amount of fragmentation. On the other hand, the electric field along the drift tube maintains a sufficiently high ion collision energy to reduce clustering of the H_3O^+ and RH^+ ions with water molecules (Holzinger et al., 2000) (see in reactions below).

$$H_3O^+ + n\,H_2O \rightleftharpoons H_3O^+(H_2O)n$$

$$RH^+ + n\,H_2O \rightleftharpoons RH^+(H_2O)n$$

However, the signal of H_3O^+ and $H_3O^+(H_2O)$ cluster cannot remain constant during experiments due to a varying intensity of the ion source and also due to the humidity of the sampled air, which regulates the H_3O^+ to $H_3O^+(H_2O)$ ratio (De Gouw et al., 2003). To account for the varying reagent ion signals, the measured product ion signals in cps are normalized to a drift tube pressure of 2.3 mbar and a total of 1 million parent ion signal by using the following equation:

$$[m]_{ncps} = [m]_{cps} \times \frac{2.3}{P_d} \times \frac{10^6}{[H_3O^+]_{cps} + [H_3O^+(H_2O)]_{cps} + [H_3O^+(H_2O)_2]_{cps}} \quad (2.1)$$

where $[m]_{ncps}$ expresses the product ion signal in units of ncps (normalized counts per second); P_d is the drift tube pressure in mbar; $[m]_{cps}$ is the ion signals of product ions in cps; $[H_3O^+]_{cps}$, $[H_3O^+(H_2O)]_{cps}$, and $[H_3O^+(H_2O)_2]_{cps}$ are that of H_3O^+, $H_3O^+(H_2O)$, and $H_3O^+(H_2O)_2$, respectively. The isotope $H_3^{18}O^+$ and $H_3^{18}O^+(H_2O)$ at m/z 21 and m/z 39 were used in our case since H_3O^+, $H_3O^+(H_2O)$ signals were usually saturated. The use of normalized signal ensures reliable comparison between datasets where the primary ion number and the drift tube pressure may alter slightly, which is often the case.

2.1.2 Mass separation and ion detection

PTR-MS instruments were originally equipped with a quadrupole mass analyzer (QMS) for the ion detection. This has the limit of not providing much analytical information besides the nominal mass of the detected ions, because of the unit mass resolution. The identification problem is more crucial when qualitatively unknown mixtures of compounds are to be investigated (Lindinger et al., 1998). A few years later a Time-Of-Flight (TOF) mass analyzer was also used in the ion detection systems. It is built upon the simple relation between the ion time-of-flight t and the ion mass-to-charge ratio (m/z), as lighter ions fly through a vacuum faster than heavier ions having the same kinetic energy (Blake et al., 2004). In principles, in TOF spectra, the ion time-of-flight t is proportional to the square root of the ion m/z (Eq. 2.2):

$$t = A\sqrt{\frac{m}{z}} + t_0 \quad (2.2)$$

where t_0 and A are constants determined via mass calibration with accurately known mass peaks. Typical peaks at m/z 21.022 ($H_3^{18}O^+$), m/z 29.997 (NO^+), m/z 59.049 (protonated acetone) that are usually present in PTR-TOF-MS spectra are used for mass calibration for the instrument in order to reach a good mass accuracy. A high molecule mass compound m/z 180.937 (protonated 1,2,4-trichlorobenzene) was added into the drift tube for calibrating the higher m/z scale. Temperature shifts during experiments can cause a slow change in the length of the ions flight path over time, hence a regular calibration of the mass axis during data post-processing is indispensable. Ion signals are detected by a multi-channel plate (MCP) detector (PHOTONIS, Sturbridge, USA). The PTR-TOF-MS is able to generate an entire mass spectra of complex VOC mixtures on a time response shorter than 100 μs (35 μs in our case) in a chosen mass range. Theoretically TOF-MS has a mass range beyond 10000 amu (mass range of 0-340 amu in our case) and a mass resolution of $m/\Delta m$ = 7000 (Δm is defined as the full width at half maximum (FWHM)) for an ion signal in V-mode, and even higher resolutions but lower sensitivity in W-mode (Jordan et al., 2009). This high mass resolution makes identification of most nominal isobaric masses possible. Figure 2.2 shows the possibility of separating the contribution of $C_4H_7O^+$ (m/z 71.050) signals from the $C_5H_{11}^+$ (m/z 71.087) signals.

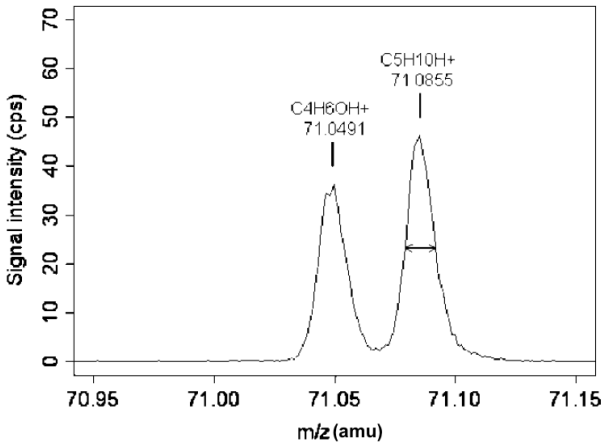

FIGURE 2.2: An example of the separation of isobaric molecules at the high mass resolution of the PTR-TOF-MS. Figure adapted from Fabris et al., 2010.

2.1.3 Mass spectra analysis

A PTR-TOF-MS mass spectrum typically contains hundreds of mass peaks and several isobaric peaks per unit m/z that need to be automatically identified and quantified. The PTR-TOF Data Analyzer software (Müller et al., 2013) was used for data analysis in this study. Prior to a baseline correction applied at each unit m/z interval, the raw mass spectra produced by the PTR-TOF-MS instrument was corrected for Poisson counting statistics and instrumental dead times. These two effects normally cause an underestimation of ion signals for high count rates. A non-extending dead time (induced by the amplifier-discriminator time response) of 12 ns and an extending dead time (induced by the MCP time response) of 1.2 ns were used. In the analyzer software, three mass peaks—two water signals at m/z 21.022 and m/z 39.033, and the externally added compound at m/z 180.937—were used for mass axis calibration and reference peak shape determination. A discriminator level of 0.01 cps was set to filter analysis only for unit m/z peaks above this threshold. An upper m/z threshold of 250 amu defined the mass range of interest with mass peaks above this value being analyzed only at unit mass resolution.

Measured ion signals from the PTR-TOF-MS provide information of both mass peak position and peak area. The peak position is governed by the the protonated VOC m/z value while the peak area is proportional to the number of ions that reach the MCP detector in the set acquisition time. Every detected mass peak can be assigned with an empirical chemical formula (i.e., $C_xH_yO_z$). A complete mass list of combinations (C, H, O, and N if present) sorted by increasing m/z that represent ions in the mass range of 21 to 250 amu was used in the mass peak identification. Individual signal intensity of compounds in the mass spectra can be then derived from respective peak area under the curve fitted by the PTR-TOF-MS data analyzer.

Different compounds can have the same chemical formula thus can be detected by the PTR-TOF-MS at the same mass peak. For that reason, compound attribution to defined VOC was done in combination of the empirical PTR-TOF-MS mass peak analysis and the literature of VOC oxidation mechanisms (Atkinson et al., 2003b; Rivera-Rios et al., 2014; Volkamer et al., 2002). For example, the oxidation of isoprene by OH radical leads to formation of several isomers due to different NO_x levels. MVK (C_4H_6O) and MACR (C_4H_6O) are the most well-known high-NO isoprene oxidation products. By contrast, under low-NO condition,

isoprene hydroxy hydroperoxides (ISOPOOHs, $C_5H_{10}O_3$) are the dominant first-generation oxidation products. Furthermore, Rivera-Rios et al., 2014 have demonstrated that ISOPOOH readily decomposes to MVK and MACR on heated metal surface, and both GC and PTR methods observe ISOPOOHs as MVK and MACR. Our calibrations show that 4,3-ISOPOOH detected as a product ion at m/z 71, has an efficiency of 36% of the sensitivity of MVK (see *AppendixA*), an efficiency of 44% was reported by Rivera-Rios et al., 2014. In addition, they showed that under 50 ppt of NO, the product ratio of ISOPOOHs/(MVK+MACR) is more than 90%, therefore in experiments where NO was less than 50 ppt, the first-generation products from isoprene photo-oxidation were considered as only ISOPOOHs. Besides that, in the low-NO experiments, the product fragment detected at the m/z 71 might be the sum of ISOPOOHs and the isobaric IEPOX, as IEPOX is the major oxidation product (yield of ∼79%) observed from both ISOPOOH isomers (Paulot et al., 2009b). unfortunately no IEPOX sensitivity available in this study, so the ISOPOOHs concentration was obtained by treating the signal detected at m/z 71 with the sensitivity of 4,3-ISOPOOH, then roughly divided the resulted concentration by 2.
The PTR-TOF-MS cannot distinguish isomeric compounds, only the sum of monoterpenes and sesquiterpenes can be detected, hence in this study the compounds attribution for m/z 137 and m/z 205 were done with the compositions provided by an offline GC-FID/MS measurements (see Chapter 2.2).

2.1.4 Quantification of VOCs concentrations

There are two approaches for quantifying VOCs concentration with PTR-MS: via calculation based on the known proton transfer rate coefficients or via calibration. The equation below (Eq. 2.3) illustrates the formula for calculating the volume mixing ratio (VMR) of a compound m.

$$[m]_{VMR} = \frac{1}{k \cdot t} \frac{[m]_{cps}}{[PI]_{cps}} \frac{T_d}{T_0} \frac{22400}{N_A} \frac{p_0}{p_d} \frac{T_r(PI)}{T_r(m)} \tag{2.3}$$

T - Temperature [K] (T_d - drift temperature, T_0 - standard temperature)
p - pressure [mbar] (P_d - drift pressure of 2.3 mbar, p_0 - standard pressure)
$[PI]$ - cps on Primary Ions at m/z 21 ($[H_3\,{}^{18}O^+]_{cps} \times$ 500)
$[m]$ - cps on product ions
$T_r(PI)$ - transmission factor for Primary Ions (m/z 21)
$T_r(m)$ - transmission factor for mass of product ion
t - reaction time $\sim 10^{-4}$ s
k - reaction rate [$cm^3 s^{-1}$]

Here, the transmission factor T_r is ruled by (i) the extraction efficiency of ions from the drift tube into the TOF-MS, (ii) the transmission efficiency of the TOF-MS, and (iii) the detection efficiency of the electron multiplier for each mass (De Gouw et al., 2007). The transmission factors correct the mass dependent discrimination of a system. The transmission curve was determined experimentally (Acir, in prep) and showed a 2-degree polynomial increase of transmission factor when going from mass 21 to larger masses. The accuracy of the calculated VOC concentration is limited by uncertainties such as the reaction time, which depends on the drift tube voltages, drift tube pressure, drift tube length, and ion mobility; additionally the accuracy is limited by the transmission factor and the reaction rate leading to an accuracy often less than 50%.
For atmospheric measurements a higher accuracy is generally required, and the accuracy

can be improved by calibrating the instrument using standard mixtures of VOCs in synthetic air or nitrogen. Three types of calibration were used in this study: (i) a self-built diffusion source; (ii) a Liquid Calibration Unit (LCU) for water soluble substances; and (iii) a multi-component gas standard together with the LCU, for regular calibrations to check the instrument performance.
Figure 2.3 shows the calibration of α-pinene at 60% relative humidity done by using the diffusion source (Gautrois et al., 1999). This diffusion source consists of 4 individual thermostated vials, in which pure liquid volatile chemicals can be added and diluted by a dynamic dilution system under a set temperature of 30°C (Julabo, F25-MP, Germany). The liquid or solid phase chemical is volatilized and diffused into a carrier gas of pure nitrogen (Linde, purity > 99.9999%). The diffusion resistance is constrained by the length and inner diameter of the neck of the glass vial. Gas phase compounds can be transported via a valve system into a mixing chamber where a dilution flux of ultra-pure zero air (Linde, purity > 99.9999%) is introduced. Concentrations of the chemical compounds released from the diffusion source can be thus determined from the mass loss rate of the individual compound and the dilution flux. Additionally, the zero air can be humidified through a thermostatic Milli-Q water bubbler before it enters the mixing chamber, thereby the relative humidity of the zero air is regulated with the ambient temperature and the Milli-Q water temperature (Julabo, F32-MC, Germany). As shown in Figure 2.3, the measured signal in ncps (normalized counts per second) as a function of known concentration in ppb (part per billion) gives the calibration curve. In this way the slope of the linear curve fit gives a sensitivity of 9.58 expressed in units of ncps/ppb. Combined error of the α-pinene concentration and error associated with the dilution procedure determine the accuracy ($\pm$ 1.8%) of calibration, which is shown together with other calibration results in *AppendixA*. The standard deviation (σ) of the zero air background measurements provides the limit of detection (LOD), which is defined as the lowest signal that can be distinguished from the background noise with statistical significance, a signal-to-noise ratio of 3 (3σ) is recommended in the PTR-MS community. The typical LOD of the instrument was $\sim$60 ppt for dry α-pinene calibration and was $\sim$110 ppt for calibration at 60% relative humidity.

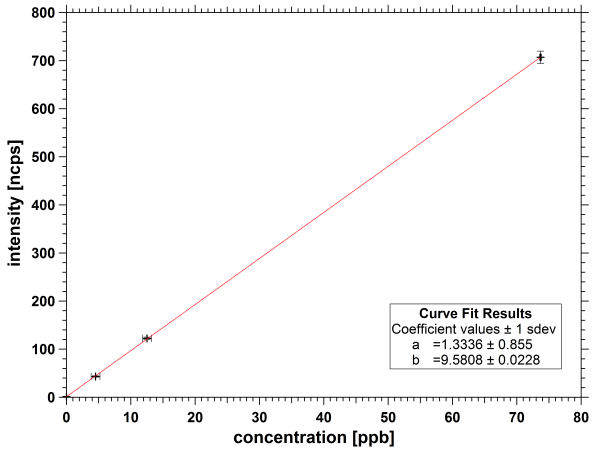

FIGURE 2.3: Example of one α-pinene calibration at 60% relative humidity. y-axis is the averaged signal at protonated α-pinene mass (m/z 137) in ncps and the x-axis is the averaged known concentration in ppb. The sensitivity of 9.58 ncps/ppb is obtained by the slope of the curve fit. Error bars show one standard deviation (1 σ).

For some water soluble VOCs such as acetic acid, calibrations as aqueous diluted standard were performed by using an advanced Liquid Calibration Unit (LCU-a, Ionicon Analytik, Austria). The LCU contains 2 liquid ports (0-50 μl/min) which can be connected to aqueous standard or pure water for calibration or humidified air supply measurements. In addition, the LCU contains two ports for the gas flow, one in the range of 500-1000 ml/min for the dilution carrier gas, and one additional gas input (0-20 ml/min) to admix a controlled flow of various gases (i.e., CO_2 or a standard gas) to the carrier gas in the evaporation chamber. In the LCU the liquid standard is pulled through the liquid port and then mixed with a carrier gas flow in a nebulizer producing a fine mist. These micro-droplets are ejected into a heated (100°C) evaporation chamber. At the end, a gas flow containing compounds at defined trace concentrations and humidity are introduced in PTR-MS through the gas inlet system. Concentrations were determined from the concentration in the aqueous standard and the flows introduced in the evaporation chamber.
A multi-component gas standard together with the LCU was also used for calibration on a regular time base. The self-made gas standard contains 16 VOCs in the mass range of 33 to 139 amu from 632.6 to 685.2 ppb. Calibrations with the gas standard were routinely done under dry/wet conditions in order to check the performance of the instrument. VOCs concentrations in the range of a few ppb to hundreds ppb under variable humidity conditions can be achieved by setting the flow rates in LCU. The sensitivities and the accuracies obtained by all 3 calibration methods are shown in *AppendixA*, together with a comparison of α-pinene sensitivity obtained by two calibration methods.
PTR-TOF-MS can monitor hundreds of VOCs at the same time. It is very time consuming and expensive to calibrate each single compound for the instrument. In principle, when the instrumental conditions change the calibration factors may change, hence a separate calibration should be preformed for every new instrumental condition. Moreover, a gas standard for every VOC is not always available and even some VOCs can interact with others, synthesizing suitable gas standards is difficult for many VOCs. As a consequence, an estimated sensitivity of 10 ncps/ppb was used for determining concentrations of un-calibrated VOCs. The sensitivity assumption of 10 was based on the general calibration result —with calibrated α-pinene, methanol, and acetone sensitivities being $\sim$6, $\sim$10, and $\sim$20 ncps/ppb, respectively. These three compounds represent some of the most common VOCs in the atmosphere with various masses. An accuracy of approximately 25% was used in further error propagation. This value is selected from the upper-limit of accuracies in all calibrations in the whole study. More sensitivities used in this study can be found in *AppendixA*.

2.2 Gas-Chromatograph (GC)

Measurements of VOCs in the atmospheric simulation chamber SAPHIR (Chapter 3.1) were simultaneously performed by an online gas-chromatograph 7890N (Agilent, Santa Clara, USA) equipped with a flame ionization detector and a mass spectrometer detector in parallel (GC-FID/MS). The gas chromatograph uses a capillary column (Agilent J&W DB 624) selected mostly by the column's dimensions (30m of length, 0.25 mm of diameter and 1.4 μm of film thickness) as well as phase properties. Different VOCs compounds are separated based on their chemical and physical properties as the sample mixture travels the length of the chromatographic column. The two-detector system allows better mass peak identification (done by the MS) and substance quantification (done by the FID). The GC-FID/MS system has a $\sim$30min time resolution consisting of 10 mins sampling time and $\sim$20 mins absorption/desorption time.
Calibrations for the GC-FID/MS system were performed with two gas standard mixtures,

one containing 57 hydrocarbons and oxygenated VOCs (OVOCs) with concentrations in the range of 100 ppb-1 ppm and the other one containing 74 hydrocarbon species with concentrations from 1 ppb to 3 ppb. The accuracies for the GC-FID/MS system were within 13%. Offline analysis of absorbent tubes (stainless steel) from the plant chamber SAPHIR-PLUS (Chapter 3.1) was also conducted with a GC-FID/MS, which has the same characteristics as the online one described above. Monoterpene and sesquiterpene compositions provided by the offline GC-FID/MS measurements (Table 5.1, Chapter 5) were then used in PTR-TOF-MS measurements for the quantification of these two terpenes.

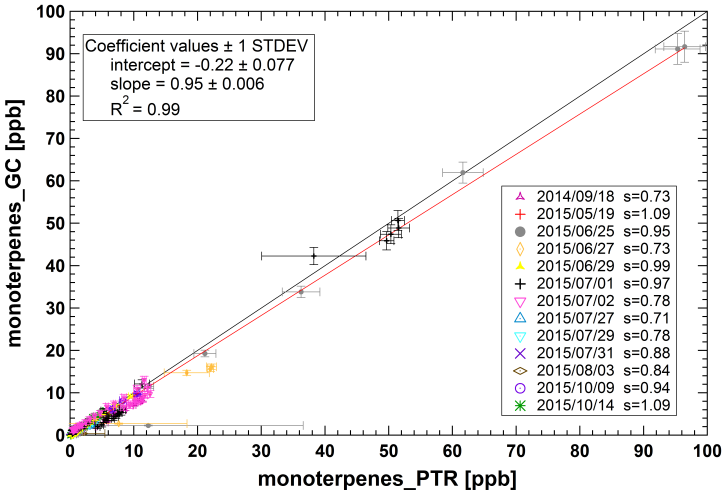

FIGURE 2.4: Overall monoterpenes in SAPHIR measured by the online GC-FID/MS vs. PTR-TOF-MS. The 1:1 ratio line is plotted in black. Slopes of linear fit for each experiment are also shown in the right box.

To cross validate the concentrations obtained by PTR-TOF-MS measurements, concentrations of most abundant compounds were compared to the online GC-FID/MS measurements. Monoterpenes are the major emitted compounds by selected sets of trees, and the mainly used BVOC reactants in this study (see experimental section in Chapter 3.2 and Chapter 3.3), thereby one example of measured monoterpenes concentrations in SAPHIR from both instruments is shown in Figure 2.4. Although, overall the GC-FID/MS measured lower mixing ratio than the PTR-TOF-MS, the correlation between the two instruments shows a good agreement (0.95) of only ∼5% of discrepancy, which is within the accuracy of both instruments (13% and 6%, respectively, see Table 3.1). The largest discrepancy happened in the Exp.BP10 (2015/07/27 s=0.71) when the measured VOC was dominated by tree-emitted monoterpenes. In this case, a low agreement of 0.71 was obtained, possibly due to losses from sampling prior to the GC analysis or due to the uncertainty of the PTR-TOF-MS measurements. Furthermore, a less accurate monoterpene speciation could lead to a bias on the quantification of monoterpenes in the PTR-TOF-MS measurements since different sensitivities were obtained for different monoterpenes.

2.3 Laser Flash Photolysis-Laser Induced Fluorescence (LP-LIF)

The total OH reactivity, k_{OH}, was determined as the inverse of the chemical OH lifetime by a laser flash photolysis/laser-induced fluorescence method (LP-LIF) (Lou et al., 2010). This technique introduces artificially generated OH into sampled ambient air and measure directly the total OH reactivity. Laser flash photolysis (LP) of O_3 is used to produce OH and laser-induced fluorescence (LIF) is applied to monitor the first-order decay of OH. Ambient air is drawn continuously through a laminar flow tube at atmospheric pressure, with a flow rate of 18 slm (standard litre per minute). The flow tube has a length of 8 m and an internal diameter of 40 mm. Short UV laser pulses (266 nm, 10 ns) from a frequency-quadrupled Nd:YAG laser (Big Sky, CFR200) pass through the flow tube and generate OH radicals ($\sim 10^9$ cm^{-3}) by laser-flash photolysis of O_3 in humid air (Reaction 1.7 and 1.8). Since the OH radicals react subsequently with the trace gases in the ambient air, change in concentrations of OH radicals in the sampled air is then probed by using a low pressure (3.5 mbar) florescence detection cell.The probe laser radiation (308 nm) comes from a tuneable, frequency-doubled 8.5 kHz pulsed UV laser (New Laser Generation, Tintura). The time-dependent OH decay is determined as:

$$[OH] = [OH]_0 \times exp(-k_{OH}t) \tag{2.4}$$

where k_{OH} is the total pseudo-first-order decay rate of OH, and $[OH]_0$ is the OH concentrations when t=0. The total OH reactivity k_{OH} for ambient air is finally retrieved from a numerical curve fit to the observed OH decay after subtraction of the zero air decay (Figure 2.5).

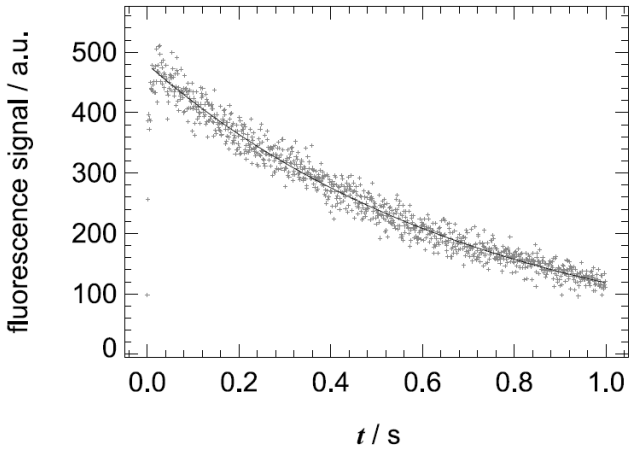

FIGURE 2.5: Example of an OH decay curve in synthetic air in presence of ozone and water vapor from one experiment in SAPHIR. Crosses represent the recorded raw time-dependent OH fluorescence signal at a time resolution of 1 ms. The line is the exponential fit to the data and corresponds to an OH reactivity as reciprocal $1/e$ lifetime (1.5 s^{-1}). Data from the first 10 ms are not considered in the fit because the signal is not stable in this interval.

The OH fluorescence signal is collected in a time-resolved mode by a multichannel plate (MCP) photo-detector. The limit of detection of the LP-LIF instrument is 0.3 s^{-1} and the integration time for the k_{OH} measurements was typically 1 min for all experiments shown in this study. This LP-LIF system was found to have a good linearity for reactivities up to

60 s^{-1} with an accuracy in the range of 5-10%. At k_{OH} higher than 60 s^{-1} an increasing negative bias appeared in the data, due to the non-exponential curvature of the OH decay curves (Hofzumahaus et al., 2009). Therefore, in experiments with k_{OH} higher than 60 s^{-1}, a dilution of the air sample at the inlet of the LP-LIF was applied and the k_{OH} was determined by taking into account this dilution factor, note that this dilution cause further uncertainty on the measured k_{OH}.

Chapter 3

Experimental section

3.1 Chamber svaporystem

Experiments were performed in the atmosphere simulation chamber SAPHIR (Simulation of Atmospheric PHotochemistry in a large Reaction chamber) located in Forschungszentrum Jülich, Germany (Figure 3.1). A detailed description of the chamber and its properties was reported by Rohrer et al., 2005. The cylindrical shape SAPHIR chamber consists of a double-wall Teflon (FEP) film with 5 m diameter, 20 m length, and 270 m^3 volume, which is attached to a steel frame. The large chamber volume and the inertness of Teflon film minimize reactant and product loss to the chamber walls. The Teflon film used has a transmittance of about 85% for visible light, UV-A and UV-B. A louvre shading system allows changes between dark and fully illuminated chamber within 60 s and protects the chamber from dangerous weather conditions.

FIGURE 3.1: The atmosphere simulation chamber SAPHIR in Forschungszentrum Jülich

During experiment time, the space between the inner and the outer Teflon wall is flushed with ultra purity air and SAPHIR is kept at a slight overpressure of about 50 Pa to prevent leakages of outside air into the chamber. Ultra-pure synthetic air (Linde, purity > 99.9999%)

mixed from evaporated liquid nitrogen and oxygen can go through the chamber via two flow controllers. The large one with a flow rate up to 500 $m^3\ h^{-1}$ is used to flush the chamber to reach clean starting conditions. The smaller one with a flow up to 15 $m^3\ h^{-1}$ (normally 7-9 $m^3\ h^{-1}$) is used in experiments to refill the chamber from losses due to the sampling of various instruments and leaks. To this clean and dry air, trace gases can be added according to experiment purpose. Humidity in the chamber can be introduced by evaporating Milli-Q water, which is added together with a large flow of synthetic air.
O_3 is provided by an ozonizator (Ozat CFS-1A, Ozonia, Switzerland) which generates O_3 in a silent discharge in ultra pure O_2. In the photo-oxidation experiments, chamber roof was opened in order to produce OH radicals i) by photolysis of O_3 to yield $O(^1D)$ which subsequently reacts with water vapor to form OH (Eq. 1.7 and Eq. 1.8); ii) additionally by photolysis of HONO (Eq. 1.10), which is released from the chamber walls of SAPHIR under illumination (Rohrer et al., 2005). The latter reaction constitutes the dominant source of OH radicals in the AVOC photo-oxidation experiments when no O_3 was added.

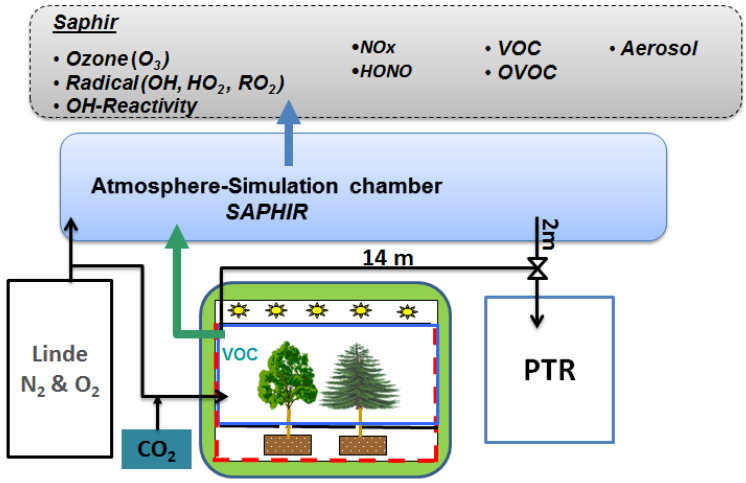

FIGURE 3.2: Schematic of the chambers experimental setup

Hohaus et al., 2016 have described the environmentally controlled flow-through plant chamber SAPHIR-PLUS, which can be coupled to the SAPHIR chamber. It has a volume of about 9.32 m^3 with outer dimensions of 2.39 m $\times$ 3.84 m $\times$ 2.84 m, also a double-wall Teflon film and a slight overpressure of about 50 Pa to prevent leakages of outside air into the chamber. Maximum 6 potted trees can be installed in the chamber, with the pots being isolated by Teflon films in a hermetically sealed interspace. Each pot is mounted with a soil moisture sensor (UMS GmbH München, EC-5) and a water drip which waters automatically if the soil moisture falls below a defined threshold and stops until the soil moisture reaches the threshold again. Illumination for photosynthetic activities of plants is controlled by a light control unit. 15 LED panels (5×3) are installed on a movable frame beneath the ceiling of the chamber. Each LED panel can be controlled individually by the process control unit. The intensity of photosynthetically active radiation (PAR) is in the range of 0 to 800 μmol $m^{-2}\ s^{-1}$, as measured by a quantum sensor (LI-190SZ-50, LI-COR GmbH, Germany) at a distance of 1 m. A gas exchange unit with adjustable flow rate from 0 to 42 $m^3\ h^{-1}$ flushes purge air and sustains CO_2 for photosynthesis of plants through the plant chamber. Water vapor can be

added to the purge air by vaporising Milli-Q water to reach a relative humidity in the chamber between 0 and 100 %. Temperature inside the chamber is controlled by heating/cooling the water-based thermofluid (0 to 50 °C) with an externally installed unit.
Plant emitted BVOCs mixed with synthetic air in SAPHIR-PLUS can be transferred to the SAPHIR simulation chamber via a 1.89 m long transfer line tube with an inner diameter of 80 mm. This perfluoroalkoxy (PFA) tube is temperature-controlled and the typical temperature is set to 60°C. Figure 3.2 shows a schematic of the chambers experimental setup.
A quantitative transfer of plant emitted BVOCs to SAPHIR is required for investigations in SAPHIR. To explore if a significant leakage of the mixed BVOCs, or a compound-dependent loss occurs during the transfer, the transfer efficiency —fraction of measured VOC concentration to that of calculated —was studied with a VOC mixture of 5 VOCs with various molar masses and polarities (acetone, isoprene, α-pinene, nopinone, and methyl salicylate (MESA)). A reference gas (CO_2) was used as a chemically inert tracer not interacting with wall surfaces, and was expected to be transferred without loss. Transfer efficiency experiments were done under different relative humidity conditions to explore the influence of water content. Transfer efficiencies of SAPHIR-PLUS inlet to outlet (upper panel) and of SAPHIR-PLUS outlet to SAPHIR (lower panel) were averaged and showed in Figure 3.3 as a function of relative humidity.

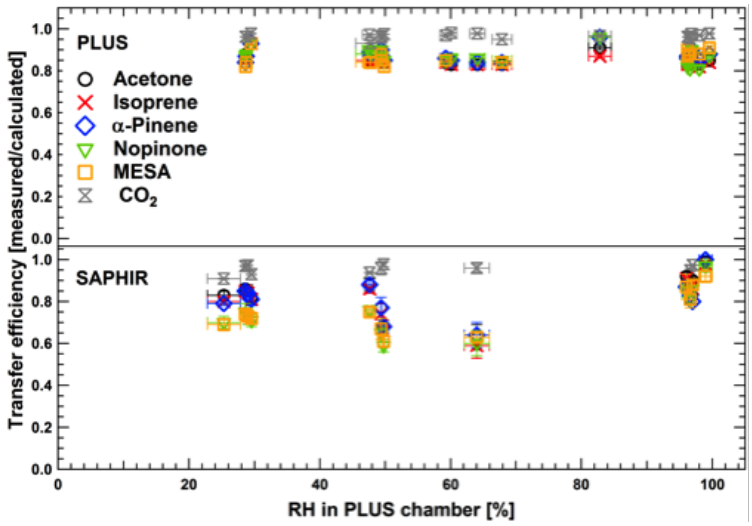

FIGURE 3.3: Transfer efficiency (upper panel between SAPHIR-PLUS inlet and outlet, lower panel between SAPHIR-PLUS outlet and SAPHIR) as a function of relative humidity levels, error bars shown are the standard deviation (1σ) (Hohaus et al., 2016).

An average BVOCs transfer efficiency of 0.85 (lowest of 0.81) between the SAPHIR-PLUS inlet and the outlet is obtained. However, it is slightly lower between the SAPHIR-PLUS outlet and the SAPHIR chamber at an average of 0.8, with the lowest of 0.59 found at 60% relative humidity. There is no remarkable difference in the transfer efficiency for different VOCs, ensuring the emission pattern remain unaltered. Additionally no systematic dependence on relative humidity is observed. The VOC mixture is shown to be effectively transferred from the plant chamber to SAPHIR, therefore SAPHIR-PLUS can be used as a representative source of BVOC emissions.

TABLE 3.1: List of instruments used in the experiments and the respective time resolution and characteristic error.

Parameter	Measurement method & Model	Time resolution (s)	Accuracy 1σ
VOCs	PTR-TOF-MS[a] PTR-TOF-MS 8000 IONICON	60	6%
VOCs	GC-FID/MS[b] Agilent 7890N	1800	13%
HCHO	Hantzsch-Reaction[c] AERO Laser al4001	10s	15%
HONO	LOng Path Absorption Photometry (LOPAP)[d] QUMA Elektronik	300	10%
CO	Reductive Gas Analyzer (RGA)[e] Trace Analytical RGA-3	60	5%
NO	Chemiluminescences(CL)[f] Eco Physics TR780	180	5%
NO_2		180	7.5%
O_3		180	5%
OH HO_2 RO_2	Laser Induced Fluorescence (LIF)[g] Jülich RO_x-LIF-System	60	10%
OH reactivity	LP-LIF[h] Jülich RO_x-LIF-System	60	10%
Photolysis frequency (jNO_2)	SpectroRadiometry (SR)[i] Bentham 300	60	13%
CH_4, CO_2, H_2O	Cavity Ring-Down Spectroscopy (CRDS)[j] Picarro G2301		
Aerosol size distribution	Scanning Mobility Particle Sizer (SMPS)[k] TSI 3080		
Temperature	UltraSonic Anemometer (USA) Metek USA-1	60	
Pressure	Pressure valve Setra Systems 270	60	
Flow rate	Mass Flow Controller Brooks	60	

[a] See Chapter 2.1
[b] See Chapter 2.2
[c] Kelly et al., 1994
[d] Heland et al., 2001
[e] Wegener et al., 2007
[f] Rohrer et al., 1992
[g] Fuchs et al., 2008
[h] See Chapter 2.3
[i] Bohn et al., 2005
[j] Crosson, 2008
[k] Sioutas, 1999

The biogenic emissions from SAPHIR-PLUS are sampled by the PTR-TOF-MS through a heated (normally 60°C) perfluoroalkoxy (PFA) tube (Figure 3.2), having a length of ∼14 m and an inner diameter of 4 mm. VOCs in SAPHIR are sampled via a PFA tube less than 2 m of length with 1.65 mm of inner diameter, heated up to 60°C. Air is sampled at a rate of 600 sccm (standard cm^3min^{-1}), thus the time for air to pass the SAPHIR-PLUS sampling line to the PTR-TOF-MS is ∼18 s and ∼0.4 s for the SAPHIR sampling line. A valve system

allows switching within one second among measurements from chambers and the synthetic air. The synthetic air measurements are then used in data analysis for the subtraction of instrumental-background.
In addition to the described PTR-TOF-MS, the online GC-FID/MS and the LP-LIF, the SAPIHR chamber is equipped with a comprehensive set of instruments locating in containers under the chamber or being installed directly in the chamber. In this study, several inorganic compounds (i.e., CO, NO, NO_2, O_3) were monitored, as well as temperature, pressure and relative humidity. Photolysis frequencies were provided from measurements with a spectral radiometer (SR). Laser induced fluorescence (LIF) was applied to measure OH concentrations, as well as HO_2 and RO_2 radicals. The chemical composition of formed SOA was monitored with a high-resolution time-of-flight aerosol mass spectrometer (AMS). The particle number concentration and number size distributions of aerosols were detected by a condensation particle counter (CPC) and a scanning mobility particle sizer (SMPS). A detailed summary of instruments used in the campaigns during 2014 and 2015 are listed in Table 3.1, as well as errors and time resolutions of measured parameters for the evaluation of the experiments.

3.2 Experiments characterizing plant emission intensity and patterns

In order to evaluate whether plants in the SAPHIR-PLUS chamber emit BVOC concentrations and patterns as expected from known physiological processes, BVOC emissions from six 1-year-old potted *Quercus ilex* (Holm oak) trees under variable light and temperature conditions were monitored (see Hohaus et al., 2016).
Quercus ilex is reported to emit large amount of monoterpenes and small quantity of isoprene with emissions being light and temperature dependent (Kesselmeier et al., 1999; Staudt et al., 1998, 1995). Methanol has the largest contribution to biogenic OVOC emitted by trees, especially for young, growing trees (Folkers et al., 2008; Mellouki et al., 2015). Hence VOC emissions of methanol, isoprene, and monoterpenes were analyzed in this study as a function of light intensity and of temperature.
For every single experiment day a diurnal light cycle was preset in SAPHIR-PLUS with a 12 h day/night period. The light intensity increased gradually from 0 and reached the maximum of 1100 μmol m^{-2} s^{-1} in 6 hours, followed by a 6 hours gradual decrease to dark condition and stay in dark for 12 h before another daytime cycle.
Plant emission dependence on temperature in a range from 13 to 31°C was investigated. Temperature was kept constant for each experiment day despite the influence of ∼1.5 °C due to LED lamps, at least two consecutive days at one temperature step were conducted. For each experiment day, 4 hours data of emissions at the highest illumination were averaged and normalized to the concentrations at 30°C (also 4 hours averaged data at peak illumination). The same set of experiments was used to study the light response of the *Quercus ilex* emissions. For the light dependence study, concentrations of plant emitted compounds were normalized with concentrations at maximum light intensity $C_{I,max}$.
Note that these six young *Quercus ilex* used in the set of experiments were kept in the plant chamber SAPHIR-PLUS for 109 consecutive days, during that time period the plants showed no signs of stress effects, that is to say, no sesquiterpenes were detected and the plant emission pattern was stable during the whole set of experiments. Results are shown and discussed in Chapter 5.1.

3.3 VOCs oxidation experiments

Experiments in SAPHIR during the summer of 2014 and 2015 were performed in several campaigns including: 1) k_{OH} measurements of BVOCs from plant emissions, which investigates the change in OH reactivity of tree-emitted BVOCs under O_3 and OH oxidations; 2) "Isoprene degradation" experiments, which focuses on the isoprene oxidation mechanism; 3) "Anthropogenic enhancement", exploring the anthropogenic influence on biogenic SOA formation; and 4) k_{OH} inter-comparison of a variety of k_{OH} measurement technics.
Various campaign purposes provided a broad suite of complementary measurements with abundant atmosphere oxidation scenarios. PTR-TOF-MS data was taken from these campaigns and analyzed to investigate oxidation processes of VOCs under different atmospheric oxidation conditions. To better structure the findings, experiments are classified into BVOC and AVOC parts and presented with increasing complexity of the system. Table 3.2 and Table 3.3 present the summary of experiments chosen in this study. Relative humidities shown in the tables are initial conditions which declined during the experiment due to the replenishment flow.
While the experiments are performed under specific campaign purposes, the common experimental procedure for VOC oxidation experiments in SAPHIR is the following: I) before starting each experiment, the SAPHIR simulation chamber is purged overnight with a clean synthetic air at a flow rate of 150 m^3h^{-1}, in order to reduce concentrations of any contaminations below the detection limit of measuring instruments (e.g., ppt levels of nitrogen oxides, O_3, and hydrocarbons in the chamber); II) a typical experiment starts at early morning with addition of water vapor along with the synthetic air flow of $\sim$150 m^3h^{-1} to reach the defined relative humidity, the humidification is completed after approximately 45 min; III) afterwards, the VOC of interest is added with a liquid injection system along with the experimental air flow ($\sim$9 m^3h^{-1}); IV) the oxidant of choice is added after quantifying the initial concentration of VOCs.
All experiments are conducted under atmospheric pressure at ambient temperature. In experiments using plant emitted BVOCs, SAPHIR is connected to SAPHIR-PLUS for several hours for transport of plant emission, afterwards is the addition of other VOCs of interest or the addition of oxidants. Ozonolysis experiments are performed in the dark chamber. In the photo-oxidation experiments, the chamber is exposed to sunlight by opening the louvre shading roof. Experimental operations can be seen (vertical colored lines) in the figures of time series of OH reactivity ($AppendixB$). For some experiments in the campaign "Anthropogenic enhancement", after the initial formation of particles, aerosols undergo both physical and chemical processes with time, for these SOA ageing experiments, the chamber roof is typically closed in the evening and opened again in the next morning. In the NO_3 oxidation experiment (Exp.BS2 in Table 3.2), NO is injected to form NO_3 radical in the presence of O_3 in the dark chamber by the reaction 1.15 and 1.16. In some experiments, a VOC-OH tracer containing 2-methylfuran (C_5H_6O) or a mixture of 2-methylfuran and mesitylene (C_9H_{12}) is added along with the experiment. The standard serves as a VOC-OH tracer gas for the determination of OH concentration which is not a topic in this study. However, their addition influences the OH reactivity measurement as shown later in Chapter 7.

3.3.1 BVOCs Oxidation

In a first series of experiments (Exp.BS1-BS9 in Table 3.2), single BVOC oxidation processes were studied in the SAPHIR chamber. β-Pinene ($C_{10}H_{16}$), limonene ($C_{10}H_{16}$), isoprene (C_5H_8) and their oxidation products from O_3 and OH oxidation were monitored with PTR-TOF-MS. Isoprene is the most abundantly emitted biogenic hydrocarbon in the atmosphere. β-pinene and limonene are also of interest as representative BVOCs due to their high emission rate

TABLE 3.2: A summary of BVOCs oxidation experiments and the initial conditions. MT=monoterpene, SQT=sesquiterpene, and ISOP=isoprene.

Experiments	RH (%)	VOC[a] (ppb)	O_3 (ppb)	NO_x (ppb)
BS1 β-pinene + O_3	60	120	740	-
BS2 Limonene + O_3	60	25	150	30 (NO)
BS3 Limonene + OH[b]	70	10, 10, 10	-	20 (NO)
BS4 Isoprene + OH, high NO	60	4.3, 4, 4.2	-	1 (NO)
BS5 Isoprene + OH, medium NO	60	4.7, 4, 4	-	0.6[c]
BS6 Isoprene + OH, low NO	60	3.8, 4, 4	110	0.05[c]
BS7 Isoprene + OH, mid NO[b]	75	5, 5, 5	150	0.08[c]
BS8 Isoprene + OH, low NO[b]	60	5, 5.2, 4.3	150	0.05[c]
BS9 [CO + Isoprene] + O_3[d]	80	2.4, 1.9, 4.4	80	-
BM1 [β-pinene + limonene] + O_3	60	60 + 12	400	-
BM2 Forest mixture I[e] + O_3	80	1, 2, 3, 4, 5	50	-
BM3 Forest mixture II[f] + O_3	80	32, 12, 0.4, 0.3, 0.8	50	-
BP1 *Quercus ilex* emissions + O_3	60	12 MT	50	-
BP2 *Picea abies* emissions + O_3	60	1.2 MT + 1.6 SQT	50	-
BP3 *Picea abies* emissions + OH	60	1.2 MT + 2 SQT	50	-
BP4 *Betula pendula* emissions + O_3	60	1 MT + 1.6 SQT	50	-
BP5 *Betula pendula* emissions + OH	60	0.6 MT + 0.6 SQT	50	-
BP6 *Quercus robur* emissions + OH	60	9 ISOP	90	0.05[c]
BP7 *Quercus robur* emissions + OH	60	1.7, 2.4 ISOP	120	0.1[c]
BP8 *Pinus sylvestris* emissions + O_3	60	50 MT	300	-
BP9 *Pinus sylvestris* emissions + OH	60	12 MT	-	-
BP10 *Fagus sylvatica* emissions + O_3	60	3.8 MT	50	-
BP11 *Fagus sylvatica* emissions + O_3[b]	60	4 MT	50	-
BP12 *Fagus sylvatica* emissions + OH	60	3.6 MT	50	-
BP13 *Pinus sylvestris* & *Fagus sylvatica* emissions + O_3	80	5 MT	70	-

[a] Concentration in BP1-BP13 is the measured concentration of the major tree-emitted BVOCs in SAPHIR at the time before addition of oxidants or before SAPHIR decoupling from SAPHIR-PLUS. MT= monoterpenes, SQT= sesquiterpenes, and ISOP= isoprene.
[b] A VOC-OH tracer containing 2-methylfuran was added.
[c] Measured maximum concentration of NO in the chamber.
[d] A VOC-OH tracer containing 2-methylfuran and mesitylene was added.
[e] Forest mixtureI consists of α-pinene, myrcene and limonene (68% : 10.5% : 21.5%).
[f] Forest mixtureII consists of acetaldehyde and MVK / MACR mixture (1 : 1), with β-caryophyllene.

among monoterpenes (Mellouki et al., 2015).
The β-pinene ozonolysis experiment (Exp.BS1) was performed in the dark chamber following the typical experimental procedure as explained above. The time series of observed concentration of β-pinene and of major oxidation products are shown in Chapter 6.1 (Figure 6.1). In the limonene ozonolysis case (Exp.BS2), NO was added several hours after the ozonolysis in order to explore the NO_3 oxidation over night. In the limonene photooxidation experiment (Exp.BS3), NO was added to serve as an anthropogenic compound prior to the limonene injection and a VOC-OH tracer was added along with the experiment, two limonene injections were repeated afterwards. The amount of VOCs in each injection is listed in Table 3.2, different injections are separated by commas. Kim et al., 2011 suggest that the contribution of unmeasured OVOC to the total OH reactivity should be carefully

evaluated for appropriate NO conditions to constrain the source of missing OH reactivity. Additionally, as mentioned in the Chapter 1, isoprene oxidation mechanisms under different NO concentrations lead to distinct products. In the isoprene photo-oxidation study, different NO regimes from tens ppt to 1 ppb were investigated (Exp.BS4-BS9). 1 ppb of NO was added in the chamber to reach a high NO level while more than 100 ppb of O_3 were injected to achieve low NO concentration. In experiments BS7-BS9, a VOC-OH tracer was added. In Exp.BS9, even though the chamber roof was opened to produce OH radicals, the added large amount of CO (1 ppm) served as an OH scavenger leading to isoprene oxidation mainly by ozone, therefore this experiment will be referred later as isoprene ozonolysis.
In the second set of experiments (Exp.BM1-BM3 in Table 3.2), synthetic BVOC mixtures were used to present more complex systems. The same experiment procedures as described above were performed in SAPHIR, with exception of VOCs being added in several steps. In Exp.BM1 60 ppb of β-pinene plus 12 ppb of limonene were injected in the SAPHIR chamber to investigate the monoterpene mixture ozonolysis. The Forest mixtureI in Exp.BM2 consists of 3 monoterpenes, including α-pinene (68%), myrcene (10.5%) and limonene (21.5%). This monoterpene mixture was added in 5 steps before the O_3 addition in order to test the sensitivity of calculated and measured OH reactivity at different OH reactivity levels. The Forest mixtureII in Exp.BM3 simulates a more complicated atmospheric environment, with OVOCs and β-caryophyllene presenting stressed tree emissions: acetaldehyde was injected first, about one hour later the MVK/MACR (1 : 1) mixture was added, then 3 times of β-caryophyllene injections were implemented followed by the addition of O_3.
With increasing complexity of the simulated atmosphere system, finally the oxidation of real plant emission provided from SAPHIR-PLUS were studied (Exp.BP1-BP13 in Table 3.2). Several different species of trees representing some of the most widely distributed monoterpene-emitting plants were used in the experiments, including: *Quercus ilex* (Holm oak, Exp.BP1), *Picea abies* (Norway spruce, Exp.BP2-3), *Betula pendula* (European birch, Exp.BP4-5), *Pinus sylvestris* (Scots pine, Exp.BP8-9), and *Fagus sylvatica* (European beech, Exp.BP10-12). At the end the emission from a mix of 3 *Pinus sylvestris* and 3 *Fagus sylvatica* (Exp.BP13) was transferred into SAPHIR to investigate its reaction with O_3. A set of 6 *Quercus robur* (English oak, Exp.BP6-7), representing an isoprene emitter was also used in the experiment. All experiments with plant emissions were implemented at humid condition as the humid air was transferred from the plant chamber to SAPHIR. Initial concentrations of the mainly emitted BVOCs in SAPHIR are listed in Table 3.2. The plant chamber was connected twice to SAPHIR in the Exp. BP7. Monoterpene concentrations were determined with the help of the monoterpene composition provided by offline GC-FID/MS measurements.

3.3.2 AVOCs Oxidation

The total global AVOCs emissions have been estimated to be 129 Tg for the year 2000 (Von Schneidemesser et al., 2015). Anthropogenic air pollution poses an increasingly serious concern for public health, agriculture, and global climate change. Reactive AVOCs produce much larger amounts of SOA than predicted from models (Volkamer et al., 2006). The chemical transformation of AVOCs and the relative importance of oxidation products remained unknown. Therefore, atmospheric oxidation processes of AVOCs need to be studied in detail. Experiments from the campaign of "Anthropogenic enhancement" and of k_{OH} intercomparison in 2015 were taken and presented, again with increasing complexity of the atmosphere system.
Typical AVOCs are aromatic hydrocarbons. Benzene (C_6H_6) is one of the most important AVOCs, which is known as a natural constituent of crude oil and an important component of petrol. In the "Anthropogenic enhancement" campaign, deuterated benzene (C_6D_6, benzene-D_6 in Table 3.3) was used as an anthropogenic marker substance for identification reasons in

the AMS measurements. As it is highly common that anthropogenic activities come along with high NO_x concentrations, experiments under different NO_x regimes were performed. The first two AVOC oxidation experiments explore single benzene-D_6 photo-oxidations at low- and high-NO_x levels (Table 3.3, Exp.AS1-AS2). In the high NO_x experiment, 40 ppb of

TABLE 3.3: A summary of AVOCs oxidation experiments and the initial conditions. Brackets indicate the order of addition.

Experiments	RH (%)	VOC[a] (ppb)	O_3 (ppb)	NO_x (ppb)
AS1 benzene-D_6 + OH, low NO_x	75	290	-	0.3[b]
AS2 benzene-D_6 + OH, high NO_x	75	290	-	40 (NO)
AM1 Urban mixture + OH[c]	85	54, 18	90	10, 15, 20, 20 (NO_2)
AM2 CO + Urban mixture + O_3[c]	85	22, 14, 14, 14	90	10, 10 (NO_2)
AB1 Photo-oxidation of [benzene-D_6] + [BVOCs[d]]	75	8	-	0.3[b]
AB2 Photo-oxidation of [BVOCs[e]] + [benzene-D_6]	75	9	-	0.5[b]
AB3 Photo-oxidation of [BVOCs[e] + benzene-D_6]	75	11	-	0.3[b]
AB4 Photo-oxidation of [BVOCs[e]] + [benzene-D_6 + NO]	75	10	-	40 (NO)
AB5 Photo-oxidation of [BVOCs[e] + NO + benzene-D_6]	75	8	-	40 (NO)
AB6 Photo-oxidation of [benzene-D_6] + [BVOCs[e]]	75	3	-	0.3[b]
AB7 Photo-oxidation of [benzene-D_6 + NO] + [BVOCs[e]]	75	1.2	-	40 (NO)

[a] Concentration in AB1-AB7 is the measured monoterpenes concentration in SAPHIR at the time before addition of oxidants or before SAPHIR decoupling from SAPHIR-PLUS. Benzene-D_6 was added at the same amount of 290 ppb.
[b] Measured maximum concentration of NO in the chamber.
[c] Adding along a VOC-OH tracer containing 2-methylfuran and mesitylene.
[d] BVOCs from a monoterpenes mixture canister.
[e] BVOCs from 6 *Pinus sylvestris* trees emission.

NO were added prior to the addition of benzene-D_6. 290 ppb of benzene-D_6 were injected in each experiment in order to reach an OH reactivity of $\sim$10 s^{-1}. OH radicals were produced by photolysis of HONO coming from SAPHIR walls by opening the roof, .

In order to increase the complexity of the simulated atmosphere system, synthetic AVOC mixtures were also used. 1-pentene (C_5H_{10}), toluene (C_7H_8) and o-xylene (C_8H_{10}) are all used in industrial productions and released from combustion processes. Those three common anthropogenic pollutants were therefore used for simulating an urban environment. Two urban mixture oxidation experiments under different NO_x variations were studied (Table 3.3, Exp.AM1-AM2). In Exp.AM1, first 90 ppb of O_3 were added in order to produce OH radicals from photolysis of O_3 in humid air. Then the injection of the urban mixture together with the continuous addition of a VOC-OH tracer was accomplished and the mixture was exposed to sunlight. One hour later 10 ppb of NO_2 were added in the chamber, followed by 3 consecutive NO_2 injections with 1 h interval. After another 1 hour a second injection of the urban mixture was made and the VOC-OH tracer addition was stopped. In Exp.AM2, an addition of O_3, NO_2 and CO was accomplished prior to the continuous addition of the VOC-OH tracer and two injections of the urban mixture. After that the chamber was exposed to sunlight followed by another injection of NO_2. Two more additions of the urban mixture were implemented later in 1 h intervals to test the sensitivity of calculated and measured OH reactivity to different OH reactivity levels.

Previous studies revealed that SOA originate from both biogenic and anthropogenic sources (Kulmala et al., 2011; Mellouki et al., 2015; Von Schneidemesser et al., 2015). Even though globally the production of biogenic SOA dominates over the anthropogenic SOA, however, locally AVOC oxidations found to enhance biogenic SOA production (Emanuelsson et al.,

2013). As shown in Table 4.1, benzene-D_6 reacts slower with OH radicals than most BVOCs. In the atmosphere, the mixtures of AVOC and BVOC have drawn special interest because of the high complexity of the degradation mechanisms, and the influence of one to the other. In order to study the importance of the chemistry of AVOC and BVOC and their interactions, experiments from "Anthropogenic enhancement" campaign simulating mixed airmass conditions were chose and presented in this study. Photo-oxidation was achieved by OH radicals formed by the photolysis of HONO. The mixed A/BVOC systems use benzene-D_6 as an anthropogenic marker substance together with BVOCs from a canister or BVOCs emitted from 6 *Pinus sylvestris* trees (Table 3.3, Exp.AB1-AB7). The canister contained a monoterpene mixture of α-pinene, 3-carene, β-pinene, limonene and myrcene (60% : 36% : 12% : 6% : 3%). 290 ppb of benzene-D_6 equivalent to an OH reactivity of $\sim$10 s^{-1} were injected in each experiment. In Exp.AB1 (Figure B.6.a), the AVOC (benzene-D_6) was added initially and exposed to sunlight for 4 h before the BVOC mixture from a canister was added, afterwards the mixture was further photo-oxidized in sunlight. In Exp.AB2 the BVOC from SAPHIR-PLUS was transferred in SAPHIR first and photo-oxidized for about 5 h, then the AVOC was injected and the mixture was kept in dark overnight. On the subsequent second day the mixture was exposed to sunlight for another 7 h. In the Exp.AB3 the BVOC from SAPHIR-PLUS and the AVOC were added together, then the mixture was exposed to sunlight for about 7 h. In the Exp.AB4, BVOC from SAPHIR-PLUS was photo-oxidized for 5 hours before the injection of AVOC and 40 ppb of NO. The Exp.AB5 was under the same procedure as the Exp.AB3, except 40 ppb of NO were added before the photo-oxidation started in order to simulate a high NO_x system. The Exp.AB6 was the same as the Exp.AB1, only with BVOC from SAPHIR-PLUS. In the Exp.AB7, NO together with the AVOC were added initially and exposed to sunlight for 3 h before the BVOC mixture from SAPHIR-PLUS was added, then the mixture was further photo-oxidized in sunlight.

Chapter 4

Data evaluation

4.1 Product yields determination

Further insight on the oxidation products of VOCs under atmospheric conditions is important to investigate their oxidation mechanism and to assess their overall reactivity. This is also important as input to atmosphere models that try to elucidate the atmospheric removal of VOCs (Grosjean et al., 1993; Lou et al., 2010; Lu et al., 2013; Zannoni et al., 2015). Yield determination experiments in this study include single monoterpene (β-pinene and limonene) ozonolysis, and the single isoprene photo-oxidation; the monoterpenes mixture and eventually the tree-emitted BVOCs oxidation. Some oxidation products have been reported in a number of previous reaction chamber studies. Nopinone has long been identified as a major product in the ozonolysis of β-pinene (Atkinson et al., 2003b; Yu et al., 1999), whereas MVK and MACR are well-known first generation products of OH-isoprene reaction in the presence of high NO (Atkinson et al., 2003b; Rivera-Rios et al., 2014; Sprengnether et al., 2002). Acetone was found in the terpene oxidations to be formed promptly via a series of highly unstable radical intermediates or slowly via the degradation of stable non-radical products (Wisthaler et al., 2001).
The PTR-TOF-MS can monitor reactants and products at the same time with a high time resolution, thus it was used in the SAPHIR chamber experiments for online measuring of VOCs at levels down to a few ppt. The gas-phase product molar yield was determined from the reactant-product time series with a time resolution of 1 minute. The VOC concentrations measured by the PTR-TOF-MS were corrected for losses through dilution and leakage (see more chamber description in Chapter 3.1). Different initial reactant/product concentrations were used along with different flushing rates by taking into account the replenishment flow and the chamber volume by the following equation describing the dilution in a well stirred reactor (Apel et al., 2008):

$$C(t) = C_0 \times exp\left(-\frac{1}{V}\int_0^t F(t^{'})\mathrm{d}t^{'}\right) \tag{4.1}$$

Here, $F(t)$ is the replenishment flow rate [m^3 h^{-1}], C_0 is the initial concentration [ppb] after injection and mixing (at t = 0); V is the SAPHIR volume [m^3]. The dilution rate of all species in the chamber under a typical replenishment flow of 9 m^3 h^{-1} was calculated to be ~3% h^{-1}.
For OH-initiated oxidation experiments, the chamber roof was opened in order to produce OH radicals. The instantaneous formation of some trace gases (e.g., HONO, acetaldehyde, acetone, formic acid and acetic acid) was previously observed when the SAPHIR chamber was exposed to sunlight and these substances are considered to be released from the chamber walls (Acir, in prep; Rohrer et al., 2005). As a consequence, the measured photo-oxidation products concentrations must be corrected for this chamber source by using the following equation:

$$S_i = a_i \times j\mathrm{NO_2} \times (0.21 + 2.6 \times 10^{-2} \times RH) \times exp[-2880/T] \quad (4.2)$$

S_i - source of analyte i in SAPHIR [$molecule \cdot cm^{-3}s^{-1}$]
a_i - scaling factor of analyte i
$j\mathrm{NO_2}$ - photolysis frequency of NO_2 [s^{-1}]
RH - relative humidity in SAPHIR [%]
T - temperature in SAPHIR [K]

The chamber source depends on the temperature (T), the intensity of light (taken into account as the photolysis frequency of NO_2) and the relative humidity (RH) in SAPHIR. The compound-specific scaling factor a was investigated in reference experiments ($e.g.$ $a_{acetone}$ = $\sim$0.1$\times$10^{13} cm^{-3}, Acir, in prep). By using this equation, about 300 ppt h^{-1} of acetone

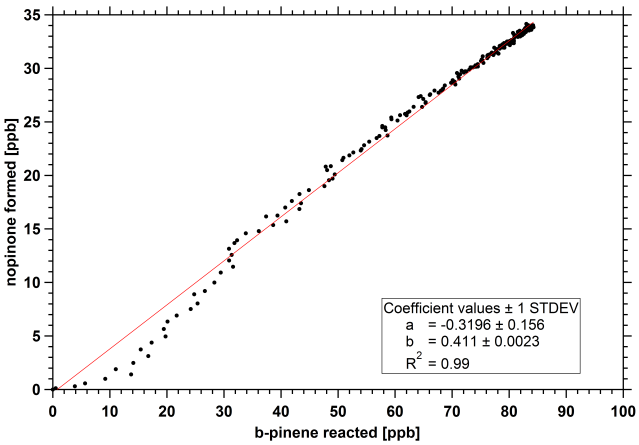

FIGURE 4.1: Plot of the nopinone produced vs.the amount of reacted β-pinene. A nopinone yield of 41.1 $\pm$ 4.2% is obtained from the slope of the linear fit. (Note that the error of slope b in the figure does not represent the error of yield determined with error propagation.)

coming from the chamber walls was calculated for a typical experiment condition (T=298 K, jNO_2=0.004 s^{-1}, RH=50%). As a consequence, in photo-oxidation yield determinations, the concentration corrections determined above were then subtracted from the experimentally observed VOC concentration at time t.
The amount of reactant consumed was calculated from the different concentrations between t_0 and t (C_t - C_0, both after correction), the product yield was hence calculated from the slope of the corrected concentration plotted as a function of the amount of consumed reactant (Atkinson et al., 1989; Volkamer et al., 2002). The average of 10 minutes data points before oxidant addition was used as the initial concentration of the reactant (C_0). For the isoprene oxidation experiments where OH radicals were produced before the addition of reactant, the measured first data point after isoprene injection was used as C_0. C_t was took when 90% of the reactant was consumed. Figure 4.1 illustrates the product yield determination of nopinone from β-pinene ozonolysis. Concentrations of β-pinene and nopinone were corrected according to equation 4.1. No chamber source correction was needed since the experiment was performed in dark condition. The slope of the linear fit gives a nopinone yield of 41.1 $\pm$ 4.2%. Note that errors of yields reported in this study were calculated by taking into account of the accuracy of both reactant and product, the standard deviation of the

initial stage, the error of dilution correction, and if applied, the error of the chamber source correction.

4.2 Missing OH reactivity investigation

Besides the direct measured OH reactivity k_{OH}^{meas} by the LP-LIF instrument, the OH reactivity calculated from the VOC and inorganic measurements k_{OH}^{cal}, was also determined in this study (equation 1.19), in order to further elucidate the number and abundance of reactive components that react with OH. Figure 4.2 explicates the approach of using PTR-TOF-MS data in the comparison of the total OH reactivity. As explained in Chapter 2.1.2, measured ion signals from the PTR-TOF-MS provide information of mass peak position and peak area. Each mass peak is assigned with an empirical chemical formula by using a mass list of combinations (C, H, O, and N if present) in the mass range of 21 up to 250 amu. The respective peak area provides information on the signal intensity of the compound. The compound concentration is obtained either by using a determined sensitivity from calibration, or by applying an estimated sensitivity of 10 ncps/ppb when no calibration was performed for the compound.

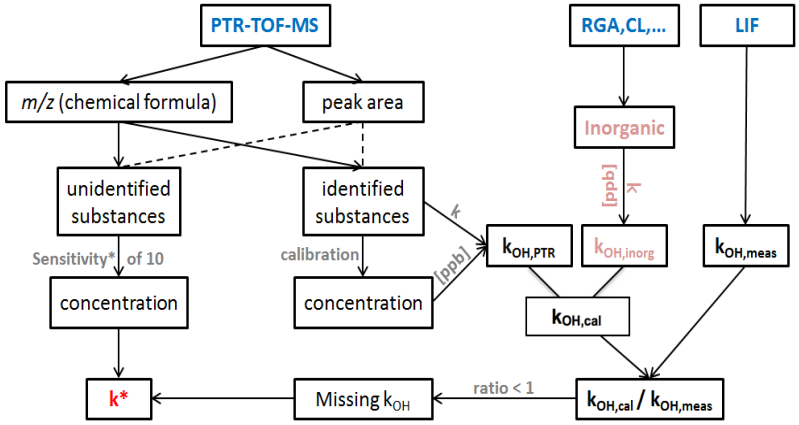

FIGURE 4.2: Schematic of how missing k_{OH} was determined by comparing OH reactivity calculated from PTR-TOF-MS data ($k_{OH,PTR}$) and inorganic compounds ($k_{OH,inorg}$) to the OH reactivity measured from LIF data ($k_{OH,LIF}$). k^* is the weighted average rate constant derived from the concentration of unidentified compounds in the PTR data in order to close the k_{OH} budget.

The concentration of all the compounds that cannot be identified in the PTR-TOF-MS measurements (not included in Table 4.1) was summed. For instance in the β-pinene ozonolysis experiment, the sum of unidentified compounds resulted in a maximum concentration of ~60 ppb whereas that of the total identified compounds was ~80 ppb (Figure 4.3). This is one of the cases with the highest relative contribution of unidentified compounds. In all experiments the amount of unidentified compounds is always much less than that of identified compounds, except for the limonene ozonolysis where the maximum concentration of unidentified compounds (~16 ppb) was almost the same as the sum of all identified compounds (~18 ppb).
For all identified substances, their concentrations and the respective rate constants were then used in the calculation of the OH reactivity $k_{OH,PTR}$ (see Figure 4.2). The rate constants for

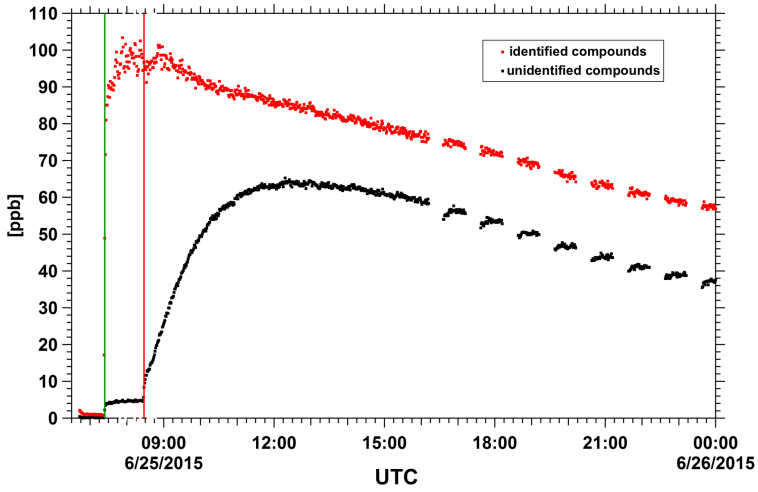

FIGURE 4.3: Time series of concentrations of identified compounds (red dots) and unidentified compounds (black dots) from PTR-TOF-MS measurements. Green vertical line indicates the injection time of VOC, red vertical line the injection time of O_3.

1,2-and 4,3-ISOPOOHs reported by St. Clair et al., 2015 with an efficiency of 20% were used for the calculation of OH reactivity, as the reaction between ISOPOOHs and OH reforms OH immediately. Monoterpene identification and quantification were done with the help of the offline GC-FID/MS as mentioned previously and corresponding rate constants were then used in the OH reactivity calculation. As for sesquiterpene signal at m/z 205, quantification was done with the calibrated sensitivity of β-caryophyllene, and the OH reactivity was calculated by taking into account additionally the contribution of α-humulene. Rate constants used for all identified compounds can be found in Table 4.1 and sensitivities in *AppendixA*.
By combining $k_{OH,PTR}$ with $k_{OH,inorg}$, the OH reactivity from inorganic compounds as CO, NO, NO_2, and O_3 (measurements from a RGA and CL, more details see Chapter 3.1), the calculated total OH reactivity k_{OH}^{cal}, was obtained.
The missing OH reactivity is the difference between k_{OH}^{cal} and k_{OH}^{meas} in case the calculated one is smaller than the measured one. In some cases with a higher calculated k_{OH} in this study (within the uncertainty), the reactive components in the atmosphere were considered as fully identified and quantified by the reactants measurements.
Previous field studies speculated that the missing OH reactivities resulted from unknown / unmeasured compounds (Lou et al., 2010; Nölscher et al., 2012; Zannoni et al., 2015). To investigate whether the unidentified substances from the PTR-TOF-MS measurements can be used in explaining the observed missing OH reactivity ($k_{OH,meas}$ - $k_{OH,cal}$), the concentration of all unidentified compounds ($\sum_i [X_i]_{un-id}$) was used. As a result an average rate constant k^* was derived:

$$k^* = \frac{k_{OH,meas} - k_{OH,cal}}{\sum_i [X_i]_{un-id}} \tag{4.3}$$

This derived k^* quantifies the reaction rate of all unidentified compounds in reaction with OH radicals, which gives in terms of chemical kinetics a further insight at each stage of an

TABLE 4.1: The OH rate constants k used in calculation of the OH reactivity (at room temperature and its temperature dependence).

Compound [a]	k **(298 K)** $(cm^3 molecule^{-1} s^{-1})$	k **(T)**	**Reference**
NO	1.0×10^{-11}	$7.4 \times 10^{-31}(T/300)^{-2.4}[N_2]$	IUPAC (Jun 2012)
NO_2	9.97×10^{-12}	$3.3 \times 10^{-30}(T/300)^{-4.5}[N_2]$	IUPAC (Jun 2012)
CO	2.41×10^{-13}	-	NIST (1997)
O_3	7.3×10^{-14}	$1.7 \times 10^{-12} \exp(940/T)$	IUPAC (Oct 2001)
acetaldehyde[b]	1.5×10^{-11}	$4.4 \times 10^{-12} \exp(365/T)$	Atkinson et al., 2003a
acetone[b]	1.7×10^{-13}	-	Atkinson et al., 2003a
acetic acid	6.9×10^{-13}	$4.0 \times 10^{-14} \exp(850/T)$	IUPAC (May 2009)
α-humulene	2.93×10^{-10}	-	Atkinson et al., 2003a
α-pinene[c]	5.23×10^{-11}	$1.21 \times 10^{-11} \exp(436/T)$	Atkinson et al., 2003a
β-caryophyllene	2.0×10^{-10}	-	IUPAC (Jun 2014)
benzene-D_6	1.14×10^{-12}	-	NIST (1986)
β-pinene[c]	7.43×10^{-11}	$1.55 \times 10^{-11} \exp(401/T)$	Atkinson et al., 2003a
butanone[b]	1.22×10^{-12}	$2.53 \times 10^{-18} T^2 \exp(503/T)$	Atkinson et al., 2003a
cyclohexanone	6.39×10^{-12}		NIST (1998)
ethanol	3.2×10^{-12}	$6.1 \times 10^{-18} T^2 \exp(530/T)$	Atkinson et al., 2003a
formaldehyde[d]	9.37×10^{-12}	$1.2 \times 10^{-14} T \exp(287/T)$	Atkinson et al., 2003a
formic acid	4.5×10^{-13}	-	IUPAC (Dec 2007)
hydroxyacetone	3.0×10^{-12}	-	NIST (2001)
isoprene[b]	1.01×10^{-10}	$2.56 \times 10^{-11} \exp(410/T)$	NIST (2002)
limonene[c]	1.64×10^{-10}	$4.28 \times 10^{-11} \exp(401/T)$	Atkinson et al., 2003a
mesitylene[b]	5.83×10^{-11}	-	NIST (1998)
methanol[b]	9.4×10^{-13}	$6.0 \times 10^{-18} T^2 \exp(170/T)$	Atkinson et al., 2003a
methyl vinyl ketone[b]	2.0×10^{-11}	$2.6 \times 10^{-12} \exp(610/T)$	Atkinson et al., 2003a
methacrolein	2.9×10^{-11}	$8.0 \times 10^{-12} \exp(380/T)$	Atkinson et al., 2003a
methylglyoxal	1.5×10^{-11}	-	Atkinson et al., 2003a
myrcene[c]	2.15×10^{-10}	-	Atkinson et al., 2003a
nopinone[b]	1.5×10^{-11}	-	Atkinson et al., 2003a
o-xylene[b]	1.36×10^{-11}	-	Atkinson et al., 2003a
phenol	3.27×10^{-11}	-	NIST (2002)
pinonaldehyde	4.4×10^{-11}	-	Atkinson et al., 2003a
toluene[b]	5.63×10^{-12}	$1.18 \times 10^{-12} \exp(338/T)$	Atkinson et al., 2003a
1-pentene[b]	3.14×10^{-11}	-	Atkinson et al., 2003a
1-butanol	8.5×10^{-12}	$5.3 \times 10^{-12} \exp(140/T)$	IUPAC (Aug 2007)
1,2-ISOPOOH	7.5×10^{-11}	–	St. Clair et al., 2015
4,3-ISOPOOH	1.18×10^{-10}	–	St. Clair et al., 2015
2-methylbut-3-en-2ol	5.6×10^{-11}	-	NIST (2007)
2-methylfuran	6.18×10^{-11}	-	NIST (1992)
2,3-dimethyl-2-butene	1.1×10^{-10}	-	Atkinson et al., 2003a
2,5-dimethylfuran	1.32×10^{-10}	-	NIST (1992)
3-carene[c]	8.8×10^{-11}	-	Atkinson et al., 2003a

[a] Compounds in bold are VOCs used as reactants in experiments.
[b] Sensitivity used in PTR-TOF-MS measurements is listed in A.2.
[c] Sensitivity used in PTR-TOF-MS measurements is listed in A.1
[d] Concentration taken from Hantzsch measurements if available, otherwise, a sensitivity of 10 [ncps/ppb] was used in PTR-TOF-MS measurements.

integral chemical reaction.
Overall uncertainties of the calculated total OH reactivity include random and systematic errors. Random errors from measurements precision dominated only in the low range of OH reactivity, and were not taken into account in this study as they were relatively small (< 2%

when the concentration was > 1 ppb). Systematic errors include the accuracy of each single measurement $[X_i]$, as well as the error of the respective rate constant k_{OH+X_i}. Only the most abundant VOC species making the largest contributions to the k_{OH}^{cal} (> 30%) and inorganic compounds were included in the uncertainty calculation. For all the other identified compounds making minor contributions to the k_{OH}^{cal}, an uncertainty of 25% was assumed.

TABLE 4.2: The error of rate constants k at 298K.

Substance	k_err **at 298K [%]**	**Source**
NO	10	IUPAC (Jun 2012)
NO_2	15	IUPAC (Jun 2012)
O_3	15	IUPAC (Oct 2001)
α-pinene	25	Atkinson et al., 2003a
acetaldehyde	20	Atkinson et al., 2003a
β-caryophyllene	15	IUPAC (Jun 2014)
β-pinene	25	Atkinson et al., 2003a
benzene-D_6	30	NIST (1986)
isoprene	20	NIST (2002)
ISOPOOH	16	St. Clair et al., 2015
formaldehyde	15	Atkinson et al., 2003a
limonene	20	Atkinson et al., 2003a
methacrolein	25	Atkinson et al., 2003a
methyl vinyl ketone	30	Atkinson et al., 2003a
phenol	10	NIST (2002)

Moreover, for experiments with SOA formation during VOC oxidations, the particulate surface act as an OH sink. In order to examine whether the contribution of aerosol can explain the observed missing OH reactivity, the OH reactivity of aerosol particles (k_p) was estimated by using the formula from IUPAC heterogeneous processes:

$$\frac{d[X]_g}{dt} = -k_p[X]_g = -\gamma\frac{\bar{c}}{4}[SS]_g[X]_g \tag{4.4}$$

$[X]_g$ = concentration of X in the gas phase (molecules cm^{-3})
c = mean thermal velocity of $[X]_g$ (m s^{-1})
$[SS]_g$ = specific surface area of the condensed phase (cm^{-1})
γ = reactive uptake coefficient, probability of a gas-phase molecule that collides with the surface will react with the surface (0-1).

where c is calculated from the gas kinetic theory and a mean value of 630 m s^{-1} was used for [OH]; γ for OH radicals on aerosol is difficult to measure, a γ value of 0.5 was used in the calculation (Chapleski et al., 2016). Note that a γ value of 1 could double the calculated OH reactivity of aerosols.

4.3 O/C ratio calculation

The atomic oxygen-to-carbon (O/C) ratio characterizes the oxidation state of VOCs, which increases along the oxidation process (t) and results to a ratio of 2 (O:C=2 as in CO_2) in a complete oxidation. The O/C ratio can be derived by elemental analysis of mass spectra obtained in the PTR-TOF-MS measurement, with the assigned empirical formula (which gives the corresponding atomic O/C ratio of compound i, $(O/C)_i$) for a mixture of compounds

and the respective concentration $[X_i]$:

$$(O/C)_t = \sum_i (O/C)_i \times [X_i]_t \tag{4.5}$$

In the atmosphere, aged air masses have a higher O/C ratio than air masses containing fresh released VOCs because of oxidation processes, thus by calculating the O/C ratio in one oxidation experiment, the variation of oxidation as a function of time can be tracked.

Chapter 5

Plant emitted BVOC measurements

The newly-built plant chamber SAPHIR-PLUS provides an environment in which parameters can be chosen for plant physiology investigation. Sufficient transfer efficiency from PLUS to SAPHIR ensures the use of the plant chamber as a source of BVOC emissions from real plants in atmospheric simulation experiments in SAPHIR. Seven sets of plants were used in this study, including isoprene-emitting trees, monoterpene-emitting trees, stressed trees and mixed tree species. The BVOC emissions measured in SAPHIR-PLUS are presented in this chapter.

5.1 Overall plant emissions

The overall monoterpene and sesquiterpene speciation for the seven sets of trees determined from the offline GC-FID/MS data is shown in Table 5.1. Emissions of each plant set were sampled in SAPHIR-PLUS with absorbent tubes at the highest light intensity. Numbers in brackets indicate the measured mixing ratios, note that the concentrations of isoprene were obtained with the PTR data.
Five most abundant monoterpenes (α-pinene, β-pinene, Δ^3-carene, limonene, myrcene) were calibrated with the PTR-TOF-MS, their sensitivities can be found in *AppendixA*. The other monoterpenes detected by the offline GC-FID/MS were grouped into these 5 compounds, according to their rate constants in reaction with OH radicals (see Table 4.1). Only two sesquiterpenes(β-caryophyllene and α-humulene) having considerable proportions are listed in Table 5.1, other sesquiterpenes were also grouped into these 2 compounds with their rate constants in reaction with OH.
Comparisons with reported emission of different tree species are also laid out in Table 5.1. The emission of *Quercus ilex* was mainly monoterpenes but only a small amount of isoprene, which was in accordance with the findings from Staudt et al., 1995 and Kesselmeier et al., 1999. The highest emitted monoterpene was α-pinene as expected. No sesquiterpenes were detected by the offline GC-FID/MS, suggested that the status of the six *Quercus ilex* was "normal". By contrast, more sesquiterpenes than monoterpenes were detected in the *Picea abies* emission, indicating a "stressed" status of these six trees. For this tree species, no β-pinene was detected, but the β-pinene/sabinene accounted for 20% in the study of Grabmer et al., 2006, the rest monoterpene composition was similar to their findings. The six *Betula pendula* were also considered as "stressed" as high sesquiterpenes emissions were detected. *Quercus robur* as an isoprene emitter, showed low concentrations of monoterpenes and sesquiterpenes during the peak emission. The set of six *Pinus sylvestris* was used for two campaigns through a long period, therefore its emission was sampled in three times with one-week interval. The emissions of isoprene and sesquiterpenes were fairly small comparing to the large amount of monoterpenes emitted by our *Pinus sylvestris*. A big quantity of Δ^3-carene but a few α-pinene were found for the six *Fagus sylvatica*, this did not match the observation from Kim et al., 2011, where the major monoterpene emission was α-pinene. The mix trees comprised three *Pinus sylvestris* and three *Fagus sylvatica* emitted unexpectedly higher quantity of β-

TABLE 5.1: Plant emissions detected in SAPHIR-PLUS in comparison with emissions reported in the literature. Monoterpene and sesquiterpene speciations were obtained with the offline GC data. Numbers in brackets indicating measured mixing ratios in ppb. Mixing ratios of isoprene were from the PTR measurements.

Tree species	Monoterpenes speciation (%)					sesquiterpenes speciation (%)		isoprene	Reference
	α-pinene	β-pinene	Δ^3-carene	limonene	myrcene	α-humulene	β-caryophyllene		
Quercus ilex	28.0 (2.1)	19.0 (1.4)	23.0 (1.7)	17.6 (1.3)	12.4 (0.9)	-	-	(0.4)[a]	This work
	~40	~ 30	~18[b]	0	2	-	-	-	Staudt et al., 1995
	43	28	29[b]	0	0	-	-	-	Staudt et al., 1998
	34.2	22.2	26.1	9.6	7.9	-	-	-	J. Kesselmeier et al., 1997
Picea abies	43.1 (0.5)	0.0 (0.0)	4.3 (0.1)	27.8 (0.3)	24.8 (0.3)	0.0	100.0 (5.1)	(0.5)[a]	This work
	42	20[c]	7	27	4	-	-	-	Grabmer et al., 2006
Betula pendula	14.1 (0.5)	0.0	8.3 (0.3)	26.4 (1.0)	51.2 (2.0)	18.7 (1.0)	81.3 (4.2)	(0.6)[a]	This work
Quercus robur	49.4 (0.1)	0.0	0.0	0.0	50.6 (0.1)	4.0 (0.01)	96.0 (0.2)	(106)[a]	This work
Pinus sylvestris	16.1 (5.0)	2.6 (0.8)	61.2 (19.0)	6.6 (2.1)	13.5 (4.2)	0.0	100.0 (1.8)	(0.7)[a]	This work
	34.4 (20.6)	3.8 (2.3)	47.1 (28.2)	6.0 (3.6)	8.7 (5.2)	1.0 (0.05)	99.0 (4.0)	(1.3)[a]	This work
	19.0 (21.0)	1.9 (2.1)	61.4 (68.1)	5.3 (5.9)	12.4 (13.7)	3.6 (0.07)	96.4 (2.0)	(2.2)[a]	This work
	23-64	2-7	1-60	0-13	2-5	-	-	-	Janson et al., 2001
	45.5	9	39.6	2.3	3.3	-	-	-	Bäck et al., 2012
Fagus sylvatica	1.4 (0.3)	1.1 (0.2)	40.9 (8.4)	40.7 (8.4)	15.9 (3.3)	0.5 (0.02)	99.5 (3.5)	(1.0)[a]	This work
	54	9	2	30	5	-	-	-	Kim et al., 2011
Mix trees	31.7 (6.2)	21.8 (4.2)	20.8 (4.0)	12.2 (2.4)	13.5 (2.6)	1.6(0.05)	98.4(2.9)	(0.8)[a]	This work

[a] concentration measured by the PTR-TOF-MS.
[b] sabinene
[c] β-pinene/sabinene

pinene but lower proportion of Δ^3-carene comparing to the emissions from these two trees species.

5.2 Light- and temperature-dependent plant emissions

The evergreen *Quercus ilex* (Holm oak) is reported to be an important mediterranean monoterpenes emitter with small quantity of methanol and isoprene emissions. BVOC emissions monitored in this study were dominated by monoterpenes, minor emissions of isoprene and methanol were also observed with the overall emission pattern typical for *Quercus ilex* trees in the growing season (Kesselmeier et al., 1999; Staudt et al., 1998). One example of the *Quercus ilex* emission of monoterpenes (red circles) and isoprene (blue triangles) is shown in Figure 5.1. Monoterpenes emission was close to zero when the lights were off in SAPHIR-PLUS and gradually escalated with light intensity. The highest concentration ($\sim$ 13 ppb) in that day was observed shortly after the light maximum, then dropped rapidly with light intensity. Same diurnal emission behavior for isoprene despite its small emitted amount (< 0.5 ppb).

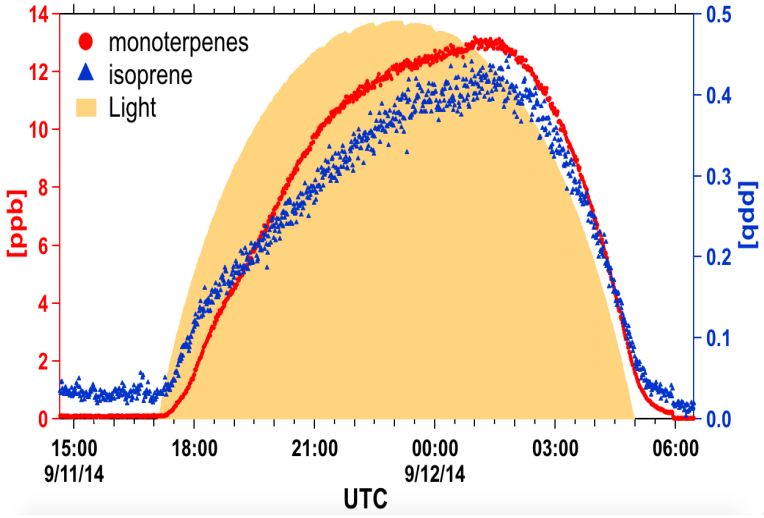

FIGURE 5.1: Observed monoterpenes (red circles, scale on the left) and isoprene (blue triangles, scale on the right) emissions from *Quercus ilex*. Light condition is shown in yellow background.

VOCs are produced in plant leaves and released into the atmosphere by passing through the stomata. Some VOCs can be stored after synthesis in special cells or organs and their release is regarded as a volatilization out of storage organs. Other VOCs do not have storage pools in the plant organs so their synthesis and emissions are directly interrelated (Kesselmeier et al., 1999).

Monoterpenes and methanol are reported to be stored in plant secretory tissues whereas isoprene is reported to have no storage pool found in any plants (Kesselmeier et al., 1999; Niinemets et al., 2003; Rapparini et al., 2004). For these three compounds, Figure 5.2 shows the dependence of their relative emissions on light intensity at three different air temperatures. Emissions were normalized with the emission at the maximum illumination ($C/C_{I,max}$). As already acknowledged, monoterpenes and isoprene relative emissions by *Quercus ilex* responded strongly to the diurnal cycle of light intensity (Figure 5.2, upper and middle panel).

Their relative emissions were close to 0 under dark conditions and reached the maximum slightly after the highest light intensity. The normalized isoprene and monoterpenes emission responses to light in all temperature regimes exhibited similar patterns. Isoprene emission was found to be triggered by illumination and is never stored in plants after its production as no isoprene storage exists (Kesselmeier et al., 1999). Monoterpenes emission in our study seemed to be directly linked to a photosynthesis-dependent process as well. Previous studies regarding *Quercus ilex* also pointed out that for this tree species, monoterpenes emission responses to light are similar to isoprene, as no monoterpenes storage pools exist, hence the emissions are more related to actual photosynthetic activity than to temperature (Kesselmeier et al., 1999; Staudt et al., 1995, 1993).

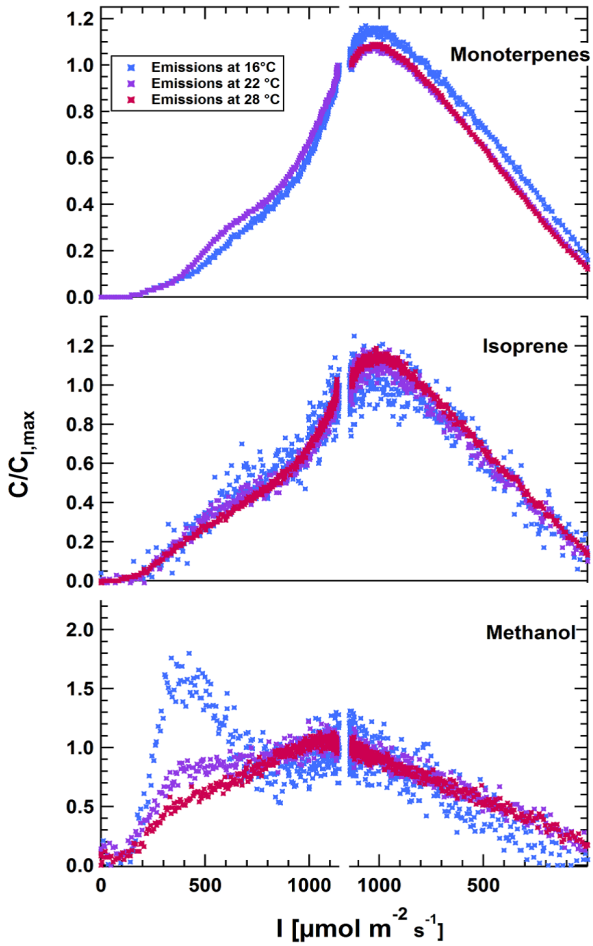

FIGURE 5.2: Response of emissions to light intensity for *Quercus ilex* under different temperature conditions. Concentrations of monoterpenes, isoprene and methanol were normalized with observed concentrations at maximum light intensity ($C_{I,max}$)

Methanol relative emission emerged an abrupt escalation shortly after the beginning of illumination. This was more pronounced at lower temperature regimes after normalization, since $C_{I,max}$ was smaller under lower temperature conditions (Figure 5.2, lower panel). This phenomenon has been observed previously for different plant species both in field and laboratory experiments under controlled conditions (Folkers et al., 2008; Kesselmeier et al., 1999; Niinemets et al., 2003). The reason of the large burst of VOC emission in the morning was described by physic-chemical processes: during darkness when stomata are nearly closed, the plant produced soluble VOCs (i.e., carboxylic acid, aldehydes, alcohols) are accumulated in aqueous phase in the plant leaves; in the morning, when stomata open, VOCs are released as a pulse in gas phase into the atmosphere. The observed morning eruption were the most evident for methanol in our study due to its high emission rate from *Quercus ilex* and its high solubility in water (Folkers et al., 2008; Niinemets et al., 2003).
For the temperature dependence study, 4 hours averaged peak emissions around simulated noon time were normalized to the peak emissions at 30 °C (also 4 hours averaged data at peak illumination), results are shown in Figure 5.3. The monoterpenes relative emissions (red circles) responses to temperature followed an exponential escalation from 13 to 31°C, confirming the well-known strong temperature dependency of monoterpenes emissions from *Quercus ilex*. In previous emission studies, a formula described by Tingey et al., 1980 is usually used to simulate the temperature dependence of monoterpenes emission:

$$E = E_s \times exp[\beta \times (T - T_s)] \tag{5.1}$$

E is the emission at temperature T, E_s is the emission at standard temperature T_s of 30 °C, the slope β found in the literature ranges between 0.057 and 0.144 $°C^{-1}$. A generally accepted average slope value of 0.09 $°C^{-1}$ (Guenther, 1993) was plotted in Figure 5.3. In this study, monoterpenes emissions increased with a slope of 0.11 $\pm$ 0.02 $°C^{-1}$ which is in good agreement with the literature.

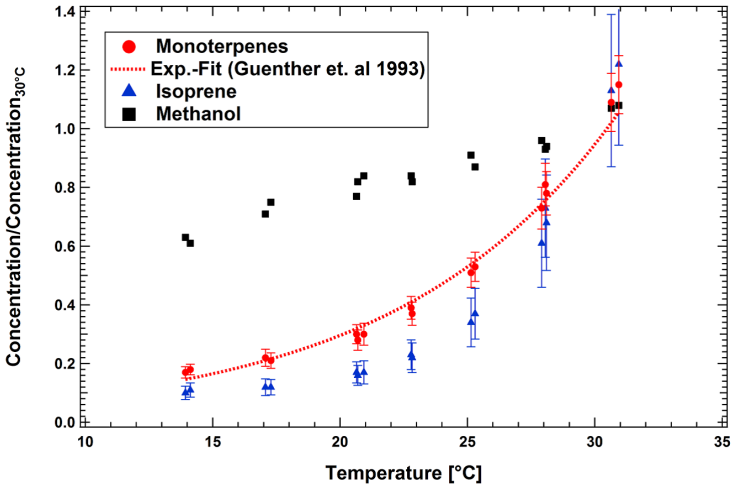

FIGURE 5.3: Response of emissions to increases in temperature for *Quercus ilex*. Error bars were calculated by using error propagation based on the standard deviation for the concentration at 30 °C and the measured temperatures. An empirical slope of 0.09 (Guenther, 1993) is shown as the red dotted line.

Isoprene relative emission (blue triangles) also exhibited an exponential increase with temperature, this can be explained by an enzyme activation: the enzyme isoprene synthase is activated with rising temperature, leading to increased emissions. It is worth mention that an enzyme denaturation was also found at high temperatures (i.e., > 33 °C) reducing emissions (Guenther, 1993).
Methanol relative emission (black squares) on the other hand escalated linearly with temperature, with a 10% increase in peak emissions every ∼4 °C in the temperature range from 13 to 31 °C. Results of characteristics of plant emissions were published on Atmospheric Measurement Techniques as Hohaus et al., 2016.

Chapter 6

Product yields from BVOCs oxidations

Product yields give insight on the atmospheric fate of VOCs, yet few studies of product yields from plant emitted BVOCs oxidation have been reported. In this chapter, product yields determined from BVOC oxidations with different complexity of the BVOC systems are listed and compared to the literature: from single monoterpene (β-pinene and limonene) ozonolysis and the single isoprene photo-oxidation, to the monoterpenes mixture ozonolysis, and at last to the tree-emitted BVOCs oxidation.

6.1 Single BVOCs

The first set of experiments includes oxidation of three single BVOCs: isoprene, β-pinene and limonene, which are among the most abundant tree-emitteded BVOCs in ambient air (Grosjean et al., 1993; Guenther et al., 2012).
An example of the monitored VOCs variations is demonstrated (Figure 6.1) for the ozonolysis of β-pinene, with a time resolution of 1 min. Gaps are measurements in the plant chamber SAPHIR-PLUS, that are not discussed here. At the beginning of the experiment, overnight

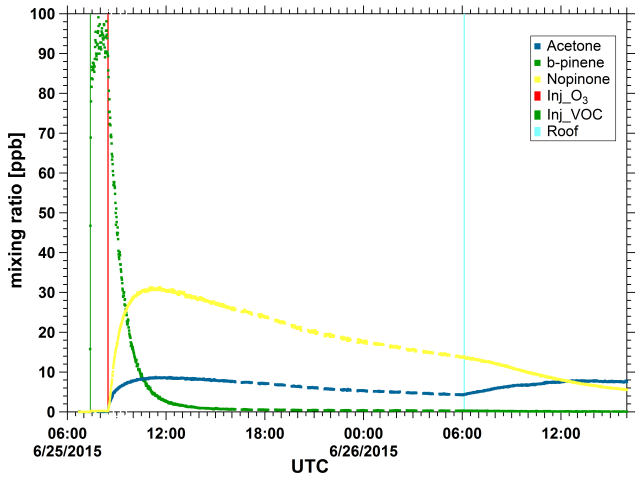

FIGURE 6.1: Time series of observed concentration (ppb) of the injected β-pinene and its major products. Vertical lines show the times of addition of VOCs (green), O_3 (red), and the time when roof was opened (blue).

purged SAPHIR was humidified to the set humidity of 60%, background measurements were made after the completion of humidification. Afterwards, β-pinene (m/z 137, green dots in the figure) was injected into the chamber to achieve a proposed mixing ratio of 120 ppb,

the adding time is marked with the green vertical line. Yet approximately 100 ppb were detected by the PTR-TOF-MS, resulting in a recovery of 0.83. After quantifying the initial concentration of β-pinene, O_3 was added about one hour later (red vertical line) and the mixture was kept in the dark overnight. The initial conditions of relative humidity and the concentrations of all additives can be seen in Table 3.2. The chamber roof was opened the next morning (blue vertical line) in order to produce OH radicals from photolysis of O_3 and HONO. During the initial phase of the ozonolysis, concentrations of nopinone (m/z 139, yellow dots) and acetone (m/z 59, dark blue dots) were found to raise proportionally to the consumption of β-pinene, less than 10% of β-pinene was left in the chamber after 2 hours. A large production of nopinone of over 30 ppb in concentration was observed the first 90 min after O_3 injection, the acetone formed was about 9 ppb. Concentrations seen here were all before dilution corrections (Chapter 4.1). The molar yield of formed nopinone and acetone were 0.41±0.04 and 0.1±0.09, respectively.

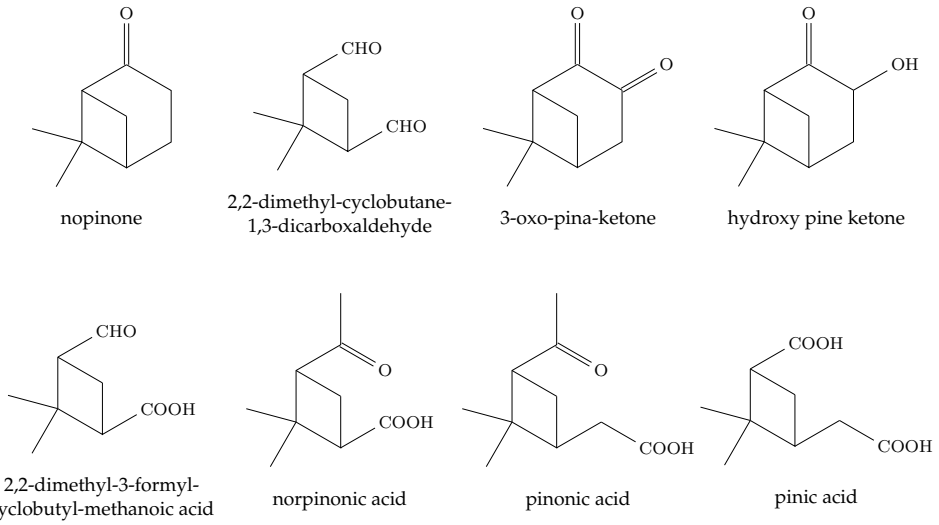

FIGURE 6.2: Structure of high mass products from β-pinene ozonolysis.

Table 6.1 lists detected products with their molar yields from the reaction of β-pinene ozonolysis, together with yields reported in the literature (in italic). Nopinone is long known as the major product from the reaction of β-pinene with OH and O_3, its structure together with that of other high-molecular products are shown in Figure 6.2. Previous studies reported nopinone molar yields vary from 0.158-0.17 to 0.51 $\pm$ 0.09 for the β-pinene/O_3 reaction. A nopinone molar yield of 0.41 $\pm$ 0.04 was determined in our study. Considering that the reaction of β-pinene with O_3 produces hydroxyl radicals (Atkinson et al., 2003b), our high nopinone yield could be influenced by nopinone formed in the β-pinene/OH reaction. Our nopinone yield is in agreement with that determined by Hatakeyama et al., 1989, where no OH scavenger was used as well. Further, H_2O has shown to affect the yields of nopinone regarding experiments performed in the presence of cyclohexane as OH scavenger (Winterhalter et al., 2000). Hakola et al., 1994 and Lee et al., 2006 conducted their experiment at relative humidities of ∼5%. The H_2O concentrations were not reported in other studies in the presence of cyclohexane (Grosjean et al., 1993; Yu et al., 1999), these experiments were assumed to be performed under dry conditions. In fact, in the study of Winterhalter et al., 2000, a higher nopinone yield of 0.51 $\pm$ 0.09 was found at high relative humidity (∼ 50%),

comparing to the low nopinone yield of 0.16 ± 0.04 under dry condition (∼ 5% of relative humidity). Note that our experiment was conducted under high humidity (60%) condition in order to better compare the result to plant emitted β-pinene ozonolysis in a natural environment.

TABLE 6.1: Products formed, and their yields, from the reactions of β-pinene with O_3.

m/z detected	Chemical formula	Substance	Yield	Reference
139	$C_9H_{14}O$	nopinone	0.41±0.04	This work
			0.4±0.02	Hatakeyama et al., 1989
			0.22[a]	Grosjean et al., 1993
			0.23±0.05[a]	Hakola et al., 1994
			0.158-0.17[a]	Yu et al., 1999
			0.16±0.04[a]	Winterhalter et al., 2000
			0.51±0.09[ab]	Winterhalter et al., 2000
			˜0.4[a]	Atkinson et al., 2003b
			0.17±0.02[a]	Lee et al., 2006
59	C_3H_6O	acetone	0.1±0.09	This work
			0.07±0.05[a]	Reissell et al., 1999
			0.04[a]	Atkinson et al., 2003b
			0.009±0.009[a]	Atkinson et al., 2003b
			0.036±0.003[a]	Lee et al., 2006
47	CH_2O_2	formic acid	0.15±0.05	This work
			0.02-0.05[a]	Atkinson et al., 2003b
			0.04±0.004[a]	Lee et al., 2006
141	$C_8H_{12}O_2$	2,2-dimethyl-cyclobutane-1,3-dicarboxaldehyde	0.02±0.01	This work
			0.0029-0.0035[a]	Yu et al., 1999
153	$C_9H_{12}O_2$	3-oxo-pina-ketone	0.14±0.04	This work
			0.018-0.076[a]	Yu et al., 1999
			0.061±0.01[a]	Lee et al., 2006
155	$C_9H_{14}O_2$	hydroxy pine ketone	0.14±0.04[c]	This work
			0.15±0.05	Winterhalter et al., 2000
			0.066-0.079[a]	Yu et al., 1999
			0.047±0.01[a]	Lee et al., 2006
157	$C_8H_{12}O_3$	2,2-dimethyl-3-formyl-cyclobutyl-methanoic acid	0.01±0.003[c]	This work
171	$C_9H_{14}O_3$	norpinonic acid	0.01±0.002[c]	This work
			0.046-0.143[a]	Yu et al., 1999
			0.001±0.0003[a]	Lee et al., 2006
185	$C_{10}H_{16}O_3$	pinonic acid	0.02±0.004[c]	This work
			0.0041-0.0056[a]	Yu et al., 1999
			0.011±0.003[a]	Lee et al., 2006
187	$C_9H_{14}O_4$	pinic acid	0.001±0.001[c]	This work
			0.017-0.025[a]	Yu et al., 1999
			0.02±0.01[a]	Winterhalter et al., 2000

[a] In the presence of an OH scavenger.
[b] At higher relative humidity.
[c] Considered as a secondary product.

As for acetone, a molar yield of 0.1 ± 0.09 was observed, slightly higher (yet within the uncertainty) than in other studies where an OH scavenger was added. Figure 6.3.a shows the correlation between concentrations of consumed β-pinene and formed acetone in ppb. As explained in Chapter 4.1, both concentrations were corrected for the dilution loss and the C_t was chosen when 90% of the reactant was consumed. Figure 6.3.b lays out variations of consumed β-pinene and acetone yield as a function of time. To get a more comprehensive picture, a longer period is plotted, which starts 10 mins before the O_3 injection and ends several hours after the oxidation. At the first 60 mins of the oxidation, a higher acetone yield of up to 0.19 was observed. This high yield could be due to the β-pinene/OH reaction, since the β-pinene/O_3 reaction also produces OH radicals as reported in previous studies ($0.35^{+0.18}_{-0.12}$ in yield, Atkinson et al., 2003b). Additionally, acetone yields of 0.13 and 0.27 from OH-initiated oxidation of β-pinene were found by Wisthaler et al., 2001 and by Kaminski, 2014, respectively, both were higher than the reported acetone yields of reaction between β-pinene with O_3.

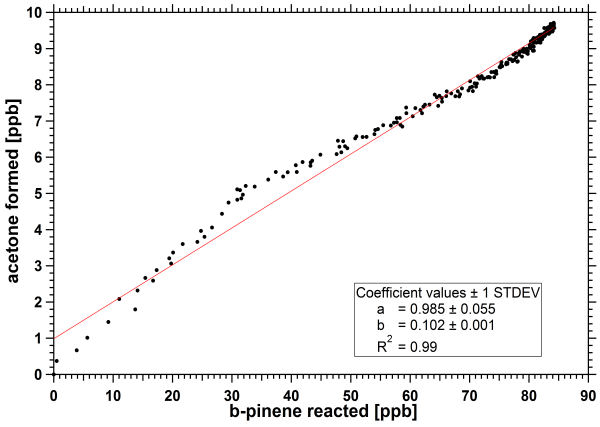

a) Acetone yield from β-pinene ozonolysis.

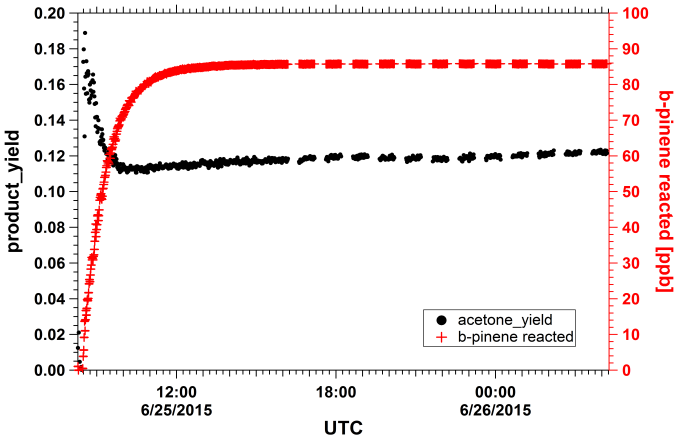

b) Acetone yield and consumed β-pinene as a function of time.

FIGURE 6.3: Measured yield of acetone from the β-pinene/O_3 reaction.

The highest reported formic acid yield from β-pinene ozonolysis was 0.04 $\pm$ 0.004 (Lee et al., 2006), where experiments were conducted at < 10% relative humidity. Our humid experimental condition could be the cause of the large disagreement (0.15 $\pm$ 0.05 in this study) on the formic acid yield.
Hydroxy pine ketone detected at m/z 155 in the PTR-TOF-MS spectra was quantified with an assumed sensitivity of 10 ncps/ppb and had a yield of 0.14 $\pm$ 0.04 from the β-pinene ozonolysis, whereas a yield in the range between 0.047 and 0.15 was found in the literature. The produced hydroxy pine ketone was not linear to the consumed β-pinene. It revealed a suppressed increase along the amount of reacted β-pinene, and a higher value after the total consumption of β-pinene (see Figure C.1 in $AppendixC$). Potential losses on the chamber walls at the beginning of the experiment may result in the suppressed increase. Nevertheless, this behavior fit the conjecture of Winterhalter et al., 2000, where the hydroxy pine ketone was reckoned a secondary product.
The 3-oxo-pina-ketone yield was 0.14 $\pm$ 0.04, much higher compared to 0.018-0.076 reported in previous studies. 3-oxo-pina-ketone at m/z 153 was also quantified with the assumed sensitivity, more, the signal detected at m/z 153 was only tentatively assigned as 3-oxo-pina-ketone according to the reported product m/z from β-pinene ozonolysis. PTR measurements cannot determine if one particular compound completely represents an observed oxidation product mass. Signals at m/z 153 could be interfered by other substances/fragments as the PTR cannot separate isomeric compounds, plus the 3-oxo-pina-ketone could itself, fragment onto other m/z. Consequently, the mixing ratio of 3-oxo-pina-ketone might be possibly overestimated or underestimated. This study gives a reference of observed product yields and compares them to the literature, products might even be named differently but were proposed the same structure in different studies. We try to explain the disagreement between our observation and other studies. The yields in the previous studies have been determined under different conditions (e.g., the reactant concentration level, the temperature and the relative humidity). It is very difficult to distinguish whether a measurement error or the measurement conditions are the reason for differences among the reported yields.
The other high mass product yields were low and exhibited slight disagreement with previous studies, their structures could be seen in Figure 6.2. 2,2-dimethyl-cyclobutane-1,3-dicarboxaldehyde yield was 0.02 $\pm$ 0.01 in this study, yet an even lower yield of 0.0029-0.0035 was reported by Yu et al., 1999. They also identified the product 2,2-dimethyl-3-formyl-cyclobutyl-methanoic acid, unfortunately no yield was reported there, whereas a yield of 0.01 $\pm$ 0.003 was observed in our experiments. The rest high mass acids: norpinonic acid, pinonic acid, and pinic acid, having nominal reported yields (< 0.02) were observed with low yields in this study as well. All correlations between the formed product and the consumed reactant, together with time series of the consumed reactant and the product yield could be found in $AppendixC$.
Limonene, a monoterpene with two double bounds, one endo- and one terminal, is reported to have a very high potential to be an important source of biogenic SOA (Maksymiuk et al., 2009; Zhang et al., 2006), yet its gas-phase oxidation products were not well characterized. Ozone reacts with limonene via addition to the two unsaturated carbon-carbon double bonds. Grosjean et al., 1993 found that the observed product limona ketone (4-acetyl-1-methylcyclohexene) were consistent with ozone addition on the terminal C=C bond and no carbonyl products were directly formed by the addition of ozone on the endo- double bond. However, Zhang et al., 2006 reported that the terminal double bond was oxidized simultaneously with the endo- double bond. Nørgaard et al., 2006 also observed that the product limonene endo-ozonide at the high mass of 185 amu was formed secondarily by ozone addition on the endo- double bond in the gas-phase ozonolysis of limonene. The proposed structure of the secondary endo-limonene ozonides and the isomeric limononic acid are shown in Figure 6.4, together with structures of some other high mass products from

limonene ozonolysis.

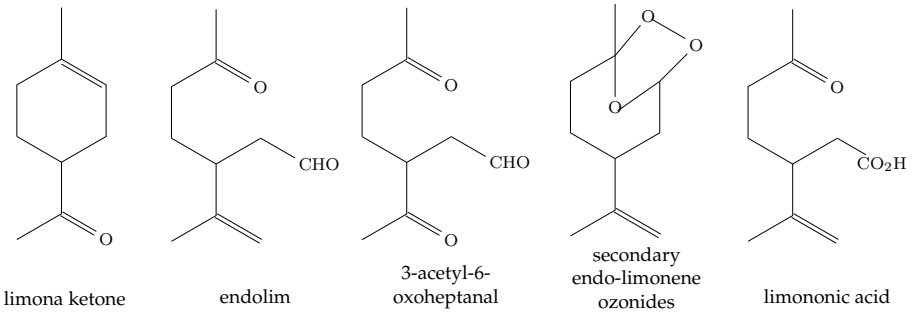

FIGURE 6.4: Structure of high mass products from limonene ozoznolysis.

No significant oxidation products from the reaction of limonene with O_3 were reported by previous studies (see Table 6.2). Reissell et al., 1999 investigated the acetone formation in the limonene ozonolysis and found an acetone yield smaller than 0.02. Hakola et al., 1994 detected limona ketone (4-acetyl-1-methylcyclohexene) as the only gas-phase product from dark limonene ozonolysis with a molar yield less than 0.04. Grosjean et al., 1993 found the formation of both formaldehyde (0.1) and limona ketone (0.02). Atkinson et al., 2003b iden-

TABLE 6.2: Products formed, and their yields, from the reactions of limonene with O_3.

m/z **detected**	**Chemical formula**	**Substance**	**Yield**	**Reference**
47	CH_2O_2	formic acid	0.16±0.04	This work
			0.03-0.1[a]	Atkinson et al., 2003b
59	C_3H_6O	acetone	0.02±0.002	This work
			< 0.02[a]	Reissell et al., 1999
			∼0.02[a]	Atkinson et al., 2003b
61	$C_2H_4O_2$	acetic acid	0.16±0.02	This work
139	$C_9H_{14}O$	limona ketone	0.01±0.003	This work
			≤0.04[a]	Hakola et al., 1994
			0.02[a]	Grosjean et al., 1993
			˜0.01[a]	Atkinson et al., 2003b
			0.0076±0.0008	Ham et al., 2016
			0.0081±0.0009[a]	Ham et al., 2016
169	$C_{10}H_{16}O_2$	endolim	0.008±0.003	This work
			˜0.01[a]	Atkinson et al., 2003b
			0.16±0.005	Ham et al., 2016
			0.05±0.008[a]	Ham et al., 2016
171	$C_9H_{14}O_3$	3-acetyl-6-oxoheptanal	0.003±0.001	This work
			0.015±0.002	Ham et al., 2016
185	$C_{10}H_{16}O_3$	limononic acid	0.006±0.002	This work
			0.021±0.001	Ham et al., 2016
			0.019±0.003[a]	Ham et al., 2016

[a]In the presence of an OH radical scavenger.

tified the two mentioned products with yields of 0.19 and ∼0.01, respectively, as well as the formation of endolim (3-isopropenyl-6-oxo-heptanal, 0.01), acetone (0.02), and formic acid (0.03-0.1).
Ham et al., 2016 studied the limonene ozonolysis in both the presence/absence of an OH scavenger and observed 5 major products, the 2-acetyl-5-oxohexanal (m/z 156) reported in their study could not be attributed to detected masses here.
Acetone yield in our experiment was 0.02 ± 0.002 in accordance with the previous yield reports. The most common products limona ketone and endolim molar yields observed here were 0.01 ± 0.003 and 0.008 ± 0.003, respectively, both were in agreement with reported yields. The product 3-acetyl-6-oxoheptanal observed at m/z 171 had a yield of 0.003 ± 0.001, Ham et al., 2016 reported a 3-acetyl-6-oxoheptanal yield of 0.015 ± 0.002 from the limonene + O_3 reaction but this product was not observed when cyclohexane was added as an OH scavenger. Limononic acid at m/z 185 having a yield of 0.006 ± 0.002 is also smaller than the two values reported by Ham et al., 2016, with or without an OH scavenger. Note that their experiments were also conducted in a humid chamber (50% of relative humidity), though no humidity influence on the limonene ozonolysis product has been reported. A high formic acid yield of 0.16 ± 0.04 was observed, comparing to that of 0.03-01 reported by Atkinson et al., 2003b. The acetic acid yield determined in this study was 0.16 ± 0.06 yet its yield has not been reported from the limonene ozonolysis.
The dominant loss mechanism for isoprene in the atmosphere is reaction with OH radicals (Guenther, 1993; Sprengnether et al., 2002). The organic peroxy radicals (RO_2) formed from the OH-initiated isoprene oxidation primarily reacts with either HO_2 or with NO, the latter is well-known anthropogenic in origin. Under pristine low NO conditions, reactions with HO_2 dominate the fate of RO_2, to form hydroperoxides (ISOPOOHs). On the other hand under polluted urban conditions, reactions with NO lead to the formation of formaldehyde and MVK/MACR and HO_2 radicals that react in turn with NO to regenerate OH and form NO_2 (Fuchs et al., 2013; Peeters et al., 2014; Rivera-Rios et al., 2014; St. Clair et al., 2015). The chemical structure of the four major products are shown in Figure 6.5.

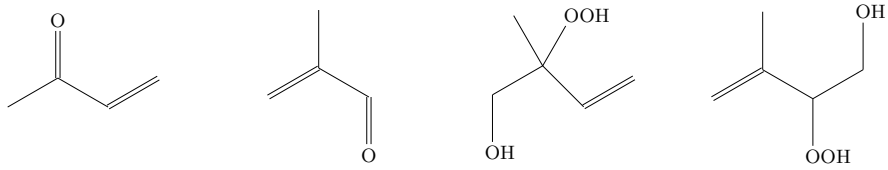

FIGURE 6.5: Structure of products from isoprene photo-oxidation.

Isoprene photo-oxidation products presented here were all corrected for both dilution loss and chamber source, since experiments were conducted under sunlight irradiation. Previous studies reported the major oxidation products MVK + MACR yields range from 0.52 ± 0.02 to 0.72 ± 0.07 under high NO conditions, a yield of 0.68 was calculated by Galloway et al., 2011 with the Leeds Master Chemical Mechanism (MCM) v. 3.2. In this study, MVK + MACR yields of 0.79 ± 0.15 at high NO level (> 1 ppb) and of 0.83 ± 0.16 under middle NO condition (∼0.5 ppb) were observed (Table 6.3), this was slightly higher than reported yields but were consistent within experimental uncertainties. A few studies reported ISOPOOHs yield from isoprene photo-oxidation at low NO level. The molar yield of ISOPOOHs was 0.8 ± 0.15 in our experiment, in reasonable agreement with yields obtained by Paulot et al., 2009b (> 0.7). The time series of products yields under different NO conditions exhibited interesting differences (Figure 6.6). Under high- and mid- NO conditions (Figure 6.6.a and b), MVK +

TABLE 6.3: Products formed, and their yields, from the reactions of isoprene with OH radicals at different NO levels

m/z detected	Formula	Substance	Yield (high NO)	Yield (mid NO)	Yield (low NO)[a]	Reference
71	C_4H_6O	MVK+MACR	0.79±0.15	0.83±0.16		This work
			0.54±0.12[b]			Tuazon et al., 1990
			0.61±0.06			Atkinson et al., 2003b
			0.54±0.07			Atkinson et al., 2003b
			0.72±0.07			Sprengnether et al., 2002
			0.68±0.04			Karl et al., 2006
			0.66			Paulot et al., 2009a
			0.52±0.02			Galloway et al., 2011
			0.68[c]			Galloway et al., 2011
			0.7±0.03			Liu et al., 2013
71	$C_5H_{10}O_3$	ISOPOOH			0.8±0.15	This work
					> 0.7	Paulot et al., 2009b
73	$C_3H_4O_2$	methylglyoxal	0.12±0.02[d]	0.17±0.05[d]	0.19±0.06[d]	This work
			0.042[e]			Galloway et al., 2011

[a] Added O_3 as a NO scavenger.
[b] Corrected by Atkinson, 1997 to take into account $O(^3P)$ atom reactions.
[c] Calculated with MCM v.3.2 for high NO_x conditions.
[d] Considered as a secondary product.
[e] Inferred from the mechanism presented by Paulot et al., 2009a.

MACR yields revealed a prompt increase to more than 1 at the beginning of the oxidation. As the chamber source has been corrected, this abnormal high yield could be from bias on the MVK + MACR concentration. Signals at m/z 71 in the PTR measurements were evaluated with only MVK sensitivity, the PTR might be more sensible for monitoring MACR, lead to a slight overestimation on the concentration, and this could affect the momentary yield determination since small amount of isoprene (∼2.4) was used in the experiments. However, the PTR measurements provided an insight on the MVK + MACR yield variation over the time, it decreased along the whole experiment, indicating the instant reaction of both compounds to form higher generation products. On the other hand, ISOPOOHs yield under low-NO conditions (Figure 6.6.c) emerged a gradual increase after the photo-oxidation started, its yield also dropped during the photo-oxidation, yet the decrease was much slower than that of MVK + MACR. The IEPOX formed from the reaction of ISOPOOHs oxidation, having fragments also at m/z 71, could affect the observed ISOPOOHs yield and cause this lingering decrease. As mentioned in Chapter 2.1.3, signals at m/z 71 were treated with only ISOPOOH sensitivity and roughly divided by 2 to get the ISOPOOHs concentration.
Theoretical work of Dibble, 2004 suggested a mechanism for methylglyoxal formation as a first-generation product from isoprene oxidation under high NO_x conditions. Paulot et al., 2009a sketched a mechanism of OH-initiated oxidation of isoprene under high NO_x conditions, revealing the formation of methylglyoxal in several first steps of the oxidation. Galloway et al., 2011 inferred a methylglyoxal yield of 0.042 from the mechanism presented by Paulot et al., 2009a, and developed a new isoprene oxidation scheme laying out that the methylglyoxal production can be first-generation production from isoprene, and secondary production via MVK, MACR. They have also reported the methylglyoxal yield from OH reactions with MVK and MACR being 0.24 ± 0.001 and 0.08 ± 0.005, respectively. Time series of methylglyoxal yields in this study revealed continuous increase during the whole oxidation (*AppendixC*, Figure C.3, Figure C.4, and Figure C.5), implying its secondary production from the isoprene oxidation products. The methylglyoxal yields were from 0.12 ± 0.02 to 0.19

$\pm$ 0.06 at different NO levels, with the highest yield being observed surprisingly in low-NO experiment. Methylglyoxal was indeed reported as higher-generation product in the reaction scheme of low-NO isoprene photo-oxidation (Peeters et al., 2014), yet no molar yield was given. Jacobs et al., 2013 reported a yield of 0.12 of methylglyoxal from IEPOX—the well-known high-generation isoprene photo-oxidation product at low-NO level.
We also observed the formation of formic and acetic acids, however, the correlations between produced acids and consumed isoprene manifested poor linearity (< 0.3), so their yields were not discussed in this study.

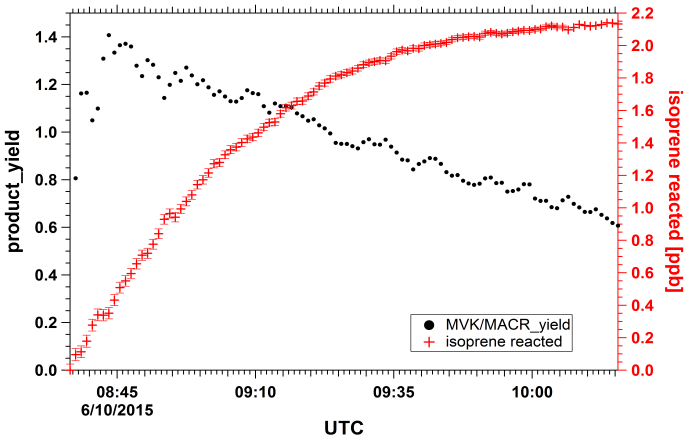

a) At high-NO level, MVK + MACR yield and consumed isoprene as a function of time.

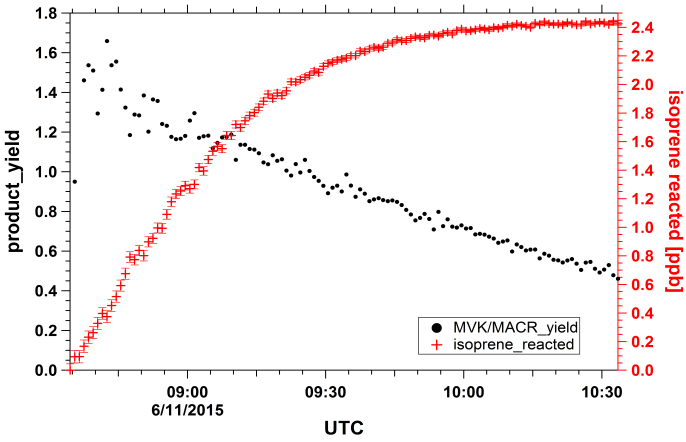

b) At mid-NO level, MVK + MACR yield and consumed isoprene as a function of time.

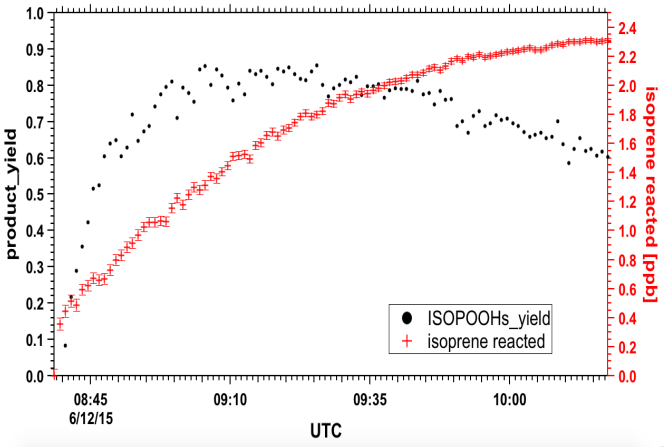

c) At low-NO level, ISOPOOHs yield and consumed isoprene as a function of time.

FIGURE 6.6: First-generation products yields from isoprene photo-oxidations.

6.2 BVOC mixture

Product yields from the ozonolysis of two monoterpene mixtures (Exp.BM1 and BM2) are listed in Table 6.4, together with yields calculated (in italic) from the literature, and from the single BVOC ozonolysis yields reported above. The formic acid yield was 0.2 ± 0.05 in the β-pinene and limonene mixture (Exp.BM1), higher than the yields obtained in both ozonolysis of single β-pinene (0.15 ± 0.05) and single limonene (0.16 ± 0.04). However, this value was considered in consistence with the calculated yield (0.15 ± 0.04) from the two single BVOC ozonolysis by taking into account the uncertainty. The observed acetic acid yield (0.08 ± 0.02) from the BM1 ozonolysis was higher than the calculated one (0.03 ± 0.003) as no acetic acid yield was obtained in the β-pinene ozonolysis. The rest product yields found in the BM1 ozonolysis were in accordance with that in the two single BVOC ozonolysis regarding the uncertainties. Note that signals detected at m/z 139 were treated with nopinone sensitivity in the PTR measurements.

Higher acids yields were observed in the ozonolysis of monoterpene mixture Exp.BM2 comparing to the Exp.BM1, especially in acetic acid yields, suggested higher acetic yields from α-pinene and myrcene comparing to that from limonene. Acetone yields from myrcene was the highest (0.21±0.03-0.29, Atkinson et al., 2003b) among reported monoterpenes ozonolysis. Hence the myrcene-containing mixture BM2 was expected to have a higher acetone yield than BM1. An acetone yield of 0.14 ± 0.04 was obtained in the BM2 ozonolysis, that calculated with the yields reported by Reissell et al., 1999 was 0.09 ± 0.02. Higher acetone yield in this study was reasonable since no OH scavenger was used in our ozonolysis experiments. As explained above, acetone yields from monoterpene reaction with OH were usually higher than reaction with O_3. The product at m/z 75 having a yield of 0.07 ± 0.06 was identified as hydroxyacetone from the myrcene ozonolysis, as myrcene is the only monoterpene with reported hydroxyacetone yield (Atkinson et al., 2003b). The observed yield was higher than the calculated one (0.02) after taking into account of the myrcene proportion in the BVOC mixture, yet commensurable with the calculated result regarding the large uncertainty. The pinonaldehyde yield of 0.06 ± 0.03 was much lower than that calculated (0.35 ± 0.04) with yield reported by Hatakeyama et al., 1989 where no OH scavenger was used as well. Nevertheless, the pinonaldehyde yield was in minor differences with other studies.

TABLE 6.4: Observed products, and their yields, from the ozonolysis of BVOC mixture. Yields shown in italic are calculated from yields reported in the literature, or from the single BVOC ozonolysis yields shown above.

m/z detected	Chemical formula	Substance	Yield BM1[a] + O_3	Yield BM2[b] + O_3	Reference
47	CH_2O_2	formic acid	0.20±0.05 *0.15±0.04*	0.22±0.09	This work This work[**]
59	C_3H_6O	acetone	0.10±0.03 *0.09±0.08* 	0.14±0.04 *0.09±0.02*[c]	This work This work[**] Reissell et al., 1999
61	$C_2H_4O_2$	acetic acid	0.08±0.02 *0.03±0.003*	0.21±0.03	This work This work[**]
75	$C_3H_6O_2$	hydroxyacetone	-	0.07±0.06 *0.02*[c]	This work Atkinson et al., 2003b
139	$C_9H_{14}O$	nopinone/limona ketone	0.35±0.09 *0.34±0.04*	-	This work This work[**]
141	$C_8H_{12}O_2$	2,2-dimethyl-cyclobutane-1,3-dicarboxaldehyde	0.03± 0.004 *0.02±0.01*	-	This work This work[**]
151	$C_{10}H_{14}O$	pinonaldehyde	-	0.06±0.03 *0.13±0.03*[c] *0.35±0.04* *0.04-0.13*[c] *0.11±0.02*[c] *0.10±0.02*[c]	This work Hakola et al., 1994 Hatakeyama et al., 1989 Yu et al., 1999 Atkinson et al., 2003b Atkinson et al., 2003b
153	$C_9H_{12}O_2$	3-oxo-pina-ketone	0.16±0.06 *0.12±0.04*	-	This work This work[**]
155	$C_9H_{14}O_2$	hydroxy pine ketone	0.14±0.01 *0.12±0.03*	-	This work This work[**]
157	$C_8H_{12}O_3$	2,2-dimethyl-3-formyl-cyclobutyl-methanoic acid	0.01±0.002 *0.01±0.002*	-	This work This work[**]
171	$C_9H_{14}O_3$	norpinonic acid	0.01±0.001 *0.01±0.002*	-	This work This work[**]
185	$C_{10}H_{16}O_3$	pinonic acid	0.01±0.002 *0.02*±0.004	-	This work This work[**]

[a] A monoterpene mixture of β-pinene (83%) and limonene (17%).
[b] A forest mixture I consists of α-pinene (68%), limonene (21.5%) and myrcene (10.5%).
[**] Yield calculated with the obtained β-pinene and limonene yields shown above.
[c] In the presence of an OH radical scavenger.

6.3 BVOCs from plant emission

In the final set of experiments, oxidation product yields from emissions of five sets of plants were monitored and listed in Table 6.5 for monoterpene-dominant and isoprene-dominant emissions. Over 98% of the six *Quercus ilex* trees emission were monoterpenes, they were also the major emitted by six *Pinus sylvestris* trees, more than 97% in comparison with isoprene and sesquiterpenes. Monoterpenes accounted for > 92% in the six *Fagus sylvatica* trees emission. Mix tree (three *Pinus sylvestris* and three *Picea abies*) emission consisted of over 97% of monoterpenes. As for the the six *Quercus robur* trees, isoprene was > 99% of the total emitted BVOCs. Yields were also inferred with reported values and the corresponding monoterpene proportion for different tree emission oxidations (shown in italic in Table 6.5), depending on their availabilities. For the reason that no important products at mass 138 amu

were reported in monoterpenes oxidations other than nopinone from β-pinene oxidations, the oxidation product detected at m/z 139 in the PTR-TOF-MS was reckoned as nopinone in the yield determinations of tree emissions. Same reason for the product at m/z 151 being identified as pinonaldehyde.

Formic acid and acetic acid have been found to be the mainly released organic acids by land vegetation, and are blamed for up to 60% of the acidity in precipitation in remote areas (J. Kesselmeier et al., 1997; Kesselmeier et al., 1999). Formic acid yields listed here were always higher than the inferred yields, which were calculated with the monoterpene speciation and yields reported by Atkinson et al., 2003b. Note that here the inferred result presented an upper-limit yield for each plant emission oxidation. Unfortunately, no reported formic acid yield available for Δ^3-carene ozonolysis, this would affect its calculated yield especially from the oxidation of *Pinus sylvestris* emission, where 61% of the emitted monoterpenes were Δ^3-carene. No formic acid yield was successfully determined for the oxidation of *Fagus sylvatica* emission, because of the poor linear regression between the formed formic acid and the consumed monoterpenes. The notable high formic acid yield in the ozonolysis of mix tree emission could be affected by re-evaporation of water vapor that condensed on the sampling line at night, since formic acid is highly soluble in water. Note that this experiment was performed in October with low outside temperature, condensation might happen when the sample air passed through the outdoor valve system. Possibly the same reason for the observed high yields of acetic acid and acetone, that have high water solubility. Acetone yields

TABLE 6.5: Products formed, and their yields, from the reactions of plant emitted monoterpenes with O_3 and of plant emitted isoprene with OH radicals. Yields shown in italic are calculated from yields reported in the literature, or from the single BVOC ozonolysis yields shown above.

m/z detected	Substance	*Quercus ilex*	*Pinus sylvestris*	*Fagus sylvatica*	*Mix trees*	*Quercus robur*
47	formic acid	0.28±0.08 *0.11*[a]	0.15±0.04 *0.1*[a]	- *0.09*[a]	0.57±0.22 *0.11*[a]	
59	acetone	0.13±0.06 *0.12±0.02*[b]	0.17±0.02 *0.19±0.03*[b]	0.15±0.01 *0.14±0.02*[b]	0.2±0.01 *0.13±0.02*[b]	
61	acetic acid	0.23±0.2	0.13±0.03	-	0.35±0.03	
139	nopinone	0.07±0.01 *0.08±0.008*[*]	0.03±0.01 *0.02±0.003*[*]	0.42±0.08 *0.01±0.002*[*]	0.07±0.02 *0.09±0.009*[*]	
151	pinonaldehyde	0.03±0.01 *0.05*[c]	0.11±0.03 *0.03*[c]	- *0*[c]	- *0.06*[c]	
71	MVK+MACR					0.57±0.11
73	methylglyoxal					0.14±0.04

[a] Yield calculated based on the monoterpene speciation and the upper-limit formic acid yields reported by Atkinson et al., 2003b.

[b] Yield calculated based on the monoterpene speciation and the acetone yields reported by Reissell et al., 1999.

[*] Yield calculated based on the monoterpene speciation and the nopinone yield reported in the β-pinene ozonolysis.

[c] Yield calculated based on the monoterpene speciation and the upper-limit of pinonaldehyde yield reported by Yu et al., 1999.

calculated with the monoterpene speciation and yields reported by Reissell et al., 1999 are shown in the table. A slightly higher acetone yield was observed in the mix tree emission oxidation, possible explanations were discussed above. The rest acetone yields were consistent

with the inferred results regarding the uncertainties. No acetic acid yields available for any of the monoterpenes, so its yields determined here could not be compared to the literature. Nopinone yields calculated with the β-pinene proportion and the yield reported in earlier β-pinene ozonolysis were in good agreement with the measured yields, except the anomaly in the *Fagus sylvatica* emission ozonolysis, only 1.1% of the emitted monoterpene is β-pinene, yet a nopinone yield of 0.42 ± 0.08 was observed.
For the shown photo-oxidation of *Quercus robur* tree emissions, the main oxidation products at m/z 71 were identified as MVK and MACR as the monitored NO level was over 0.1 ppb in the system. Both the MVK + MACR yield (0.57 ± 0.11) and the methylglyoxal yield (0.14 ± 0.04) from the photo-oxidation of *Quercus robur* tree emission were in accordance with yields presented above (single isoprene photo-oxidation at high-NO, Table 6.3), within the uncertainty range. The slight lower MVK + MACR yield agreed even better with yields reported in the literature.
It is well known that BVOC emissions significantly exceed AVOC emissions on the global scale, with emission rate of the diverse BVOCs dependent on plant species, vegetation period and temperature (Guenther et al., 2012; Kesselmeier et al., 1999; Koppmann, 2008). BVOCs emitted by plants, in particular isoprene and monoterpenes, as well as their oxidation products are involved in the atmospheric chemistry. For example, the long lifetime of acetone (See Table 1.2) allows for transport to the upper-troposphere, where its photolysis becomes an important source for PAN (peroxyacetyl nitrate). PAN acts as a temporary reservoir for NO_x and has a potential to form aerosols (Arnold et al., 1986; Janson et al., 2001). Atmospheric formic and acetic acids, could be both primary emitted or secondary formed from VOC oxidations. They could increase the acidity of rainwater and have the potential to modify the hygroscopic properties of SOA since they are highly water-soluble (Wang et al., 2007). As it shown above, the reactions of O_3 with biogenic emitted terpenes are also important sources of OH radicals in the atmosphere (Atkinson et al., 2003b). Information on VOCs oxidation products is important to better understand the mechanism of oxidation and the formation of SOA. Moreover, the atmospheric SOA has been found to be largely affected by products from VOC ozonolysis (Donahue et al., 2007; Lee et al., 2006). Therefore, knowledge on the nature and the yields of products from different tree-emitted BVOC oxidation is crucial for comprehending the impact of the biogenic SOA formation. To date, no studies have been carried out to determine product yields from oxidations of real tree-emitted terpenes. Our study provides product yields from different tree emissions which are comparable with yields from single BVOC oxidation found in previous studies. Therefore, this product study can help to precise regional chemical transport models and to develop global climate models.

Chapter 7

Results and discussion of the OH reactivity

This chapter discusses the comparison between measured OH reactivity from the LP-LIF measurements (k_{OH}^{meas}) and calculated OH reactivity from the PTR-TOF-MS and the inorganic measurements (k_{OH}^{cal}), with the equation demonstrated in Chapter 1.1 (Eqn 1.19). Note that from the PTR measurements, only identified substances with respective rate constant were included in k_{OH}^{cal} (Table 4.1). Results are presented here in BVOC and AVOC parts with increased complexity of the system, to examine if there is a trend of missing OH reactivity with more complex atmospheric system.

7.1 Missing OH reactivity for BVOCs oxidations

Figure 7.1 displays the limonene ozonolysis experiment (Exp.BS2), where NO was added to explore the night time NO_3 oxidation. At the injection of 25 ppb of limonene (green vertical line), the k_{OH}^{cal} was larger than the k_{OH}^{meas}, probably due to the large uncertainties for the LP-LIF instrument above 60 s^{-1} of OH reactivity (as explained in Chapter 2.3). After the injection of O_3 (red vertical line), the OH reactivity decreased rapidly and was less than 3 s^{-1} after 2 hours (lower panel), no discernible major product was observed. At this stage the measured OH reactivity was ~13 s^{-1} with a missing fraction of 75% compared to the calculated one (mid-panel). As a matter of fact, the biggest missing OH reactivity in the whole study was found in the limonene ozonolysis period (see Figure 7.8 for the overview of the whole set of experiments). For all the unidentified compounds, a higher k^* value was obtained at the beginning of the oxidation to close the observed large missing OH reactivity (upper panel). Note that at this stage of experiment, the sum of unidentified compounds manifested a rapid increase, indicating the existence of some reactive oxidation products, which was generated rapidly and was not included in the k_{OH} calculation. The derived k^* decreased gradually with the oxidation process to about 1×10^{-11} cm^3 $molecule^{-1}$ s^{-1} by the end of the day. The added NO lead to the formation of NO_3 radicals with O_3 present in the dark chamber. By the time the NO was added (grey vertical line), compounds left in the chamber returned an OH reactivity of about 2 s^{-1} whereas the k_{OH}^{meas} was ~9 s^{-1}, resulting in a missing fraction of more than 70%. After the addition of NO, the ratio of k_{OH}^{cal} over k_{OH}^{meas} increased but not the absolute missing OH reactivity, this is reflected also in the smooth decay of the k^*. No increase of the missing OH reactivity during the night, implying that nitrate chemistry is not an important source of the unmeasured oxidized products.
No important oxidation products with high molar yield were reported for the limonene ozonolysis as discussed above. The only two products (formic acid and acetic acid) having yields of more than 10% are much less reactive than the other products (see Chapter 6.1 for more details on the product yield). Gas-phase reaction of O_3 and limonene cannot explain

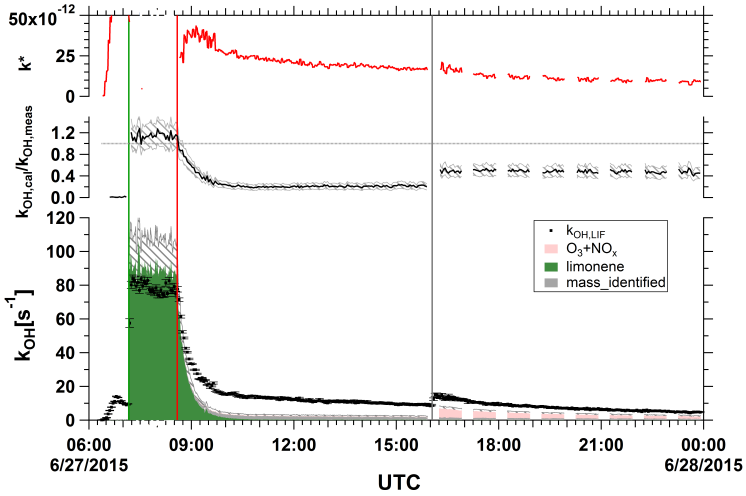

FIGURE 7.1: Exp.BS2: Limonene ozonolysis and night time nitrate oxidation. Lower panel shows the k_{OH}^{cal} with respect to the contribution of species in different colors, together with the k_{OH}^{meas} (black dots). The calculation uncertainty of k_{OH}^{cal} is shown in grey shadow, black error bars are one σ of the k_{OH}^{meas}. Colored vertical lines indicate the injection time of VOC (green line), O_3 (red), and NO (grey line). Middle panel shows the ratio of k_{OH}^{cal} over k_{OH}^{meas} (black line) with the upper and lower limit of the uncertainty (grey shadow). Upper panel is the rate constant (k^*) derived from the unidentified compounds to explain the missing k_{OH}.

alone the observed large missing OH reactivity. Grosjean et al., 1993 found that aerosol products account for 22% of total carbon of the reacted limonene in the reaction with ozone, additionally, the unsaturated carbonyl products also react with ozone and lead to low-volatility OVOCs. Zhang et al., 2006 confirmed the potential of limonene to be a very important source of biogenic SOA. In our limonene ozonolysis experiment, a SOA mass concentration of about 40 $\mu g/m^3$ was found, with a high total surface concentration of 2.5 $\times$ 10^9 nm^2 cm^{-3}. However, the calculated OH reactivity on aerosol particles was only 0.2 s^{-1} by using the proposed reactive uptake coefficient of 0.5 (see Eqn 4.4), which is not able to explain the large missing fraction of OH reactivity. Mogensen et al., 2011 analyzed the particles formation events occurred during a field campaign with the measured data set of OH reactivity and observed that the missing OH reactivity increased during the particle formation event. They found that the missing OH reactivity could not be explained by OH loss on particles surface, but rather by OH oxidation with VOCs to form higher oxidized semi-volatile compounds. In our case with the PTR measurements, those higher oxidized, possibly highly reactive products might be excluded in the OH reactivity calculation since only identified compounds were considered.

Experiment BM3 (Figure 7.2) simulated a more complicated atmospheric environment with OVOCs and β-caryophyllene presenting stressed tree emissions. No significant missing OH reactivity was observed during the injections of acetaldehyde and MVK/MACR mixture. Nevertheless, a missing fraction of about 10% appeared after the injection of β-caryophyllene. As there was no oxidation during this period, the missing OH reactivity is likely to be caused by the weak accuracy of the PTR measurements, since the lowest accuracy (> 20%, see *Appendix.A*) was obtained for β-caryophyllene among all compounds in this study.

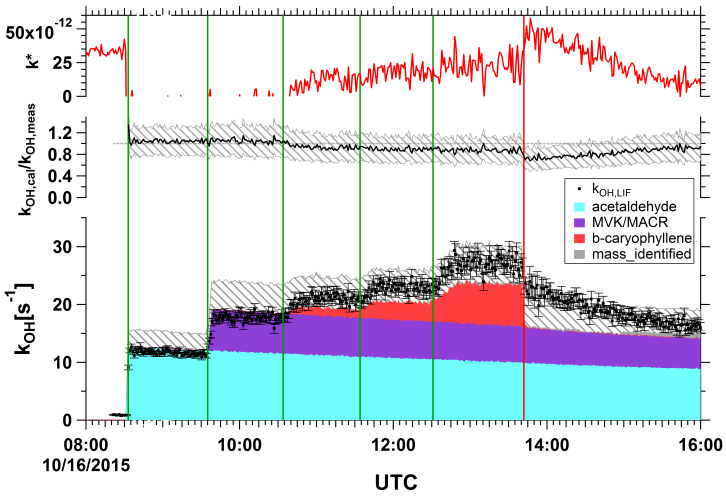

FIGURE 7.2: Exp.BM3: Forest mixture II ozonolysis. Lower panel shows the k_{OH}^{cal} with respect to the contribution of species in different colors, together with the k_{OH}^{meas} (black dots). The calculation uncertainty of k_{OH}^{cal} is shown in grey shadow, black error bars are one σ of the k_{OH}^{meas}. Colored vertical lines indicate the injection time of VOCs (green line) and O_3 (red). Middle panel shows the ratio of k_{OH}^{cal} over k_{OH}^{meas} (black line) with the upper and lower limit of the uncertainty (grey shadow). Upper panel is the rate constant (k^*) derived from the unidentified compounds to explain the missing k_{OH}.

After the addition of O_3, a prompt depletion of β-caryophyllene within minutes was observed. The missing OH reactivity revealed a drastic increase, probably due to the significant secondary organic aerosol formation from the ozonolysis of β-caryophyllene. Aerosol mass yield from 12% to almost 100% have been observed for β-caryophyllene oxidations (Helmig et al., 2006). Unfortunately there was no aerosol measurements in our experiment to calculate the OH reactivity on aerosol particles. Grosjean et al., 1993 investigated gas-phase products from the dark ozonolysis of β-caryophyllene and observed the only product was formaldehyde (80% yield). Whereas Calogirou et al., 1997 identified the formation of formaldehyde (14% yield) and several semi-volatile ketoaldehydes (β-caryophyllone aldehyde, β-nocaryophyllone aldehyde, etc.) as the main gas-phase reaction products. Jaoui et al., 2003 reported higher yields of β-caryophyllone aldehyde and β-nocaryophyllone aldehyde than those reported by Calogirou et al., 1997, together with other products resulted a total carbon mass yield of 24.5% in the gas-phase. Lee et al., 2006 used PTR-MS to study the gas-phase products of reaction between O_3 and β-caryophyllene, and reported product yields as: formaldehyde (76 ± 20)%, acetaldehyde (0.9 ± 0.3)%, acetone (1.1 ± 0.3)%, formic acid (3.9 ± 1)%, acetic acid (20 ± 5)%, with a total carbon mass yield of (39 ± 2)%. The measured k_{OH} remained high even if almost no β-caryophyllene ozonolysis products were detected in this study. This was likely to infer that some reactive products contributing to the missing OH reactivity were not included in the calculation due to their unsuccessful identification in the PTR measurements.

The sum of the unidentified compounds in the PTR measurements was less than 5 ppb, and remained nearly constant during the whole oxidation process. A k^* value of about 5×10^{-11} cm^3 molecule^{-1} s^{-1} was derived at the first stage of the β-caryophyllene ozonolysis. After $\sim$2 hours oxidation, the k^* value decreased gradually to about 1×10^{-11} cm^3 molecule^{-1} s^{-1}.

Considering that there was no significant deviation on the unidentified oxidation products, these results implicated the existence of some very reactive products that were generated immediately in the β-caryophyllene ozonolysis and were transformed into less reactive second order products.
Finally a more complex system with real plant emission was studied with the help of the plant chamber. SAPHIR was coupled to SAPHIR-PLUS for several hours till the transferred plant emission reached the desired concentration in SAPHIR. Figure 7.3 exhibits the ozonolysis of emissions from 6 *Quercus ilex* trees (Exp.BP1). Monoterpene dominated the emissions (> 97%) and its speciation was determined by the offline GC-FID/MS (see Table 5.1). The k_{OH} from monoterpenes was calculated by using their respective rate constants.

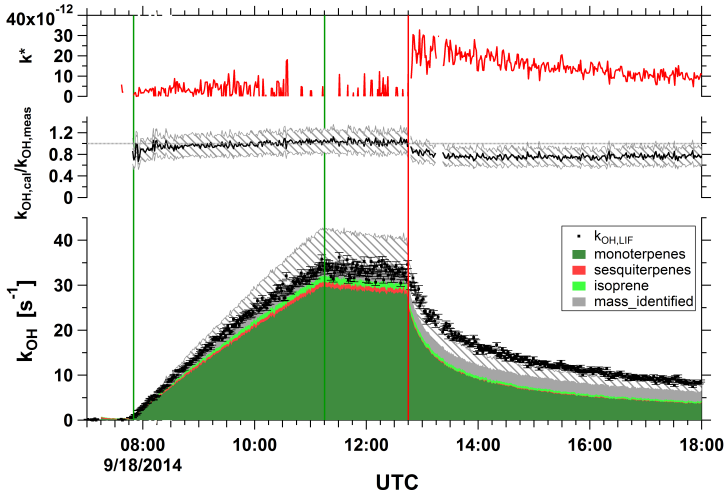

FIGURE 7.3: Exp.BP1: Ozonolysis of *Quercus ilex* tree emissions. Lower panel shows the k_{OH}^{cal} with respect to the contribution of species in different colors, together with the k_{OH}^{meas} (black dots). The calculation uncertainty of k_{OH}^{cal} is shown in grey shadow, black error bars are one σ of the k_{OH}^{meas}. Colored vertical lines indicate the start/end time of coupling with the plant chamber (green line), and the injection of O_3 (red). Middle panel shows the ratio of k_{OH}^{cal} over k_{OH}^{meas} (black line) with the upper and lower limit of the uncertainty (grey shadow). Upper panel is the rate constant (k^*) derived from the unidentified compounds to explain the missing k_{OH}.

No missing OH reactivity was observed during the transfer period when no oxidation was occurring, a missing fraction was observed after the injection of O_3. The k_{OH}^{cal} over k_{OH}^{meas} ratio dropped from ~1 to ~0.8 after the ozonolysis. In addition, the derived k^* value showed the same pattern as observed in the two previous examples, a mildly higher value at the beginning of the oxidation period and then decreased slowly to about 1×10^{-11} cm^3 molecule^{-1} s^{-1}. A rapid increase of the unidentified product at the first minutes of the ozonolysis was detected. This was possibly consisted of unmeasured high-amount reactive compounds that could be the explanation for the abrupt increase of the missing OH reactivity at the beginning of the oxidation.
The pattern is slightly different in the photo-oxidation of *Quercus robur* tree emissions (Figure 7.4, Exp.BP6). OH radicals were generated from photolysis of O3 and HONO by operating the chamber roof (blue vertical lines). A missing OH reactivity already emerged at the transfer stage where the dominant compound in the system was emitted isoprene (> 99%).

The main oxidation products at m/z 71 were identified as ISOPOOHs since the injected O_3 lead to a very low NO level (< 50 ppt) in the system. The generated acetaldehyde was from both the isoprene photo-oxidation and the chamber source (Rohrer et al., 2005). As observed in previous examples, the missing OH reactivity revealed an increase during the oxidation period compared to the reactant period (transfer stage), and the derived k^* value decreased again to about 1×10^{-11} cm^3 molecule^{-1} s^{-1} at the end of the experiment. The missing OH reactivity at the transfer stage might be caused by an underestimation of the isoprene concentration from the PTR measurements. In fact, about 10% underestimation of the isoprene concentration was constantly observed in the whole set of experiments comparing to the online GC-FID/MS data (see Figure A.2 in *Appendix.A*). For comparison, the total OH reactivity calculated with the GC measurements was also plotted in the figure in red crosses. It did close the OH reactivity gap during the transfer period. However, after the oxidation, an even bigger discrepancy between measured and calculated OH reactivity was observed for the GC measurements. These results implied the existence of some reactive products that were not detected by both methods.

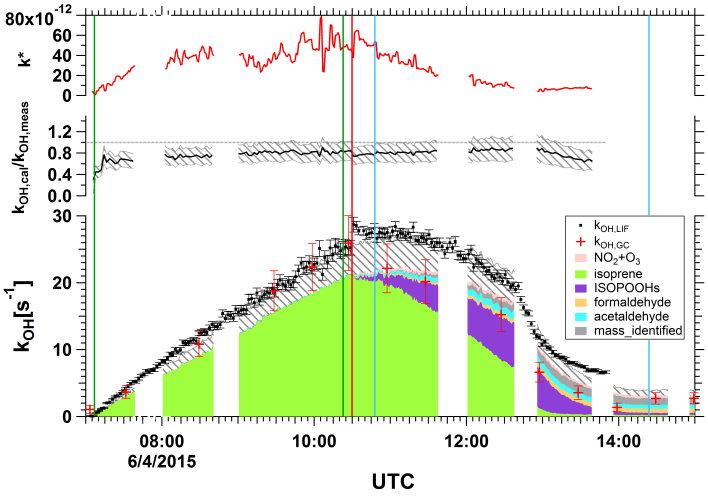

FIGURE 7.4: Exp.BP6: photo-oxidation of *Quercus robur* emissions. Lower panel shows the k_{OH}^{cal} with respect to the contribution of species in different colors, together with the k_{OH}^{meas} (black dots). The calculation uncertainty of k_{OH}^{cal} is shown in grey shadow, black error bars are one σ of the k_{OH}^{meas}. k_{OH} calculated with GC data is shown in red crosses with error bars showing the calculation uncertainty. Colored vertical lines indicate the start/end time of coupling with the plant chamber (green line), the injection of O_3 (red), and the roof operation (blue). Middle panel shows the ratio of k_{OH}^{cal} over k_{OH}^{meas} (black line) with the upper and lower limit of the uncertainty (grey shadow). Upper panel is the rate constant (k^*) derived from the unidentified compounds to explain the missing k_{OH}.

7.2 Missing OH reactivity for AVOCs oxidations

In the single AVOC photo-oxidation experiment AS1 (Figure 7.5), the calculated and measured OH reactivity were very close when there was only benzene-D_6 in the system. Small

fraction (∼10%, within the uncertainty) of missing OH reactivity was observed. Both k_{OH}^{cal} and k_{OH}^{meas} demonstrated an increase after the roof was opened, indicating that the benzene-D_6 photo-oxidation products were more reactive than the reactant (Volkamer et al., 2002). The major oxidation product identified was phenol-D_6 and its concentration measured by the PTR-TOF-MS was only ∼3 ppb at the end of the experiment, while the GC-FID/MS measured 18 ppb. Total OH reactivity calculated with the GC data was thus plotted in Figure 7.5 in red crosses. Yet the GC data displayed much higher OH reactivity than the measured one (black dots in the Figure) during the photo-oxidation phase. However, the discrepancy between measured OH reactivity and calculated from PTR measurements was within the error range. The bias on the phenol-D_6 concentration measured by PTR was probably caused by the deuteration of the phenol-D_6 as the calibration factor of phenol was used.

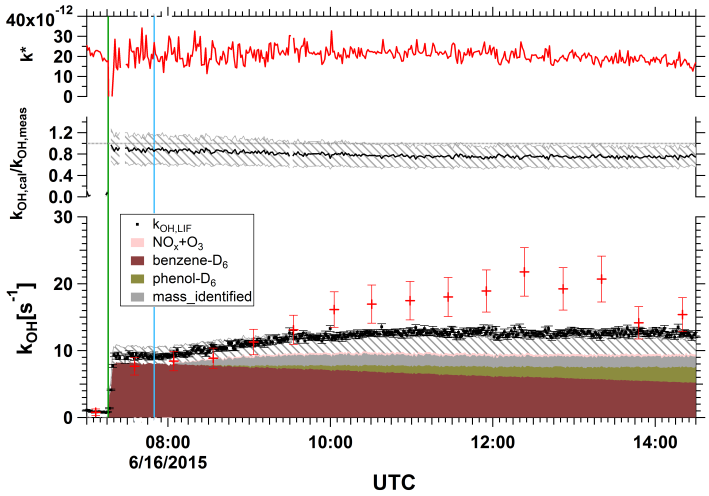

FIGURE 7.5: Exp.AS1: Photo-oxidation of benzene-D_6 (low NO_x). Lower panel shows the k_{OH}^{cal} with respect to the contribution of species in different colors, together with the k_{OH}^{meas} (black dots). The calculation uncertainty of k_{OH}^{cal} is shown in grey shadow, black error bars are one σ of the k_{OH}^{meas}. Colored vertical lines indicate the injection of VOC (green line) and the roof operation (blue). Middle panel shows the ratio of k_{OH}^{cal} over k_{OH}^{meas} (black line) with the upper and lower limit of the uncertainty (grey shadow). Upper panel is the rate constant (k^*) derived from the unidentified compounds to explain the missing k_{OH}.

The $k_{OH}^{cal}/k_{OH}^{meas}$ ratio showed a slight decrease along the photo-oxidation process. A stable k^* value of about 2×10^{-11} cm^3 molecule^{-1} s^{-1} was derived for all unidentified compounds to close the observed missing OH reactivity. As the sum of the unidentified compounds were increasing during the whole experiment (< 7 ppb), this seemed to imply that the unidentified products were becoming less reactive with OH. Furthermore, the SOA mass concentration measured in the experiment was small (∼ 4 μg/m^3), with a low total surface concentration of about 2×10^8 nm^2 cm^3. By using the Eqn 4.4, this returned an OH reactivity on aerosol particles of 0.02 s^{-1}, yet together with measured gas-phase VOCs, this is not able to close the missing OH reactivity. These results suggested that there were some gas-phase reactive products which were not identified and included in the OH reactivity calculation by the PTR measurements.

The calculated and measured OH reactivity exhibited no discrepancy for the two urban mixture oxidation experiments (Exp.AM1 and Exp.AM2). Figure 7.6 elucidates the second urban mixture oxidation experiment. The experiment was conducted in October where the overhead sunlight was not strong (the recorded photolysis frequency $j\mathrm{NO_2}$ was more than 2 times higher in June). 1 ppm of CO was added (the second grey vertical line) to cleanse OH radicals produced from the photolysis of O_3 and HONO. This lead to the reaction of AVOC only with the added O_3. The oxidation of AVOCs was more slowly comparing to BVOCs, only 20% of AVOCs were consumed at the end of the experiment. No evident reactive oxidation products were detected. Furthermore no evident missing OH reactivity was observed during the whole experiment, leading to a derived k^* value close to 0. This result proved the good agreement between the PTR-TOF-MS and the LP-LIF instruments, as well as the high sensitivity of both methods to the atmosphere system changes.

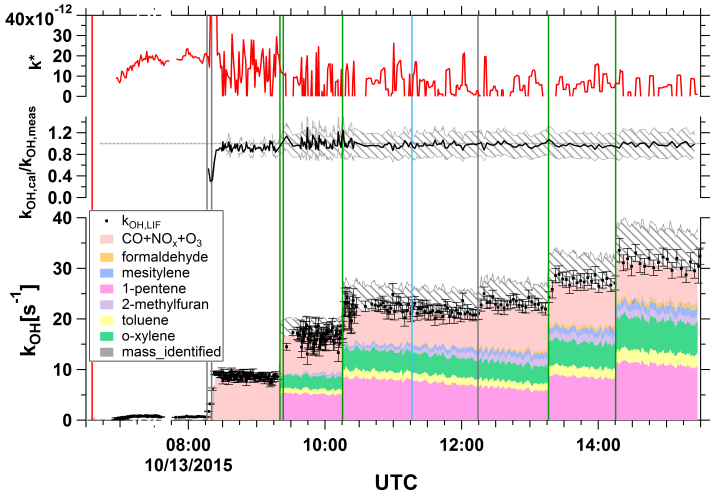

FIGURE 7.6: Exp.AM2: Ozonolysis of Urban mixture [1]. Lower panel shows the k_{OH}^{cal} with respect to the contribution of species in different colors, together with the k_{OH}^{meas} (black dots). The calculation uncertainty of k_{OH}^{cal} is shown in grey shadow, black error bars are one σ of the k_{OH}^{meas}. Colored vertical lines indicate the injection of VOCs (green line), injection of O_3 (red), injection of NO_2/CO (grey), and the roof operation (blue). Middle panel shows the ratio of k_{OH}^{cal} over k_{OH}^{meas} (black line) with the upper and lower limit of the uncertainty (grey shadow). Upper panel is the rate constant (k^*) derived from the unidentified compounds to explain the missing k_{OH}.

In the more complex system, mixed air masses containing AVOC and tree-emitted BVOC were simulated. Again in the Exp.AB3 (Figure 7.7), the total OH reactivity calculated with the online GC-FID/MS data (red crosses) showed higher values than the measured one during the oxidation period due to measured high phenol-D_6 concentration (in comparison to that measured by the PTR). The OH reactivity calculated with the PTR measurements demonstrated an overestimation of the k_{OH}^{cal} for the A/BVOC mixture. This could be caused by the overestimated monoterpene concentration in the PTR measurements or the uncertainty of monoterpene speciation from the offline GC data. The $k_{OH}^{cal}/k_{OH}^{meas}$ ratio continuously declined during the photo-oxidation stage, the missing fraction was more than 20% at the end

[1] Adding along a VOC-OH trace standard containing 2-methylfuran and mesitylene.

of the experiment. This returned a k^* value of about 1.5×10^{-11} cm^3 molecule^{-1} s^{-1} for all unidentified compounds (< 14 ppb). In addition, the SOA total surface concentration was about $3.5{\times}10^8$ nm^2 cm^3, thus the OH reactivity on aerosol particles was calculated to be 0.03 s^{-1}, again not able to explain the missing OH reactivity. These results implicated once more the presence of gas-phase reactive products, which have slightly lower reaction rate constant than phenol (3.27×10^{-11} cm^3 molecule^{-1} s^{-1}) but are more reactive than benzene-D_6 (1.14×10^{-12} cm^3 molecule^{-1} s^{-1}).

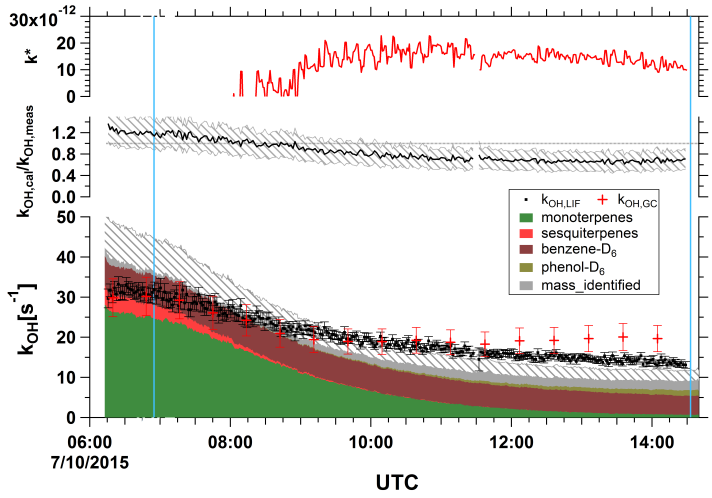

FIGURE 7.7: Exp.AB3: Photo-oxidation of the BVOC [2]and benzene-D$_6$ mixture. Lower panel shows the k_{OH}^{cal} with respect to the contribution of species in different colors, together with the k_{OH}^{meas} (black dots). The calculation uncertainty of k_{OH}^{cal} is shown in grey shadow, black error bars are one σ of the k_{OH}^{meas}. Colored vertical lines indicate the roof operation (blue). Middle panel shows the ratio of k_{OH}^{cal} over k_{OH}^{meas} (black line) with the upper and lower limit of the uncertainty (grey shadow). Upper panel is the rate constant (k^*) derived from the unidentified compounds to explain the missing k_{OH}.

7.3 Discussion of missing OH reactivity

An overview of the OH reactivity comparison is demonstrated in bars (Figure 7.8) for the whole set of experiments (Exp.AS2 was not included in the overview due to the lack of measurements during the reactant stage). Bars present the mean k_{OH}^{cal} over k_{OH}^{meas} ratio of selected 2 stages of each experiment—reactant phase (in black) and product phase (in red). Error bars show respective uncertainties determined via error propagation. The reactant phase was selected i) several hours before the injection of oxidants when there was only reactant in the chamber; or ii) only the first five-minute data points for experiments where reactants were added after opening the chamber roof. The product phase was defined as period starting from 50% loss of the major reactant during the oxidation. However, due to the slow reaction of AVCOs with OH radicals, in the oxidation experiments containing AVOCs, the selected product phase started when only 20% of AVOC reactant was consumed. Due to the high un-

[2]BVOCs from 6 *Pinus sylvestris* trees emission.

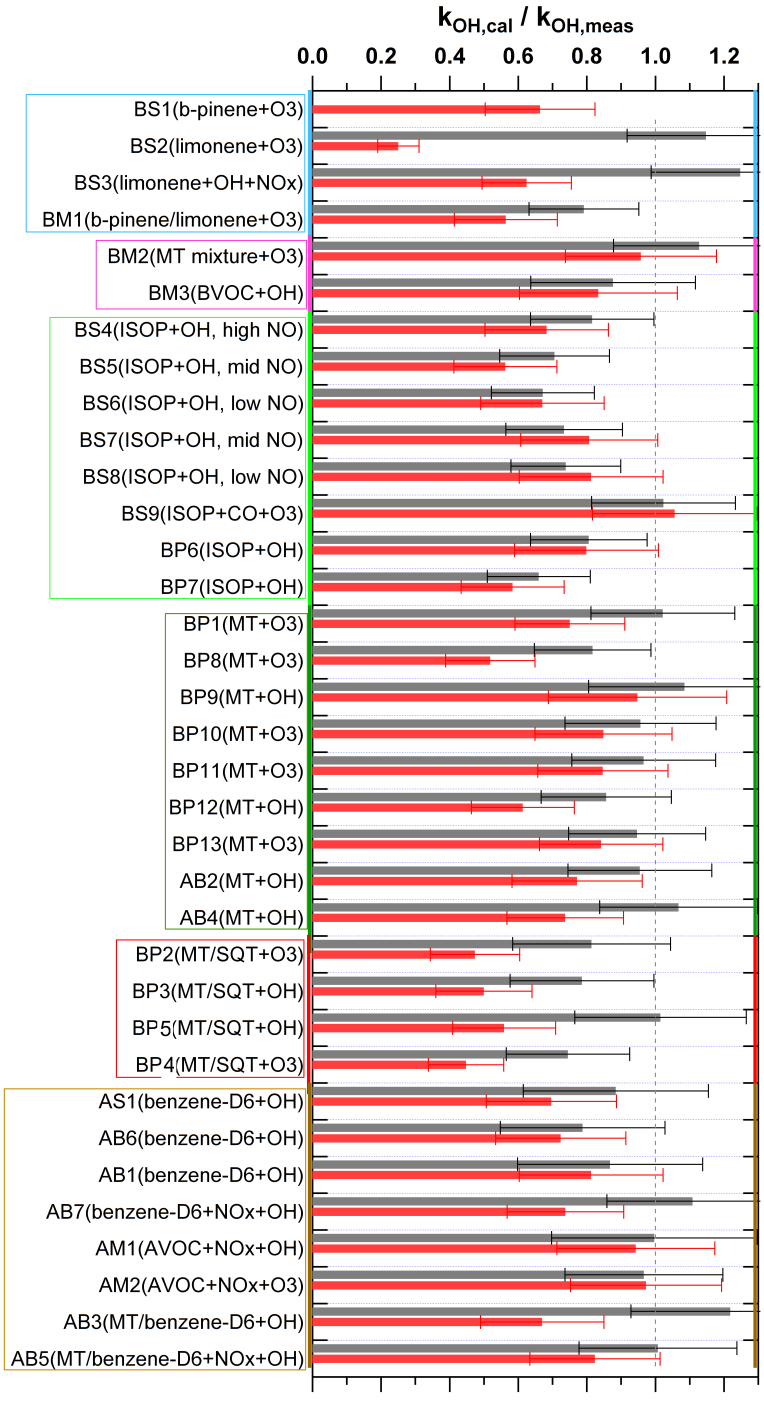

FIGURE 7.8: Overview of mean $k_{OH}^{cal}/k_{OH}^{meas}$ ratio for reactant phase (in black) and product phase (in red), error bars showing respective uncertainties determined via error propagation. MT= monoterpenes, SQT= sesquiterpenes, and ISOP= isoprene.

certainty for the LP-LIF instrument above 60 s^{-1} of OH reactivity, plus no dilution performed for the sampled air, there was no data for the reactant phase in the β-pinene ozonolysis experiment (Exp.BS1, time series is shown in *Appendix.A*).
In general, the discrepancy (missing fraction of the OH reactivity) was larger in the oxidation phase than in the reactant phase (except for Exp.BS7-9 and Exp.AM2), indicating that more oxidation products from reactive primary biogenic/anthropogenic precursors were not included in our OH reactivity calculation. The exceptional cases of the three isoprene photo-oxidation experiments BS7-9, and the urban mixture oxidation experiment AM2 will be discussed below.
The biggest missing OH reactivity was observed in the limonene ozonolysis period (Exp.BS2 in Figure 7.9, blue box), where only less than 25% of OH reactivity could be explained by the VOCs measurements. Note that more than 100% of OH reactivity was calculated than the measured one when there was only limonene in the system (within error range). On the other hand, the ozonolysis of β-pinene (Exp.BS1) had a smaller missing OH reactivity with about ~65% recovered by the VOCs measurements since the main oxidation product nopinone was well characterized. Nopinone molar yield is comparable with literature (41.1%, see Chapter 6.1 for more details). Formaldehyde was also identified as an important product from reaction of β-pinene and O_3, yields ranged from 42 to 76% were reported (Atkinson et al., 2003b; Grosjean et al., 1993; Hatakeyama et al., 1989; Winterhalter et al., 2000). Unfortunately no formaldehyde data available from the Hantzsch measurements in this experiment. The high instability of the PTR-TOF-MS for quantifying formaldehyde (underestimation by a factor of 3 to 5, see Chapter 2.1.1) might be a reason for the underestimation of the OH reactivity. The ozonolysis of β-pinene/limonene mixture (Exp.BM1) had a k_{OH}^{cal} over k_{OH}^{meas} ratio of ~55% in the product phase, which is, as expected, in between of ~25% and ~65% for the two single BVOC oxidations discussed above. The reason that a notable missing fraction was already revealed at the reactant phase is due to the high OH reactivity (> 170 s^{-1}) measured at this stage. The photo-oxidation of limonene under high NO_x condition (Exp.BS3) revealed less unknown oxidation products than in the limonene ozonolysis experiment. About 63% of OH reactivity could be explained by the VOCs measurements in the product phase. Formaldehyde data from the Hantzsch measurements was used in the k_{OH}^{cal}, as a matter of fact, the mixing ratio was ~4 times higher than what measured by the PTR-TOF-MS.

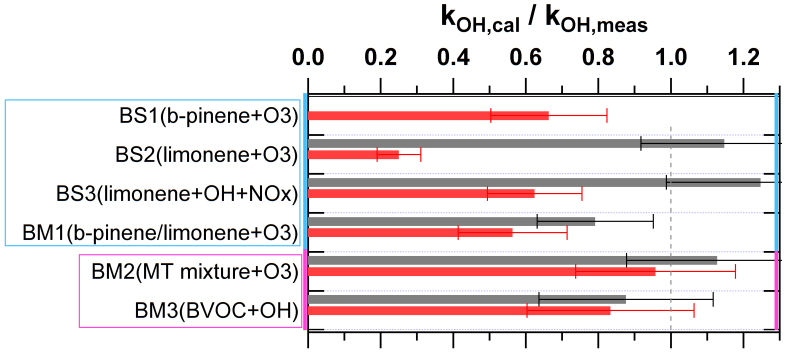

FIGURE 7.9: Mean $k_{OH}^{cal}/k_{OH}^{meas}$ ratio of reactant phase (in black) and product phase (in red) for single BVOC and BVOC mixtures, error bars showing respective uncertainties determined via error propagation. MT= monoterpenes.

When the system complexity was increased in the forest mixture simulation experiments, calculated OH reactivity of two BVOC mixture oxidation experiments—BM2 and BM3 (Figure 7.9, pink box)—showed better agreement with measured ones. The less missing OH reactivity in the monoterpene mixture ozonolysis (Exp.BM2) than in the single limonene ozonolysis (Exp.BS2) confirmed again the poor understanding in the limonene oxidation. In the oxidation period, Exp.BM3 (sesquiterpenes and OVOCs mixture) had a smaller k_{OH}^{cal} over k_{OH}^{meas} ratio of 83% compared to 96% in Exp.BM2. However, the observed missing OH reactivities were not significant when considering the relative uncertainties. The highly reactive oxidation products of sesquiterpenes are most likely the source of the observed missing OH reactivity, since those products were not successfully identified and included in the PTR data calculation. On the other side the higher gas-particle portioning of sesquiterpenes (from 12 to almost 100%, Helmig et al., 2006) compered to monoterpenes (18-32%, Emanuelsson et al., 2013) could be another reason for the difference in the missing OH reactivity.

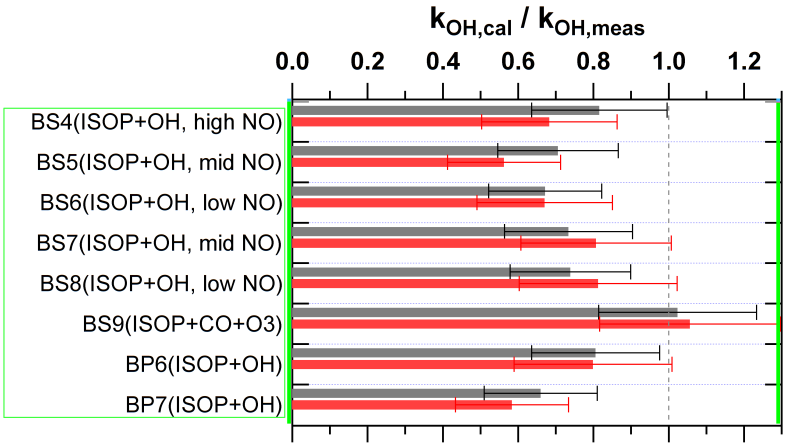

FIGURE 7.10: Mean $k_{OH}^{cal}/k_{OH}^{meas}$ ratio of reactant phase (in black) and product phase (in red) for isoprene experiments, error bars showing respective uncertainties determined via error propagation. ISOP= isoprene.

Light green box encloses all results from injected or plant emitted isoprene oxidation experiments (Figure 7.10). For the first time, higher $k_{OH}^{cal}/k_{OH}^{meas}$ ratios were found in the oxidation phase for the experiments BS7-9. In addition, notable missing OH reactivities already emerged during the injection of isoprene except for the isoprene ozonolysis experiment BS9. It is worth mention that, for the Exp.BS9, in addition to the fact that CO was added as an OH scavenger, this experiment was conducted in October when the photolysis frequency was low, therefore one hour data after only 30% of isoprene loss was averaged as the product phase. No missing OH reactivity was observed for the Exp.BS9. For the rest isoprene photooxidation experiments, the missing OH reactivity at the reactant phase suggests an underestimation of the isoprene concentration from the PTR-TOF-MS measurements. k_{OH} calculated from GC-FID/MS measurements confirmed the presence of unmeasured OVOCs since it revealed even more missing OH reactivity than the PTR data during the oxidation period. Different product identification from distinct isoprene oxidation pathways—MVK/MACR under high- and mid-NO conditions and ISOPOOHs in low-NO isoprene oxidations—did not show any tendency in the missing OH reactivity, identified different products could be seen in *AppendixB*.

Dark green box in Figure 7.11 encloses plant emitted monoterpenes oxidation experiments. Considering the uncertainties, almost all measured OH reactivity could be explained by measured monoterpenes at the reactant stage. The only exception happened in the Exp.BP8 (18% missing OH reactivity) where the highest OH reactivity was measured during the whole set of experiments (> 200 s^{-1}). This extreme high value could cause large measurements bias in the LP-LIF instrument as explained before (see Chapter 2.3). Additionally, higher missing OH reactivity (5-48%) was always found in the oxidation phase and no systematic differences between the photo-oxidation and ozonolysis of plant emitted monoterpenes.

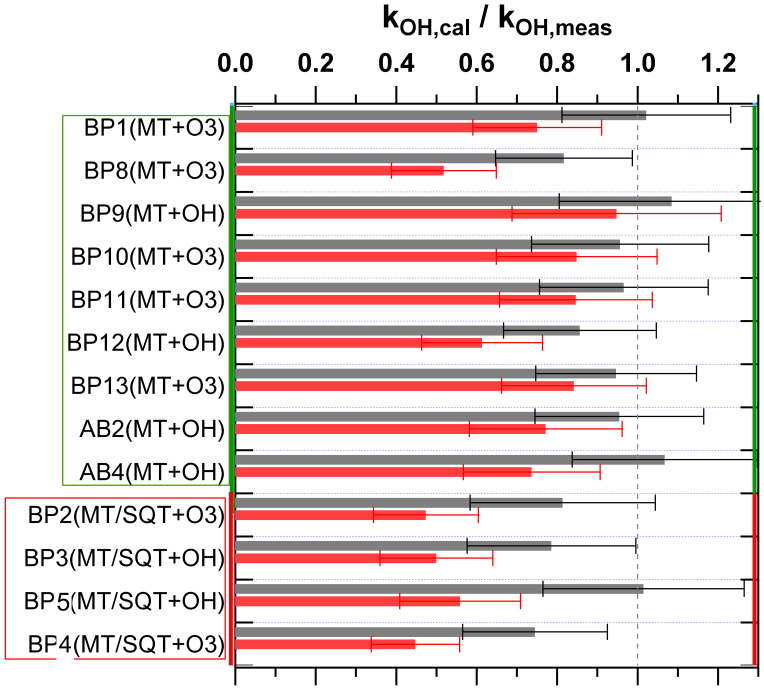

FIGURE 7.11: Mean $k_{OH}^{cal}/k_{OH}^{meas}$ ratio of reactant phase (in black) and product phase (in red) for tree emitted MT (monoterpenes) or SQT (sesquiterpenes) experiments, error bars showing respective uncertainties determined via error propagation.

For oxidations of sesquiterpene-abundant plant emissions (red box in Figure 7.11), bigger missing OH reactivity (44-55%) in the product phase than in the reactant phase (0-25%) was again observed, suggesting unmeasured high reactive products from sesquiterpenes oxidation. In general, discrepancy in both phases was higher than when the plant emission mainly consisted of monoterpenes. The bigger discrepancy in the reactant phase might be a result from the low measurement accuracy for sesquiterpenes in the PTR-TOF-MS measurements (see sensitivity table in *AppendixA*). The discrepancy in the product phase might be caused by unmeasured high reactive products or by the higher gas-particle portioning of sesquiterpenes as mentioned before. Nölscher et al., 2012 used the Comparative Reactivity Method (CRM) to measure the total OH reactivity in a Finnish boreal forest, they quantified VOCs mixing ratio with a GC-MS and obtained an averaged k_{OH}^{cal} over k_{OH}^{meas} ratio of 42% under normal boreal conditions. However, their biggest discrepancy of only 11% of the total OH

reactivity recovered by VOCs measurements was observed when sesquiterpenes dominated in the heat stress emissions.
Overall the discrepancy was not significant for all photo-oxidation experiments containing AVOCs (Figure 7.12, brown box). Same rise in missing OH reactivity from reactant to oxidation period was observed again, suggesting more unmeasured oxidation products resulting from reactive primary biogenic/anthropogenic precursors. Nevertheless, in the Exp.AM2, a slightly better closure was found in the oxidation phase. The largest discrepancy happened in the product phase of the Exp.AB3 when the heterogenous system consisted of both biogenic and anthropogenic VOC reactants. An overestimation of 22% of OH reactivity was calculated for the A/BVOC mixture, possibly caused by the overestimated monoterpene concentration from the PTR measurements or the uncertainty of monoterpene speciation from the offline GC data. Not likely to be caused from bias on the AVOC measurements since the same amount of 290 ppb of benzene-D_6 was injected in all experiments, and no remarkable inconsistency of the benzene-D_6 concentration was discovered in the Exp.AB3. Nevertheless, only ~67% of the measured OH reactivity was recovered by VOCs monitored in the photo-oxidation phase. The missing OH reactivity did not show any tendency when the complexity of the AVOC system increased, nor when the NO_x level changed.

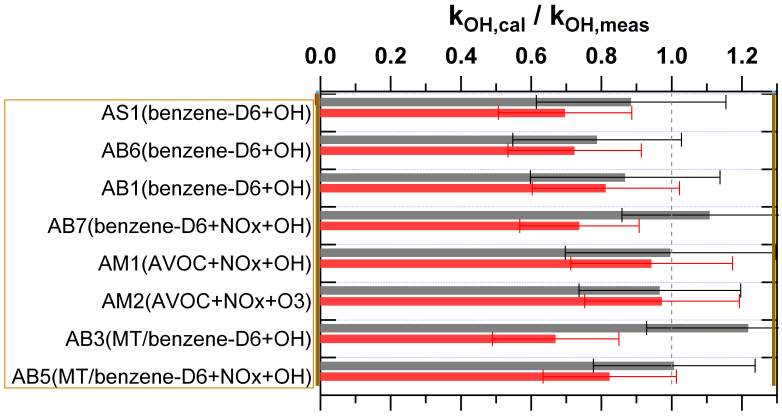

FIGURE 7.12: Mean $k_{OH}^{cal}/k_{OH}^{meas}$ ratio of reactant phase (in black) and product phase (in red) for experiments containing AVOCs, error bars showing respective uncertainties determined via error propagation. MT= monoterpenes.

Globally, the biggest missing OH reactivity in our study was found in the limonene ozonolysis, not much oxidation products were found for the reaction between limonene and O_3. This resulted also missing OH reactivity for oxidations of mixtures containing limonene. Poor agreement between measured and calculated OH reactivity found in the isoprene oxidation experiments might be improved with improvement of the PTR-TOF-MS calibration on quantifying isoprene. Distinct oxidation pathways of the isoprene oxidation did not show a systematic difference on the missing OH reactivity. The oxidation of sesquiterpenes mixture had a bigger missing OH reactivity than that of monoterpenes mixture. The same pattern was also observed in oxidations of these two compounds from tree emissions: in general when the BVOC system was dominated by sesquiterpenes the missing OH reactivity is larger than that in the system containing mainly monoterpenes. Single AVOC oxidation revealed a smaller missing OH reactivity than the two single BVOC oxidations. The oxidations of AVOC mixtures had less missing OH reactivity than that of BVOC mixtures as well. Additionally no trend was observed when the AVOC system became more complex.

The atomic oxygen-to-carbon (O/C) ratio, which characterizes the oxidation state of the atmosphere system, was derived from the PTR measurements for each experiment. In order to get a further insight on the correlation between missing OH reactivity and the oxidation progress, the k_{OH}^{cal} over k_{OH}^{meas} ratio was plotted against the O/C ratio in Figure 7.13. Same reactant (in black) and product (in red) phase as discussed above was used but the error bars indicate standard deviation of the $k_{OH}^{cal}/k_{OH}^{meas}$ ratio for the averaged phase.
O/C ratio ranged from 0.003 to 0.807 in the whole set of experiments. The smallest ratio was found in the Exp.AS1 when 290 ppb of benzene-D_6 (O/C=0) were injected, a small amount of other common compounds such as acetone, which is always present in the ambient air, might be the cause of the small value of the O/C ratio. The biggest O/C ratio lied in the product phase of Exp.BS7 where formaldehyde (O/C=1) was added prior to the isoprene photooxidation. In each experiment O/C ratio always increased from reactant phase to product phase (more details see Table B.1 and Table B.2). The $k_{OH}^{cal}/k_{OH}^{meas}$ ratio showed a downward tendency when the O/C ratio increased. Considering that the O/C ratio was calculated with all VOCs measured (identified and unidentified) from the PTR data, this correlation between the $k_{OH}^{cal}/k_{OH}^{meas}$ and the O/C ratio suggests an unknown OH sink of oxygenated compounds which were not included in our OH reactivity calculation.

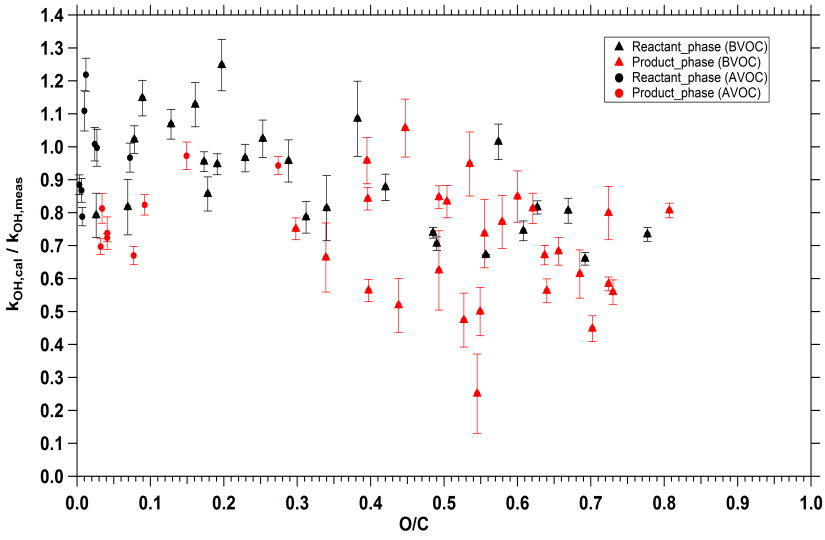

FIGURE 7.13: An overview of $k_{OH}^{cal}/k_{OH}^{meas}$ ratio vs the O/C ratio. Reactant phase is shown in black and product phase in red, with distinction between AVOC (round dot) and BVOC (triangle) systems. Error bar is one σ of the averaged period.

k^* value derived from the missing OH reactivity and the unidentified compounds was averaged for the same reactant (in black) and product (in red) phase as shown in Figure 7.14. No systematic difference was noted for derived k^* between AVOC and BVOC reactions nor between reactant and product phases. In case there was an overestimation of the calculated OH reactivity, the k^* value was negative therefore was excluded from discussion. The averaged k^* value ranged from 1.1×10^{-12} to 159.4×10^{-12} cm^3 molecule^{-1} s^{-1}. The extreme high k^* values happened when the measured OH reactivities were higher than 60 s^{-1} (Exp.BM1 and

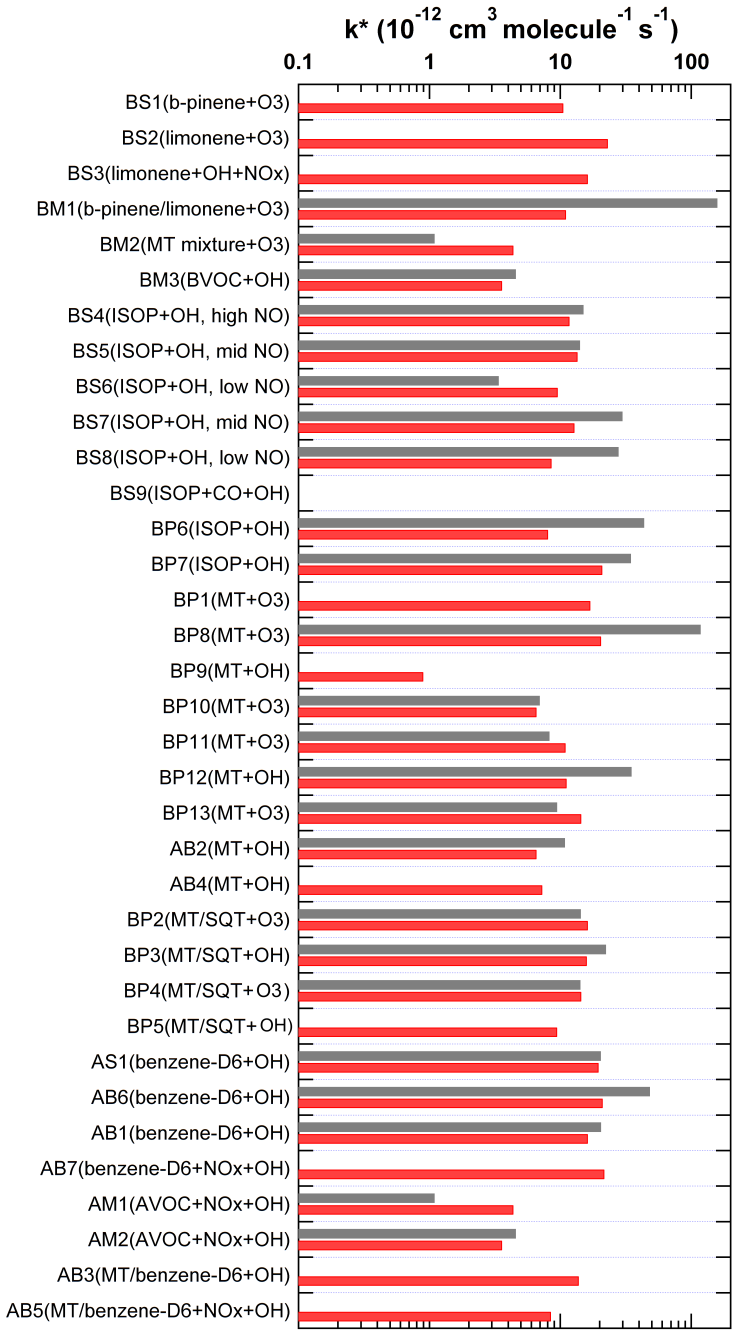

FIGURE 7.14: An overview of averaged k^* values for reactant and product period.

Exp.BM8). But the highest derived k^*=159.4 $\times$ 10^{-12} cm^3 molecule^{-1} s^{-1}, is still in a reasonable order, smaller than the rate constant of β-caryophyllene (200.0 $\times$ 10^{-12} cm^3 molecule^{-1} s^{-1}). In general, the k^* was in the vicinity of 1 $\times$ 10^{-11} cm^3 molecule^{-1} s^{-1}, this number is slightly lower than the reaction rate constant of two common atmospheric oxidation products nopinone and methylglyoxal (1.5 $\times$ 10^{-11} cm^3 molecule^{-1} s^{-1}), it is also lower than the isoprene oxidation products MVK and MACR (2.0 $\times$ 10^{-11} and 2.9 $\times$ 10^{-11} cm^3 molecule^{-1} s^{-1}, respectively). It is only mildly higher than the reported median rate constant for ketones (0.57 $\times$ 10^{-11} cm^3 molecule^{-1} s^{-1}, Atkinson et al., 2003a). Furthermore, an even higher rate constant of 5$\times$$10^{-11}$ cm^3 molecule^{-1} s^{-1} was assumed by Nölscher et al., 2012 in their total OH reactivity measurements from a boreal forest field campaign. More rate constant range for reactions of different VOC species with OH radicals reported by Atkinson et al., 2003a can be found in Figure 7.15. Our study on the rate constant for unidentified compounds measured by PTR-TOF-MS suggests the possibility of closing the missing OH reactivity as long as the mixing ratio and the rate constant of those unidentified compounds are well characterized. The large uncertainty on rate constants was also speculated by Mogensen et al., 2011 as one cause for the missing OH reactivity observed in their model results in a field campaign. For further OH reactivity studies, a value of at least 1 $\times$ 10^{-11} cm^3 molecule^{-1} s^{-1} is needed for VOCs without reported rate constants.

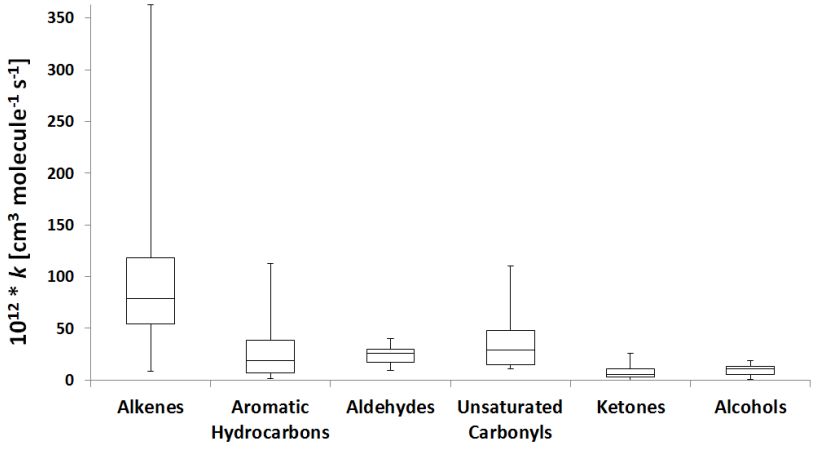

FIGURE 7.15: Room-temperature (298 K) rate constants for the gas-phase reactions of OH radicals with different VOC species reported by Atkinson et al., 2003a. The bottom and top of the box show the 25^{th} and 75^{th} percentiles with the band inside the box showing the median, the ends of the whiskers represent the minimum and the maximum of the reported rate constant.

Chapter 8

Summary and conclusion

This thesis presented results from: 1) characterisation of the newly built plant chamber SAPHIR-PLUS; 2) light- and temperature-dependence of plant emissions; 3) yields determination of different atmosphere system; and 4) OH reactivity comparison in a number of atmospheric scenarios.

The average BVOCs transfer efficiency from PLUS inlet to outlet was 0.85, and was 0.8 from PLUS to the atmosphere simulation chamber SAPHIR. Transfer efficiencies did not demonstrate any significant difference for different VOCs, and no systematic dependence on relative humidity as well. The plant chamber proved to be an excellent facility for use as a source of direct plant emissions in atmospheric simulation experiments.

36 experiments from campaigns in 2014 and 2015 were selected and analyzed. By using the online PTR-TOF-MS, real time change in the measured VOCs was monitored. The identification of VOCs was completed with empirical PTR mass peak analysis and previously reported VOC oxidation products under different conditions (Atkinson et al., 2003b; Rivera-Rios et al., 2014; Volkamer et al., 2002). Monoterpene and sesquiterpene mixtures were better characterized with the help of the GC-FID/MS. The intercomparison between these two VOC-instruments during the selected campaigns exhibited that the measured concentrations of the main reactants used in this study (isoprene, monoterpenes and benzene-D_6) were linearly correlated and differed within 15%.

The newly built plant chamber SAPHIR-PLUS, was implemented to study emissions of BVOCs from 7 sets of plants, from mono-species to mixed trees, from isoprene-emitting trees to monoterpene-emitters. The BVOC emission from six *Quercus ilex* (Holm oak) showed indeed a diurnal profile. Emissions of different compounds under temperature and light influence were in agreement with observations from laboratory plant enclosure and field studies. Isoprene and monoterpenes emission responses to light were strongly photosynthesis-dependent as no storage pools exist for these two compounds in *Quercus ilex* (Guenther, 1993; Kesselmeier et al., 1999; Staudt et al., 1998). Methanol emission emerged a morning burst as observed in previous studies, this phenomenon was explained by its high emission rate from *Quercus ilex* and its high solubility in water (Folkers et al., 2008; Niinemets et al., 2003). Isoprene and monoterpenes emission showed an exponential increase with temperature, with a slope β of $0.11 \pm 0.02\ ^{\circ}C^{-1}$ for the monoterpenes emission, in good agreement with the literature. Methanol emission also escalated with temperature but showed a linear dependence.

Oxidation product studies using real plant emitted BVOCs have not been reported to date. Product yields from ozonolysis of monoterpene—from single injected β-pinene, limonene, to the monoterpene mixture, and finally to the tree-emitted monoterpenes—were investigated in the atmosphere simulation chamber SAPHIR. Isoprene photo-oxidations from single injected to tree-emitted were also simulated. As reported in previous studies, the most important oxidation product from β-pinene ozonolysis in this work was nopinone with a yield of 0.41 ± 0.04. No major products were observed in the limonene ozonolysis, yet the reported common products were successfully identified with commensurable minute yields.

Product yields in ozonolysis of two BVOC mixtures exhibited good agreement with the literature, also with the single BVOC ozonolysis. 5 sets of trees were used in the yield study. The notably high formic (0.57 ± 0.22) and acetic acids (0.35 ± 0.03) yields, as well as the high acetone yield (0.2 ± 0.01) from the ozonolysis of mix trees emission could be explained by experimental flaw, possibly from water condensation in the sampling tube. Apart from that, product yields observed in ozonolysis of tree-emitted monoterpenes were admissibly consistent with the literature or with our single BVOC ozonolysis (one anomaly is the high nopinone yield (0.42 ± 0.08) from *Fagus sylvatica* emission, since only 1.1% of the emission is β-pinene). Acetone is the common product from monoterpene ozonolysis, its yields from our ozonolysis experiments were in accordance with yields found in the literature, except for the mix trees emission as explained above. Different products were identified for photo-oxidations of isoprene at different NO levels, all product yields (from 0.79 to 0.83) showed higher values than the reported yields yet within the uncertainties. MVK + MACR yields (0.57 ± 0.11) from the isoprene-emitting trees were in the expected range as well.
The individual contribution of the VOCs together with inorganic compounds (O_3, NO_x and CO) to the total OH reactivity was calculated and compared to the OH reactivity measured by the LP-LIF instrument. The missing OH reactivity, representing the difference between calculated and measured OH reactivity, was generally bigger in the oxidation phases, implying the production of some reactive compounds which were not included in the OH reactivity calculation. The missing OH reactivity was the largest (75%) in the ozonolysis of limonene due to the lack of detection of limonene oxidation products. OH reactivity attributed to aerosol particles ($0.2\ s^{-1}$) also cannot ameliorate the observed large missing OH reactivity in the ozonolysis of limonene. Our understanding of atmospheric limonene chemistry is still limited and this should be taken into account for future OH reactivity studies involving limonene emissions. As discussed in Chapter 6, no important oxidation products from limonene ozonolysis were observed in other studies as well. For isoprene photo-oxidation experiments, the reported two distinct oxidation pathways under different NO conditions did not demonstrate a remarkable difference on the missing OH reactivity. Moreover, the missing OH reactivity found in the isoprene oxidation experiments can be possibly improved with improvement of the PTR-MS calibration on quantifying isoprene, since the PTR was speculated to measured 10% less of isoprene in the whole study, likely from the bias of isoprene concentration in our gas standard used in calibrations. The oxidations of sesquiterpene-dominating system showed a bigger missing OH reactivity (44-55%) than that in the oxidations of monoterpene-dominating system (5-48%). Sesquiterpene is known as stress-induced emission, highly reactive oxidation products of sesquiterpenes are speculated to cause the observed large missing OH reactivity, those products were probably not identified in the PTR therefore not included in the OH reactivity calculation. Moreover the reported higher gas-particle portioning of sesquiterpenes (12-100%, Helmig et al., 2006) compering to monoterpenes (18-32%, Emanuelsson et al., 2013) could cause higher missing OH reactivity as well. Our results were consistent with Nölscher et al., 2012, where in a Finnish boreal forest a missing OH reactivity of 89% under heat-stressed conditions, and 58% under normal tree emission was reported. Overall the missing OH reactivities were smaller in oxidation experiments containing AVOCs, previous studies reported less missing OH reactivities in rural sites than in the tropical forest sites as well. These results suggested that the OH sink terms in aged BVOCs air masses were poorly constrained, particularly in air mass containing limonene or sesquiterpenes, while the AVOCs in reaction with OH was better understand.
The atomic oxygen-to-carbon (O/C) ratio calculated with all VOCs measured (identified and unidentified) from the PTR measurements, showed a positive correlation with the missing OH reactivity, and confirmed again unknown OH sinks of oxygenated compounds.
Furthermore, the observed missing OH reactivity speculated to be unmeasured/unknown

VOCs, could be interpreted by the PTR measurements. By including all the masses in the PTR mass spectra, with a roughly assumed sensitivity of 10 ppb/ncps, the gap between calculated and measured OH reactivity could be closed with an averaged reaction rate constant k^*, of about 1×10^{-11} cm^3 molecule^{-1} s^{-1}. This k^* value obtained in our work, is slightly lower than the reaction rate constant of some common atmospheric oxidation products (e.g., nopinone, methylglyoxal, MVK and MACR), and is only higher than the reported median rate constant for ketones. For further OH reactivity studies, a value of at least 1×10^{-11} cm^3 molecule^{-1} s^{-1} is suggested for VOCs without reported rate constants.
This work highlighted the use of OH reactivity as a tool to better evaluate the completeness of measured VOC budget. Deploying the OH reactivity method in future chamber studies and at field sites would be of great benefit to better understand atmospheric processes, especially focusing on plants emissions and photochemical transformation.

Appendix A

Sensitivity table

TABLE A.1: Sensitivities used in this work for the VOCs calibrated with the diffusion source or the LCU.

Substance	m/z detected	Calibration date (Year.Month)	relative humidity (%)	Sensitivity (ncps/ppb)	Accuracy (%)
α-pinene	137	2014.09	0	10.0	1.9
			30	8.8	3.2
			50	8.2	3.9
			80	8.5	3.0
		2015.05	0	9.8	1.9
			30	8.7	1.0
			50	8.1	1.0
			80	7.7	1.3
		2015.06	0	6.0	1.9
			60	6.1	2.6
		2015.07	0	7.6	1.5
			60	6.4	1.8
		2015.09	0	12.6	1.0
			60	9.6	1.8
β-pinene	137	2014.10	0	10.5	2.3
			30	9.8	4.8
			50	9.8	4.7
			80	9.2	4.0
		2015.05	0	10.6	2.0
			30	9.5	1.2
			50	9.0	2.8
			80	7.4	1.7
		2015.06	60	7.3	1.9
limonene	137	2014.10	0	10.4	9.6
			30	9.0	7.3
			50	8.9	8.7
			80	8.7	6.7
		2015.07	0	5.9	6.4
			30	6.0	5.2
		2015.09	0	9.4	3.8
			30	7.4	3.3
Δ^3-carene	137	2014.09	0	12.4	3.8
			30	10.6	4.9
			50	10.1	3.1
			80	10.2	4.9
		2015.05	0	11.9	3.1
			30	10.6	1.6
			50	10.9	3.9
			80	9.3	2.1

TABLE A.1: (continued)

Substance	m/z detected	Calibration date (Year.Month)	relative humidity (%)	Sensitivity (ncps/ppb)	Accuracy (%)
		2015.06	0	8.5	1.3
			60	7.5	1.2
		2015.09	0	12.8	1.9
			60	10.0	2.8
myrcene	137	2015.09	0	8.7	4.8
			30	7.5	2.8
β-caryophellene	205	2015.05	0	4.5	24
			30	4.5	24
			50	4.5	24
			80	4.4	24
		2015.06	0	4.8	23
			60	5.9	21
acetic acid	61	2015.04[1]	60	7.8	5.3
ISOPOOH	71	2015.08[1]	60	5.3	5.4
1-pentene	71	2015.09	0	10.4	1.7
			60	10.0	3.7
o-xylene	107	2015.10	0	19.5	3.0
			60	15.2	1.8
phenol	101	2015.03[1]	60	13.3	5.3

[1] Calibrated with the LCU.

TABLE A.2: Sensitivities used in this work for the VOCs calibrated with the gas standard at relative humidity of ˜60%. Calibration accuracy in % is given in brackets.

Substance	**m/z detected**	**Calibration time**				
		2014.09	2015.05	2015.07	2015.08	2015.09
methanol[a]	33	10.4 (±6.4)	9.8 (±6.2)	11.0 (±6.1)	8.2 (±6.6)	8.9 (±6.9)
acetaldehyde[b]	45	20.2 (±5.9)	19.6 (±5.8)	18.1(±5.8)	17.9 (±5.8)	17.9 (±5.9)
acetone[c]	59	23.8 (±6.0)	22.3 (±5.9)	20.0 (±5.9)	19.9 (±5.9)	20.3 (±6.1)
isoprene[d]	69	15.2 (±5.8)	14.1 (±5.8)	12.2 (±5.8)	12.3 (±5.9)	12.7 (±6.1)
MVK[e]	71	17.9 (±5.9)	16.1 (±5.9)	14.6 (±5.9)	13.9 (±5.9)	14.8 (±6.3)
2-butanone[f]	73	23.8 (±5.8)	21.0 (±5.8)	18.6 (±5.9)	18.5 (±5.9)	19.4 (±6.3)
benzene[g]	79	13.5 (±5.8)	11.8 (±5.8)	10.3 (±5.9)	10.1 (±5.9)	10.7 (±5.9)
3-pentanone[h]	87	22.6 (±6.0)	19.5 (±6.1)	17.2 (±6.3)	17.5 (±6.0)	18.1 (±6.3)
toluene[i]	93	16.5 (±5.8)	13.3 (±6.0)	12.1 (±6.0)	12.1 (±6.0)	16.5 (±6.5)
o-xylene[j]	107	18.2 (±5.8)	15.3 (±6.2)	12.8 (±6.0)	12.8 (±6.1)	13.6 (±6.1)
chlorobenzene[k]	113	14.5 (±5.8)	11.7 (±5.9)	10.4 (±5.9)	10.5 (±5.9)	11.0 (±6.0)
mesitylene[l]	121	19.7 (±6.0)	15.2 (±6.0)	12.9 (±6.1)	13.1 (±6.2)	14.2 (±6.3)
α-pinene[m]	137	8.2 (±5.9)	6.3 (±5.8)	5.3 (±5.8)	5.3 (±5.9)	6.0 (±5.9)
nopinone[n]	139	25.7 (±6.1)	16.6 (±6.2)	18.0 (±5.8)	14.9 (±6.3)	18.5 (±6.5)

[a] 99.9% pure, Sigma-Aldrich.
[b] 99.5% pure, Fluka Analytical.
[c] 99.8% pure, Merck.
[d] 99.5% pure, Fluka Analytical.
[e] 99% pure, Fluka Analytical.
[f] 99.5% pure, Fluka Analytical.
[g] 99.5% pure, Merck.
[h] 99.5% pure, Fluka Analytical.
[i] 99.5% pure, Sigma-Aldrich.
[j] 99.5% pure, Fluka Analytical.
[k] 99.8% pure, Sigma-Aldrich.
[l] 99% pure, Fluka Analytical.
[m] 98.5% pure, Fluka Analytical.
[n] 98% pure, Sigma-Aldrich.

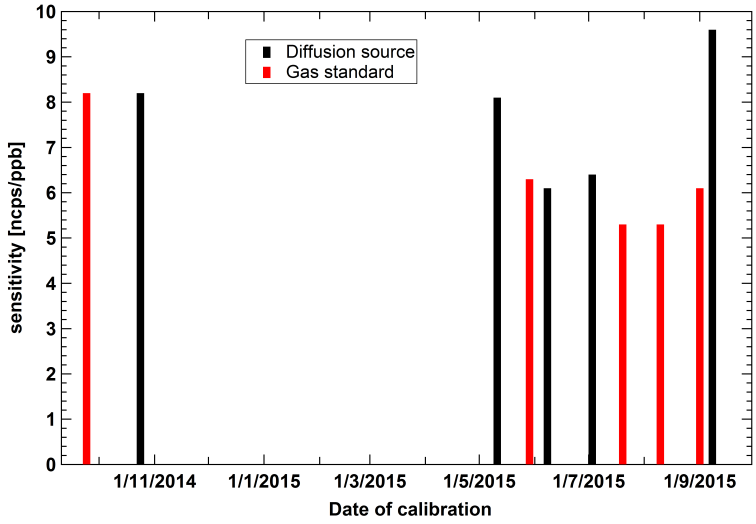

FIGURE A.1: comparison of α-pinene sensitivity obtained by diffusion source (black) and gas standard (red) calibrations at 60% of relative humidity.

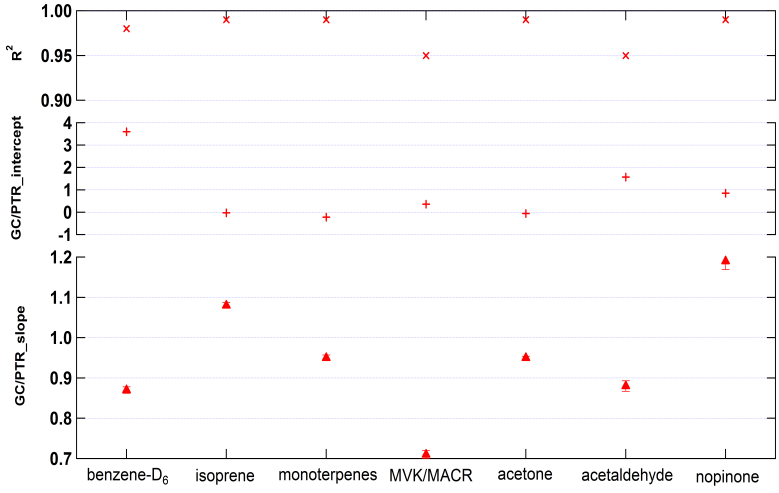

FIGURE A.2: Overall comparison between GC and PTR measurements for some abundant compounds in this study.

Appendix B

kOH comparison time series

The common experimental procedure for VOC oxidation experiments in SAPHIR is: I) overnight purification with a clean synthetic air to reduce contaminations in the SAPHIR simulation chamber ; II) a typical experiment starts at early morning with addition of water vapor to reach the defined relative humidity, the humidification is completed after approximately 45 min; III) addition of the VOC of interest (time point shown as green vertical line); IV) addition of the oxidant. All experiments are conducted under atmospheric pressure at ambient temperature. Ozonolysis experiments are performed in the dark chamber. In the photo-oxidation experiments, the chamber is exposed to sunlight by opening the roof. Experimental operation time point is marked with vertical colored lines in the following figures: green line the start/stop injection of VOC, red the injection of O_3, grey the injection of $NO/NO_2/CO$, and blue the roof operation. Lower panel shows the k_{OH}^{cal} with respect to the contribution of species in different colors, together with the k_{OH}^{meas} (black dots). The calculation uncertainty of k_{OH}^{cal} is shown in grey shadow, black error bars are one σ of the k_{OH}^{meas}. Middle panel shows the ratio of k_{OH}^{cal} over k_{OH}^{meas} (black line) with the upper and lower limit of the uncertainty (grey shadow). Upper panel is the rate constant (k^*) derived from the unidentified compounds to explain the missing k_{OH}.

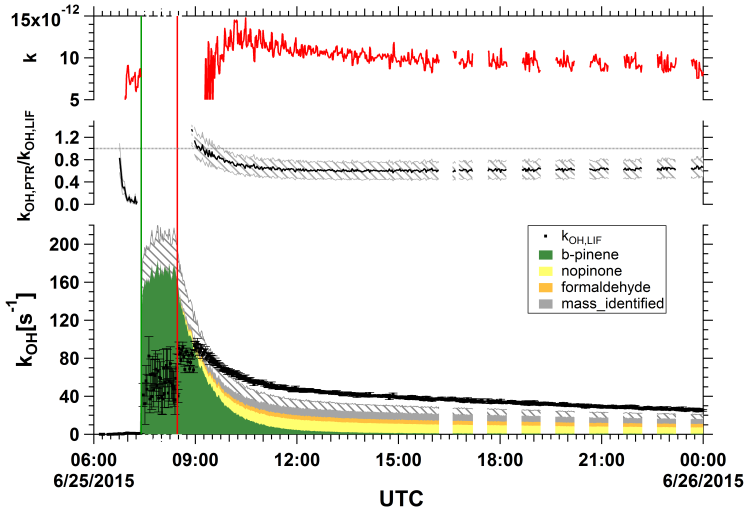

a) BS1: β-Pinene ozonolysis

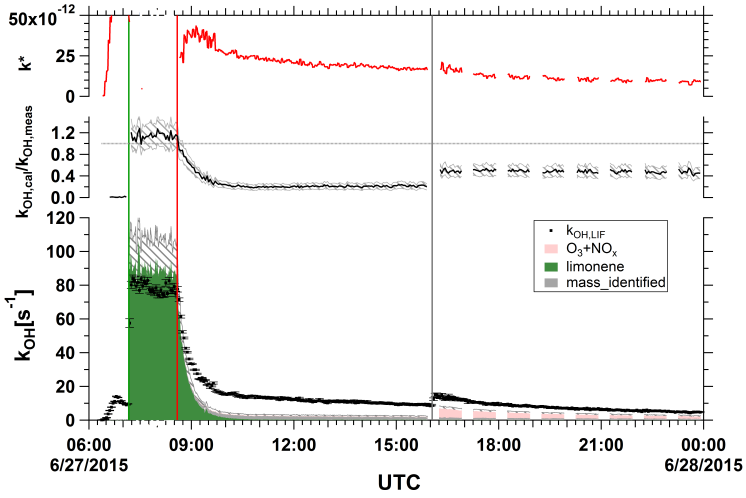

b) BS2: Limonene ozonolysis

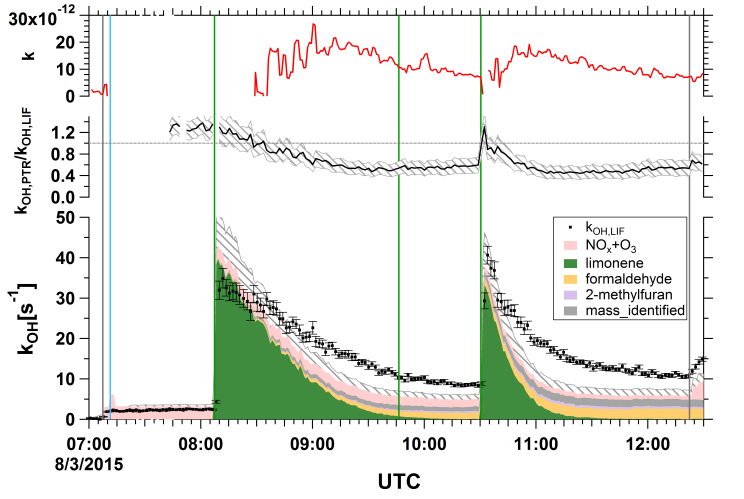

c) BS3: Limonene photooxidation

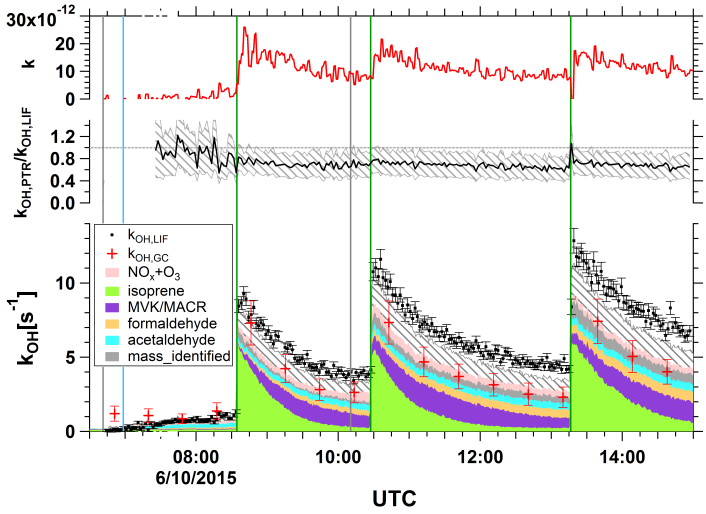

d) BS4: Isoprene photooxidation (high NO)

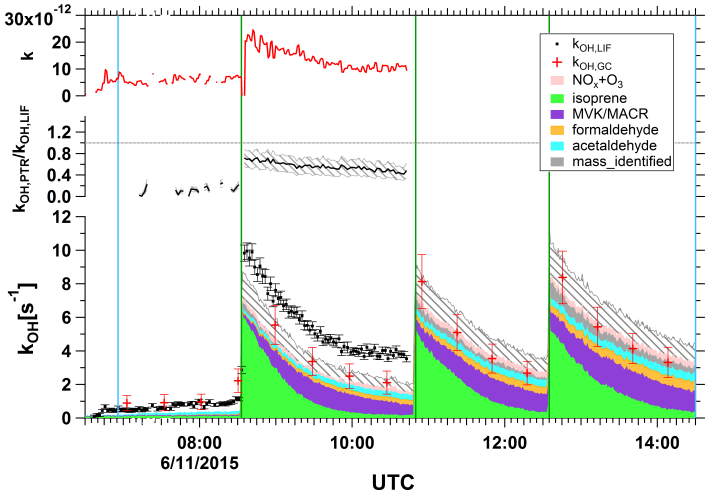

e) BS5: Isoprene photooxidation (medium NO)

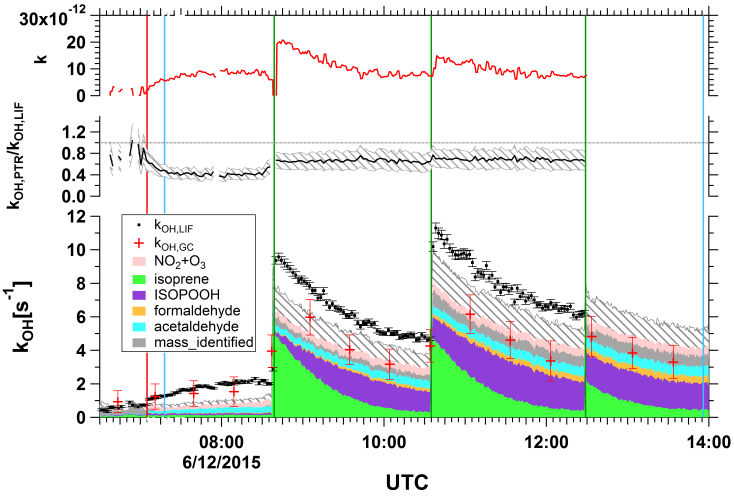

f) BS6: Isoprene photooxidation (low NO)

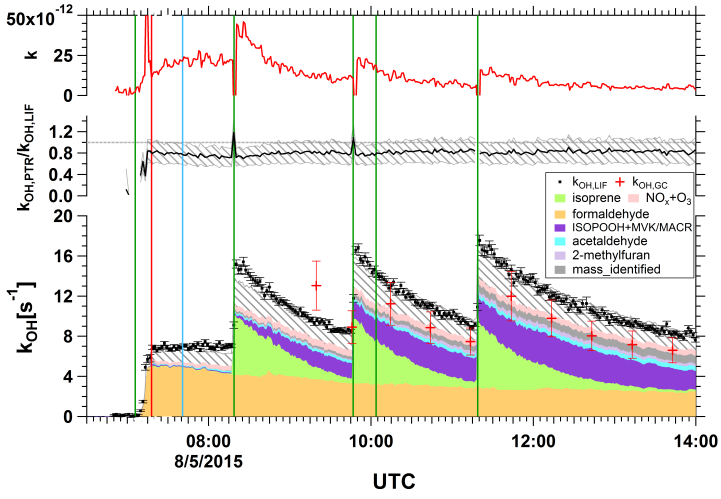

g) BS7: Isoprene photooxidation (medium NO)

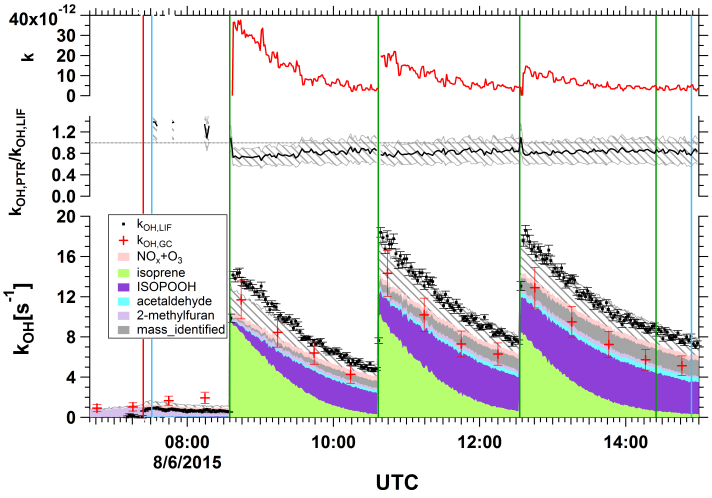

h) BS8: Isoprene photooxidation (low NO)

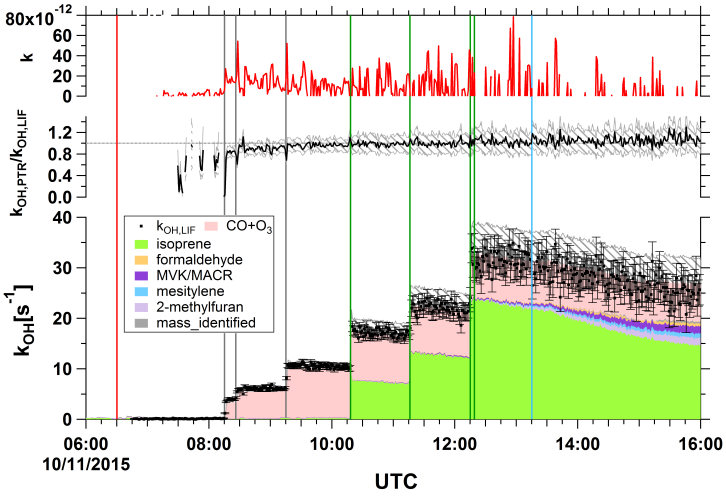

i) BS9: Linear CO/isoprene ozoznolysis

FIGURE B.1: Time series of k_{OH}^{cal} and k_{OH}^{meas} for oxidations of single BVOC. Lower panel shows the k_{OH}^{cal} with respect to the contribution of species in different colors, together with the k_{OH}^{meas} (black dots). The calculation uncertainty of k_{OH}^{cal} is shown in grey shadow, black error bars are one σ of the k_{OH}^{meas}. Colored vertical lines indicate the start/stop injection of VOC (green line), injection of O_3 (red), injection of $NO/NO_2/CO$ (grey line), and the roof operation (blue line). Middle panel shows the ratio of k_{OH}^{cal} over k_{OH}^{meas} (black line) with the upper and lower limit of the uncertainty (grey shadow). Upper panel is the rate constant (k^*) derived from the unidentified compounds to explain the missing k_{OH}.

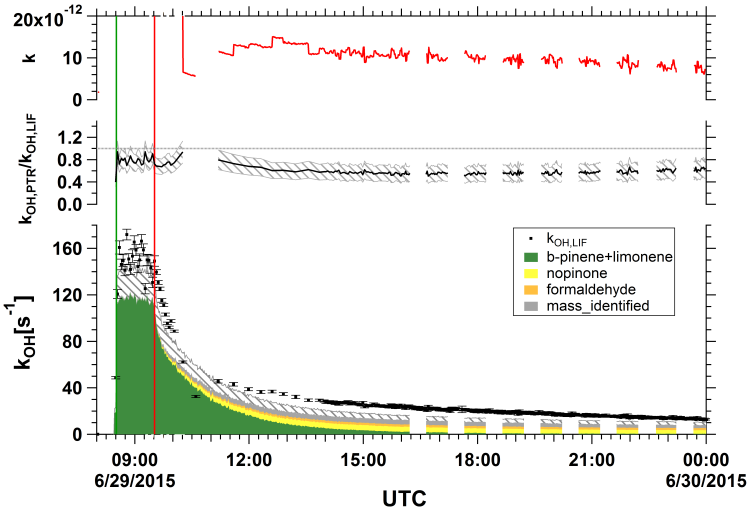

a) BM1: Ozonolysis of β-pinene and limonene.

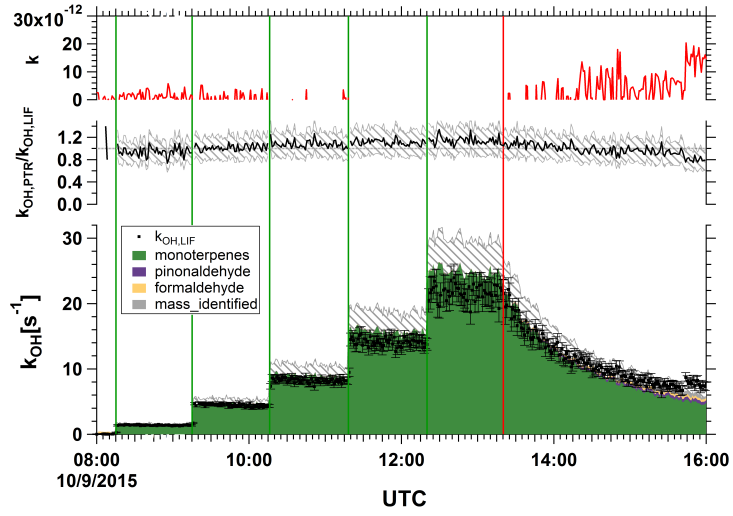

b) BM2: Forest mixture I Ozonolysis

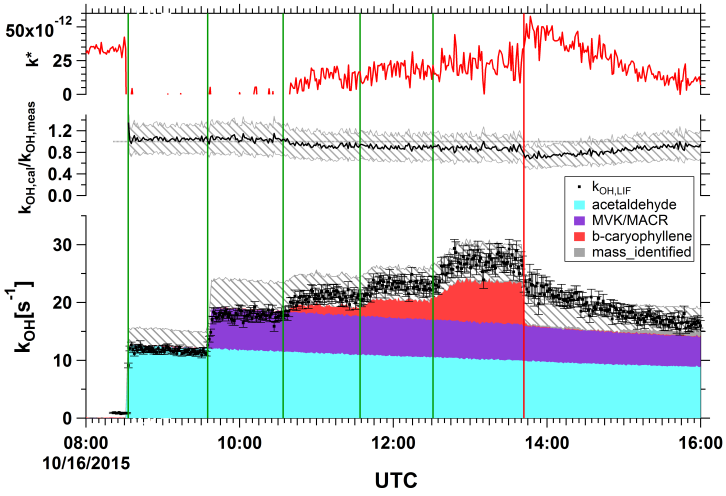

c) BM3: Forest mixture II Ozonolysis

FIGURE B.2: Time series of k_{OH}^{cal} and k_{OH}^{meas} for ozonolysis of BVOC mixtures. Lower panel shows the k_{OH}^{cal} with respect to the contribution of species in different colors, together with the k_{OH}^{meas} (black dots). The calculation uncertainty of k_{OH}^{cal} is shown in grey shadow, black error bars are one σ of the k_{OH}^{meas}. Colored vertical lines indicate the injection time of VOCs (green line) and O_3 (red). Middle panel shows the ratio of k_{OH}^{cal} over k_{OH}^{meas} (black line) with the upper and lower limit of the uncertainty (grey shadow). Upper panel is the rate constant (k^*) derived from the unidentified compounds to explain the missing k_{OH}.

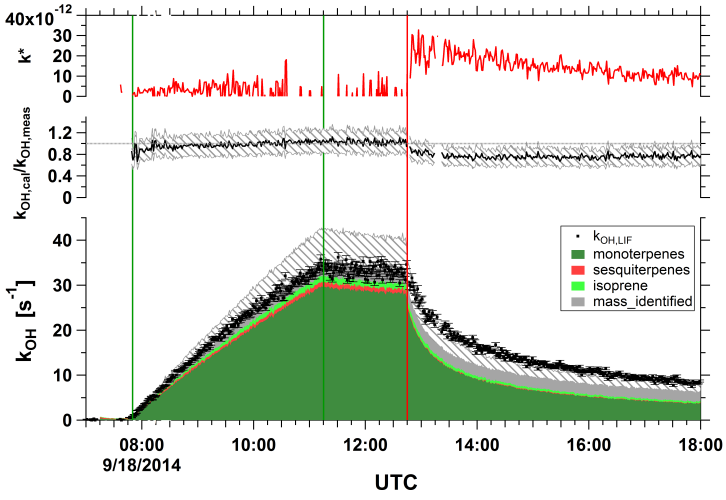

a) BP1.Ozonolysis of BVOC from *Quercus ilex* tree emissions

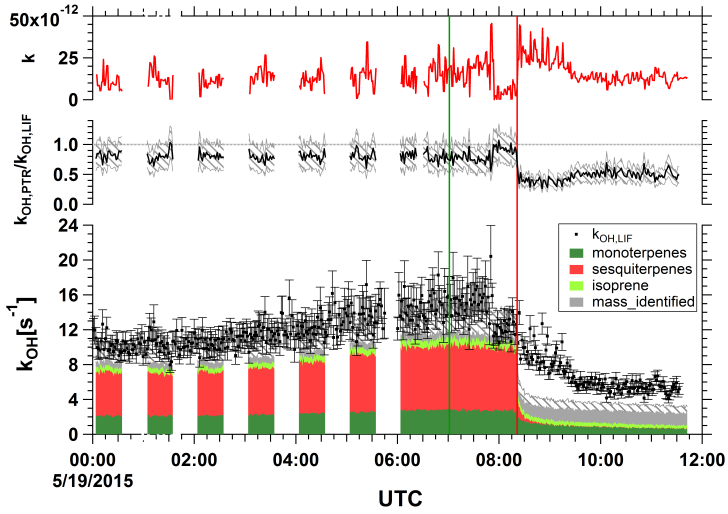

b) BP2.Ozonolysis of BVOC from *Picea abies* tree emissions

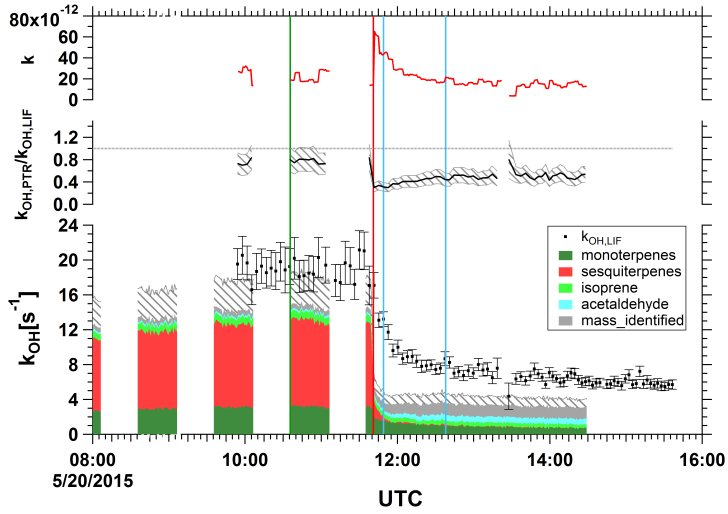

c) BP3.Photooxidation of BVOC from *Picea abies* tree emissions

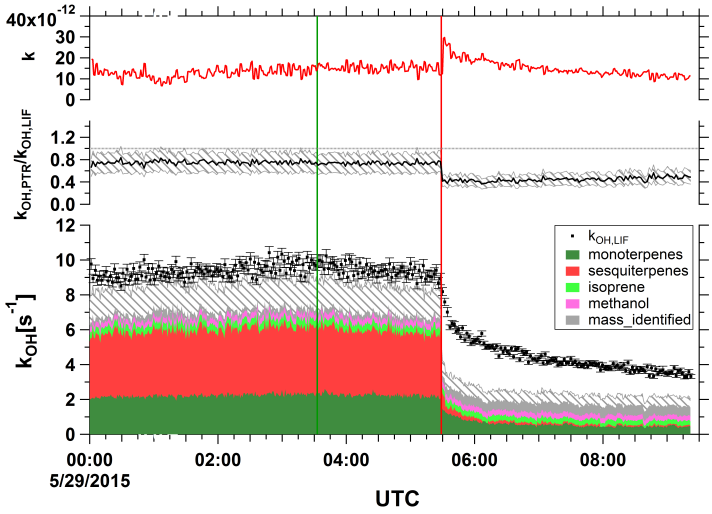

d) BP4.Ozonolysis of BVOC from *Betula pendula* tree emissions

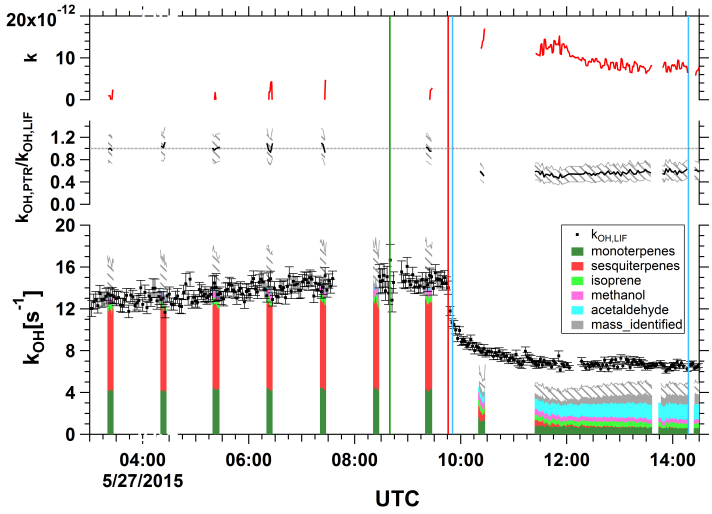

e) BP5.Photooxidation of BVOC from *Betula pendula* tree emissions

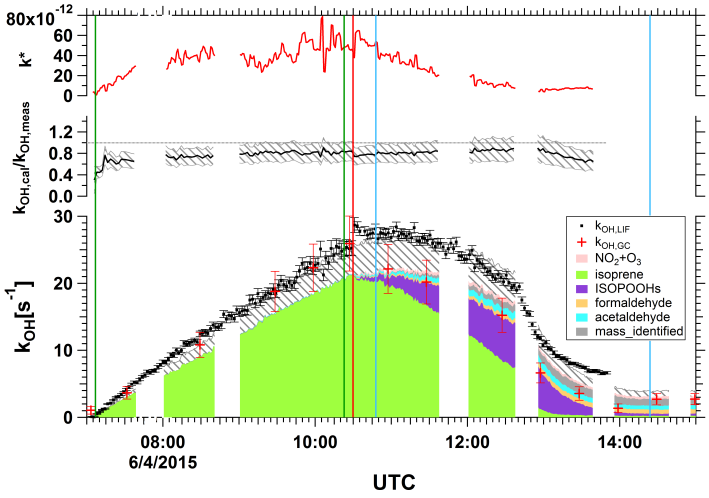

f) BP6.Photooxidation of BVOC from *Quercus robur* tree emissions

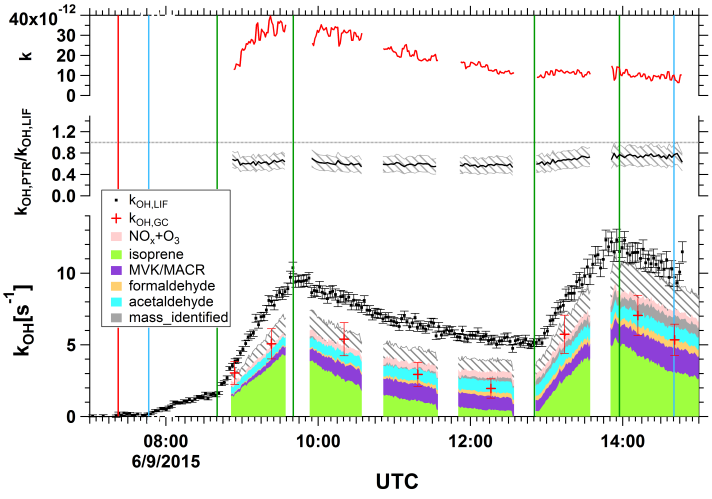

g) BP7.Photooxidation of BVOC from *Quercus robur* tree emissions

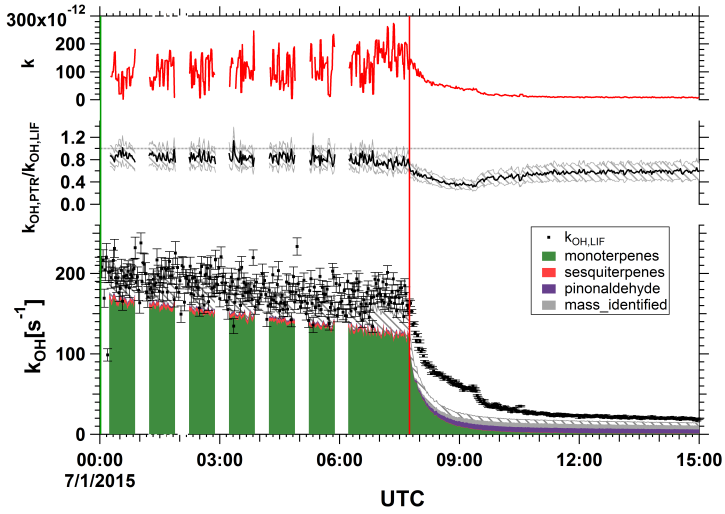

h) BP8.Ozonolysis of BVOC from *Pinus sylvestris* tree emissions

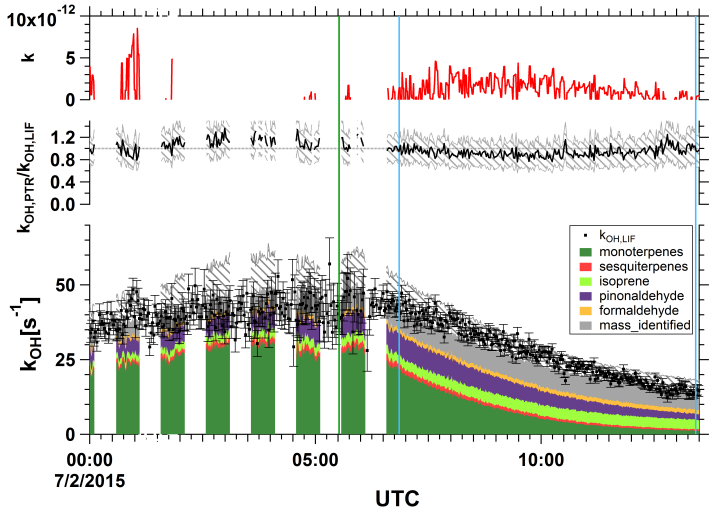

i) BP9.Photooxidation of BVOC from *Pinus sylvestris* tree emissions

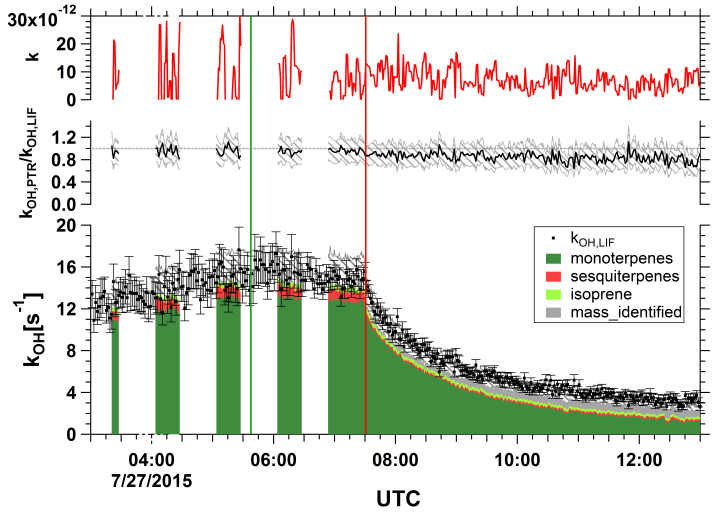

j) BP10.Ozonolysis of BVOC from *Fagus sylvatica* tree emissions

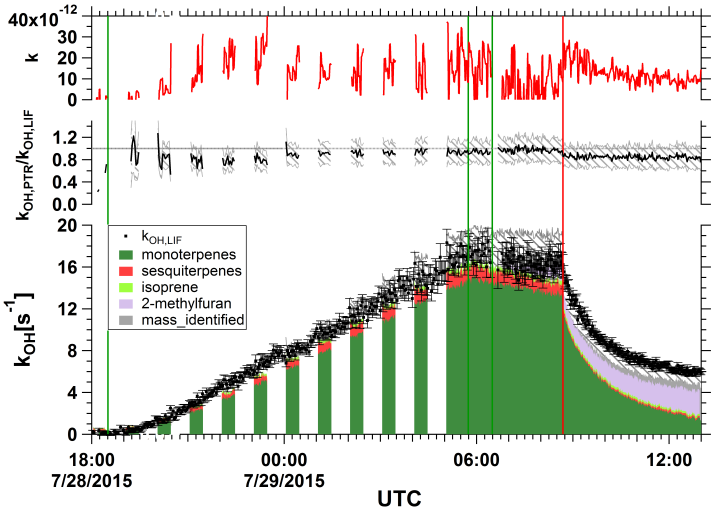

k) BP11.Ozonolysis of BVOC from *Fagus sylvatica* tree emissions

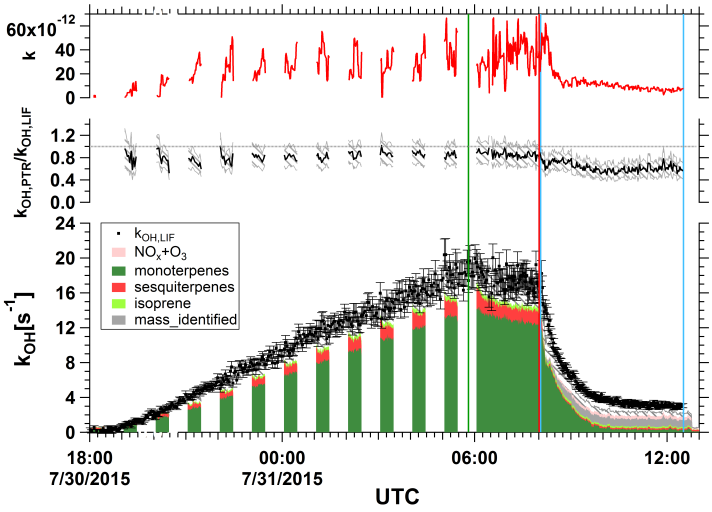

l) BP12.Photooxidation of BVOC from *Fagus sylvatica* tree emissions

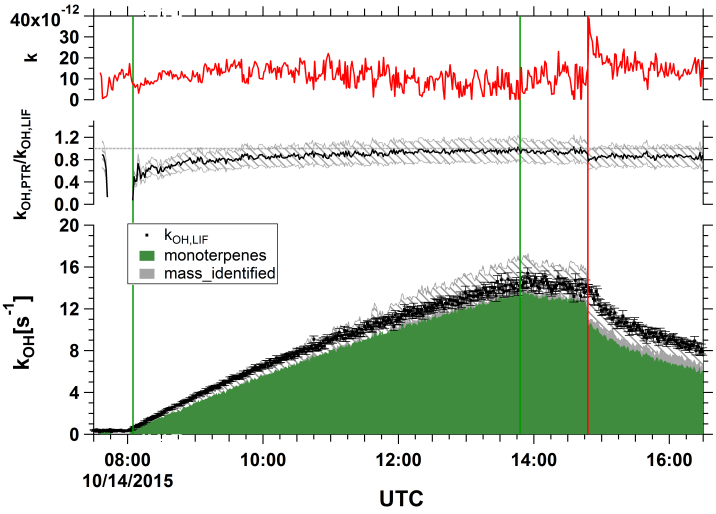

m) BP13.Ozonolysis of BVOC from *Pinus sylvestris* and *Fagus sylvatica* tree emissions

FIGURE B.3: Time series of k_{OH}^{cal} and k_{OH}^{meas} for the oxidation of BVOC from plant emissions. Lower panel shows the k_{OH}^{cal} with respect to the contribution of species in different colors, together with the k_{OH}^{meas} (black dots). The calculation uncertainty of k_{OH}^{cal} is shown in grey shadow, black error bars are one σ of the k_{OH}^{meas}. Colored vertical lines indicate the start/end time of coupling with the plant chamber (green line), the injection of O_3 (red), and the roof operation (blue line). Middle panel shows the ratio of k_{OH}^{cal} over k_{OH}^{meas} (black line) with the upper and lower limit of the uncertainty (grey shadow). Upper panel is the rate constant (k^*) derived from the unidentified compounds to explain the missing k_{OH}.

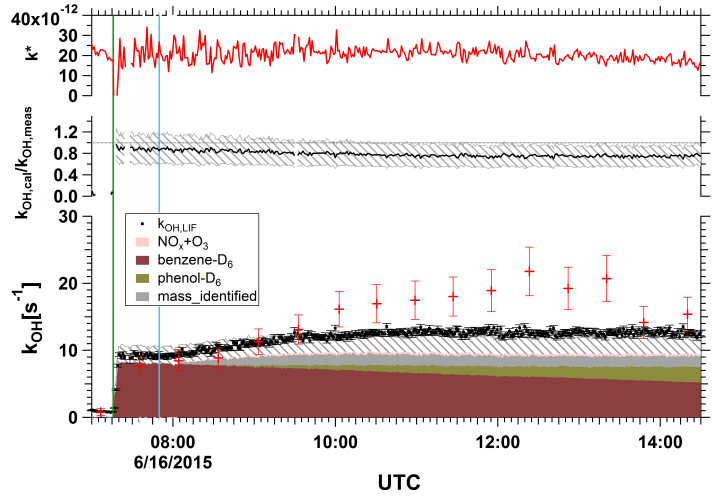

AS1: Photo-oxidation of benzene-D_6 (low NO_x)

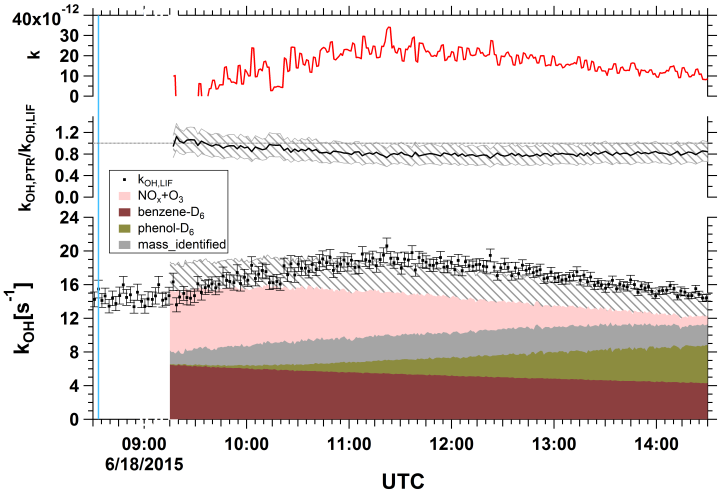

AS2: Photo-oxidation of benzene-D_6 (high NO_x)

FIGURE B.4: Time series of k_{OH}^{cal} and k_{OH}^{meas} for the oxidation of benzene-D_6. Lower panel shows the k_{OH}^{cal} with respect to the contribution of species in different colors, together with the k_{OH}^{meas} (black dots). The calculation uncertainty of k_{OH}^{cal} is shown in grey shadow, black error bars are one σ of the k_{OH}^{meas}. Colored vertical lines indicate the injection of VOC (green line) and the roof operation (blue). Middle panel shows the ratio of k_{OH}^{cal} over k_{OH}^{meas} (black line) with the upper and lower limit of the uncertainty (grey shadow). Upper panel is the rate constant (k^*) derived from the unidentified compounds to explain the missing k_{OH}.

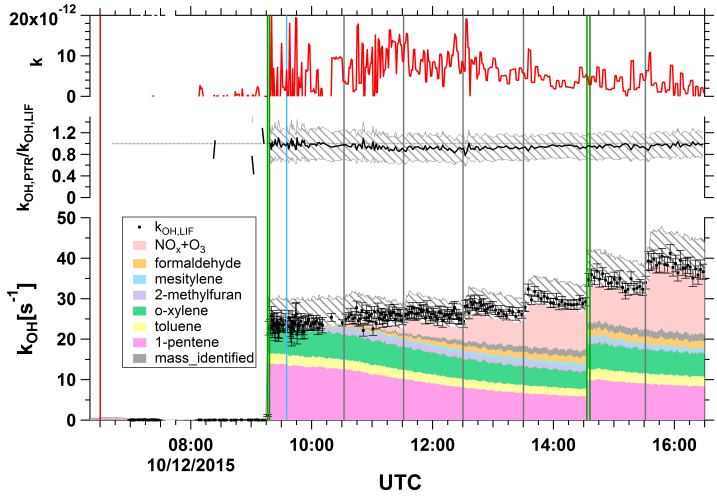

a) AM1: Photo-oxidation of Urban mixture

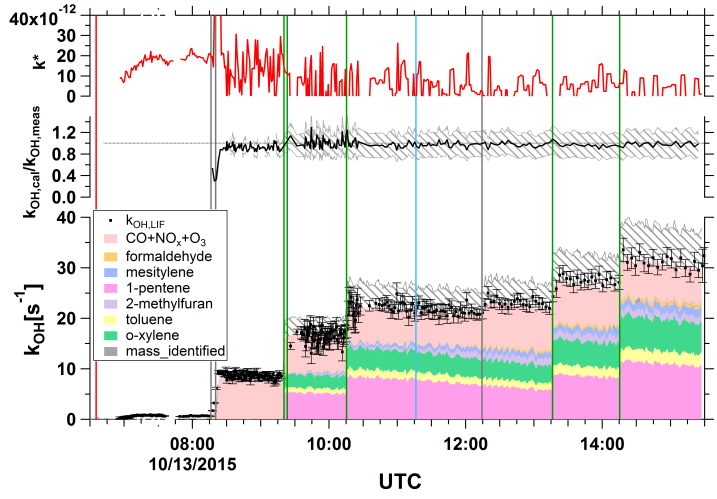

b) AM2: Photo-oxidation of Urban mixture and CO

FIGURE B.5: Time series of k_{OH}^{cal} and k_{OH}^{meas} for oxidations of the urban mixture. Lower panel shows the k_{OH}^{cal} with respect to the contribution of species in different colors, together with the k_{OH}^{meas} (black dots). The calculation uncertainty of k_{OH}^{cal} is shown in grey shadow, black error bars are one σ of the k_{OH}^{meas}. Colored vertical lines indicate the injection of VOCs (green line), injection of O_3 (red), injection of NO_2/CO (grey), and the roof operation (blue). Middle panel shows the ratio of k_{OH}^{cal} over k_{OH}^{meas} (black line) with the upper and lower limit of the uncertainty (grey shadow). Upper panel is the rate constant (k^*) derived from the unidentified compounds to explain the missing k_{OH}.

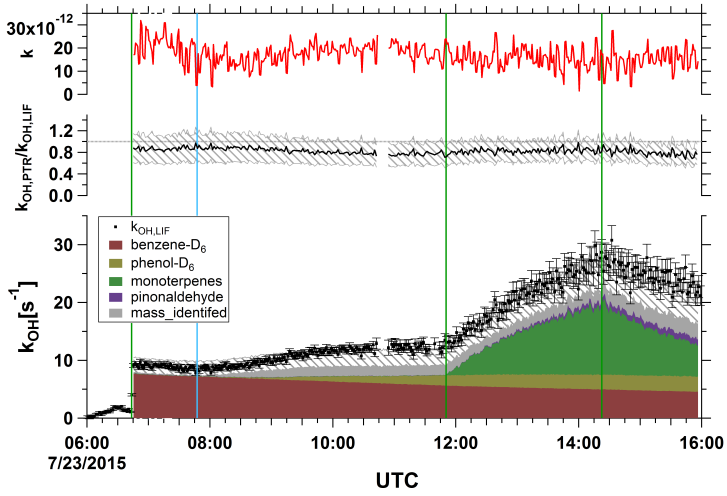

a) AB1: Photooxidation of [benzene-D_6] + [BVOC]

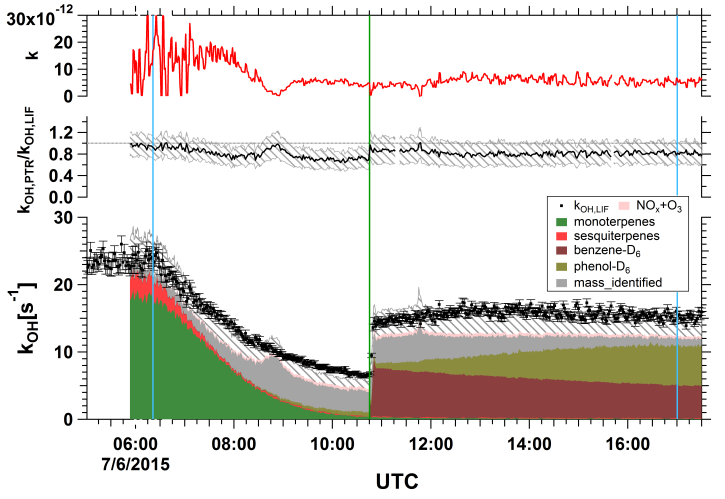

b) AB2: Photooxidation of [BVOC] + [benzene-D_6]

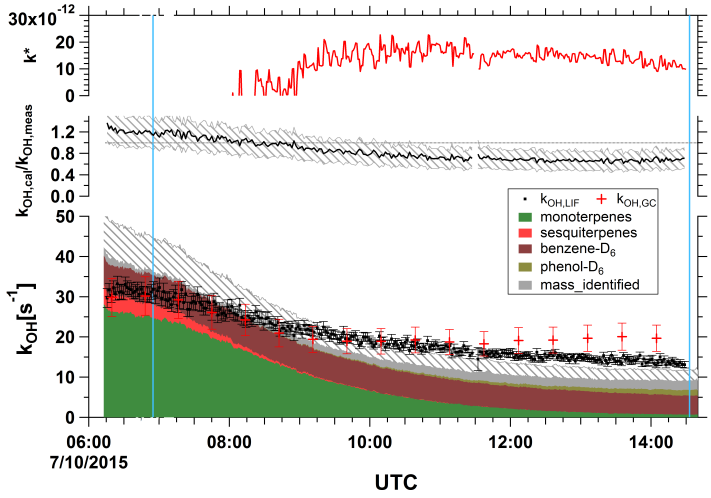

c) AB3: Photooxidation of [BVOC + benzene-D_6]

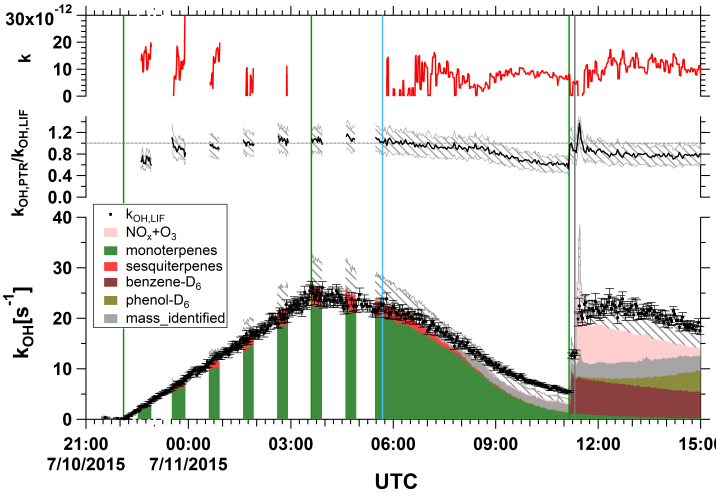

d) AB4: Photooxidation of [BVOC] + [benzene-D_6 + NO]

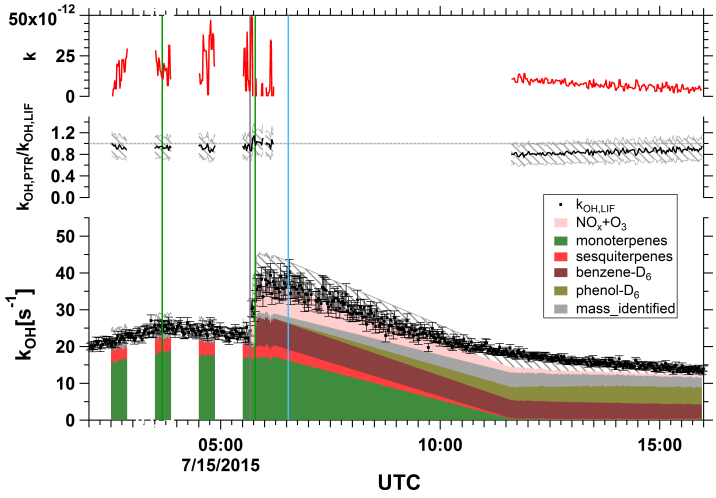

e) AB5: Photooxidation of [BVOC + NO + benzene-D_6]

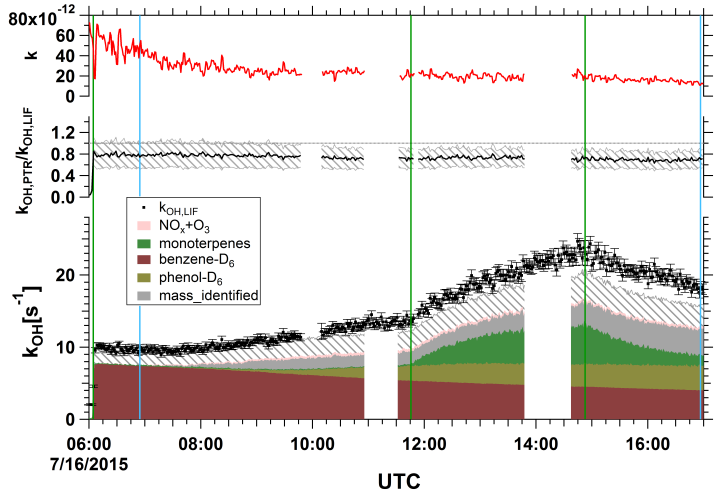

f) AB6: Photooxidation of [benzene-D_6] + [BVOC]

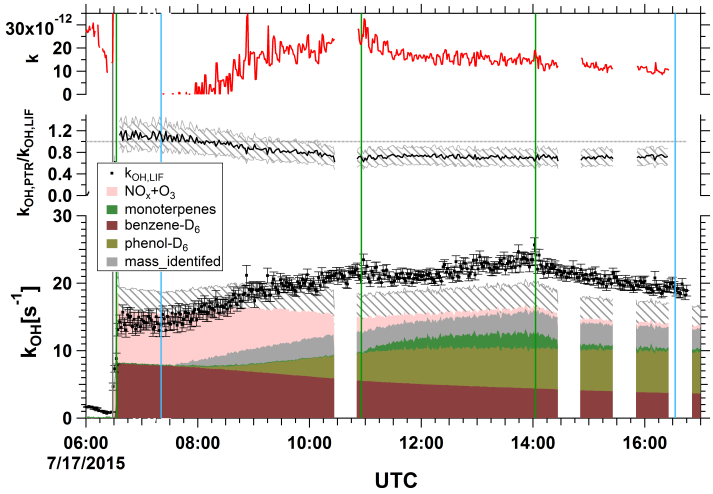

g) AB7: Photooxidation of [benzene-D_6 + NO] + [BVOC]

FIGURE B.6: Time series of k_{OH}^{cal} and k_{OH}^{meas} for oxidations of the mixture of AVOC and BVOC from tree emission. Lower panel shows the k_{OH}^{cal} with respect to the contribution of species in different colors, together with the k_{OH}^{meas} (black dots). The calculation uncertainty of k_{OH}^{cal} is shown in grey shadow, black error bars are one σ of the k_{OH}^{meas}. Colored vertical lines indicate the start/end time of coupling with the plant chamber (green line), the injection of NO (grey), and the roof operation (blue).. Middle panel shows the ratio of k_{OH}^{cal} over k_{OH}^{meas} (black line) with the upper and lower limit of the uncertainty (grey shadow). Upper panel is the rate constant (k^*) derived from the unidentified compounds to explain the missing k_{OH}.

TABLE B.1: A summary of experiments of BVOCs oxidation.

Experiments	reactant phase/product phase		
	$k_{OH}^{cal}/k_{OH}^{meas}$	O/C	k^{*a}
BS1 β-pinene + O_3	-	0.01±0.01	-
	0.66±0.16	0.34±0.06	10.6±2.7
BS2 Limonene + O_3	1.15±0.23	0.09±0.03	-
	0.25±0.06	0.55±0.07	23.2±6.4
BS3 Limonene + OH[b]	1.25±0.26	0.2±0.01	-
	0.6±0.13	0.49±0.08	16.3±4.0
BS4 Isoprene + OH, high NO	0.82±0.18	0.63±0.01	15.1±6.7
	0.68±0.18	0.66±0.02	11.8±3.0
BS5 Isoprene + OH, medium NO	0.71±0.16	0.49±0.01	14.2±7.7
	0.56±0.15	0.64±0.04	13.6±2.6
BS6 Isoprene + OH, low NO	0.67±0.15	0.56±0.03	3.4±5.2
	0.67±0.18	0.64±0.03	9.6±2.1
BS7 Isoprene + OH, mid NO[b]	0.73±0.17	0.78±0.01	30.0±23.7
	0.81±0.2	0.81±0.01	12.9±3.0
BS8 Isoprene + OH, low NO[b]	0.74±0.16	0.49±0.01	28.0±18.1
	0.81±0.21	0.62±0.03	8.6±4.0
BS9 [CO + Isoprene] + OH[c]	1.02±0.21	0.25±0.01	-
	1.06±0.24	0.48±0.01	-
BM1 [β-pinene + limonene] + O_3	0.79±0.16	0.03±0.01	159.4±60.2
	0.56±0.15	0.4±0.05	11.1±1.6
BM2 Forest mixture I + OH	1.13±0.25	0.16±0.01	1.1±9.2
	0.96±0.22	0.4±0.01	4.4±2.3
BM3 Forest mixture II + OH	0.88±0.24	0.42±0.05	4.6±7.8
	0.83±0.23	0.5±0.01	3.6±6.5
BP1 *Quercus ilex* emissions + O_3	1.02±0.21	0.08±0.01	-
	0.75±0.16	0.3±0.04	17±4.2
BP2 *Picea abies* emissions + O_3	0.81±0.23	0.34±0.01	14.4±8.9
	0.47±0.13	0.53±0.02	16.3±6.8
BP3 *Picea abies* emissions + OH	0.79±0.21	0.31±0.02	22.4±5.9
	0.5±0.14	0.55±0.01	16.0±4.1
BP4 *Betula pendula* emissions + O_3	0.75±0.18	0.61±0.01	14.3±2.3
	0.45±0.11	0.7±0.01	14.5±3.1
BP5 *Betula pendula* emissions + OH	1.01±0.25	0.57±0.07	-
	0.56±0.04	0.73±0.04	9.5±2.3
BP6 *Quercus robur* emissions + OH	0.81±0.17	0.67±0.01	43.9±11.0
	0.8±0.21	0.72±0.05	8.1±2.3
BP7 *Quercus robur* emissions + OH	0.66±0.15	0.69±0.01	34.8±2.2
	0.58±0.15	0.72±0.07	21.0±3.0
BP8 *Pinus sylvestris* emissions + O_3	0.82±0.17	0.07±0.01	118.4±56.9
	0.52±0.13	0.44±0.06	20.6±19.2
BP9 *Pinus sylvestris* emissions + OH	1.08±0.28	0.38±0.54	-
	0.95±0.26	0.54±0.04	0.9±1.2
BP10 *Fagus sylvatica* emissions + O_3	0.96±0.22	0.29±0.06	7.0±10.4
	0.85±0.2	0.6±0.06	6.6±3.8
BP11 *Fagus sylvatica* emissions + O_3[b]	0.97±0.21	0.23±0.03	8.3±10.1
	0.85±0.19	0.49±0.04	11.0±3.1
BP12 *Fagus sylvatica* emissions + OH	0.86±0.19	0.18±0.02	35.2±14.3
	0.61±0.15	0.69±0.06	11.2±3.2
BP13 mixed tree emissions + O_3	0.95±0.2	0.19±0.01	9.5±5.9
	0.84±0.18	0.4±0.01	14.5±3.3

[a] (10^{-12} cm^3 $molecule^{-1}$ s^{-1})
[b] A VOC-OH trace standard containing 2-methylfuran.
[c] A VOC-OH trace standard containing 2-methylfuran (C_5H_6O) and mesitylene (C_9H_{12}).

TABLE B.2: A summary of experiments of AVOCs oxidation.

Experiments	**reactant phase/product phase**		
	$k_{OH}^{cal}/k_{OH}^{meas}$	**O/C**	k^{*a}
AS1 benzene-D_6 + OH, low NO_x	0.89±0.27	0.01±0.01	20.5±5.7
	0.7±0.19	0.03±0.01	19.7±2.6
AM1 Urban mixture + OH[b]	1.0±0.3	0.03±0.01	1.1±9.2
	0.94±0.23	0.27±0.01	4.4±2.3
AM2 Urban mixture + OH[b]	0.97±0.23	0.07±0.01	4.6±7.8
	0.97±0.22	0.15±0.01	3.6±6.5
AB1 Photo-oxidation of [benzene-D_6] + [BVOCs[c]]	0.87±0.27	0.01±0.01	20.6±6.2
	0.81±0.21	0.03±0.01	16.3±4.3
AB2 Photo-oxidation of [BVOCs[d]] + [benzene-D_6]	0.96±0.21	0.17±0.01	10.9±8.0
	0.77±0.19	0.58±0.09	6.6±4.2
AB3 Photo-oxidation of [BVOCs[d] + benzene-D_6]	1.22±0.29	0.01±0.01	-
	0.67±0.18	0.08±0.01	13.9±2.1
AB4 Photo-oxidation of [BVOCs[d]] + [benzene-D_6 + NO]	1.07±0.23	0.13±0.01	-
	0.74±0.17	0.56±0.07	7.3±2.3
AB5 Photo-oxidation of [BVOCs[d] + NO + benzene-D_6]	1.01±0.23	0.02±0.01	-
	0.82±0.19	0.09±0.01	8.5±2.0
AB6 Photo-oxidation of [benzene-D_6] + [BVOCs[d]]	0.79±0.24	0.01±0.01	48.6±8.7
	0.72±0.19	0.04±0.01	21.2±2.8
AB7 Photo-oxidation of [benzene-D_6 + NO] + [BVOCs[d]]	1.11±0.25	0.01±0.01	-
	0.74±0.17	0.04±0.01	21.8±3.9

[a] (10^{-12} cm^3 $molecule^{-1}$ s^{-1})
[b] Adding along a VOC-OH trace standard containing 2-methylfuran and mesitylene.
[c] BVOCs from a monoterpenes mixture canister.
[d] BVOCs from 6 *Pinus sylvestris* trees emission

Appendix C

Yield plot

Yields of oxidation products observed for all oxidation experiments are presented here. Left side figure shows the time series of consumed reactant and product yield for the whole experiment, starting from 10 mins before the O_3 injection, or in photo-oxidation experiment, from the moment when the reactant is added. Right side figure is the correlation between product and reactant, selected data points end when 90% of the reactant is consumed. All concentrations were corrected for dilution loss, and in photo-oxidation experiments, were also corrected for the chamber source.

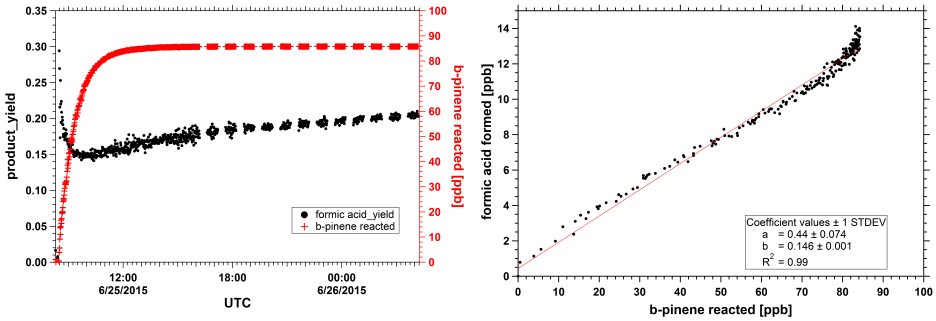

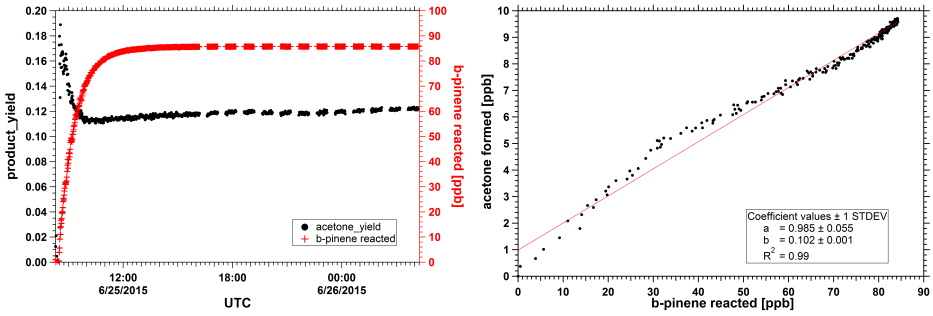

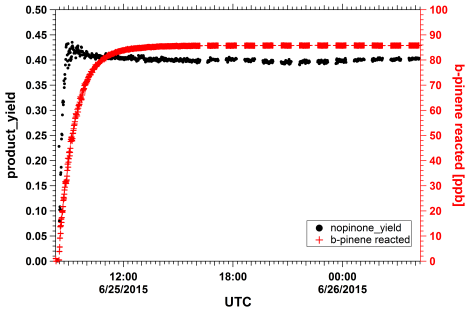
product_yield
b-pinene reacted [ppb]
nopinone_yield
b-pinene reacted
12:00
6/25/2015
18:00
00:00
6/26/2015
UTC

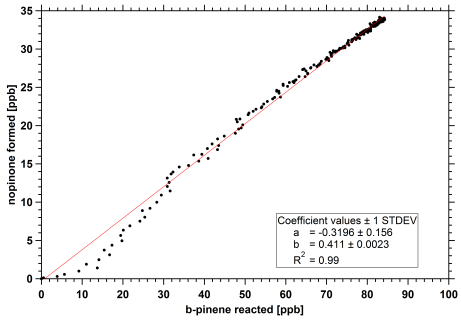
nopinone formed [ppb]
b-pinene reacted [ppb]
Coefficient values ± 1 STDEV
a = -0.3196 ± 0.156
b = 0.411 ± 0.0023
R² = 0.99

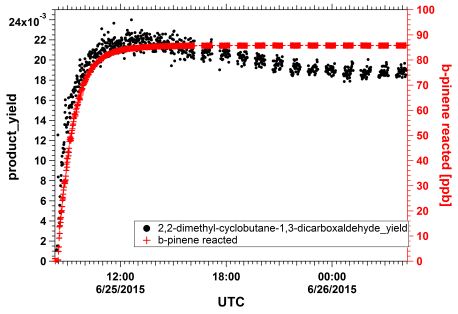
24x10⁻³
product_yield
b-pinene reacted [ppb]
2,2-dimethyl-cyclobutane-1,3-dicarboxaldehyde_yield
b-pinene reacted
12:00
6/25/2015
18:00
00:00
6/26/2015
UTC

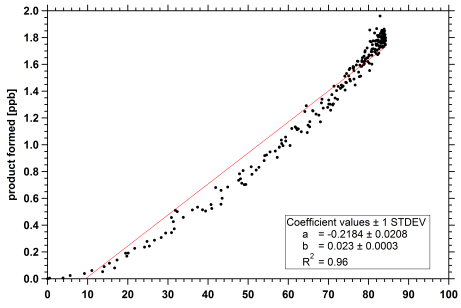
product formed [ppb]
b-pinene reacted [ppb]
Coefficient values ± 1 STDEV
a = -0.2184 ± 0.0208
b = 0.023 ± 0.0003
R² = 0.96

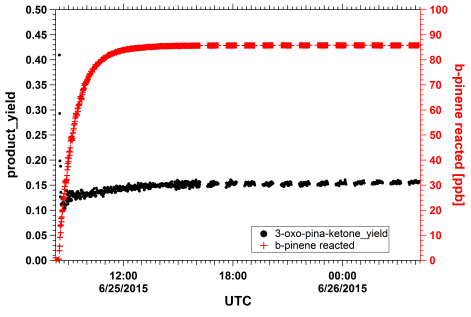
product_yield
b-pinene reacted [ppb]
3-oxo-pina-ketone_yield
b-pinene reacted
12:00
6/25/2015
18:00
00:00
6/26/2015
UTC

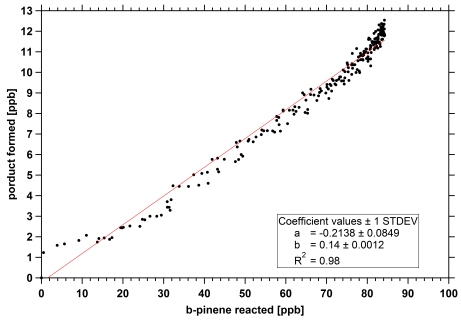
porduct formed [ppb]
b-pinene reacted [ppb]
Coefficient values ± 1 STDEV
a = -0.2138 ± 0.0849
b = 0.14 ± 0.0012
R² = 0.98

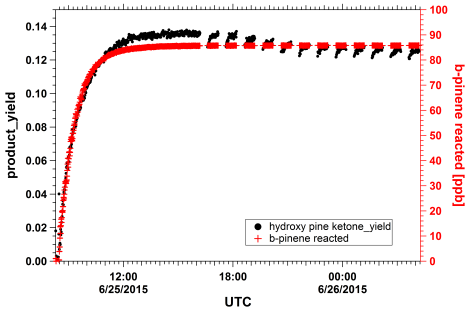
product_yield
b-pinene reacted [ppb]
hydroxy pine ketone_yield
b-pinene reacted
12:00
6/25/2015
18:00
00:00
6/26/2015
UTC

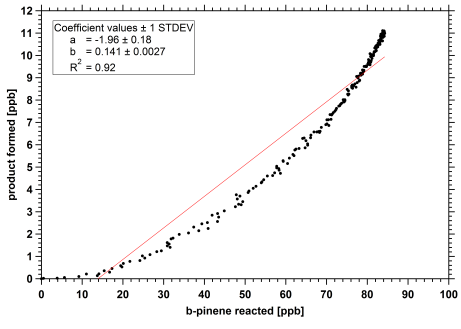
Coefficient values ± 1 STDEV
a = -1.96 ± 0.18
b = 0.141 ± 0.0027
R² = 0.92
product formed [ppb]
b-pinene reacted [ppb]

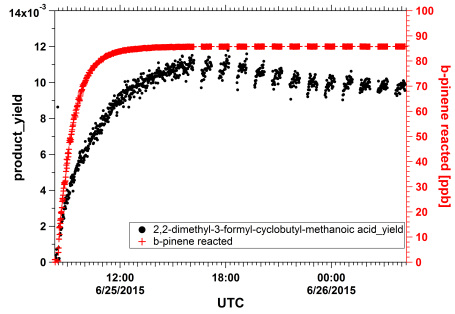
14x10-3
product_yield
b-pinene reacted [ppb]
2,2-dimethyl-3-formyl-cyclobutyl-methanoic acid_yield
b-pinene reacted
12:00
6/25/2015
18:00
00:00
6/26/2015
UTC

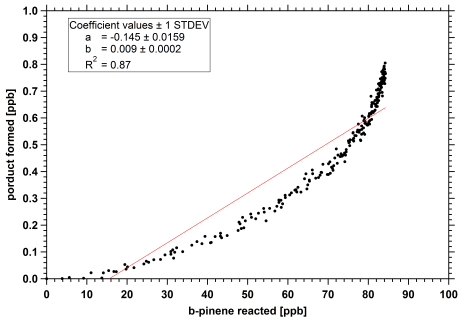
Coefficient values ± 1 STDEV
a = -0.145 ± 0.0159
b = 0.009 ± 0.0002
R2 = 0.87
porduct formed [ppb]
b-pinene reacted [ppb]

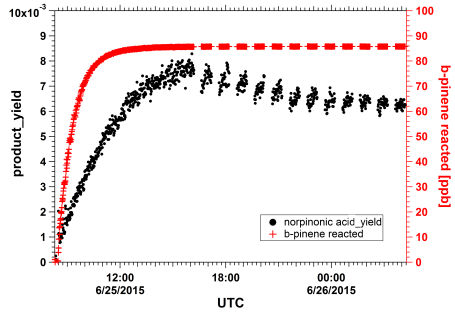
10x10-3
product_yield
b-pinene reacted [ppb]
norpinonic acid_yield
b-pinene reacted
12:00
6/25/2015
18:00
00:00
6/26/2015
UTC

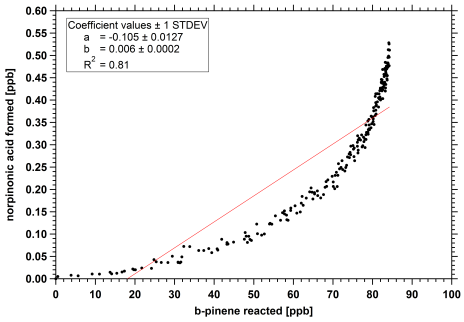
Coefficient values ± 1 STDEV
a = -0.105 ± 0.0127
b = 0.006 ± 0.0002
R2 = 0.81
norpinonic acid formed [ppb]
b-pinene reacted [ppb]

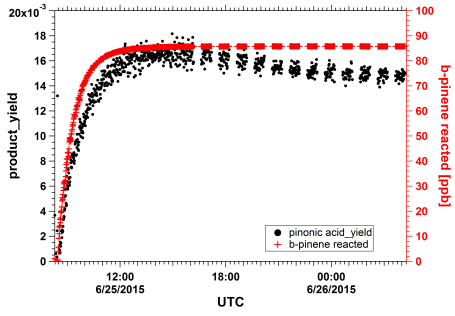
20x10-3
product_yield
b-pinene reacted [ppb]
pinonic acid_yield
b-pinene reacted
12:00
6/25/2015
18:00
00:00
6/26/2015
UTC

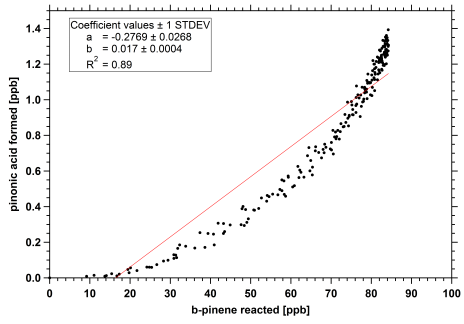
Coefficient values ± 1 STDEV
a = -0.2769 ± 0.0268
b = 0.017 ± 0.0004
R2 = 0.89
pinonic acid formed [ppb]
b-pinene reacted [ppb]

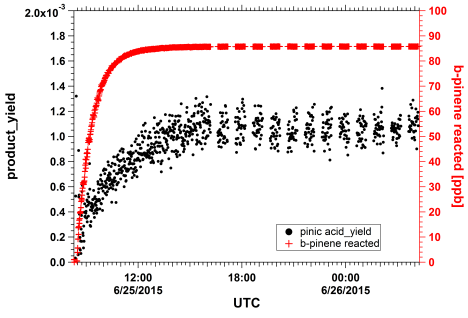
2.0x10-3
product_yield
b-pinene reacted [ppb]
pinic acid_yield
b-pinene reacted
12:00
6/25/2015
18:00
00:00
6/26/2015
UTC

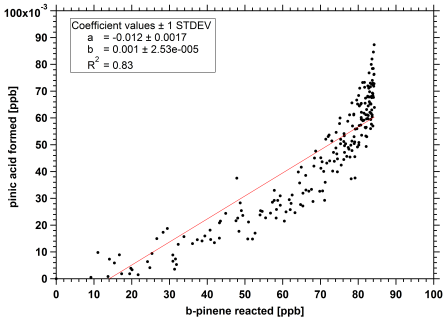
100x10-3
Coefficient values ± 1 STDEV
a = -0.012 ± 0.0017
b = 0.001 ± 2.53e-005
R2 = 0.83
pinic acid formed [ppb]
b-pinene reacted [ppb]

FIGURE C.1: Products formed, and their yields, from the reactions of β-pinene with O_3. Left is the product yield and the consumed amount of β-pinene as a function of time, right is the correlation between product and the reactant.

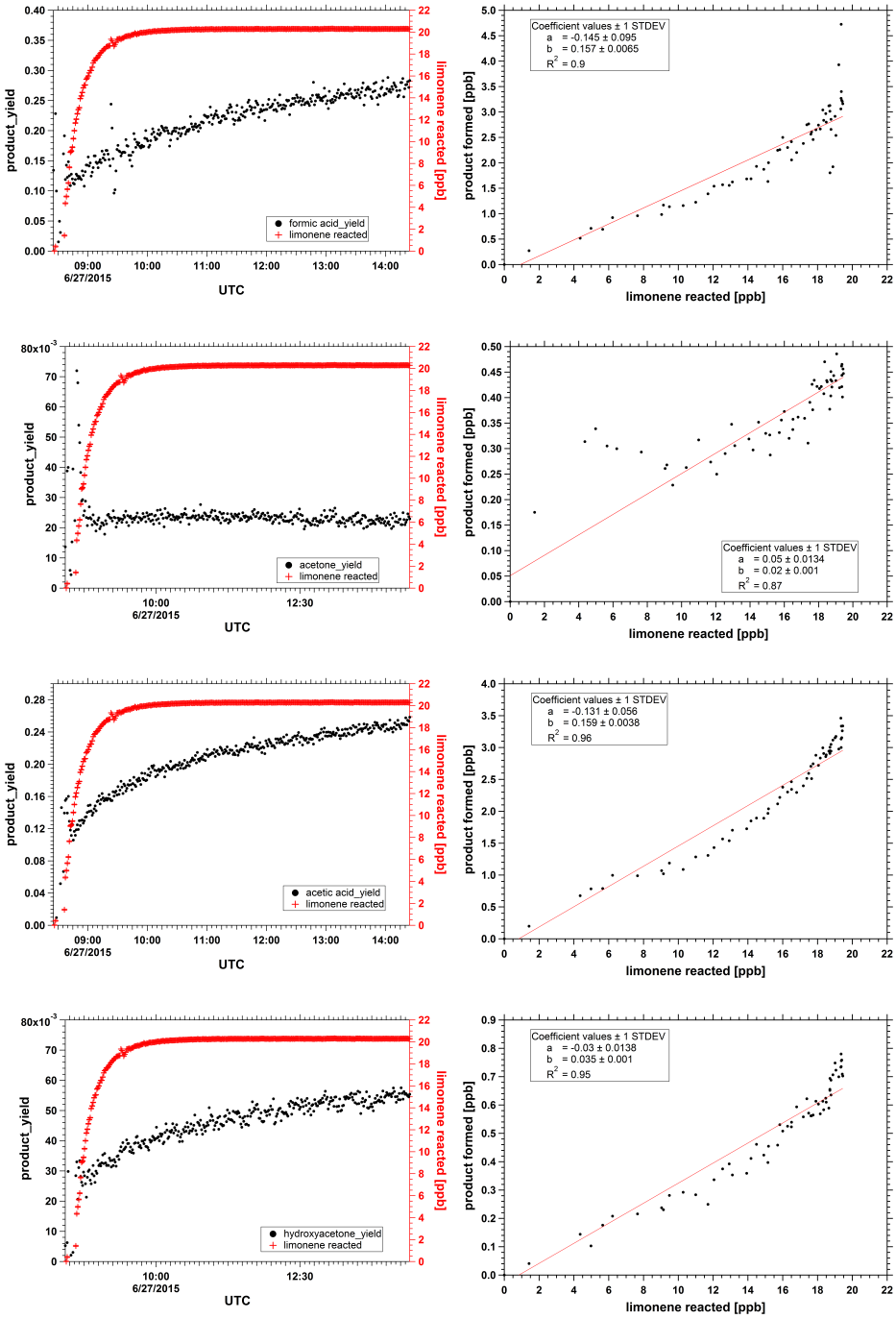

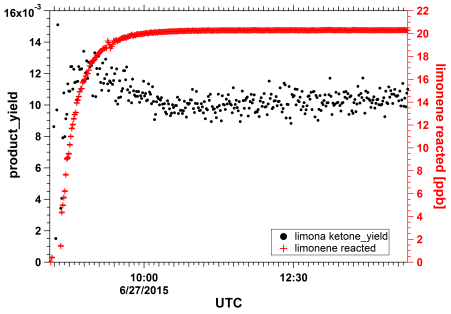
16x10-3
product_yield
limonene reacted [ppb]
limona ketone_yield
limonene reacted
10:00
6/27/2015
12:30
UTC

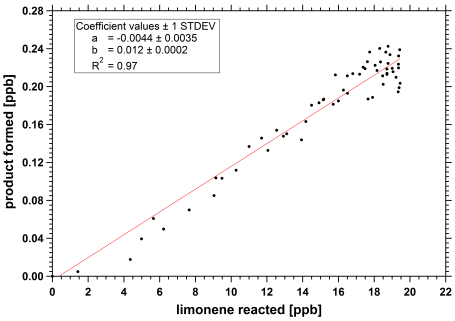
Coefficient values ± 1 STDEV
a = -0.0044 ± 0.0035
b = 0.012 ± 0.0002
R2 = 0.97
product formed [ppb]
limonene reacted [ppb]

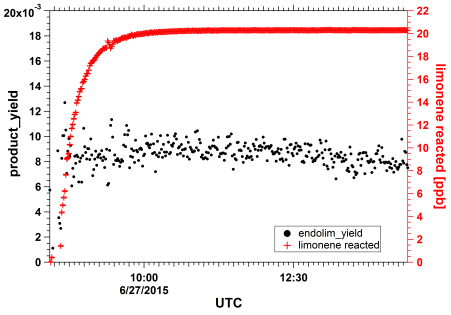
20x10-3
product_yield
limonene reacted [ppb]
endolim_yield
limonene reacted
10:00
6/27/2015
12:30
UTC

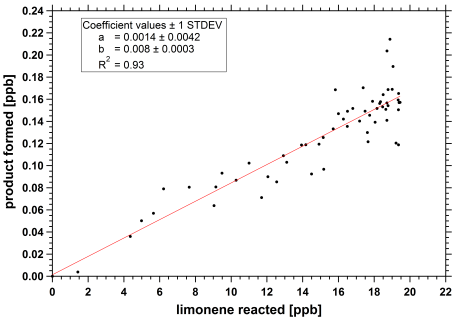
Coefficient values ± 1 STDEV
a = 0.0014 ± 0.0042
b = 0.008 ± 0.0003
R2 = 0.93
product formed [ppb]
limonene reacted [ppb]

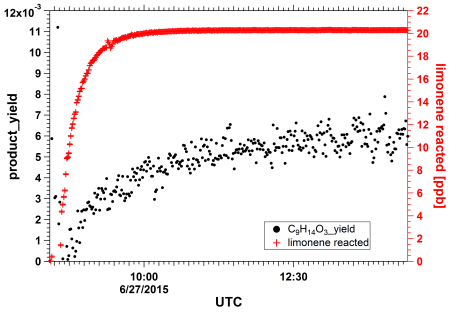
12x10-3
product_yield
limonene reacted [ppb]
C9H14O3_yield
limonene reacted
10:00
6/27/2015
12:30
UTC

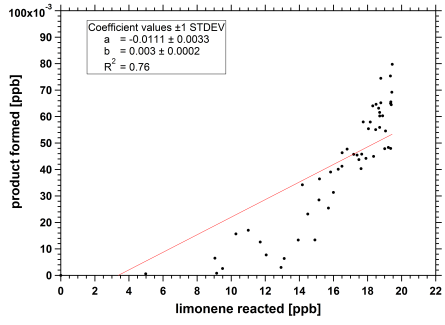
100x10-3
Coefficient values ±1 STDEV
a = -0.0111 ± 0.0033
b = 0.003 ± 0.0002
R2 = 0.76
product formed [ppb]
limonene reacted [ppb]

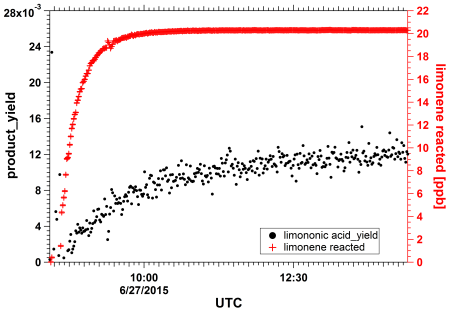
28x10-3
product_yield
limonene reacted [ppb]
limononic acid_yield
limonene reacted
10:00
6/27/2015
12:30
UTC

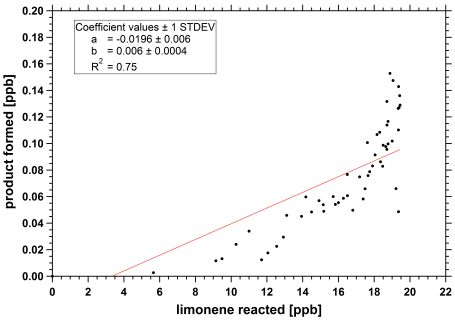
Coefficient values ± 1 STDEV
a = -0.0196 ± 0.006
b = 0.006 ± 0.0004
R2 = 0.75
product formed [ppb]
limonene reacted [ppb]

FIGURE C.2: Products formed, and their yields, from the reactions of limonene with O_3. Left is the product yield and the consumed amount of limonene as a function of time, right is the correlation between product and the reactant.

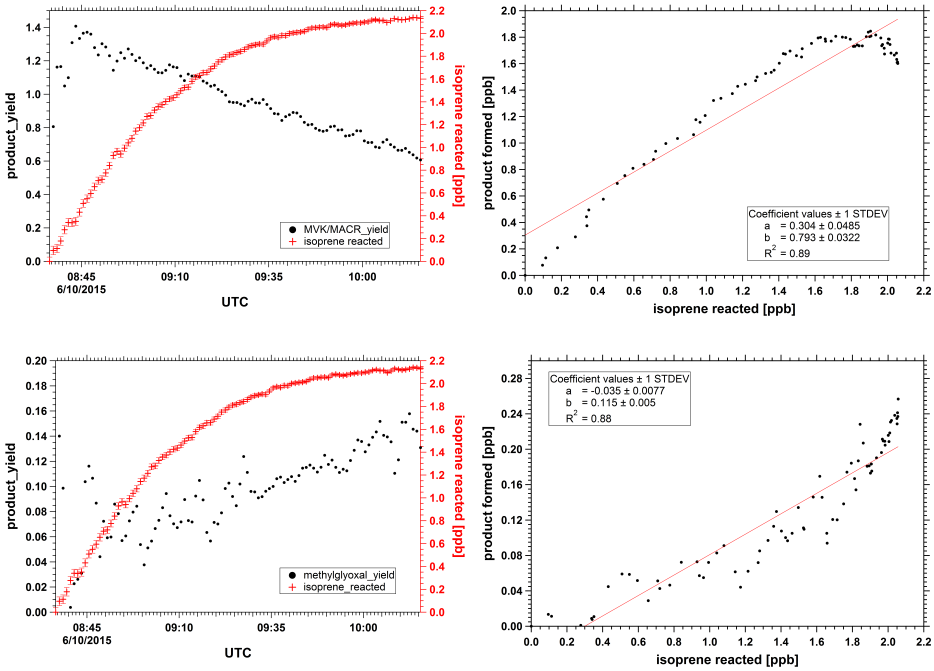

FIGURE C.3: Products formed, and their yields, from the reactions of isoprene with OH radicals at high NO level. Left is the product yield and the consumed amount of limonene as a function of time, right is the correlation between product and the reactant.

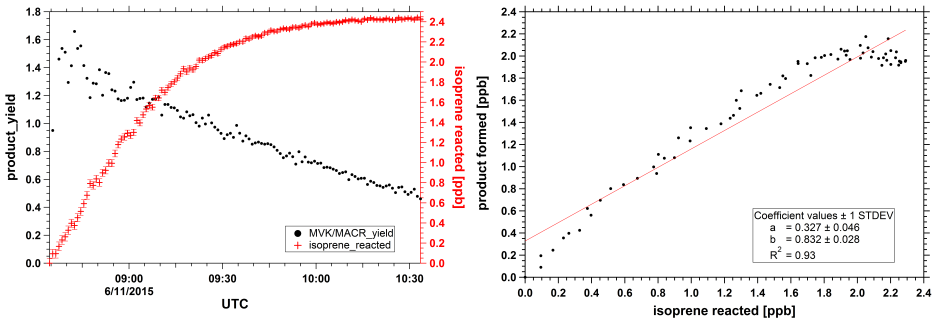

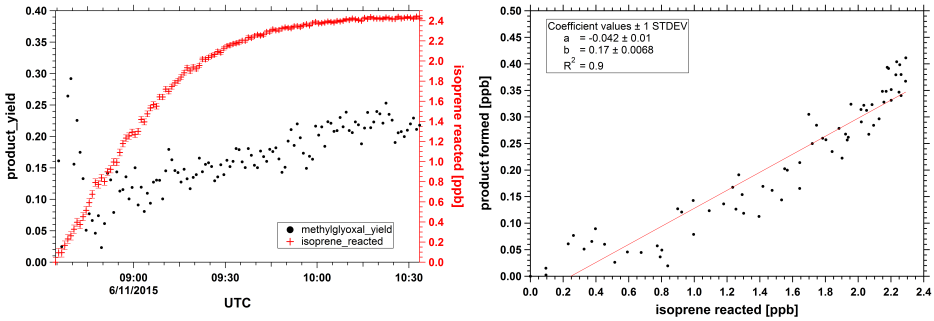

FIGURE C.4: Products formed, and their yields, from the reactions of isoprene with OH radicals at middle NO level. Left is the product yield and the consumed amount of limonene as a function of time, right is the correlation between product and the reactant.

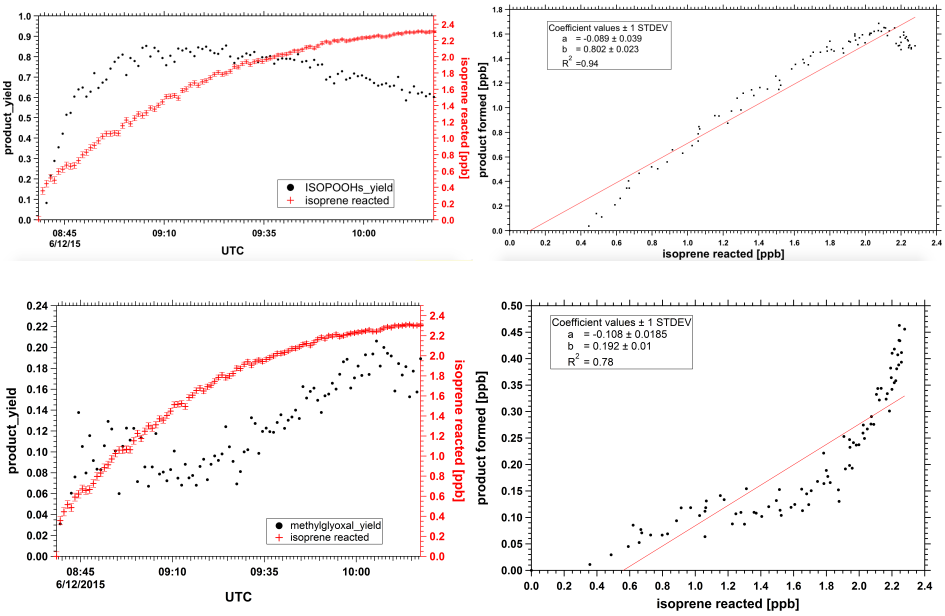

FIGURE C.5: Products formed, and their yields, from the reactions of isoprene with OH radicals at low NO level. Left is the product yield and the consumed amount of limonene as a function of time, right is the correlation between product and the reactant.

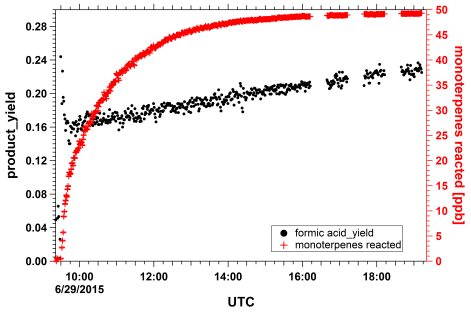
product_yield
monoterpenes reacted [ppb]
formic acid_yield
monoterpenes reacted
10:00
6/29/2015
12:00
14:00
16:00
18:00
UTC

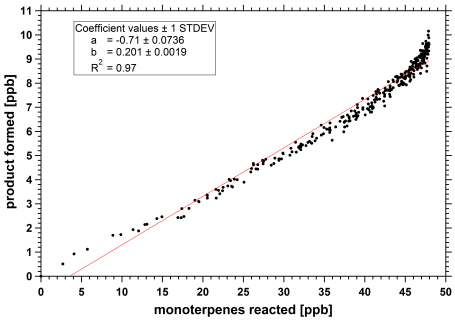
Coefficient values ± 1 STDEV
a = -0.71 ± 0.0736
b = 0.201 ± 0.0019
R2 = 0.97
product formed [ppb]
monoterpenes reacted [ppb]

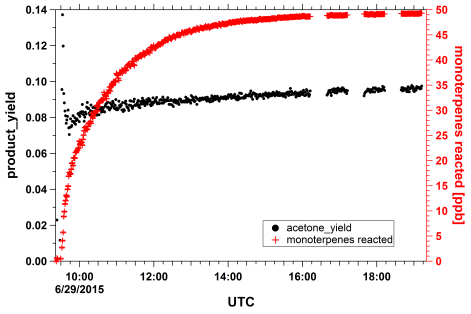
product_yield
monoterpenes reacted [ppb]
acetone_yield
monoterpenes reacted
10:00
6/29/2015
12:00
14:00
16:00
18:00
UTC

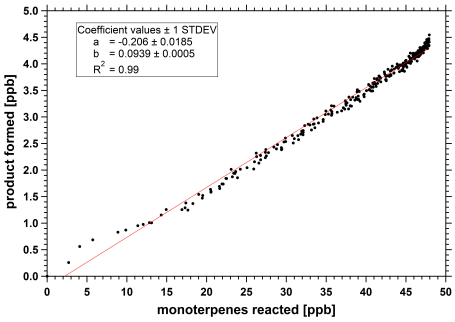
Coefficient values ± 1 STDEV
a = -0.206 ± 0.0185
b = 0.0939 ± 0.0005
R2 = 0.99
product formed [ppb]
monoterpenes reacted [ppb]

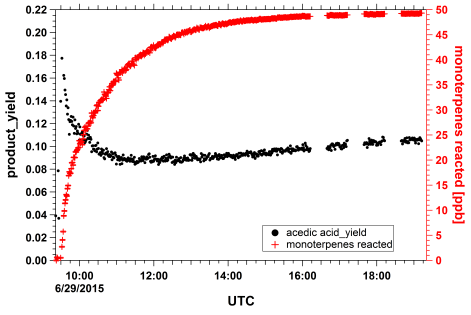
product_yield
monoterpenes reacted [ppb]
acedic acid_yield
monoterpenes reacted
10:00
6/29/2015
12:00
14:00
16:00
18:00
UTC

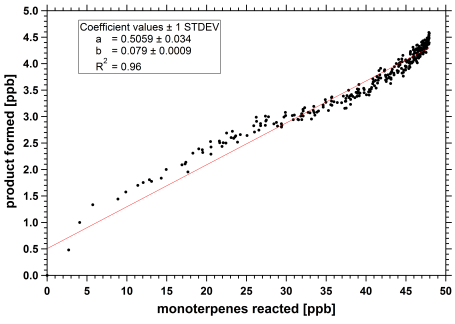
Coefficient values ± 1 STDEV
a = 0.5059 ± 0.034
b = 0.079 ± 0.0009
R2 = 0.96
product formed [ppb]
monoterpenes reacted [ppb]

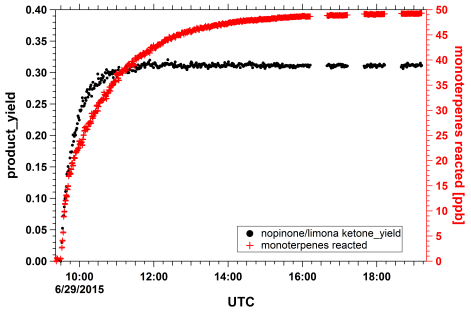
product_yield
monoterpenes reacted [ppb]
nopinone/limona ketone_yield
monoterpenes reacted
10:00
6/29/2015
12:00
14:00
16:00
18:00
UTC

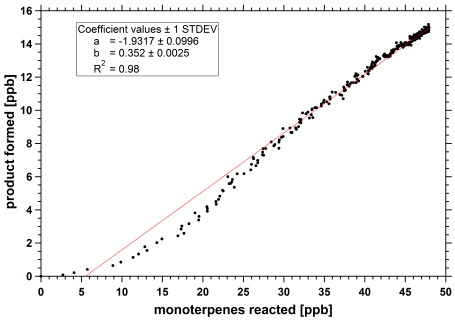
Coefficient values ± 1 STDEV
a = -1.9317 ± 0.0996
b = 0.352 ± 0.0025
R2 = 0.98
product formed [ppb]
monoterpenes reacted [ppb]

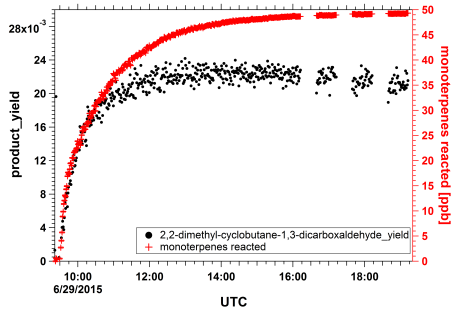
28x10-3
product_yield
monoterpenes reacted [ppb]
2,2-dimethyl-cyclobutane-1,3-dicarboxaldehyde_yield
monoterpenes reacted
10:00
6/29/2015
12:00
14:00
16:00
18:00
UTC

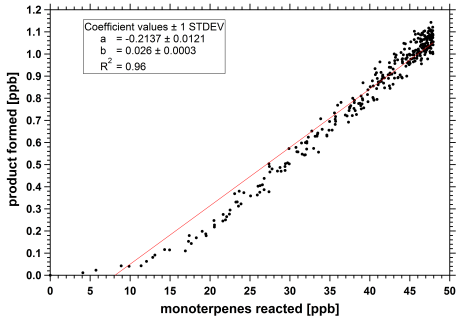
Coefficient values ± 1 STDEV
a = -0.2137 ± 0.0121
b = 0.026 ± 0.0003
R2 = 0.96
product formed [ppb]
monoterpenes reacted [ppb]

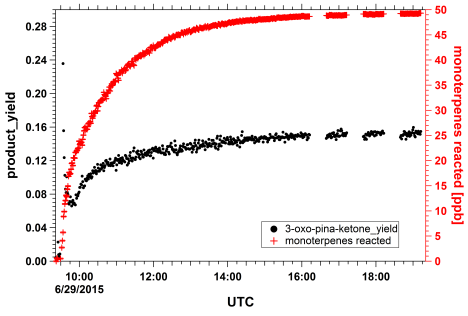
product_yield
monoterpenes reacted [ppb]
3-oxo-pina-ketone_yield
monoterpenes reacted
10:00
6/29/2015
12:00
14:00
16:00
18:00
UTC

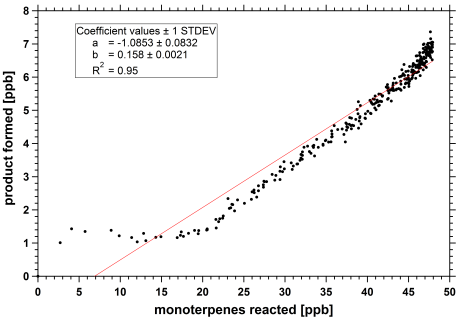
Coefficient values ± 1 STDEV
a = -1.0853 ± 0.0832
b = 0.158 ± 0.0021
R2 = 0.95
product formed [ppb]
monoterpenes reacted [ppb]

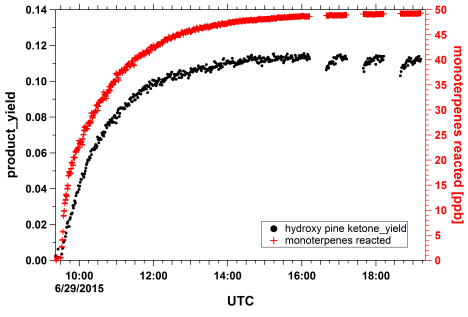
product_yield
monoterpenes reacted [ppb]
hydroxy pine ketone_yield
monoterpenes reacted
10:00
6/29/2015
12:00
14:00
16:00
18:00
UTC

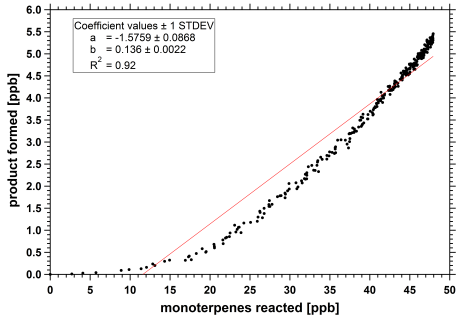
Coefficient values ± 1 STDEV
a = -1.5759 ± 0.0868
b = 0.136 ± 0.0022
R2 = 0.92
product formed [ppb]
monoterpenes reacted [ppb]

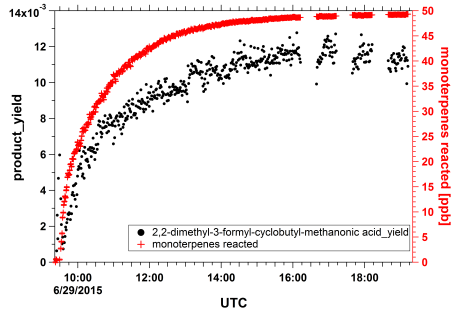
14x10-3
product_yield
monoterpenes reacted [ppb]
2,2-dimethyl-3-formyl-cyclobutyl-methanonic acid_yield
monoterpenes reacted
10:00
6/29/2015
12:00
14:00
16:00
18:00
UTC

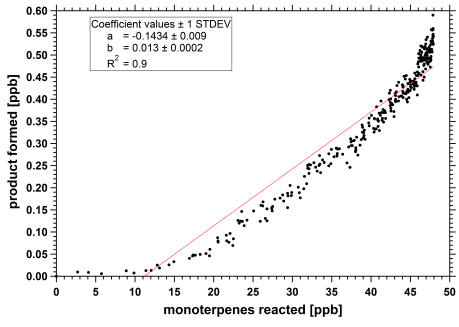
Coefficient values ± 1 STDEV
a = -0.1434 ± 0.009
b = 0.013 ± 0.0002
R2 = 0.9
product formed [ppb]
monoterpenes reacted [ppb]

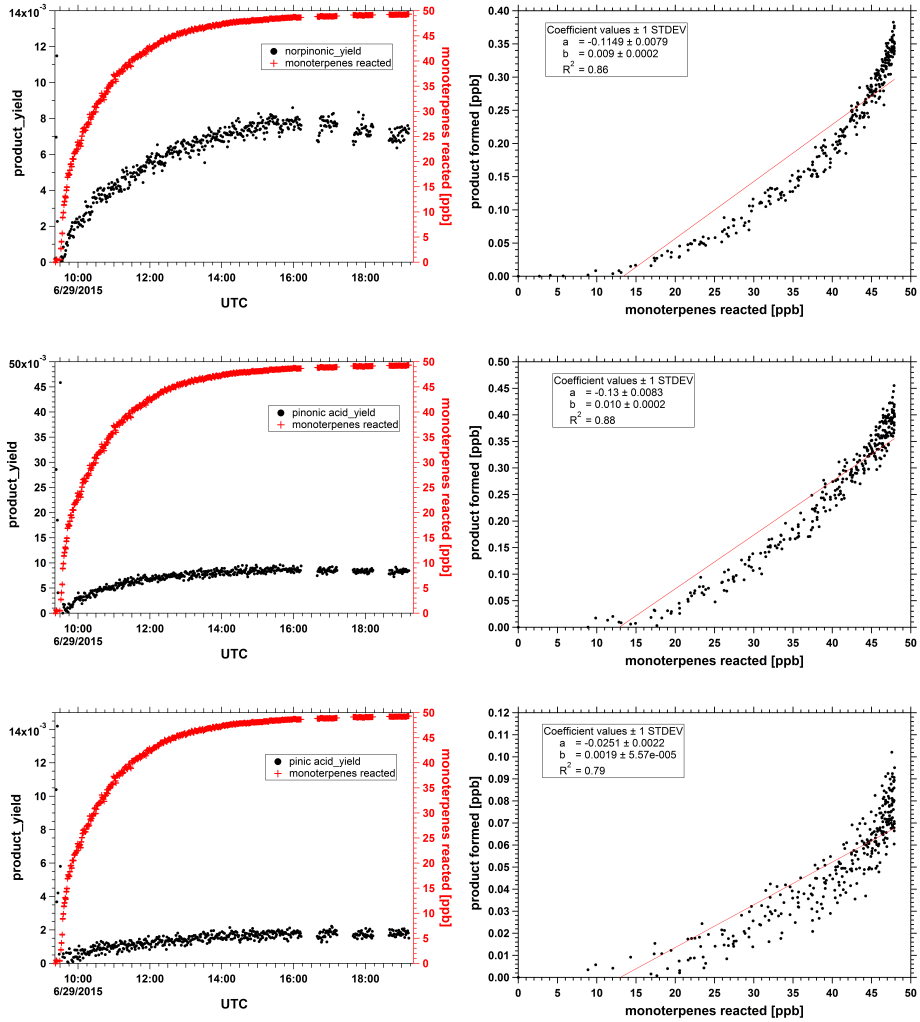

FIGURE C.6: Products formed, and their yields, from the ozonolysis of BM1 (β-pinene and limonene mixture). Left is the product yield and the consumed amount of monoterpenes as a function of time, right is the correlation between product and the reactant.

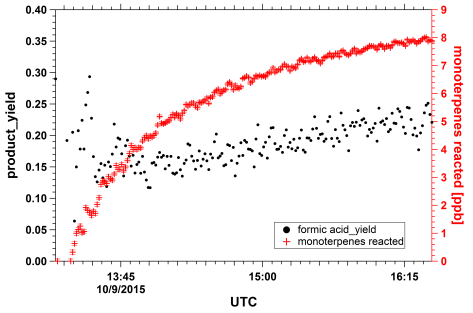
product_yield
monoterpenes reacted [ppb]
formic acid_yield
monoterpenes reacted
13:45
10/9/2015
15:00
16:15
UTC

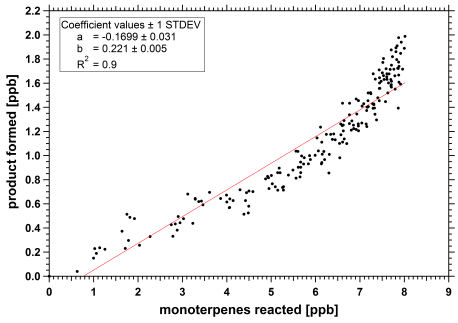
Coefficient values ± 1 STDEV
a = -0.1699 ± 0.031
b = 0.221 ± 0.005
R² = 0.9
product formed [ppb]
monoterpenes reacted [ppb]

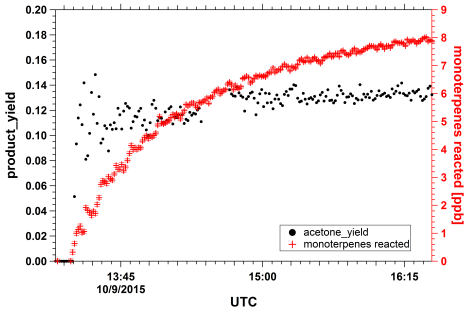
product_yield
monoterpenes reacted [ppb]
acetone_yield
monoterpenes reacted
13:45
10/9/2015
15:00
16:15
UTC

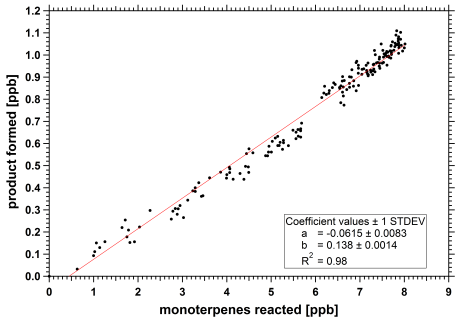
Coefficient values ± 1 STDEV
a = -0.0615 ± 0.0083
b = 0.138 ± 0.0014
R² = 0.98
product formed [ppb]
monoterpenes reacted [ppb]

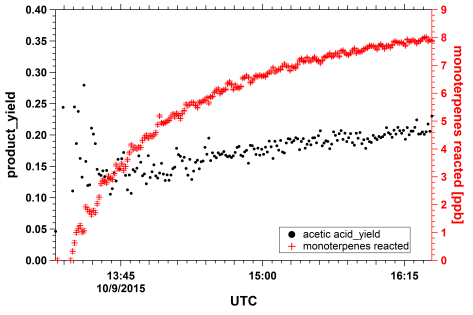
product_yield
monoterpenes reacted [ppb]
acetic acid_yield
monoterpenes reacted
13:45
10/9/2015
15:00
16:15
UTC

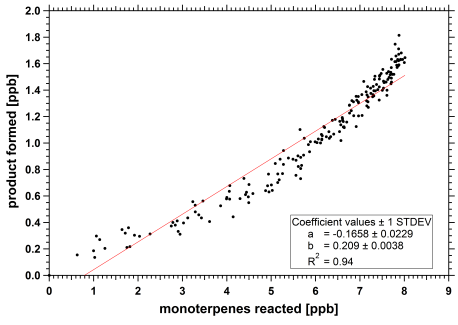
Coefficient values ± 1 STDEV
a = -0.1658 ± 0.0229
b = 0.209 ± 0.0038
R² = 0.94
product formed [ppb]
monoterpenes reacted [ppb]

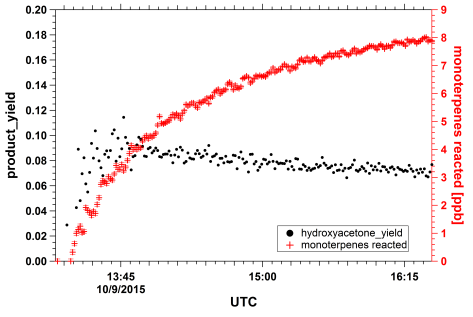
product_yield
monoterpenes reacted [ppb]
hydroxyacetone_yield
monoterpenes reacted
13:45
10/9/2015
15:00
16:15
UTC

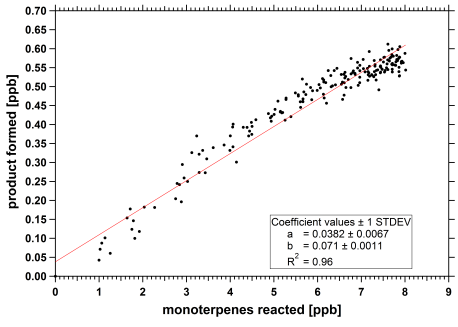
Coefficient values ± 1 STDEV
a = 0.0382 ± 0.0067
b = 0.071 ± 0.0011
R² = 0.96
product formed [ppb]
monoterpenes reacted [ppb]

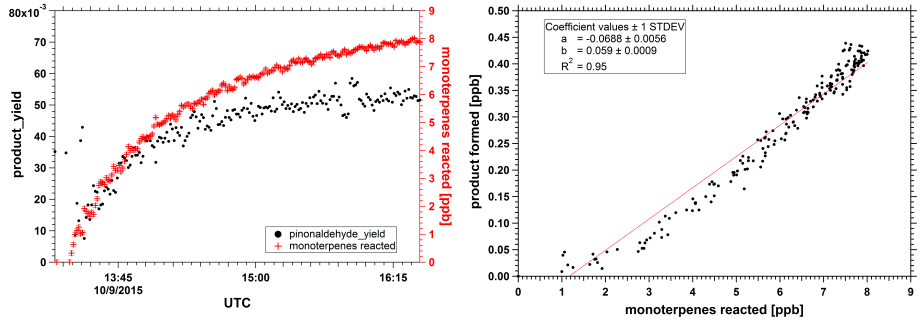

FIGURE C.7: Products formed, and their yields, from the ozonolysis of BM2 (α-pinene, myrcene and limonene). Left is the product yield and the consumed amount of monoterpenes as a function of time, right is the correlation between product and the reactant.

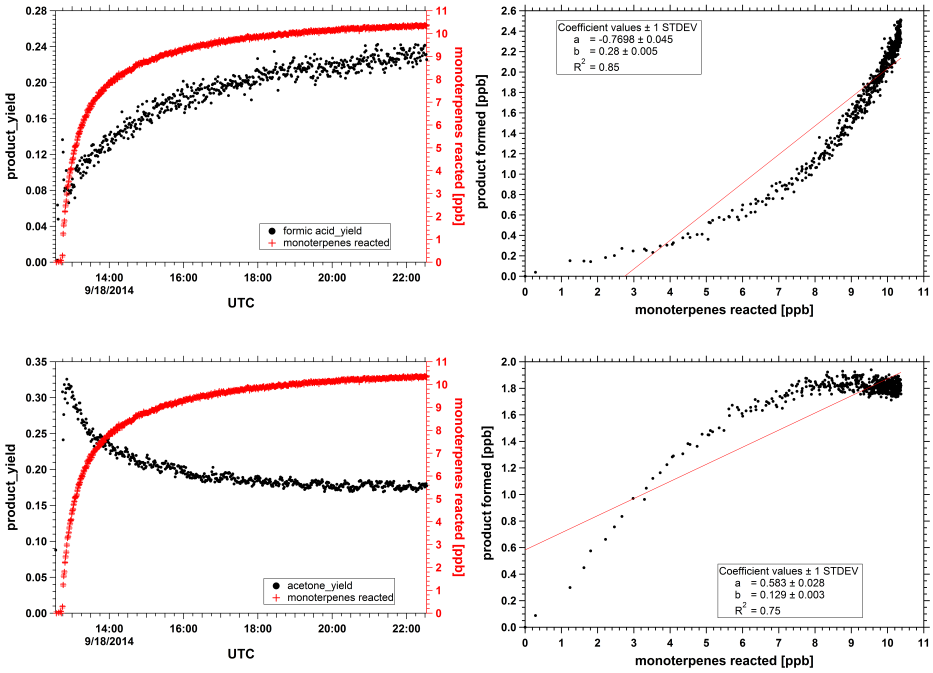

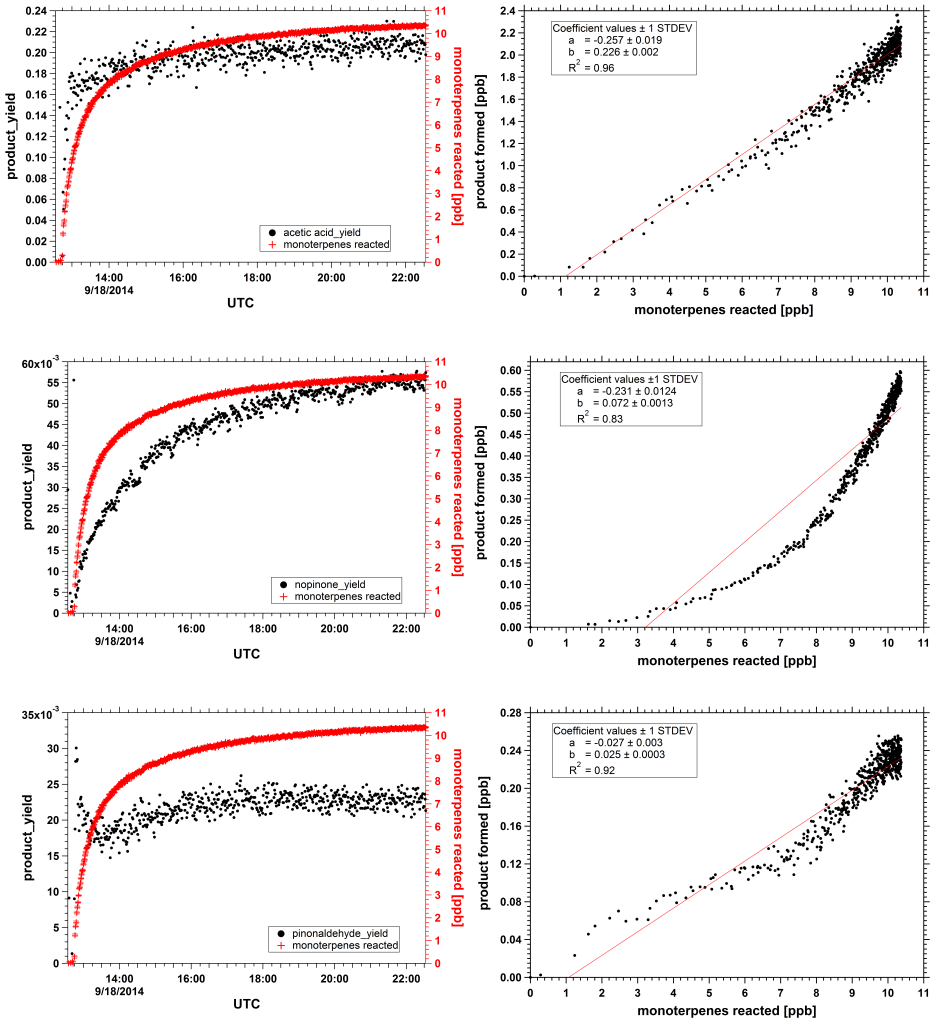

FIGURE C.8: Products formed, and their yields, from the ozonolysis of *Quercus ilex* tree emission. Left is the product yield and the consumed amount of monoterpenes as a function of time, right is the correlation between product and the reactant.

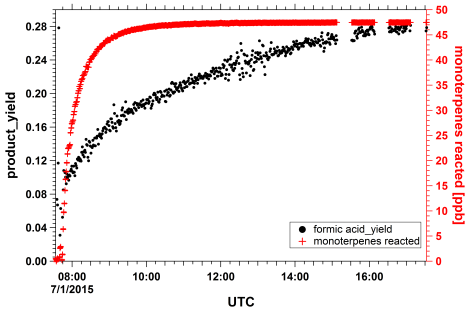
product_yield
monoterpenes reacted [ppb]
formic acid_yield
monoterpenes reacted
08:00
7/1/2015
10:00
12:00
14:00
16:00
UTC

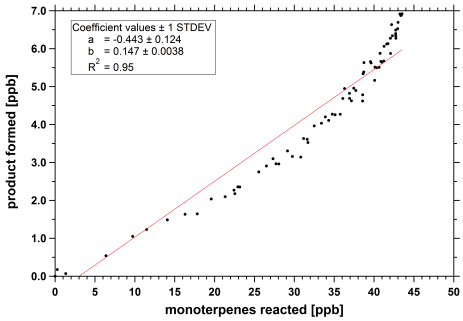
Coefficient values ± 1 STDEV
a = -0.443 ± 0.124
b = 0.147 ± 0.0038
R2 = 0.95
product formed [ppb]
monoterpenes reacted [ppb]

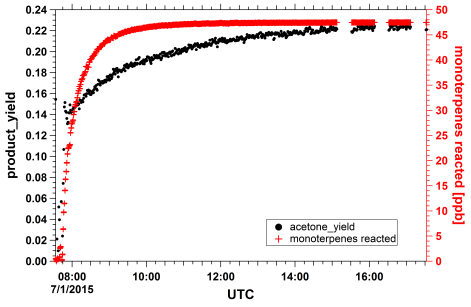
product_yield
monoterpenes reacted [ppb]
acetone_yield
monoterpenes reacted
08:00
7/1/2015
10:00
12:00
14:00
16:00
UTC

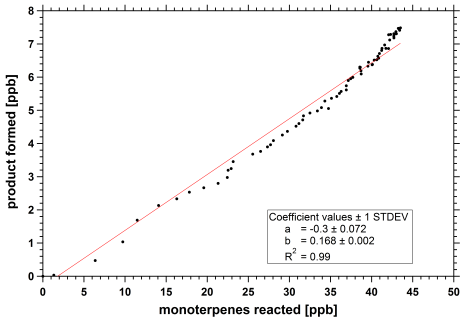
Coefficient values ± 1 STDEV
a = -0.3 ± 0.072
b = 0.168 ± 0.002
R2 = 0.99
product formed [ppb]
monoterpenes reacted [ppb]

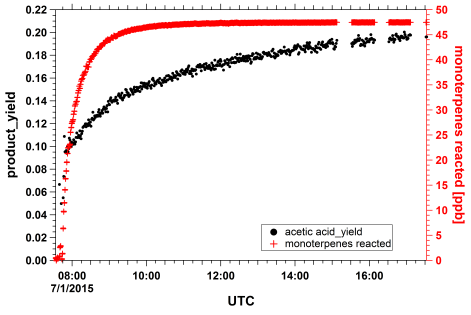
product_yield
monoterpenes reacted [ppb]
acetic acid_yield
monoterpenes reacted
08:00
7/1/2015
10:00
12:00
14:00
16:00
UTC

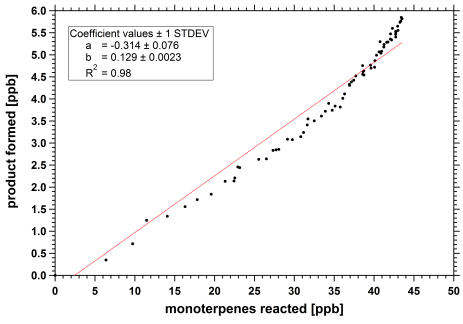
Coefficient values ± 1 STDEV
a = -0.314 ± 0.076
b = 0.129 ± 0.0023
R2 = 0.98
product formed [ppb]
monoterpenes reacted [ppb]

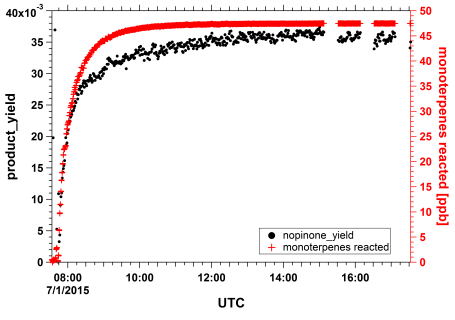
40x10-3
product_yield
monoterpenes reacted [ppb]
nopinone_yield
monoterpenes reacted
08:00
7/1/2015
10:00
12:00
14:00
16:00
UTC

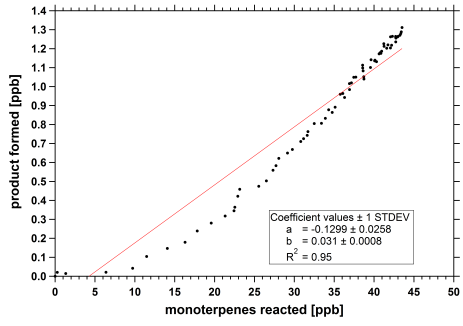
Coefficient values ± 1 STDEV
a = -0.1299 ± 0.0258
b = 0.031 ± 0.0008
R2 = 0.95
product formed [ppb]
monoterpenes reacted [ppb]

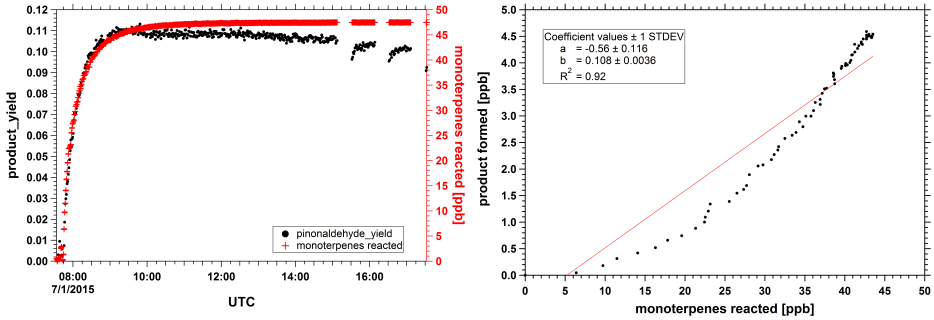

FIGURE C.9: Products formed, and their yields, from the ozonolysis of *Pinus sylvestris* tree emission. Left is the product yield and the consumed amount of monoterpenes as a function of time, right is the correlation between product and the reactant.

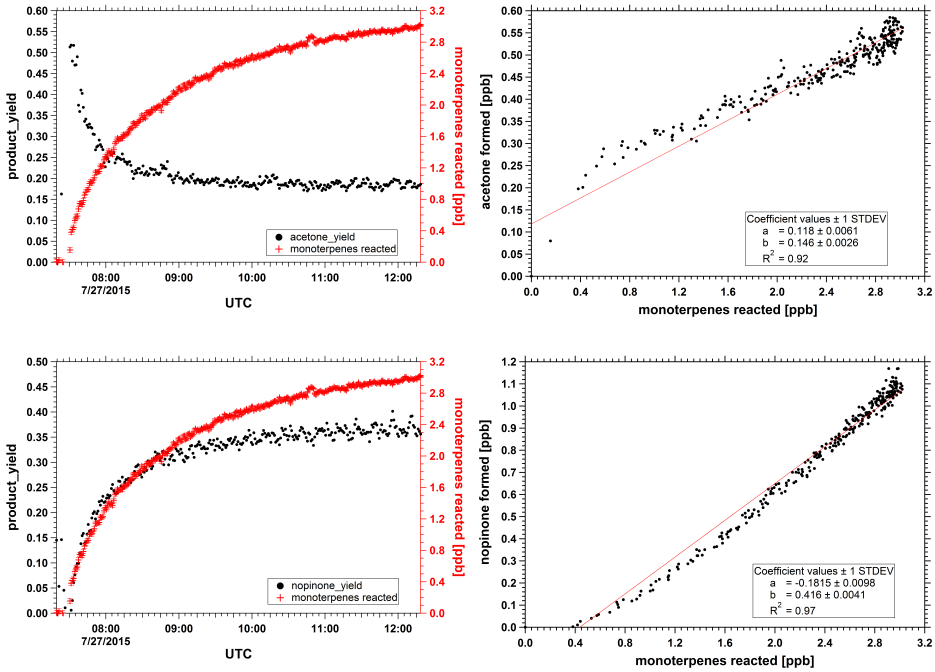

FIGURE C.10: Products formed, and their yields, from the ozonolysis of *Fagus sylvatica* tree emission. Left is the product yield and the consumed amount of monoterpenes as a function of time, right is the correlation between product and the reactant.

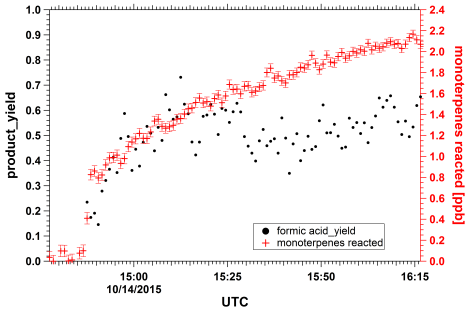
product_yield
monoterpenes reacted [ppb]
formic acid_yield
monoterpenes reacted
15:00
15:25
15:50
16:15
10/14/2015
UTC

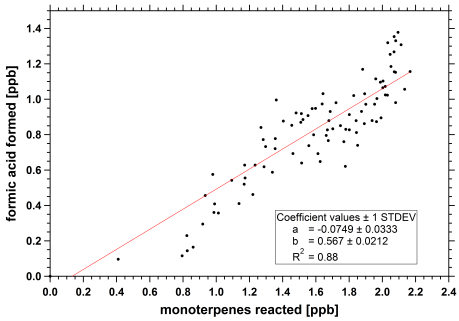
formic acid formed [ppb]
monoterpenes reacted [ppb]
Coefficient values ± 1 STDEV
a = -0.0749 ± 0.0333
b = 0.567 ± 0.0212
R2 = 0.88

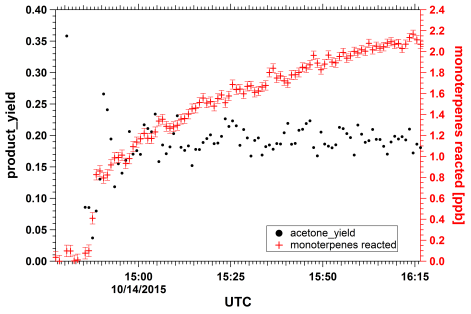
product_yield
monoterpenes reacted [ppb]
acetone_yield
monoterpenes reacted
15:00
15:25
15:50
16:15
10/14/2015
UTC

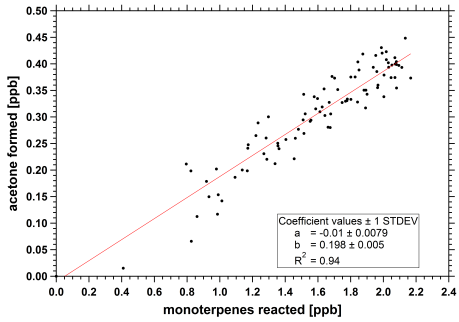
acetone formed [ppb]
monoterpenes reacted [ppb]
Coefficient values ± 1 STDEV
a = -0.01 ± 0.0079
b = 0.198 ± 0.005
R2 = 0.94

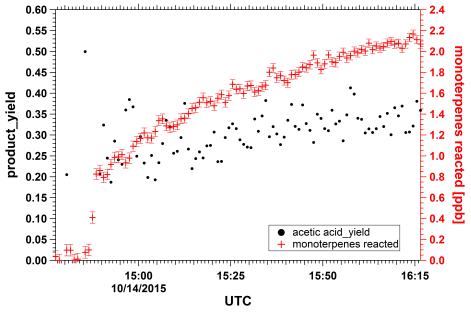
product_yield
monoterpenes reacted [ppb]
acetic acid_yield
monoterpenes reacted
15:00
15:25
15:50
16:15
10/14/2015
UTC

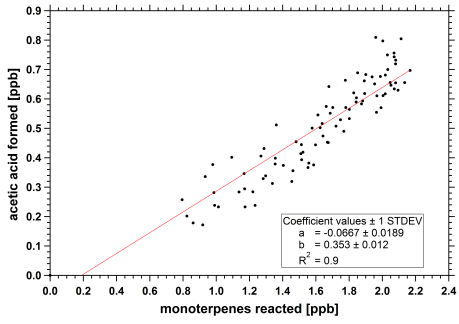
acetic acid formed [ppb]
monoterpenes reacted [ppb]
Coefficient values ± 1 STDEV
a = -0.0667 ± 0.0189
b = 0.353 ± 0.012
R2 = 0.9

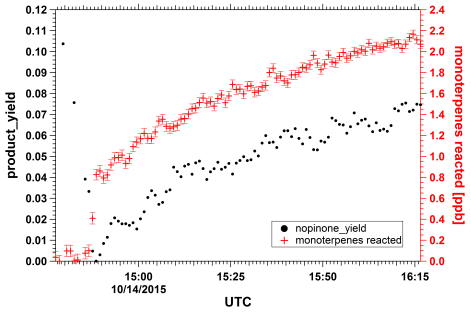
product_yield
monoterpenes reacted [ppb]
nopinone_yield
monoterpenes reacted
15:00
15:25
15:50
16:15
10/14/2015
UTC

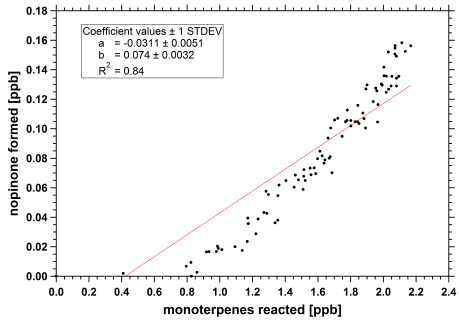
nopinone formed [ppb]
monoterpenes reacted [ppb]
Coefficient values ± 1 STDEV
a = -0.0311 ± 0.0051
b = 0.074 ± 0.0032
R2 = 0.84

FIGURE C.11: Products formed, and their yields, from the ozonolysis of mix tree (three *Pinus sylvestris* and three *Picea abies*) emission. Left is the product yield and the consumed amount of monoterpenes as a function of time, right is the correlation between product and the reactant.

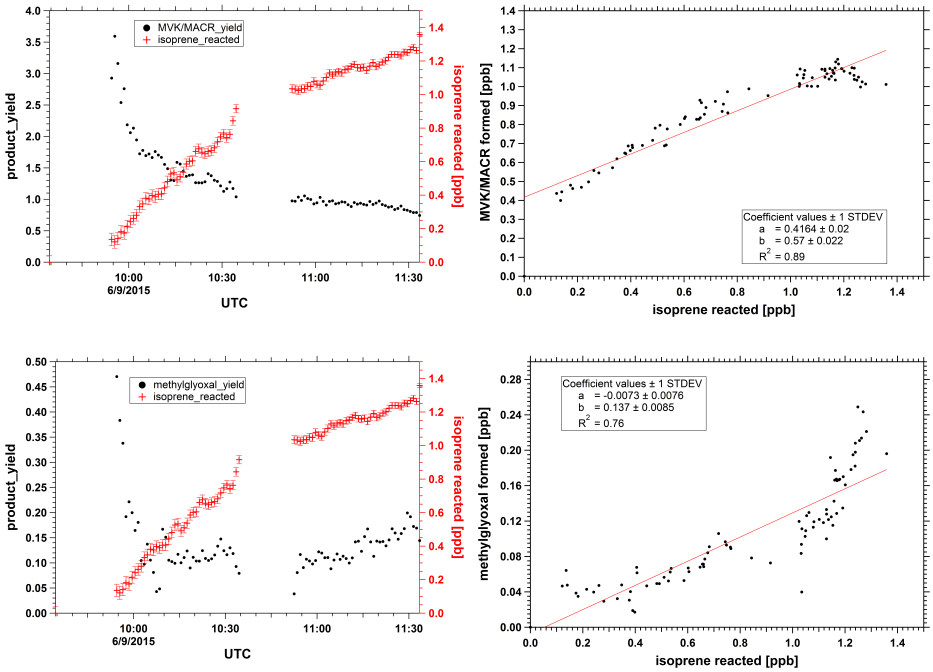

FIGURE C.12: Products formed, and their yields, from the photo-oxidation of six *Quercus robur* tree emission. Left is the product yield and the consumed amount of isoprene as a function of time, gaps indicate measurements in the plant chamber SAPHIR-PLUS; right is the correlation between product and the reactant.

Bibliography

Acir, Ismail-Hakki (in prep). "Hochauflösende Protonen-Transfer-Reaktions-Massenspektrometrie zur Bestimmung des photochemischen Abbaus von stress-induzierten Emmisionen". In:

Apel, EC, T Brauers, R Koppmann, B Bandowe, J Bossmeyer, C Holzke, R Tillmann, A Wahner, R Wegener, A Brunner, et al. (2008). "Intercomparison of oxygenated volatile organic compound measurements at the SAPHIR atmosphere simulation chamber". In: *Journal of Geophysical Research: Atmospheres* 113.D20.

Arnold, F., G. Knop, and H. Ziereis (1986). "Acetone measurements in the upper troposphere and lower stratosphere—implications for hydroxyl radical abundances". In: *Nature* 321.6069, pp. 505–507.

Atkinson, Roger (1997). "Gas-phase tropospheric chemistry of volatile organic compounds: 1. Alkanes and alkenes". In: *Journal of Physical and Chemical Reference Data* 26.2, pp. 215–290.

Atkinson, Roger (2000). "Atmospheric chemistry of VOCs and NO x". In: *Atmospheric environment* 34.12, pp. 2063–2101.

Atkinson, Roger and Janet Arey (2003a). "Atmospheric degradation of volatile organic compounds". In: *Chemical reviews* 103.12, pp. 4605–4638.

Atkinson, Roger and Janet Arey (2003b). "Gas-phase tropospheric chemistry of biogenic volatile organic compounds: a review". In: *Atmospheric Environment* 37, pp. 197–219.

Atkinson, Roger, Sara M Aschmann, Janet Arey, and William PL Carter (1989). "Formation of ring-retaining products from the OH radical-initiated reactions of benzene and toluene". In: *International Journal of Chemical Kinetics* 21.9, pp. 801–827.

Bäck, J, J Aalto, M Henriksson, H Hakola, Q He, and M Boy (2012). "Chemodiversity of a Scots pine stand and implications for terpene air concentrations". In: *Biogeosciences* 9.2, pp. 689–702.

Blake, Robert S, Christopher Whyte, Ceri O Hughes, Andrew M Ellis, and Paul S Monks (2004). "Demonstration of proton-transfer reaction time-of-flight mass spectrometry for real-time analysis of trace volatile organic compounds". In: *Analytical chemistry* 76.13, pp. 3841–3845.

Bohn, B and H Zilken (2005). "Model-aided radiometric determination of photolysis frequencies in a sunlit atmosphere simulation chamber". In: *Atmospheric Chemistry and Physics* 5.1, pp. 191–206.

Calogirou, A, D Kotzias, and A Kettrup (1997). "Product analysis of the gas-phase reaction of β-caryophyllene with ozone". In: *Atmospheric Environment* 31.2, pp. 283–285.

Chapleski, Robert C, Yafen Zhang, Diego Troya, and John R Morris (2016). "Heterogeneous chemistry and reaction dynamics of the atmospheric oxidants, O 3, NO 3, and OH, on organic surfaces". In: *Chemical Society Reviews*.

Cleveland, Cory C and Joseph B Yavitt (1997). "Consumption of atmospheric isoprene". In: *Geophysical Research Letters* 24.19, pp. 2379–2382.

Crosson, ER (2008). "A cavity ring-down analyzer for measuring atmospheric levels of methane, carbon dioxide, and water vapor". In: *Applied Physics B* 92.3, pp. 403–408.

Dales, Robert, Ling Liu, Amanda J. Wheeler, and Nicolas L. Gilbert (2008). "Public health: Quality of indoor residential air and health". In: *Cmaj* 179.2, pp. 147–152.

De Gouw, J and Carsten Warneke (2007). "Measurements of volatile organic compounds in the earth's atmosphere using proton-transfer-reaction mass spectrometry". In: *Mass Spectrometry Reviews* 26.2, pp. 223–257.

De Gouw, JA, PD Goldan, C Warneke, WC Kuster, JM Roberts, M Marchewka, SB Bertman, AAP Pszenny, and WC Keene (2003). "Validation of proton transfer reaction-mass spectrometry (PTR-MS) measurements of gas-phase organic compounds in the atmosphere during the New England Air Quality Study (NEAQS) in 2002". In: *Journal of Geophysical Research: Atmospheres* 108.D21.

Di Carlo, Piero, William H Brune, Monica Martinez, Hartwig Harder, Robert Lesher, Xinrong Ren, Troy Thornberry, Mary Anne Carroll, Valerie Young, Paul B Shepson, et al. (2004). "Missing OH reactivity in a forest: Evidence for unknown reactive biogenic VOCs". In: *Science* 304.5671, pp. 722–725.

Dibble, Theodore S. (2004). "Prompt Chemistry of Alkenoxy Radical Products of the Double H-Atom Transfer of Alkoxy Radicals from Isoprene". In: *Journal of Physical Chemistry A* 108.12, pp. 2208–2215.

Dolgorouky, C, V Gros, R Sarda-Esteve, V Sinha, J Williams, N Marchand, S Sauvage, L Poulain, J Sciare, and B Bonsang (2012). "Total OH reactivity measurements in Paris during the 2010 MEGAPOLI winter campaign". In: *Atmospheric Chemistry and Physics* 12.20, pp. 9593–9612.

Donahue, N. M., J. E. Tischuk, B. J. Marquis, and K. E. Huff Hartz (2007). "Secondary organic aerosol from limona ketone: insights into terpene ozonolysis via synthesis of key intermediates." In: *Physical Chemistry Chemical Physics Pccp* 9.23, pp. 2991–8.

Dusanter, S, D Vimal, P. S Stevens, R Volkamer, and L. T Molina (2009). "Measurements of OH and HO_2 concentrations during the MCMA-2006 field campaign - Part 1: Deployment of the Indiana University laser-induced fluorescence instrument". In: *Atmospheric Chemistry and Physics* 9.5, pp. 1665–1685.

Edwards, PM, MJ Evans, KL Furneaux, J Hopkins, T Ingham, C Jones, JD Lee, AC Lewis, SJ Moller, D Stone, et al. (2013). "OH reactivity in a South East Asian tropical rainforest during the Oxidant and Particle Photochemical Processes (OP3) project". In: *Atmospheric Chemistry and Physics* 13.18, pp. 9497–9514.

Emanuelsson, Eva U, Mattias Hallquist, Kasper Kristensen, Marianne Glasius, B Bohn, H Fuchs, B Kammer, A Kiendler-Scharr, S Nehr, F Rubach, et al. (2013). "Formation of anthropogenic secondary organic aerosol (SOA) and its influence on biogenic SOA properties". In: *Atmospheric Chemistry and Physics* 13.5, pp. 2837–2855.

Fabris, Alessandra, Franco Biasioli, Pablo M Granitto, Eugenio Aprea, Luca Cappellin, Erna Schuhfried, Christos Soukoulis, Tilmann D Märk, Flavia Gasperi, and Isabella Endrizzi (2010). "PTR-TOF-MS and data-mining methods for rapid characterisation of agro-industrial samples: influence of milk storage conditions on the volatile compounds profile of Trentingrana cheese". In: *Journal of mass spectrometry* 45.9, pp. 1065–1074.

Folkers, A, K Hüve, C Ammann, T Dindorf, J Kesselmeier, E Kleist, U Kuhn, R Uerlings, and J Wildt (2008). "Methanol emissions from deciduous tree species: dependence on temperature and light intensity". In: *Plant biology* 10.1, pp. 65–75.

Fuchs, H, I. H Acir, B Bohn, T Brauers, H. P Dorn, R Häseler, A Hofzumahaus, F Holland, M Kaminski, and X Li (2014). "OH regeneration from methacrolein oxidation investigated in the atmosphere simulation chamber SAPHIR". In: *Atmospheric Chemistry & Physics* 14.15, pp. 5197–5231.

Fuchs, H., A. Novelli, M. Rolletter, A. Hofzumahaus, E. Y. Pfannerstill, S. Kessel, A. Edtbauer, J. Williams, V. Michoud, S. Dusanter, N. Locoge, N. Zannoni, V. Gros, F. Truong, R. Sarda-Esteve, D. R. Cryer, C. A. Brumby, L. K. Whalley, D. Stone, P. W. Seakins, D. E. Heard, C. Schoemaecker, M. Blocquet, S. Coudert, S. Batut, C. Fittschen, A. B. Thames, W. H. Brune, C. Ernest, H. Harder, J. B. A. Muller, T. Elste, D. Kubistin, S. Andres, B. Bohn,

T. Hohaus, F. Holland, X. Li, F. Rohrer, A. Kiendler-Scharr, R. Tillmann, R. Wegener, Z. Yu, Q. Zou, and A. Wahner (2017). "Comparison of OH reactivity measurements in the atmospheric simulation chamber SAPHIR". In: *Atmos. Meas. Tech.* 10.10, pp. 4023–4053. ISSN: 1867-8548. DOI: 10.5194/amt-10-4023-2017.

Fuchs, Hendrik, Frank Holland, and Andreas Hofzumahaus (2008). "Measurement of tropospheric RO2 and HO2 radicals by a laser-induced fluorescence instrument." In: *The Review of scientific instruments* 79.8, pp. 084104–084104.

Fuchs, H, A Hofzumahaus, F Rohrer, B Bohn, T Brauers, HP Dorn, R Häseler, F Holland, M Kaminski, X Li, et al. (2013). "Experimental evidence for efficient hydroxyl radical regeneration in isoprene oxidation". In: *Nature Geoscience* 6.12, pp. 1023–1026.

Galloway, M. M., A. J. Huisman, L. D. Yee, A. W. H. Chan, C. L. Loza, J. H. Seinfeld, and F. N. Keutsch (2011). "Yields of oxidized volatile organic compounds during the OH radical initiated oxidation of isoprene, methyl vinyl ketone, and methacrolein under high-NOx conditions". In: *Atmospheric Chemistry & Physics* 11.11, pp. 10693–10720.

Gautrois, M. and R. Koppmann (1999). "Diffusion technique for the production of gas standards for atmospheric measurements". In: *Journal of Chromatography A* 848.1–2, pp. 239–249.

Geron, Chris, Rei Rasmussen, Robert R Arnts, and Alex Guenther (2000). "A review and synthesis of monoterpene speciation from forests in the United States". In: *Atmospheric Environment* 34.11, pp. 1761–1781.

Goldstein, A.H. and I.E. Galbally (2007). "Known and Unexplored Organic Constituents in the Earth's Atmosphere". In: *Environ Sci Technol* 41.5, pp. 1514–1521.

Grabmer, W, J Kreuzwieser, A Wisthaler, C Cojocariu, M Graus, H Rennenberg, D Steigner, R Steinbrecher, and A Hansel (2006). "VOC emissions from Norway spruce (Picea abies L.[Karst]) twigs in the field—results of a dynamic enclosure study". In: *Atmospheric Environment* 40, pp. 128–137.

Grosjean, Daniel, Edwin L Williams, Eric Grosjean, Jean M Andino, and John H Seinfeld (1993). "Atmospheric oxidation of biogenic hydrocarbons: reaction of ozone with. beta.-pinene, D-limonene and trans-caryophyllene". In: *Environmental science & technology* 27.13, pp. 2754–2758.

Guenther, AB, X Jiang, CL Heald, T Sakulyanontvittaya, T Duhl, LK Emmons, and X Wang (2012). "The Model of Emissions of Gases and Aerosols from Nature version 2.1 (MEGAN2. 1): an extended and updated framework for modeling biogenic emissions". In:

Guenther, Alex (2002). "The contribution of reactive carbon emissions from vegetation to the carbon balance of terrestrial ecosystems". In: *Chemosphere* 49.8, pp. 837–844.

Guenther, Alex, C Nicholas Hewitt, David Erickson, Ray Fall, Chris Geron, Tom Graedel, Peter Harley, Lee Klinger, Manuel Lerdau, WA McKay, et al. (1995). "A global model of natural volatile organic compound emissions". In: *Journal of Geophysical Research: Atmospheres* 100.D5, pp. 8873–8892.

Guenther, R (1993). "Isoprene and monoterpene emission rate variability: model evaluations and sensitivity analyses". In: *Journal of Geophysical Research* 98.

Hakola, Hannele, Janet Arey, Sara M Aschmann, and Roger Atkinson (1994). "Product formation from the gas-phase reactions of OH radicals and O3 with a series of monoterpenes". In: *Journal of Atmospheric Chemistry* 18.1, pp. 75–102.

Ham, Jason E, Joel C Harrison, Stephen R Jackson, and JR Wells (2016). "Limonene ozonolysis in the presence of nitric oxide: Gas-phase reaction products and yields". In: *Atmospheric Environment* 132, pp. 300–308.

Hansel, A, A Jordan, R Holzinger, P Prazeller, W Vogel, and W Lindinger (1995). "Proton transfer reaction mass spectrometry: on-line trace gas analysis at the ppb level". In: *International Journal of Mass Spectrometry and Ion Processes* 149, pp. 609–619.

Hatakeyama, Shiro, Katsuyuki Izumi, Tsutomu Fukuyama, and Hajime Akimoto (1989). "Reactions of ozone with α-pinene and β-pinene in air: Yields of gaseous and particulate products". In: *Journal of Geophysical Research: Atmospheres* 94.D10, pp. 13013–13024.

Heland, Jörg, Jörg Kleffmann, Ralf Kurtenbach, and Peter Wiesen (2001). "A new instrument to measure gaseous nitrous acid (HONO) in the atmosphere". In: *Environmental science & technology* 35.15, pp. 3207–3212.

Helmig, Detlev, John Ortega, Alex Guenther, Jeffrey D Herrick, and Chris Geron (2006). "Sesquiterpene emissions from loblolly pine and their potential contribution to biogenic aerosol formation in the Southeastern US". In: *Atmospheric Environment* 40.22, pp. 4150–4157.

Hofzumahaus, Andreas, Franz Rohrer, Keding Lu, Birger Bohn, Theo Brauers, Chih-Chung Chang, Hendrik Fuchs, Frank Holland, Kazuyuki Kita, Yutaka Kondo, et al. (2009). "Amplified trace gas removal in the troposphere". In: *science* 324.5935, pp. 1702–1704.

Hohaus, T, U Kuhn, S Andres, M Kaminski, F Rohrer, R Tillmann, A Wahner, R Wegener, Z Yu, and A Kiendler-Scharr (2016). "A new plant chamber facility, PLUS, coupled to the atmosphere simulation chamber SAPHIR". In: *Atmospheric Measurement Techniques* 9.3, pp. 1247–1259.

Holzinger, R, L Sandoval-Soto, S Rottenberger, PJ Crutzen, and J Kesselmeier (2000). "Emissions of volatile organic compounds from Quercus ilex L. measured by proton transfer reaction mass spectrometry under different environmental conditions". In: *Journal of Geophysical Research: Atmospheres* 105.D16, pp. 20573–20579.

Ingham, T, A Goddard, LK Whalley, KL Furneaux, PM Edwards, CP Seal, DE Self, GP Johnson, KA Read, JD Lee, et al. (2009). "A flow-tube based laser-induced fluorescence instrument to measure OH reactivity in the troposphere". In: *Atmospheric Measurement Techniques* 2.2, pp. 465–477.

J. Kesselmeier K. Bode, U. Hofmann, H Müller, L Schäfer, A Wolf, P Ciccioli, E Brancaleoni, A Cecinato, M Frattoni, et al. (1997). "Emission of short chained organic acids, aldehydes and monoterpenes from Quercus ilex L. and Pinus pinea L. in relation to physiological activities, carbon budget and emission algorithms". In: *Atmospheric Environment* 31, pp. 119–133.

Jacobs, M. I., A. I. Darer, and M. J. Elrod (2013). "Rate Constants and Products of the OH Reaction with Isoprene-Derived Epoxides." In: *Environmental Science & Technology* 47.22, pp. 12868–76.

Jäger, Julia (2014). *Airborne VOC measurements on board the Zeppelin NT during the PEGASOS campaigns in 2012 deploying the improved Fast-GC-MSD System*. Forschungszentrum Jülich.

Janson, Robert and Claes de Serves (2001). "Acetone and monoterpene emissions from the boreal forest in northern Europe". In: *Atmospheric Environment* 35.27, pp. 4629–4637.

Jaoui, M, S Leungsakul, and Richard M Kamens (2003). "Gas and particle products distribution from the reaction of β-caryophyllene with ozone". In: *Journal of Atmospheric Chemistry* 45.3, pp. 261–287.

Jordan, A., S. Haidacher, G. Hanel, E. Hartungen, L. Märk, H. Seehauser, R. Schottkowsky, P. Sulzer, and T.D. Märk (2009). "A high resolution and high sensitivity proton-transfer-reaction time-of-flight mass spectrometer (PTR-TOF-MS)". In: *International Journal of Mass Spectrometry* 286.2–3, pp. 122–128. ISSN: 1387-3806.

Kaminski, Martin (2014). *Untersuchung des photochemischen Terpenoidabbaus in der Atmosphärensimulationskammer SAPHIR*. Vol. 218. Forschungszentrum Jülich.

Kansal, Ankur (2009). "Sources and reactivity of NMHCs and VOCs in the atmosphere: A review". In: *Journal of Hazardous Materials* 166.1, pp. 17–26.

Karl, M, H-P Dorn, F Holland, R Koppmann, D Poppe, L Rupp, A Schaub, and A Wahner (2006). "Product study of the reaction of OH radicals with isoprene in the atmosphere simulation chamber SAPHIR". In: *Journal of atmospheric chemistry* 55.2, pp. 167–187.

Keene, William C. and James N. Galloway (1986). "Considerations regarding sources for formic and acetic acids in the troposphere". In: *Journal of Geophysical Research Atmospheres* 91.D13, pp. 14466–14474.

Kelly, TJ and CR Fortune (1994). "Continuous monitoring of gaseous formaldehyde using an improved fluorescence approach". In: *International journal of environmental analytical chemistry* 54.4, pp. 249–263.

Kesselmeier, J and M Staudt (1999). "Biogenic volatile organic compounds (VOC): an overview on emission, physiology and ecology". In: *Journal of atmospheric chemistry* 33.1, pp. 23–88.

Kim, S, A Guenther, T Karl, and J Greenberg (2011). "Contributions of primary and secondary biogenic VOC tototal OH reactivity during the CABINEX (Community Atmosphere-Biosphere INteractions Experiments)-09 field campaign". In: *Atmospheric Chemistry and Physics* 11.16, pp. 8613–8623.

Koppmann, Ralf (2008). *Volatile organic compounds in the atmosphere*. John Wiley & Sons.

Kovacs, TA, WH Brune, H Harder, M Martinez, JB Simpas, GJ Frost, E Williams, T Jobson, C Stroud, V Young, et al. (2003). "Direct measurements of urban OH reactivity during Nashville SOS in summer 1999". In: *Journal of Environmental Monitoring* 5.1, pp. 68–74.

Kulmala, Markku, Ari Asmi, HK Lappalainen, Urs Baltensperger, J-L Brenguier, MC Facchini, H-C Hansson, Øystein Hov, CD O'Dowd, U Pöschl, et al. (2011). "General overview: European Integrated project on Aerosol Cloud Climate and Air Quality interactions (EUCAARI)–integrating aerosol research from nano to global scales". In: *Atmospheric Chemistry and Physics* 11.24, pp. 13061–13143.

Lee, Anita, Allen H Goldstein, Melita D Keywood, Song Gao, Varuntida Varutbangkul, Roya Bahreini, Nga L Ng, Richard C Flagan, and John H Seinfeld (2006). "Gas-phase products and secondary aerosol yields from the ozonolysis of ten different terpenes". In: *Journal of Geophysical Research: Atmospheres* 111.D7.

Lee, James D, Jennifer C Young, Katie A Read, Jacqueline F Hamilton, James R Hopkins, Alastair C Lewis, Brian J Bandy, James Davey, Peter Edwards, Trevor Ingham, et al. (2009). "Measurement and calculation of OH reactivity at a United Kingdom coastal site". In: *Journal of atmospheric chemistry* 64.1, pp. 53–76.

Lindinger, W, A Hansel, and A Jordan (1998). "On-line monitoring of volatile organic compounds at pptv levels by means of proton-transfer-reaction mass spectrometry (PTR-MS) medical applications, food control and environmental research". In: *International Journal of Mass Spectrometry and Ion Processes* 173.3, pp. 191–241.

Liu, YJ, I Herdlinger-Blatt, KA McKinney, and ST Martin (2013). "Production of methyl vinyl ketone and methacrolein via the hydroperoxyl pathway of isoprene oxidation". In: *Atmospheric Chemistry and Physics* 13.11, pp. 5715–5730.

Lou, S, F Holland, F Rohrer, K Lu, B Bohn, T Brauers, CC Chang, H Fuchs, R Häseler, K Kita, et al. (2010). "Atmospheric OH reactivities in the Pearl River Delta–China in summer 2006: measurement and model results". In: *Atmospheric Chemistry and Physics* 10.22, pp. 11243–11260.

Lu, KD, A Hofzumahaus, F Holland, B Bohn, T Brauers, H Fuchs, M Hu, R Häseler, K Kita, Y Kondo, et al. (2013). "Missing OH source in a suburban environment near Beijing: observed and modelled OH and HO 2 concentrations in summer 2006". In: *Atmospheric Chemistry and Physics* 13.2, pp. 1057–1080.

Maksymiuk, Christina S, Chakicherla Gayahtri, Roberto R Gil, and Neil M Donahue (2009). "Secondary organic aerosol formation from multiphase oxidation of limonene by ozone: mechanistic constraints via two-dimensional heteronuclear NMR spectroscopy". In: *Physical Chemistry Chemical Physics* 11.36, pp. 7810–7818.

Mao, Jingqiu, Xinrong Ren, Shuang Chen, William H Brune, Zhong Chen, Monica Martinez, Hartwig Harder, Barry Lefer, Bernhard Rappenglück, James Flynn, et al. (2010). "Atmospheric oxidation capacity in the summer of Houston 2006: Comparison with summer measurements in other metropolitan studies". In: *Atmospheric Environment* 44.33, pp. 4107–4115.

Mao, J, X Ren, WH Brune, JR Olson, JH Crawford, A Fried, LG Huey, RC Cohen, B Heikes, HB Singh, et al. (2009). "Airborne measurement of OH reactivity during INTEX-B". In: *Atmospheric Chemistry and Physics* 9.1, pp. 163–173.

Mellouki, A, TJ Wallington, and J Chen (2015). "Atmospheric chemistry of oxygenated Volatile Organic Compounds: Impacts on air quality and climate". In: *Chemical reviews* 115.10, pp. 3984–4014.

Mogensen, D, S Smolander, Andrey Sogachev, L Zhou, V Sinha, A Guenther, J Williams, T Nieminen, MK Kajos, J Rinne, et al. (2011). "Modelling atmospheric OH-reactivity in a boreal forest ecosystem". In: *Atmospheric Chemistry and Physics* 11.18, pp. 9709–9719.

Müller, Markus, Tomáš Mikoviny, Werner Jud, Barbara D'Anna, and Armin Wisthaler (2013). "A new software tool for the analysis of high resolution PTR-TOF mass spectra". In: *Chemometrics and Intelligent Laboratory Systems* 127, pp. 158–165.

Nakashima, Yoshihiro, Hiroshi Tsurumaru, Takashi Imamura, Iustinian Bejan, John C Wenger, and Yoshizumi Kajii (2012). "Total OH reactivity measurements in laboratory studies of the photooxidation of isoprene". In: *Atmospheric environment* 62, pp. 243–247.

Niinemets, Ülo and Markus Reichstein (2003). "Controls on the emission of plant volatiles through stomata: Differential sensitivity of emission rates to stomatal closure explained". In: *Journal of Geophysical Research: Atmospheres* 108.D7.

Nölscher, AC, Efstratios Bourtsoukidis, Boris Bonn, Jürgen Kesselmeier, Johannes Lelieveld, and Jonathan Williams (2013). "Seasonal measurements of total OH reactivity emission rates from Norway spruce in 2011". In: *Biogeosciences* 10.6, pp. 4241–4257.

Nölscher, AC, T Butler, J Auld, P Veres, A Muñoz, D Taraborrelli, L Vereecken, J Lelieveld, and J Williams (2014). "Using total OH reactivity to assess isoprene photooxidation via measurement and model". In: *Atmospheric Environment* 89, pp. 453–463.

Nölscher, AC, J Williams, V Sinha, T Custer, W Song, AM Johnson, R Axinte, H Bozem, H Fischer, N Pouvesle, et al. (2012). "Summertime total OH reactivity measurements from boreal forest during HUMPPA-COPEC 2010". In: *Atmospheric chemistry and Physics* 12.17, pp. 8257–8270.

Nørgaard, AW, Jacob Klenø Nøjgaard, K Larsen, Sune Sporring, CK Wilkins, PA Clausen, and P Wolkoff (2006). "Secondary limonene endo-ozonide: a major product from gas-phase ozonolysis of R-(+)-limonene at ambient temperature". In: *Atmospheric Environment* 40.19, pp. 3460–3466.

Paulot, F., J. D. Crounse, H. G. Kjaergaard, J. H. Kroll, J. H. Seinfeld, and P. O. Wennberg (2009a). "Isoprene photooxidation: new insights into the production of acids and organic nitrates". In: *Atmospheric Chemistry & Physics* 9.4, pp. 1479–1501.

Paulot, Fabien, John D Crounse, Henrik G Kjaergaard, Andreas Kürten, Jason M St Clair, John H Seinfeld, and Paul O Wennberg (2009b). "Unexpected epoxide formation in the gas-phase photooxidation of isoprene". In: *Science* 325.5941, pp. 730–733.

Peeters, Jozef, Jean-François Müller, Trissevgeni Stavrakou, and Vinh Son Nguyen (2014). "Hydroxyl radical recycling in isoprene oxidation driven by hydrogen bonding and hydrogen tunneling: The upgraded LIM1 mechanism". In: *Journal of Physical Chemistry A* 118.38, pp. 8625–8643.

Pitts, BJ Finlayson and JN Pitts (2000). "Chemistry of the upper and lower atmosphere: Theory, experiments and applications". In: *Academic, US*.

Prinn, RG, J Huang, RF Weiss, DM Cunnold, PJ Fraser, PG Simmonds, A McCulloch, C Harth, P Salameh, S O'Doherty, et al. (2001). "Evidence for substantial variations of atmospheric hydroxyl radicals in the past two decades". In: *Science* 292.5523, pp. 1882–1888.

Rapparini, F, R Baraldi, F Miglietta, and F Loreto (2004). "Isoprenoid emission in trees of Quercus pubescens and Quercus ilex with lifetime exposure to naturally high CO2 environment". In: *Plant Cell & Environment* 27.4, pp. 381–391.

Reissell, Anni, Cheryl Harry, Sara M Aschmann, Roger Atkinson, and Janet Arey (1999). "Formation of acetone from the OH radical-and O3-initiated reactions of a series of monoterpenes". In: *Journal of Geophysical Research: Atmospheres* 104.D11, pp. 13869–13879.

Ren, Xinrong, Hartwig Harder, Monica Martinez, Robert L Lesher, Angelique Oliger, Terry Shirley, Jennifer Adams, James B Simpas, and William H Brune (2003). "HO_x concentrations and OH reactivity observations in New York City during PMTACS-NY2001". In: *Atmospheric Environment* 37.26, pp. 3627–3637.

Ren, Xinrong, William H Brune, Jingqiu Mao, Michael J Mitchell, Robert L Lesher, James B Simpas, Andrew R Metcalf, James J Schwab, Chenxia Cai, Yongquan Li, et al. (2006). "Behavior of OH and HO_2 in the winter atmosphere in New York City". In: *Atmospheric Environment* 40, pp. 252–263.

Rivera-Rios, JC, TB Nguyen, JD Crounse, W Jud, JM St Clair, T Mikoviny, JB Gilman, BM Lerner, JB Kaiser, J d Gouw, et al. (2014). "Conversion of hydroperoxides to carbonyls in field and laboratory instrumentation: Observational bias in diagnosing pristine versus anthropogenically controlled atmospheric chemistry". In: *Geophysical Research Letters* 41.23, pp. 8645–8651.

Rohrer, F, B Bohn, T Brauers, D Brüning, F-J Johnen, A Wahner, and J Kleffmann (2005). "Characterisation of the photolytic HONO-source in the atmosphere simulation chamber SAPHIR". In: *Atmospheric Chemistry and Physics* 5.8, pp. 2189–2201.

Rohrer, F and D Brüning (1992). "Surface NO and NO2 mixing ratios measured between 30° N and 30° S in the Atlantic region". In: *Journal of atmospheric chemistry* 15.3-4, pp. 253–267.

Sabillón, Danelia and Lázaro V Cremades (2001). "Diurnal and seasonal variation of monoterpene emission rates for two typical Mediterranean species (Pinus pinea and Quercus ilex) from field measurements-relationship with temperature and PAR". In: *Atmospheric Environment* 35.26, pp. 4419–4431.

Sadanaga, Yasuhiro, Ayako Yoshino, Keisuke Watanabe, Atsushi Yoshioka, Yoko Wakazono, Yugo Kanaya, and Yoshizumi Kajii (2004). "Development of a measurement system of OH reactivity in the atmosphere by using a laser-induced pump and probe technique". In: *Review of Scientific Instruments* 75.8, pp. 2648–2655.

Schnitzler, J.-P, Andrea Lehning, and R Steinbrecher (2015). "Seasonal Pattern of Isoprene Synthase Activity in Quercus robur Leaves and its Significance for Modeling Isoprene Emission Rates". In: *Plant Biology* 110.3, pp. 240–243.

Shirley, TR, WH Brune, Xinrong Ren, J Mao, R Lesher, B Cardenas, R Volkamer, LT Molina, Mario J Molina, B Lamb, et al. (2006). "Atmospheric oxidation in the Mexico City metropolitan area (MCMA) during April 2003". In: *Atmospheric Chemistry and Physics* 6.9, pp. 2753–2765.

Sinha, V, J Williams, JN Crowley, and J Lelieveld (2008). "The Comparative Reactivity Method–a new tool to measure total OH Reactivity in ambient air". In: *Atmospheric Chemistry and Physics* 8.8, pp. 2213–2227.

Sinha, V., J. Williams, J. M. Diesch, F. Drewnick, M. Martinez, H. Harder, E. Regelin, D. Kubistin, H. Bozem, and Z. Hosaynalibeygi (2012). "Constraints on instantaneous ozone production rates and regimes during DOMINO derived using in-situ OH reactivity measurements". In: *Atmospheric Chemistry and Physics* 12.15, pp. 7269–7283.

Sioutas, Constantinos (1999). "Evaluation of the measurement performance of the scanning mobility particle sizer and aerodynamic particle sizer". In: *Aerosol Science & Technology* 30.1, pp. 84–92.

Sprengnether, Michele, Kenneth L Demerjian, Neil M Donahue, and James G Anderson (2002). "Product analysis of the OH oxidation of isoprene and 1, 3-butadiene in the presence of NO". In: *Journal of Geophysical Research: Atmospheres* 107.D15.

St. Clair, Jason M, Jean C Rivera-Rios, John D Crounse, Hasse C Knap, Kelvin H Bates, Alex P Teng, Solvejg Jørgensen, Henrik G Kjaergaard, Frank N Keutsch, and Paul O Wennberg (2015). "Kinetics and products of the reaction of the first-generation isoprene hydroxy hydroperoxide (ISOPOOH) with OH". In: *The Journal of Physical Chemistry A* 120.9, pp. 1441–1451.

Staudt, M and N Bertin (1998). "Light and temperature dependence of the emission of cyclic and acyclic monoterpenes from holm oak (Quercus ilex L.) leaves". In: *Plant, Cell & Environment* 21.4, pp. 385–395.

Staudt, M and G Seufert (1995). "Light-dependent emission of monoterpenes by holm oak (Quercus ilex L.)" In: *Naturwissenschaften* 82.2, pp. 89–92.

Staudt, M, G Seufert, D Kotzias, C Spartà, and P Ciccioli (1993). "Holm oak (Quercus ilex) a strong emitter of monoterpenes". In: pp. 579–586.

Tingey, David T, Marybeth Manning, Louis C Grothaus, and Walter F Burns (1980). "Influence of light and temperature on monoterpene emission rates from slash pine". In: *Plant Physiology* 65.5, pp. 797–801.

Tuazon, Ernesto C and Roger Atkinson (1990). "A product study of the gas-phase reaction of Isoprene with the OH radical in the presence of NOx". In: *International Journal of Chemical Kinetics* 22.12, pp. 1221–1236.

Vlasenko, A, AM Macdonald, SJ Sjostedt, and JPD Abbatt (2010). "Formaldehyde measurements by Proton transfer reaction–Mass Spectrometry (PTR-MS): correction for humidity effects". In: *Atmospheric Measurement Techniques* 3.4, pp. 1055–1062.

Volkamer, Rainer, Jose L Jimenez, Federico San Martini, Katja Dzepina, Qi Zhang, Dara Salcedo, Luisa T Molina, Douglas R Worsnop, and Mario J Molina (2006). "Secondary organic aerosol formation from anthropogenic air pollution: Rapid and higher than expected". In: *Geophysical Research Letters* 33.17.

Volkamer, Rainer, Björn Klotz, Ian Barnes, Takashi Imamura, Klaus Wirtz, Nobuaki Washida, Karl Heinz Becker, and Ulrich Platt (2002). "OH-initiated oxidation of benzene Part I. Phenol formation under atmospheric conditions". In: *Physical Chemistry Chemical Physics* 4.9, pp. 1598–1610.

Von Schneidemesser, Erika, Paul S Monks, James D Allan, Lori Bruhwiler, Piers Forster, David Fowler, Axel Lauer, William T Morgan, Pauli Paasonen, Mattia Righi, et al. (2015). "Chemistry and the linkages between air quality and climate change". In: *Chemical Reviews* 115.10, pp. 3856–3897.

Wang, Ying, Guoshun Zhuang, Shuang Chen, Zhisheng An, and Aihua Zheng (2007). "Characteristics and sources of formic, acetic and oxalic acids in PM 2.5 and PM 10 aerosols in Beijing, China". In: *Atmospheric Research* 84.2, pp. 169–181.

Wegener, Robert, Theo Brauers, Ralf Koppmann, Sonia Rodríguez Bares, Franz Rohrer, Ralf Tillmann, Andreas Wahner, Armin Hansel, and Armin Wisthaler (2007). "Simulation chamber investigation of the reactions of ozone with short-chained alkenes". In: *Journal of Geophysical Research: Atmospheres* 112.D13.

Winiberg, F. A. F., T. J. Dillon, S. C. Orr, C. B. M. Groß, I. Bejan, C. A. Brumby, M. J. Evans, S. C. Smith, D. E. Heard, and P. W. Seakins (2016). "Direct measurements of OH and other product yields from the $HO_2 + CH_3C(O)O_2$ reaction". In: *Atmospheric Chemistry and Physics* 16.6, pp. 4023–4042.

Winterhalter, Richard, Peter Neeb, Dirk Grossmann, Antje Kolloff, Osamu Horie, and Geert Moortgat (2000). "Products and mechanism of the gas phase reaction of ozone with β-pinene". In: *Journal of Atmospheric Chemistry* 35.2, pp. 165–197.

Wisthaler, A, NR Jensen, R Winterhalter, W Lindinger, and J Hjorth (2001). "Measurements of acetone and other gas phase product yields from the OH-initiated oxidation of terpenes by proton-transfer-reaction mass spectrometry (PTR-MS)". In: *Atmospheric Environment* 35.35, pp. 6181–6191.

Yoshino, Ayako, Yasuhiro Sadanaga, Keisuke Watanabe, Shungo Kato, Yuko Miyakawa, Jun Matsumoto, and Yoshizumi Kajii (2006). "Measurement of total OH reactivity by laser-induced pump and probe technique—comprehensive observations in the urban atmosphere of Tokyo". In: *Atmospheric Environment* 40.40, pp. 7869–7881.

Yu, Jianzhen, David R Cocker III, Robert J Griffin, Richard C Flagan, and John H Seinfeld (1999). "Gas-phase ozone oxidation of monoterpenes: Gaseous and particulate products". In: *Journal of Atmospheric Chemistry* 34.2, pp. 207–258.

Zannoni, N (2015). *OH reactivity measurements in the Mediterranean region*.

Zannoni, N, V Gros, M Lanza, R Sarda, B Bonsang, C Kalogridis, S Preunkert, M Legrand, C Jambert, C Boissard, et al. (2015). "OH reactivity and concentrations of Biogenic Volatile Organic Compounds in a Mediterranean forest of downy oak trees". In: *Atmospheric Chemistry and Physics Discussions* 15.16, pp. 22047–22095.

Zhang, Jieyuan, Kara E Huff Hartz, Spyros N Pandis, and Neil M Donahue (2006). "Secondary organic aerosol formation from limonene ozonolysis: homogeneous and heterogeneous influences as a function of NO x". In: *The Journal of Physical Chemistry A* 110.38, pp. 11053–11063.

Acknowledgements

This work is funded by the European Commission's 7th Framework Program under Grant Agreement Number 287382 (Marie Curie Training Network PIMMS) and by the Helmholtz President's Fund (Backfeed), their financial support is sincerely appreciated.

I would like to show my deepest gratitude to my supervisor, Astrid Kiendler-scharr, for giving me the opportunity to work in her research group, her superb guidance has helped me a lot during my doctoral research.

I want to take this chance to thank my "Doktor Vater", Thorsten Benter, for his enlightening lectures and warm encouragement, which I cherish deeply in my heart.

A heartfelt thanks goes to Chris Mayhew, Nigel Mason and Kathleen Hynes for organizing and managing the PIMMS network, and for always being available to help when we ESRs needed. I have learned so much in the PIMMS network, from which I will benefit a great deal in the future.

I am thankful to Ralf Tillmann, for his knowledge of chemistry and valuable suggestions during this work. Without his consistent and insightful instruction, this thesis could not be finished.

I would like to thank Thorsten Hohaus and Stefanie Andres, for taking good care of the plants as well as the plant chamber, so that our plant emission experiments could be carried out as planed. My thanks extend to all my other colleagues who did a great job in maintaining the SAPHIR chamber.

My grateful thanks to my external supervisor, Valerie Gros, for providing me the chance to visit her laboratory in LSCE, and for her interdisciplinary suggestions on this work.

Many thanks to Lukas Maerk, Philipp Sulzer, for illumination on the knowledge of PTR-MS and for their continuous support during my stay at IONICON.

I would like to thank my amazing colleagues. My best colleague and friend Scarlet, for all the relaxing and inspiring conversations we had at work, and for all the wonderful or painful times we went through together. My jungle friend Nora, for her enlightening ideas for my research, and also her superpower of making people laugh, thanks for the cozy couch and the home-made Glülhwein in Paris, I will always cherish our good memories in Innsbruck, Vienna... in Birmingham, Ely... in Paris, Caen, St-Michel... in Jüllich, and the fantastic Italian night in London! A big thanks to Matteo and Kos, for helping me with the instruments, and for their kind host during my exchange in Innsbruck. I am also grateful to Ismail, Lina, Merci... for sharing their experience with me during my first year of PhD, and for helping me out through all the stages of this thesis. I would extend my thanks to Anna, for her constructive advises on this work.

I cannot end without thanking my family, on whose constant encouragement and love I have always relied throughout my thesis.

Band / Volume 423
Sonochemical Synthesis of Silicon Hydride Polymers and Silicon Nanoparticles from Liquid Silanes
A. P. Cádiz Bedini (2018), viii, 132, XVIII pp
ISBN: 978-3-95806-329-7

Band / Volume 424
Synthesis and Stability Assessment of Uranium Microparticles: Providing Reference Materials for Nuclear Verification Purposes
R. Middendorp (2018), X, 145 pp
ISBN: 978-3-95806-330-3

Band / Volume 425
Herstellung und Charakterisierung von Lithiumlanthanzirkonat-Funktionsschichten für Lithium-Festkörperbatterien
T. Reppert (2018), vii, 187 pp
ISBN: 978-3-95806-331-0

Band / Volume 426
Proton Conduction and Gas Permeation through Polymer Electrolyte Membranes during Water Electrolysis
M. Schalenbach (2018), VI, 212 pp
ISBN: 978-3-95806-333-4

Band / Volume 427
Improved characterization of root zone soil moisture by assimilating groundwater level and surface soil moisture data in an integrated terrestrial system model
H. Zhang (2018), x, 125 pp
ISBN: 978-3-95806-335-8

Band / Volume 428
Manipulation of magnetism in iron oxide nanoparticle / $BaTiO_3$ composites and low-dimensional iron oxide nanoparticle arrays
L. Wang (2018), VI, 151 pp
ISBN: 978-3-95806-338-9
Band wurde nicht veröffentlicht. Erscheint als Schlüsseltechnologieband 180

Band / Volume 429
Characterization of spatial-temporal varying riverbed hydraulic conductivity and its role on the estimation of river-aquifer exchange fluxes with data assimilation
Q. Tang (2018), xv, 117 pp
ISBN: 978-3-95806-339-6

Band / Volume 430
Der Einfluss von Wasserdampf auf den Sauerstofftransport in keramischen Hochtemperaturmembranen
F. Thaler (2018), ii, 93, XXXI pp
ISBN: 978-3-95806-340-2

Band / Volume 431
Analysis & modeling of metastable photovoltaic technologies: towards dynamic photovoltaic performance models
M. Görig (2018), 246 pp
ISBN: 978-3-95806-342-6

Band / Volume 432
Laser Treatment of Silicon Thin-Films for Photovoltaic Applications
C. Maurer (2018), vii, 165 pp
ISBN: 978-3-95806-347-1

Band / Volume 433
Mentalitäten und Verhaltensmuster im Kontext der Energiewende in NRW
K. Schürmann & D. Schumann (Hrsg.) (2018), 236 pp
ISBN: 978-3-95806-349-5

Band / Volume 434
Adhäsionsverhalten von wässrigen Nafion-Lösungen an dispersen Phasengrenzen
A. Schulz (2018), xii, 129 pp
ISBN: 978-3-95806-354-9

Band / Volume 435
Alterungs- und fehlertolerante optimale Betriebsführung eines Direktmethanol-Brennstoffzellensystems
R. Keller (2018), XX, 175 pp
ISBN: 978-3-95806-355-6

Band / Volume 436
Chamber study of biogenic volatile organic compounds: plant emission, oxidation products and their OH reactivity
Z. Yu (2018), ix, 139 pp
ISBN: 978-3-95806-356-3

Energie & Umwelt / Energy & Environment
Band / Volume 436
ISBN 978-3-95806-356-3

Mitglied der Helmholtz-Gemeinschaft

JÜLICH
Forschungszentrum